THE NATIONAL ACADEMIES PRESS

SHARE

LRFD Design and Construction of Shallow Foundations for Highway Bridge Structures

NCHRP REPORT 651

NATIONAL COOPERATIVE HIGHWAY RESEARCH PROGRAM

LRFD Design and Construction of Shallow Foundations for Highway Bridge Structures

TRANSPORTATION RESEARCH BOARD OF THE NATIONAL ACADEMIES

DETAILS

BUY THIS BOOK

FIND RELATED TITLES

AUTHORS

Samuel G Paikowsky; Mary C Canniff; Kerstin Lesny; Aloys Kisse; Shailendra Amatya; Robert Muganga; Transportation Research Board

NATIONAL COOPERATIVE HIGHWAY RESEARCH PROGRAM

NCHRP REPORT 651

LRFD Design and Construction
of Shallow Foundations
for Highway Bridge Structures

Samuel G. Paikowsky
Mary C. Canniff
GEOSCIENCES TESTING AND RESEARCH, INC.
North Chelmsford, MA
UNIVERSITY OF MASSACHUSETTS
Lowell, MA

Kerstin Lesny
Aloys Kisse
INSTITUTE OF SOIL MECHANICS AND FOUNDATION ENGINEERING
DEPARTMENT OF CIVIL ENGINEERING
University of Duisburg-Essen, Germany

Shailendra Amatya
Robert Muganga
GEOTECHNICAL ENGINEERING RESEARCH LABORATORY
UNIVERSITY OF MASSACHUSETTS
Lowell, MA

Subscriber Categories
Highways • Bridges and Other Structures • Geotechnology

TRANSPORTATION RESEARCH BOARD

WASHINGTON, D.C.
2010
www.TRB.org

NATIONAL COOPERATIVE HIGHWAY RESEARCH PROGRAM

Systematic, well-designed research provides the most effective approach to the solution of many problems facing highway administrators and engineers. Often, highway problems are of local interest and can best be studied by highway departments individually or in cooperation with their state universities and others. However, the accelerating growth of highway transportation develops increasingly complex problems of wide interest to highway authorities. These problems are best studied through a coordinated program of cooperative research.

In recognition of these needs, the highway administrators of the American Association of State Highway and Transportation Officials initiated in 1962 an objective national highway research program employing modern scientific techniques. This program is supported on a continuing basis by funds from participating member states of the Association and it receives the full cooperation and support of the Federal Highway Administration, United States Department of Transportation.

The Transportation Research Board of the National Academies was requested by the Association to administer the research program because of the Board's recognized objectivity and understanding of modern research practices. The Board is uniquely suited for this purpose as it maintains an extensive committee structure from which authorities on any highway transportation subject may be drawn; it possesses avenues of communications and cooperation with federal, state and local governmental agencies, universities, and industry; its relationship to the National Research Council is an insurance of objectivity; it maintains a full-time research correlation staff of specialists in highway transportation matters to bring the findings of research directly to those who are in a position to use them.

The program is developed on the basis of research needs identified by chief administrators of the highway and transportation departments and by committees of AASHTO. Each year, specific areas of research needs to be included in the program are proposed to the National Research Council and the Board by the American Association of State Highway and Transportation Officials. Research projects to fulfill these needs are defined by the Board, and qualified research agencies are selected from those that have submitted proposals. Administration and surveillance of research contracts are the responsibilities of the National Research Council and the Transportation Research Board.

The needs for highway research are many, and the National Cooperative Highway Research Program can make significant contributions to the solution of highway transportation problems of mutual concern to many responsible groups. The program, however, is intended to complement rather than to substitute for or duplicate other highway research programs.

NOTICE

The project that is the subject of this report was a part of the National Cooperative Highway Research Program, conducted by the Transportation Research Board with the approval of the Governing Board of the National Research Council.

The members of the technical panel selected to monitor this project and to review this report were chosen for their special competencies and with regard for appropriate balance. The report was reviewed by the technical panel and accepted for publication according to procedures established and overseen by the Transportation Research Board and approved by the Governing Board of the National Research Council.

The opinions and conclusions expressed or implied in this report are those of the researchers who performed the research and are not necessarily those of the Transportation Research Board, the National Research Council, or the program sponsors.

The Transportation Research Board of the National Academies, the National Research Council, and the sponsors of the National Cooperative Highway Research Program do not endorse products or manufacturers. Trade or manufacturers' names appear herein solely because they are considered essential to the object of the report.

THE NATIONAL ACADEMIES
Advisers to the Nation on Science, Engineering, and Medicine

The **National Academy of Sciences** is a private, nonprofit, self-perpetuating society of distinguished scholars engaged in scientific and engineering research, dedicated to the furtherance of science and technology and to their use for the general welfare. On the authority of the charter granted to it by the Congress in 1863, the Academy has a mandate that requires it to advise the federal government on scientific and technical matters. Dr. Ralph J. Cicerone is president of the National Academy of Sciences.

The **National Academy of Engineering** was established in 1964, under the charter of the National Academy of Sciences, as a parallel organization of outstanding engineers. It is autonomous in its administration and in the selection of its members, sharing with the National Academy of Sciences the responsibility for advising the federal government. The National Academy of Engineering also sponsors engineering programs aimed at meeting national needs, encourages education and research, and recognizes the superior achievements of engineers. Dr. Charles M. Vest is president of the National Academy of Engineering.

The **Institute of Medicine** was established in 1970 by the National Academy of Sciences to secure the services of eminent members of appropriate professions in the examination of policy matters pertaining to the health of the public. The Institute acts under the responsibility given to the National Academy of Sciences by its congressional charter to be an adviser to the federal government and, on its own initiative, to identify issues of medical care, research, and education. Dr. Harvey V. Fineberg is president of the Institute of Medicine.

The **National Research Council** was organized by the National Academy of Sciences in 1916 to associate the broad community of science and technology with the Academy's purposes of furthering knowledge and advising the federal government. Functioning in accordance with general policies determined by the Academy, the Council has become the principal operating agency of both the National Academy of Sciences and the National Academy of Engineering in providing services to the government, the public, and the scientific and engineering communities. The Council is administered jointly by both the Academies and the Institute of Medicine. Dr. Ralph J. Cicerone and Dr. Charles M. Vest are chair and vice chair, respectively, of the National Research Council.

The **Transportation Research Board** is one of six major divisions of the National Research Council. The mission of the Transportation Research Board is to provide leadership in transportation innovation and progress through research and information exchange, conducted within a setting that is objective, interdisciplinary, and multimodal. The Board's varied activities annually engage about 7,000 engineers, scientists, and other transportation researchers and practitioners from the public and private sectors and academia, all of whom contribute their expertise in the public interest. The program is supported by state transportation departments, federal agencies including the component administrations of the U.S. Department of Transportation, and other organizations and individuals interested in the development of transportation. **www.TRB.org**

www.national-academies.org

COOPERATIVE RESEARCH PROGRAMS

FOREWORD

By Waseem Dekelbab
Staff Officer
Transportation Research Board

This report develops and calibrates procedures and modifies the *AASHTO LRFD Bridge Design Specifications,* Section 10—Foundations for the Strength Limit State Design of Shallow Foundations. The material in this report will be of immediate interest to bridge engineers and geotechnical engineers involved in the design of shallow foundations.

Shallow foundations are used for a large percentage of bridges, retaining walls, and other transportation structures. Reliability-based resistance factors are needed to incorporate into design specifications for use by transportation agencies.

LRFD design specifications for shallow foundations of highway structures need to be developed using a reliability-based calibration procedure, consistent with the calibration of load and resistance factors for bridge superstructures. Load and resistance factors should account for uncertainties related to load combinations, site conditions, soil and rock type and properties, and methods of testing and analysis. It is believed that resistance factors for shallow foundations in Section 10 of the current *AASHTO LRFD Bridge Design Specifications* do not satisfy these requirements.

The objective of this project was to develop recommended changes to Section 10 of the *AASHTO LRFD Bridge Design Specifications* for the strength limit state design of shallow foundations.

This research was performed under NCHRP Project 24-31 by Geosciences Testing and Research, Inc., and the University of Massachusetts at Lowell with the assistance of the University of Duisburg-Essen, Germany. The report fully documents the research leading to the recommended design specifications for the strength limit state design of shallow foundations.

Appendixes A through H from the research agency's final report are not published herein but are available on the TRB website (www.trb.org) by searching on "NCHRP Report 651". These appendixes are titled as follows:

- Appendix A: Alternative Model Background
- Appendix B: Findings—State of Practice, Serviceability and Databases
- Appendix C: Questionnaire Summary
- Appendix D: UML-GTR ShalFound07 Database
- Appendix E: UML-GTR RockFound07 Database
- Appendix F: Shallow Foundations Modes of Failure and Failure Criteria
- Appendix G: Bias Calculation Examples
- Appendix H: Design Examples

CONTENTS

S U M M A R Y

LRFD Design and Construction of Shallow Foundations for Highway Bridge Structures

NCHRP Project 24-31, "LRFD Design Specifications for Shallow Foundations" was initiated with the objective to "develop recommended changes to Section 10 of the *AASHTO LRFD Bridge Design Specifications* for the strength limit state design of shallow foundations." The AASHTO specifications are traditionally observed on all federally aided projects and are generally viewed as the national code of U.S. highway practice; hence, they influence the construction of all foundations of highway bridges throughout the United States. This report represents the results of the studies and analyses conducted for NCHRP Project 24-31.

The current AASHTO specifications, as well as other existing codes employing reliability-based design (RBD) principles, were calibrated using a combination of reliability theory, fitting to allowable stress design (ASD) (also called working stress design [WSD]), and engineering judgment. The main challenges of the project were, therefore, the compilation of large, high-quality databases of tested foundations to failure and the development of a procedural and data management framework that would enable Load and Resistance Factor Design (LRFD) parameter evaluation for the strength limit state of shallow foundations. The presented research is the first to introduce large-scale, RBD calibration of shallow foundations utilizing databases.

The state of the art was examined via a critical literature review of design methodologies and RBD and LRFD principles. The state of the practice was established via a questionnaire, distributed to and gathered from state and federal transportation officials and supplemented by telephone interviews. The use of shallow foundations for bridge construction across the United States was found to be about 17%, and a comparison to previous questionnaires showed that this percentage had not changed much. The use varies widely, however, in regions and states across the country: from about two-thirds of all bridge foundations in Pennsylvania, Tennessee, and Connecticut to six states that do not use shallow foundations at all. About three-quarters of all shallow foundations were reported to be built on rock or Intermediate Geomaterial (IGM), and the rest were predominantly built on granular materials. The presented research focuses on the analysis and RBD calibration of foundations on granular soil and rock only.

Large databases were gathered containing 549 load test cases related to the performance of shallow foundations in/on granular materials (of which 269 cases were utilized in the calibration), and 122 cases for foundations in/on rock (of which 119 were utilized in the calibration). The database for the performance of shallow foundations on soils includes the testing of models and large foundations under vertical, eccentric, and inclined loading conditions, as well as combinations of these conditions. The database for the performance of shallow foundations on rock includes the performance of models and large shallow foundations as well as the tip area of rock sockets for which the load-displacement relations could have been distinctly obtained. Failure criteria were identified and examined for establishing the ultimate limit state of the tested foundations. The application of methods to the cases provided the measured resistance of each load test case.

Bearing capacity methods were established for analyzing the ultimate limit state of shallow foundations. The general bearing capacity equation for soils was used with bearing capacity parameters of Prandtl (N_c), Reissner (N_q), and Vesić (N_γ); shape correction and load inclination factors by Vesić (1975); and depth correction factors by Brinch-Hansen (1970). Methods from Goodman (1989) and Carter and Kulhawy (1988) were used for evaluating the bearing capacity of foundations in/on rock.

The performance of the bearing capacity methods was established via the bias defined as the ratio of measured to calculated resistances. The statistics of the bias expressed via the mean and coefficient of variation of the performance were utilized for calibrating the analyses under a specific design application, developing the relevant resistance factor. The application of the statistics to the calibration process was challenging because the factors controlling the accuracy of the design methods were not always easily identified. The performance of the general bearing capacity equation for granular material is highly dependent on the bearing capacity factor N_γ, which in turn is sensitive to the magnitude of the soil's internal friction angle. The bias of the design method was found to closely follow the bias of N_γ, which increases with the increase in the internal friction angle. Similarly, the bias of the Carter and Kulhawy (1988) method was found to be dependent on the rock quality, increasing as the rock quality (measured by RMR) decreases. Both cases required, therefore, calibrations associated with the level of the soil's friction angle and RMR, respectively.

The statistical parameters of lateral loads are not readily available or identified in the AASHTO specifications. A separate study was undertaken to develop such parameters. Examination of lateral dead and live load statistics resulted in recommended lateral load distributions used in the calibration. These parameters were utilized for developing the resistance factors of footings' sliding analysis. The soil-structure interface mechanism was identified using basic research findings and utilized to establish a framework. Data from foundation testing related to two construction methods, i.e., concrete poured on the soil and prefabricated, allowed the development and calibration of the resistances associated with these two prevailing conditions.

Based on the uncertainty established for the design methods and the loading, Monte Carlo (MC) simulation was used to determine the resistance factor for a predetermined reliability index. The resistance factors were also evaluated using the simplified closed-form solution developed based on the First Order Second Moment (FOSM) principles. The findings suggest that the simplified methodology provides conservative resistance factors similar to those obtained by the MC simulations, hence adequate for local practice parameter development.

The recommended resistance factors are soundly based on the quantified performance of the design methods and follow the parameters that control them. These parameters present a radical change to the existing specifications, briefly summarized in the following way:

- The bearing capacity of shallow foundations on granular soils is calibrated according to the soil placement (natural versus controlled) and the magnitude of the internal friction angle.
- All loading conditions—namely vertical-centric, eccentric, inclined-centric, and eccentric—are calibrated.
- The reliability of frictional resistance to sliding is quantified and calibrated.
- Specific bearing capacity methods for shallow foundations on rock are identified, quantified, and calibrated.

The implementation of the findings of this research is expected to provide a safe design of shallow foundations with a consistent level of reliability between the different design methods and with the recommendations presented in *NCHRP Report 507* for the design of deep foundations. The application of the findings in the design of shallow foundations needs to be implemented in the context of total design, i.e., the application of all limit states, of which only the ultimate limit state is addressed in the presented study.

CHAPTER 1

Background

1.1 Research Objectives

NCHRP Project 24-31, "LRFD Design Specifications for Shallow Foundations" was initiated with the objective to "develop recommended changes to Section 10 of the *AASHTO LRFD Bridge Design Specifications* for the strength limit state design of shallow foundations." The current AASHTO specifications, as well as other existing codes employing reliability-based design (RBD) principles, were calibrated using a combination of reliability theory, fitting to allowable stress design (ASD) (also called working stress design [WSD]), and engineering judgment. The main challenges of the project were, therefore, the compilation of large, high-quality databases and the development of a procedural and data management framework that would enable load and resistance factor design (LRFD) parameter evaluation and future updates. Meeting these challenges required the following specific objectives:

1. Establish the state of practice in bridge shallow foundations design and construction.
2. Define the ultimate limit states (ULSs) for individual and combined loading of shallow foundations under expected bridge loading conditions.
3. Build databases of shallow foundation performance under vertical, lateral, and moment loading conditions.
4. Establish methods for the various limit state predictions and assess their uncertainty via databases, model analyses, parametric studies, and the probabilistic approach when required.
5. Develop a procedure for calibrating resistance factors for the identified ULS.
6. Establish factors and procedures.
7. Modify AASHTO's specifications based on the above findings.

1.2 Engineering Design Methodologies

1.2.1 Working Stress Design

The WSD method, also called ASD, has been used in civil engineering since the early 1800s. Under WSD, the design loads (Q), which consist of the actual forces estimated to be applied to the structure (or a particular element of the structure), are compared to the nominal resistance, or strength (R_n) through a factor of safety (FS):

$$Q \leq Q_{all} = \frac{R_n}{FS} = \frac{Q_{ult}}{FS} \tag{1}$$

where

Q = design load,
Q_{all} = allowable design load,
R_n = nominal resistance of the element or the structure, and
Q_{ult} = ultimate geotechnical foundation resistance.

The *Standard Specifications for Highway Bridges* (AASHTO, 1997), based on common practice, presents the traditional factors of safety used in conjunction with different levels of control in analysis and construction. Although engineering experience over a lengthy period of time resulted in adequate factors of safety, their source, reliability, and performance had remained mostly unknown. The factors of safety do not necessarily consider the bias, in particular, the conservatism (i.e., underprediction) of the analysis methods; hence, the validity of their assumed effect on the economics of design is questionable.

1.2.2 Limit State Design

Demand for more economical design and attempts to improve structural safety have resulted in the re-examination of the entire design process over the past 50 years. The design

of a structure needs to ensure that while being economically viable it will suit the intended purpose during its working life. Limit state (LS) is a condition beyond which the structure (i.e., a bridge in the relevant case), or a component, fails to fulfill in some way the intended purpose for which it was designed. Limit state design (LSD) comes to meet the requirements for safety, serviceability, and economy. LSD most often refers, therefore, to two types of limit states: the ULS, which deals with the strength (maximum loading capacity) of the structure, and the serviceability limit state (SLS), which deals with the functionality and service requirements of a structure to ensure adequate performance under expected conditions (these can be, for example, under normal expected loads or extreme events like impact, an earthquake, etc.).

The ULS design of a structure and its components (e.g., a column or shallow foundation) depends upon the predicted loads and the capacity of the component to resist them (i.e., resistance). Both loads and resistance have various sources and levels of uncertainty. Engineering design has historically compensated for these uncertainties by using experience and subjective judgment. The new approach that has evolved aims to quantify these uncertainties and achieve more rational engineering designs with consistent levels of reliability. These uncertainties can be quantified using probability-based methods resulting for example with the LRFD format, which allows the separation of uncertainties in loading from uncertainties in resistance, and the use of procedures from probability theory to assure a prescribed margin of safety.

The same principles used in LRFD for ULS can be applied to the SLS, substituting the capacity resistance of the component with a serviceability limit, such as a quantified displacement, crack, deflection or vibration. Since failure under the SLS will not lead to collapse, the prescribed margin of safety can be smaller, i.e., the SLS can tolerate a higher probability of "failure" (i.e., exceedance of the criterion) compared with that for the ULS.

1.2.3 Geotechnical and AASHTO Perspective

The LSD and LRFD methods are becoming the standard methods for modern-day geotechnical design codes. In Europe (CEN, 2004; DIN EN 1997-1, 2008 including the National Annex, 1 draft 2009), Canada (Becker, 2003), China (Zhang, 2003), Japan (Honjo et al., 2000; Okahara et al., 2003), the United States (Kulhawy and Phoon, 2002; Withiam, 2003; Paikowsky et al., 2004), and elsewhere, major geotechnical design codes are switching from ASD (or WSD) to LSD and LRFD.

A variation of LRFD was first adopted by AASHTO for the design of certain types of bridge superstructures in 1977 under a design procedure known as Load Factor Design (LFD). *AASHTO LRFD Bridge Design Specifications* was published in 1994 based on NCHRP Project 12-33. From 1994 to 2006,

the AASHTO LRFD specifications applied to geotechnical engineering utilized the work performed by Barker et al. (1991). This code was mostly based on an adaptation of WSD to LRFD and only marginally addressed the SLS. Continuous attempts have been made since then to improve the scientific basis on which the specifications were developed, including NCHRP Project 20-7 (Task 88), NCHRP Projects 12-35 and 12-55 for earth pressures and retaining walls, NCHRP Project 12-24 for soil-nailing, and NCHRP Project 24-17 that calibrated for the first time the LRFD parameters for deep foundations based on extensive databases of deep foundation testing (Paikowsky et al., 2004). NCHRP Project 12-66 addresses the needs of SLS in design of bridge foundations. The project's approach has required developing serviceability criteria for bridges based on foundation performance, defining methods for the evaluation of foundation displacements and establishing their uncertainty, and calibrating the resistance factors assigned for the use of these methods based on the established SLS and target reliability. The backbone of the study has been the development of databases to establish the uncertainty of the methods used to evaluate the horizontal and vertical displacements of foundations.

Of the various AASHTO studies related to LRFD calibration and implementation, one important component remained deficient and that was the ULS of shallow foundations. The topic is problematic because the ULS of coupled loading is not easily identified, and the current specifications (AASHTO, 2008), although providing the theoretical estimation of the bearing resistance of soil (Section 10.6.3.1), contain specific language to exclude inclination factors (C10.6.3.1.2a), noting that the specified resistance factors are limited, varying for all conditions between $\phi = 0.45$ to $\phi = 0.50$.

The combination of the foundation loads in the ULS framework is quite complex and needs to be addressed systematically either via the existing nominal resistance calculation providing safety limits and appropriate resistance factors and/or a new methodology directly applicable to the evaluation of the ULS under the desired load combinations. This issue is further explored in Section 1.6.

1.3 Load and Resistance Factor Design

1.3.1 Principles

The intent of LRFD is to separate uncertainties in loading from uncertainties in resistance and then to use procedures from probability theory to ensure a prescribed margin of safety. Sections 1.3 and 1.4 outline the principles of the methodology and present the common techniques used for its implementation.

Figure 1 shows probability density functions (PDFs) for load effect (Q) and resistance (R). "Load effect" is the load cal-
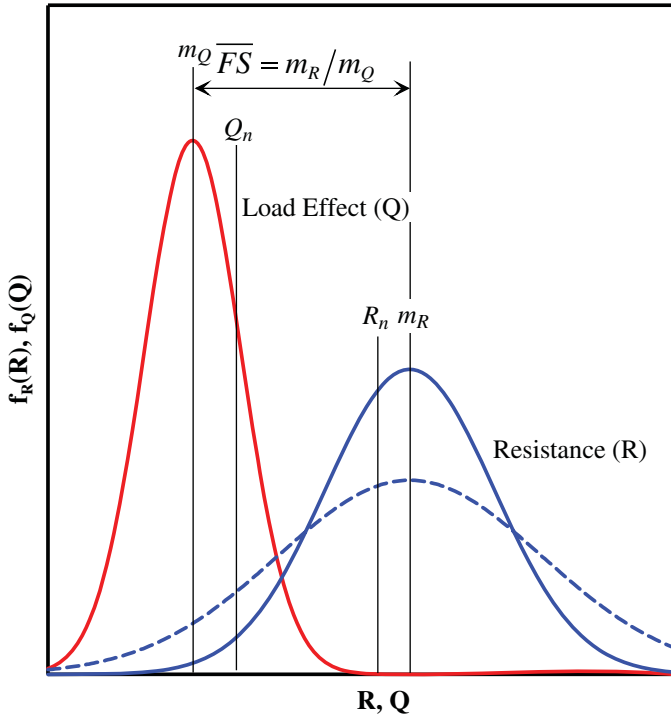
Figure 1. An illustration of PDFs for load effect and resistance.

culated to act on a particular element (e.g., a specific shallow foundation), and the resistance is its bearing load capacity. In geotechnical engineering problems, loads are usually better known than are resistances, so the Q typically has smaller variability than the R; that is, it has a smaller coefficient of variation (COV), hence a narrower PDF.

In LRFD, partial safety factors are applied separately to the load effect and to the resistance. Load effects are increased by multiplying characteristic (or nominal) values by load factors (γ); resistance (strength) is reduced by multiplying nominal values by resistance factors (ϕ). Using this approach, the factored (i.e., reduced) resistance of a component must be larger than a linear combination of the factored (i.e., increased) load effects. The nominal values (e.g., the nominal resistance, R_n, and the nominal load, Q_n) are those calculated by the specific calibrated design method and the loading conditions, respectively, and are not necessarily the means (i.e., the mean loads, m_Q, or mean resistance, m_R of Figure 1). For example, R_n is the predicted value for a specific analyzed foundation, obtained by using Vesić's bearing capacity calculation, while m_R is the mean possible predictions for that foundation considering the various uncertainties associated with that calculation.

This principle for the strength limit state is expressed in the *AASHTO LRFD Bridge Design Specifications* (AASHTO, 1994, 1997, 2001, 2006, 2007, 2008) in the following way:

$$R_r = \phi R_n \geq \sum \eta_i \gamma_i Q_i \tag{2}$$

where the nominal (ultimate) resistance (R_n) multiplied by a resistance factor (ϕ) becomes the factored resistance (R_r), which must be greater than or equal to the summation of loads (Q_i) multiplied by corresponding load factors (γ_i) and a modifier (η_i).

$$\eta_i = \eta_D \eta_R \eta_l \geq 0.95 \tag{3}$$

where η_i are factors to account for effects of ductility (η_D), redundancy (η_R), and operational importance (η_l).

Based on considerations ranging from case histories to existing design practice, a prescribed value is chosen for probability of failure. Then, for a given component design (when applying resistance and load factors), the actual probability for a failure (the probability that the factored loads exceed the factored resistances) should be equal to or smaller than the prescribed value. In foundation practice, the factors applied to load effects are typically transferred from structural codes, and then resistance factors are specifically calculated to provide the prescribed probability of failure.

The importance of uncertainty consideration regarding the resistance and the design process is illustrated in Figure 1. In this figure, the central factor of safety is $\overline{FS} = m_R/m_Q$, whereas the nominal factor of safety is $FS_n = R_n/Q_n$. The mean factor of safety is the mean of the ratio R/Q and is not equal to the ratio of the means. Consider what happens if the uncertainty in resistance is increased, and thus the PDF broadened, as suggested by the dashed curve. The mean resistance for this curve (which may represent the result of another predictive method) remains unchanged, but the variation (i.e., uncertainty) is increased. Both distributions have the same mean factor of safety one uses in WSD, but utilizing the distribution with the higher variation will require the application of a smaller resistance factor in order to achieve the same prescribed probability of failure to both methods.

The limit state function g corresponds to the margin of safety, i.e., the subtraction of the load from the resistance such that (referring to Figure 2a):

$$g = R - Q \tag{4}$$

For areas in which $g < 0$, the designed element or structure is unsafe because the load exceeds the resistance. The probability of failure, therefore, is expressed as the probability (P) for that condition:

$$p_f = P(g < 0) \tag{5}$$

In calculating the prescribed probability of failure (p_f), a derived probability density function is calculated for the margin of safety $g(R,Q)$ (refer to Figure 2a), and reliability is expressed using the "reliability index," β. Referring to Figure 2b,
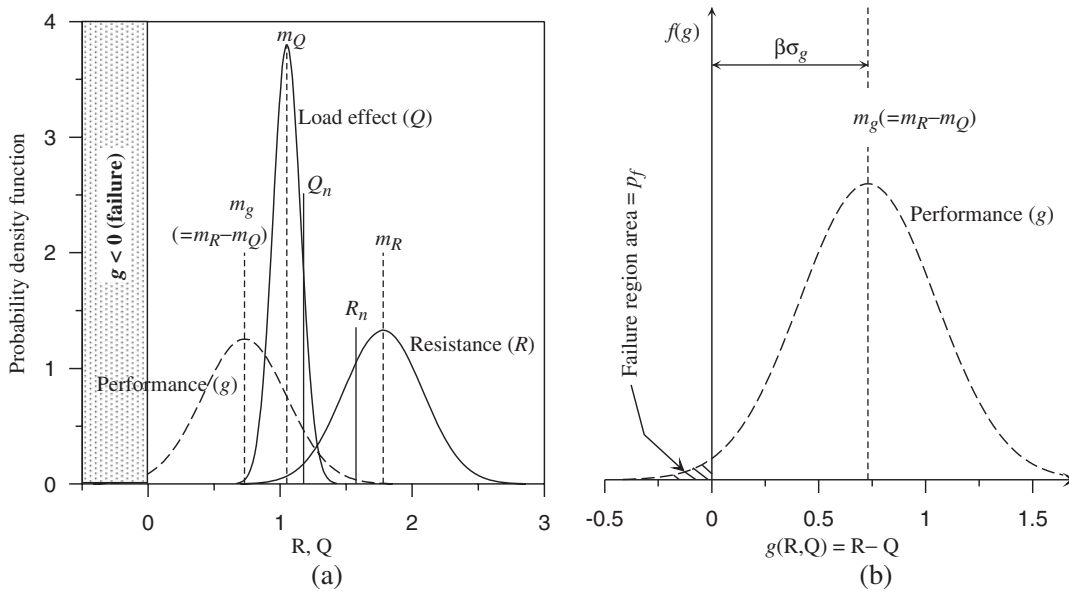
Figure 2. An illustration of probability density function for (a) load, resistance, and performance function and (b) the performance function (g(R,Q)) demonstrating the margin of safety (p_f) and its relation to the reliability index, β (σ_g = standard deviation of g).

the reliability index is the number of standard deviations of the derived PDF of g, separating the mean safety margin from the nominal failure value of g being zero:

$$\beta = m_g / \sigma_g = (m_R - m_Q) / \sqrt{\sigma_Q^2 + \sigma_R^2} \qquad (6)$$

where m_g and σ_g are the mean and standard deviation of the safety margin defined in the limit state function Equation 4, respectively.

The relationship between the reliability index (β) and the probability of failure (p_f) for the case in which both R and Q follow normal distributions can be obtained based on Equation 6 as the following:

$$p_f = \Phi(-\beta) \qquad (7)$$

where Φ is the error function defined as $\Phi(z) = \int_{-\infty}^{z} \frac{1}{\sqrt{2\pi}} \exp\left[-\frac{u^2}{2}\right] du$. The relationship between β and p_f is provided in Table 1. The relationships in Table 1 remain valid as long as the assumption is that the reliability index (β) follows a normal distribution.

As the performance of the physical behavior of engineering systems usually cannot obtain negative values (load and resistance), it is better described by a lognormal distribution. The margin of safety is taken as $\log R - \log Q$, when the resistances and load effects follow lognormal distributions. Thus, the limit state function becomes the following:

$$g = \ln(R) - \ln(Q) = \ln(R/Q) \qquad (8)$$

If R and Q follow lognormal distributions, log R and log Q follow normal distributions, thus the safety margin, g, follows a normal distribution. As such, the relationship obtained in Equation 7 is still valid to calculate the failure probability. Figure 2b illustrates the limit state function, g, for normal distributed resistance and load, the defined reliability index, β (also termed target reliability, β_T), and the probability of fail-

Table 1. Relationship between reliability index and probability of failure.

Reliability index β	Probability of failure p_f
1.0	0.159
1.2	0.115
1.4	0.0808
1.6	0.0548
1.8	0.0359
2.0	0.0228
2.2	0.0139
2.4	0.00820
2.6	0.00466
2.8	0.00256
3.0	0.00135
3.2	6.87 E^{-4}
3.4	3.37 E^{-4}
3.6	1.59 E^{-4}
3.8	7.23 E^{-5}
4.0	3.16 E^{-5}

ure, p_f. For lognormal distributions, these relations will relate to the function $g = \ln(R/Q)$ as explained above.

The values provided in Table 1 are based on series expansion and can be obtained by a spreadsheet (e.g., NORMSDIST in Excel) or standard mathematical tables related to the standard normal probability distribution function. It should be noted, however, that previous AASHTO LRFD calibrations and publications for geotechnical engineering, notably Barker et al. (1991) and Withiam et al. (1998), have used an approximation relationship proposed by Rosenblueth and Esteva (1972), which greatly errs for $\beta < 2.5$, the typical zone of interest in ULS design calibration ($\beta = 2$ to 3) and errs even more in the zone of interest for SLS calibrations ($\beta < 2.0$).

For lognormal distributions of load and resistance one can show (e.g., Phoon et al., 1995) that Equation 6 becomes the following:

$$\beta = \frac{m_{RN} - m_{QN}}{\sqrt{\sigma_{QN}^2 + \sigma_{RN}^2}}$$

$$= \frac{\ln\left[(m_R / m_Q) \sqrt{(1 + COV_Q^2)/(1 + COV_R^2)} \right]}{\sqrt{\ln\left[(1 + COV_R^2)(1 + COV_Q^2) \right]}} \qquad (9)$$

where

m_{QN}, m_{RN} = the mean of the natural logarithm of the load and the resistance,

σ_{QN}, σ_{RN} = the standard deviations of the natural logarithm of the load and the resistance, and

$m_Q, m_R,$ COV_Q, COV_R = the simple means and the coefficients of variation for the load and the resistance of the normal distributions. These values can be transformed from the lognormal distribution using the following expressions for the load and similar ones for the resistance:

$$\sigma_{QN}^2 = \ln(1 + COV_Q^2) \qquad (10)$$

and

$$m_{QN} = \ln(m_Q) - 0.5\sigma_{QN}^2 \qquad (11)$$

1.3.2 The Calibration Process

The problem facing the LRFD analysis in the calibration process is to determine the load factor (γ) and the resistance factor (ϕ) such that the distributions of R and Q will answer to the requirements of a specified β. In other words, the γ and ϕ described in Figure 3 need to answer to the prescribed target reliability (i.e., a predetermined probability of failure) described in Equation 9. Several solutions are available and are described below, including the recommended procedure for the research reported herein (see Section 1.3.5).
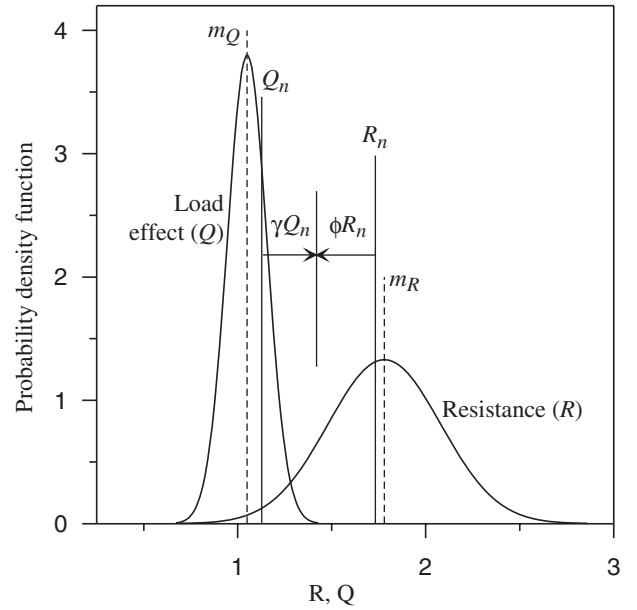
Figure 3. An illustration of the LRFD factors determination and application (typically $\gamma \geq 1$, $\phi \leq 1$) relevant to the zone in which load is greater than resistance ($Q > R$).

1.3.3 First Order Second Moment

The First Order Second Moment (FOSM) method of calibration was proposed originally by Cornell (1969) and is based on the following. For a limit state function $g(m)$:

mean $\qquad m_g \approx g(m_1, m_2, m_3, \ldots, m_n) \qquad (12)$

variance $\qquad \sigma_g^2 \approx \sum_{i=1}^{n} \left(\frac{\partial_g}{\partial_{\chi_i}} \right)^2 \cdot \sigma_i^2 \qquad (13)$

or $\qquad \approx \sum_{i=1}^{n} \left(\frac{g_i^+ - g_i^-}{\Delta_{\chi_i}} \right)^2 \cdot \sigma_i^2$

where

m_1 and σ_i = the means and standard deviations of the basic variables (design parameters);

$\chi_i, i = 1, 2, \ldots, n$;

$g_i^+ = m_i + \Delta m_i$, and $g_i^- = m_i - \Delta m_i$ for small increments Δm_i; and

Δx_i is a small change in the basic variable value, x_i.

Practically, the FOSM method was used by Barker et al. (1991) to develop closed-form solutions for the calibration of the geotechnical resistance factors (ϕ) that appeared in the previous AASHTO LRFD specifications.

$$\phi = \frac{\lambda_R \left(\sum \gamma_i Q_i \right) \sqrt{\dfrac{1+COV_Q^2}{1+COV_R^2}}}{m_Q \exp\left\{ \beta_T \sqrt{\ln\left[\left(1+COV_R^2\right)\left(1+COV_Q^2\right) \right]} \right\}} \tag{14}$$

where

λ_R = resistance bias factor, mean ratio of measured resistance over predicted resistance;

COV_Q = coefficient of variation of the load;

COV_R = coefficient of variation of the resistance; and

β_T = target reliability index.

When just dead and live loads are considered, Equation 14 can be rewritten as

$$\phi = \frac{\lambda_R \left(\gamma_D \dfrac{Q_D}{Q_L} + \gamma_L \right) \sqrt{\dfrac{1+COV_{QD}^2+COV_{QL}^2}{1+COV_R^2}}}{\left(\lambda_{QD} \dfrac{Q_D}{Q_L} + \lambda_{QL} \right) \exp\left\{ \beta_T \sqrt{\dfrac{\ln\left[\left(1+COV_R^2\right)\right.}{\left(1+COV_{QD}^2+COV_{QD}^2\right)\right]}} \right\}} \tag{15}$$

where

γ_D, γ_L = dead and live load factors,

Q_D/Q_L = dead to live load ratio,

$\lambda_{QD}, \lambda_{QL}$ = dead and live load bias factors,

COV_{QD} = coefficient of variation for dead load, and

COV_{QL} = coefficient of variation for live load.

The probabilistic characteristics of the foundation loads are assumed to be those used by AASHTO for the superstructure (Nowak, 1999); thus γ_D, γ_L, λ_{QD} and λ_{QL} are fixed, and a resistance factor can be calculated for a resistance distribution (λ_R, COV_R) for a range of dead load to live load ratios.

1.3.4 First Order Reliability Method

LRFD for structural design has evolved beyond FOSM to the more invariant First Order Reliability Method (FORM) approach (e.g., Ellingwood et al., 1980; Galambos and Ravindra, 1978), while geotechnical applications have lagged behind (Meyerhof, 1994). In order to be consistent with the previous structural code calibration and the load factors to which it leads, the calibration of resistance factors for deep foundations in NCHRP Project 24-17 used the same methodology (Paikowsky et al., 2004). The LRFD partial safety factors were calibrated using FORM as developed by Hasofer and Lind (1974). FORM can be used to assess the reliability of a component with respect to specified limit states and provides a means for calculating partial safety factors ϕ and γ_i for resistance and loads, respectively, against a target reliability level, β. FORM requires only first and second moment information on resistances and loads (i.e., means and variances) and an assumption of distribution shape (e.g., normal, lognormal,

etc.). The calibration process is presented in Figure 4 and detailed by Paikowsky et al. (2004).

Each limit state (ultimate or serviceability) can be represented by a performance function of the form:

$$g(X) = g(X_1, X_2, \ldots, X_n) \tag{16}$$

in which $X = (X_1, X_2, \ldots, X_n)$ is a vector of basic random variables of strengths and loads. The performance function $g(X)$, often called the limit state function, relates random variables to either the strength or serviceability limit state. The limit is defined as $g(X) = 0$, implying failure when $g(X) \leq 0$ (but strictly $g(X) < 0$) (see Figures 2 and 4). Referring to Figure 4, the reliability index, β, is the distance from the origin (in standard normal space transformed from the space of the basic random variables) to the failure surface at the most probable point on that surface, that is, at the point on $g(X) = 0$ at which the joint probability density function of X is greatest. This is sometimes called the *design point,* and is found by an iterative solution procedure (Thoft-Christensen and Baker, 1982). This relationship can also be used to back calculate representative values of the reliability index, β, from current design practice. The computational steps for determining β using FORM are provided by Paikowsky et al. (2004).

In developing code provisions, it is necessary to follow current design practice to ensure consistent levels of reliability over different evaluation methods (e.g., pile resistance or displacement). Calibrations of existing design codes are needed to make the new design formats as simple as possible and to put them in a form that is familiar to designers. For a given reliability index, β, and probability distributions for resistance and load effects, the partial safety factors determined by the FORM approach may differ with failure mode. For this reason, calibration of the calculated partial safety factors (PSFs) is important in order to maintain the same values for all loads at different failure modes. In the case of geotechnical codes, the calibration of resistance factors is performed for a set of load factors already specific in the structural code. Thus, the load factors are fixed. A simplified algorithm was used in NCHRP Project 24-17 to determine resistance factors:

1. For a given value of the reliability index, β, probability distributions and moments of the load variables, and the coefficient of variation for the resistance, compute mean resistance, m_R, using FORM.
2. With the mean value for R computed in Step 1, the PSF, ϕ, is revised as

$$\phi = \frac{\sum\limits_{i=1}^{n} \gamma_i m_{Li}}{m_R} \tag{17}$$

where m_{Li} and m_R are the mean values of the load and strength variables, respectively, and γ_i, $i = 1, 2, \ldots, n$, are the given set of load factors.

A comparison between resistance factors obtained using FORM and resistance factors using FOSM for 160 calibrations of axial pile capacity prediction methods is presented in Figure 5. The data in Figure 5 suggest that FORM results in resistance factors that are consistently higher than those obtained by FOSM. As a rule of thumb, FORM provided resistance factors for deep foundations approximately 10% higher than those obtained by FOSM. The practical conclusions that can be obtained from the observed data are that first evaluation of data can be done by the simplified closed-form FOSM approach and the obtained resistance factors are on the low side (safe) for the resistance distributions obtained in the NCHRP 24-17 project (Paikowsky et al., 2004).

1.3.5 Monte Carlo Simulation

Monte Carlo Simulation (MCS) has become AASHTO's preferred calibration tool and is recommended for all AASHTO-related calibrations. MCS is a powerful tool for determining the failure probability numerically, without the use of closed-form solutions such as those given by Equations 14 and 15. The objective of MCS is the numerical integration of the expression for failure probability, as given by the following equation:

$$p_f = P(g \leq 0) = \frac{1}{N} \sum_{i=1}^{N} I[g_i \leq 0] \tag{18}$$

where I is an indicator function which is equal to 1 for $g_i \leq 0$, i.e., when the resulting limit state is in the failure region, and equal to 0 for $g_i > 0$, when the resulting limit state is in the safe region. N is the number of simulations carried out. As $N \rightarrow \infty$, the mean of the estimated failure probability using Equation 18 can be shown to be equal to the actual failure probability (Rubinstein, 1981).

Code calibration in its ideal format is accomplished in an iterative process by assuming agreeable load (γ) and resistance (ϕ) factors and determining the resultant reliability index, β. When the desired target reliability index, β_T, is achieved, an acceptable set of load and resistance factors has been determined. One unique set of load and resistance factors does not exist; different sets of factors can achieve the same target reliability index (Kulicki et al., 2007).

The MCS process is simple and can be carried out as follows:

- Identify basic design variables and their distributions. Load is assumed to be normally distributed.
- Generate N number of random samples for each design variable based on its distributions, i.e., using the reported statistics of load and resistance and computer-generated random numbers.
- Evaluate the limit state function N times by taking a set of the design variables generated above and count the number for which the indicator function is equal to 1.

Notes: ST = Structural
MCS = Monte Carlo Simulation
μ = mean
$g(x)$ = performance function of the limit state
= limit state function
$g(x) = 0$ = limit defining failure for $g(x) < 0$
$g_L(x)$ = linearized performance function

Figure 4.   Resistance factor analysis flow chart using FORM (Ayyub and Assakkaf, 1999; Ayyub et al., 2000; Hasofer and Lind, 1974).
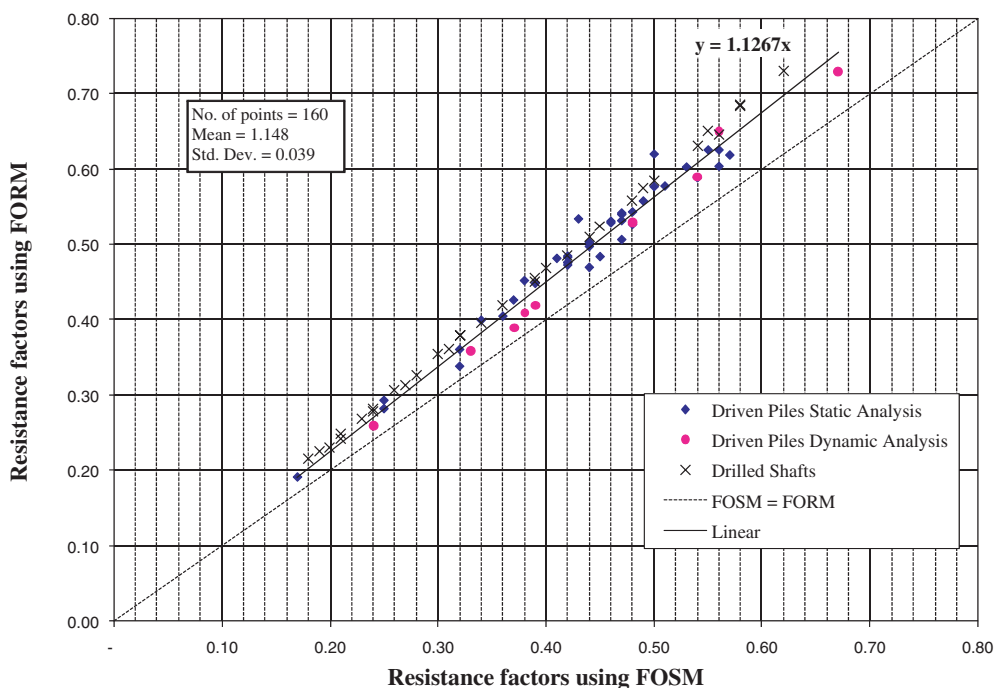
Figure 5. Comparison of resistance factors obtained using FOSM versus those obtained using FORM for a target reliability of β = 2.33 (Paikowsky et al., 2004).

- If the sum of the indicator function is N_f, i.e., the limit state function was $g_i \leq 0$ (in the failure region) for N_f number of times out of the total of N simulations carried out, then the failure probability, p_f, can be directly obtained as the ratio N_f/N.

Using the MCS process, the resistance factor can be calculated based on the fact that to attain a target failure probability of p_{fT}, N_{fT} (Number of samples to obtain target failure at the limit states) of the limit state must fall in the failure region. Since in the present geotechnical engineering LRFD only one resistance factor is used while keeping the load factors constant, a suitable choice for the resistance factor would shift the limit state function so that N_{fT} samples fall in the failure region. The resistance factor derived in this study using MCS is based on this concept.

Kulicki et al. (2007) made several observations regarding the process outlined above:

1. The solution is only as good as the modeling of the distribution of load and resistance. For example, if the load is not correctly modeled or the actual resistance varies from the modeled distribution, the solution is not accurate. In other words, if the statistical parameters are not well defined, the solution is equally inaccurate.
2. If both the distribution of load and resistance are assumed to be normally or lognormally distributed, a MCS using

these assumptions should theoretically produce the same results as the closed-form solutions.
3. The power of the MCS is its ability to use varying distributions for load and resistance.

In summary, refinement in the calibration should be pursued, not refinement of the process used to calculate the reliability index. The MCS, as discussed above, is quite adequate and understandable to the practicing engineer. Refinement should be sought in the determination of the statistical parameters of the various components of force effect and resistance and using the load distributions available for the structural analysis; this means focusing on the statistical parameters of the resistance.

1.4 Format for Design Factor Development

1.4.1 General

AASHTO development and implementation of LSD and LRFD have been driven primarily by the objectives of achieving a uniform design philosophy for bridge structural and geotechnical engineering thereby obtaining a more consistent and rational framework of risk management in geotechnical engineering.

Section 1.3 detailed the principles of LRFD and described the calibration process. The philosophies of attaining this

calibration, however, vary widely: values are chosen based on a range of already available parameters, based on expert opinion, based on comprehensive resistance calibration, or using the material factor approach. A previous effort to calibrate the ULS of deep foundations concentrated on comprehensive calibration of the resistance models as an integral entity (Paikowsky et al., 2004). This philosophy was based on the fact that in contrast to other engineering disciplines (e.g., structural analysis), the model uncertainty in geotechnical engineering is dominant. The specifications provide an ideal framework for prescribed comprehensive methodology and, hence, direct calibration of the entire methodology, when possible, results in highly accurate LRFD as demonstrated in the following sub-sections. This approach was followed by and large in the development of the SLS (NCHRP Project 12-66) and is followed (when possible) in this study as well. The calibration of shallow foundations for ULS has, however, more complex aspects that cannot be (at present time) calibrated directly. Hence, Section 1.4.2 (based primarily on Honjo and Amatya, 2005) is provided as a background to the diverse approach of the current research.

1.4.2 Material and Resistance Factor Approach

Some of the key issues in developing sound geotechnical design codes based on LSD and LRFD are definition of characteristic values and determination of partial factors together with the formats of design verification (Simpson and Driscoll, 1998; Orr, 2002; Honjo and Kusakabe, 2002; Kulhawy and Phoon, 2002). The characteristic values of the design parameters are conveniently defined as their mean values.

The approach concerning design factor development formats can be summarized as whether one should take a material factor approach (MFA) or a resistance factor approach (RFA). In MFA, partial factors are directly applied to the characteristic values of materials in the design calculation, whereas in RFA, a resistance factor is applied to the resulting resistance calculated using the characteristic values of materials. One of the modifications of RFA is a multiple resistance factor approach (MRFA) where several resistance factors are employed to be applied to relatively large masses of calculated resistances. The advantage of MRFA is claimed to be that it ensures a more consistent safety margin in design compared with RFA (Phoon et al. 1995, 2000; Kulhawy and Phoon, 2002). In general, MFA originated in Europe whereas RFA originated in North America. However, both approaches are now used interchangeably worldwide; for example, the "German approach" to EC7 coincides with RFA while Eurocode 7 allows several design approaches (both MFA and RFA), and the member state can define their preference in their National Annex to the EC7.

1.4.3 Code Calibrations

A procedure to rationally determine partial factors in the design verification formulas based on reliability analysis is termed "code calibration." Section 1.3.2 and the details in Sections 1.3.3, 1.3.4, and 1.3.5 presented the analytical meaning of the calibration in the LRFD methodology. One of the best known and most important studies in this area is by Ellingwood et al. (1982) in which load and resistance factors were determined based on a reliability analysis using FORM. Since then, a reasonable number of code calibration studies have been carried out in structural engineering (e.g., Nowak, 1999). However, rational code calibration studies for geotechnical engineering codes have only begun to be undertaken in the past decade or so (Barker et al. 1991; Phoon et al., 1995; Honjo et al., 2002; Paikowsky et al., 2004).

Barker et al. (1991) proposed resistance factors for the AASHTO bridge foundation code published in 1994 (AASHTO, 1994). The calibration was based on FOSM but used back-calculation from factors of safety and introduced a significant number of engineering judgments in determining the factors along a not-so-clearly described process. Based on the difficulties encountered in using the work of Barker et al. (1991), the partial factors for deep foundations in the AASHTO specification were revised by Paikowsky et al. (2004). In Paikowsky et al. (2004), a large database was developed and used in a directly calibrated model (an RFA approach together with a reliability analysis by FORM) to determine the resistance factors. The SLS calibration (NCHRP Project 12-66) was developed in a similar approach, using MCS to determine the factors. Examples from both studies are provided in Sections 1.4.4 and 1.4.5. Phoon et al. (1995, 2000) carried out calibration of the factors for transmission line structure foundations based on MRFA by reliability analysis. Some simplified design formats were employed, and factors were adjusted until the target reliability index was reached. Kobayashi et al. (2003) have calibrated resistance factors for building foundations for the Architectural Institute of Japan (AIJ) limit state design building code (AIJ, 2002). This code provides a set of load and resistance factors for all aspects of building design in a unified format. FORM was used for the reliability analysis, and MRFA was the adopted format of design verification as far as the foundation design was concerned.

1.4.4 Example of Code Calibrations—ULS

The capacity of the comprehensive direct model calibration resistance factor approach is demonstrated. Large databases of pile static load tests were compiled, and the static and dynamic pile capacities of various design methods were compared with the nominal strength obtained from the static load test. The geotechnical parameter variability was minimized
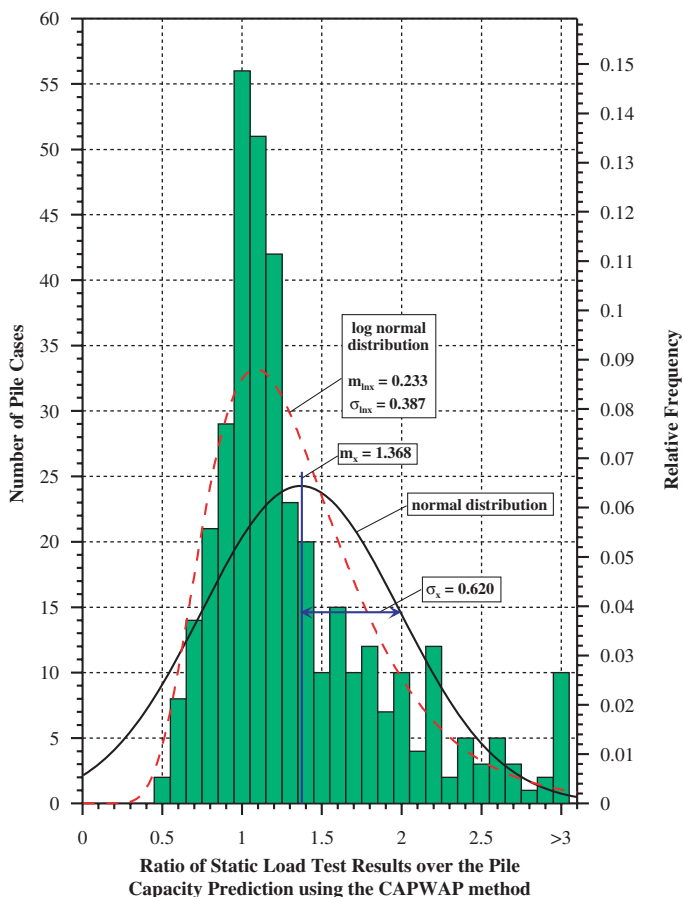
Figure 6. Histogram and frequency distributions for all (377 cases) measured over dynamically (CAPWAP) calculated pile-capacities in PD/LT2000 (Paikowsky et al., 2004).

Figure 7. Histogram and frequency distribution of measured over statically calculated pile capacities for 146 cases of all pile types (concrete, pipe, H) in mixed soil (Paikowsky et al., 2004).

(indirectly) by adhering to a given consistent procedure in soil parameters selection (e.g., NSPT [Number of Blows in a Standard Penetration Test] correction and friction angle correlations), as well as load test interpretation (e.g., establishing the uncertainty in Davisson's criterion for capacity determination and then using it consistently). Two examples for such large calibrations are presented in Figures 6 and 7 for given specific dynamic and static pile capacity prediction methods, respectively (Paikowsky et al., 2004).

Further subcategorization of the analyses led to detailed resistance factor recommendations based on pile type, soil type, and analysis method combinations. Adherence to the uncertainty of each combination as developed from the database and consistent calibrations led to a range of resistance factors (see, for example, Table 25 of *NCHRP Report 507,* Paikowsky et al., 2004). Recent versions of the specifications (AASHTO, 2006, 2008) avoided the detailed calibrations and presented one "simplified" resistance factor ($\phi = 0.45$) for static analysis of piles, along with one design method (Nordlund/ Thurman).

The first large LRFD bridge design project in New England (including superstructure and substructure) based on AASHTO 2006 specifications is currently under construction. A large static load test program preceded the design. Identifiable details are not provided, but Tables 2 and 3 present the capacity evaluation for two dynamically and statically tested piles (Class A prediction, submitted by the project consultant, Dr. Samuel Paikowsky, about one month before testing) using the calibrated resistance factors for the specific pile/soil/analysis method combination versus the "simplified" AASHTO version of the resistance factor. In both cases, the calculated factored capacity using the "simplified" resistance factor *exceeded the unfactored and factored measured resistance (by the load test) in a dangerous way,* while the use of the calibrated resistance factors led to consistent and prudent design. The anticipated substructure additional cost has increased by 100% (in comparison to its original estimate based on the AASHTO specifications), exceeded $100 million (at the time of the load test program), and delayed the project 1 year. The power of the comprehensive, direct RFA calibration based on databases versus arbitrary

Table 2. H Pile—summary (14 × 177, penetration = 112 ft).

Static:

Static Pile Capacity Combinations:

Analysis combination	Estimated capacity (R_n) (kips)	NCHRP 507 resistance factor for H piles in sand (ϕ)	Factored resistance (R_r)	NCHRP 507 resistance factor for H piles in mixed soils (ϕ)	Factored resistance (R_r)	AASHTO LRFD specifications 2006 resistance factor (ϕ)	Factored resistance (R_r)
β-Method/Thurman (Steel Only)	894	0.30	268	0.20	179	Not specified	
β-Method/Thurman (Box Area)	1,076		323		215		
Nordlund/Thurman (Steel Only)	841	0.45	379	0.35	252	0.45	379
Nordlund/Thurman (Box Area)	1,023		460		307		460
FHWA Driven Ver. 1.2 (Steel Only)	845						
FHWA Driven Ver. 1.2 (Box Area)	1,032						

Notes:

1. Resistance Factors taken from the resistance factors for redundant structures listed in Table 25 of *NCHRP Report 507* (Paikowsky et al., 2004).

▢ Recommended range for preliminary design.

Reference: *Static Pile Capacity and Resistance Factors for Pile Load Test Program*, GTR report submitted to Haley and Aldrich, Inc. (H&A), June 21, 2006 (Paikowsky, Thibodeau, and Griffin).

Note: Above DRIVEN values were obtained by inserting the friction values and unit weights directly into DRIVEN, limiting the friction angle to 36°.

Dynamic:

Sakonnet River Bridge Test Pile Program Portsmouth, RI—Summary of Dynamic Measurement Predictions and Factored Resistance (H Piles)

Pile type	Time of driving	Energy approach			CAPWAP		
		EA[1] (kips)	ϕ[2]	R_r (kips)	CAP[1] (kips)	ϕ[2]	R_r (kips)
H	EOD	481	0.55	265	310	0.65	202
	BOR	606	0.40	242	434	0.65	282[3]

[1] Values represent EOD predictions and average of all BOR predictions.
[2] All ϕ factors taken from *NCHRP Report 507* (Paikowsky et al., 2004)
[3] Only ϕ factors for BOR CAPWAP appear in AASHTO (2006) specifications and are marked by shaded cells

Reference: *Pile Capacity Based on Dynamic Testing and Resistance Factors for Pile Load Test Program,* GTR report submitted to H&A, July 17, 2006 (based on earlier submittals of data and analyses) (Paikowsky, Chernauskas, and Hart).

Static Load Test

Load Test Capacity (Davisson's Criterion):

$$Q_u = 378 \text{ kips at } 0.68 \text{ in}$$

Resistance Factors *NCHRP Report 507* and AASHTO Specifications:

$$\phi = 0.55 \quad (1 \text{ test pile large site variability})$$
$$\phi = 0.70 \quad (1 \text{ pile medium site variability})$$

Factored Resistance: R_r = 208 to 265 kips

Reference: Load Test Results presented and analyzed by H&A.

---

assignments of resistance factors is clearly demonstrated in the first significant case of its use in New England.

1.4.5 Example of Code Calibrations—SLS

The factors associated with the SLS were evaluated under NCHRP Project 12-66. Following the development of serviceability criteria for bridges (Paikowsky, 2005; Paikowsky and Lu, 2006), large databases of foundation performance were accumulated and analyzed for direct RFA calibrations (Paikowsky et al., 2009a, 2009b). Examples of databases examining the performance of displacement analyses of shallow foundations are presented in Figures 8 and 9 for the AASHTO (2008) and Schmertmann et al. (1978) settlement analysis methods, respectively. These robust analysis results allow direct calibration of resistance factors for applied loads

Table 3. 42-in Pipe Pile—summary (diam. = 42 in, wall thickness (w.t.) = 1 in, 2-in tip, penetration = 64 ft).

Static:

Static Pile Capacity Combinations: Assumed Displaced Soil Volume Based on Uniform Wall Thickness (1.0 in)

Analysis combination	Estimated capacity (R_n) (kips)	NCHRP 507 resistance factor for pipe piles in sand (ϕ)	Factored resistance (R_r)	NCHRP 507 resistance factor for pipe piles in mixed soils (ϕ)	Factored resistance (R_r)	AASHTO LRFD specifications 2006 resistance factor (ϕ)	Factored resistance (R_r)
β-Method/Thurman (Steel Only)	924		324		231		-
β-Method/Thurman (30% Tip Area)	984		345		246		-
β-Method/Thurman (50% Tip Area)	1,084	0.35	380	0.25	271	Not specified	-
β-Method/Thurman (70% Tip Area)	1,184		415		296		-
β-Method/Thurman (100% Tip Area, plugged)	1,335		467		334		-
Nordlund/Thurman (Steel Only)	690		379		241		310
Nordlund/Thurman (30% Tip Area)	750		412		262		337
Nordlund/Thurman (50% Tip Area)	850	0.55	467	0.35	297	0.45	382
Nordlund/Thurman (70% Tip Area)	950		522		332		427
Nordlund/Thurman (100% Tip Area, plugged)	1,101		605		385		495

Notes:
1. Resistance Factors taken from the resistance factors for redundant structures listed in Table 25 of *NCHRP Report 507* (Paikowsky et al., 2004).
2. Tip resistance for steel only included 2-in. wall thickness accounting for the driving shoe.

☐ Recommended range for preliminary design soil plug only.

Reference: *Static Pile Capacity and Resistance Factors for Pile Load Test Program*, GTR report submitted to Haley and Aldrich, Inc. (H&A), June 21, 2006 (Paikowsky, Thibodeau, and Griffin).

- -

Static Load Test (Open Pipe Pile)

Load Test Capacity (Davisson's Criterion):

$$Q_u = 320 \text{ kips at } 0.52 \text{ in}$$

Resistance Factors *NCHRP Report 507* and AASHTO Specifications:

$$\phi = 0.55 \text{ (1 pile large site variability)}$$
$$\phi = 0.70 \text{ (1 pile medium site variability)}$$

Factored Resistance: R_r = 176 to 224 kips

Reference: Load Test Results presented and analyzed by H&A.

---

for a given SLS criterion (displacement). The data in Figures 8 and 9 are related to the following: 1 ft (0.30 m) $\leq B \leq$ 28 ft (8.53 m), B_{avg} = 8 ft (2.44 m), $1.0 \leq L/B \leq 6.79$, L/B_{avg} = 1.55, 25.2 ksf (1,205 kPa) $\leq q_{max} \leq$ 177.9 ksf (8,520 kPa) for which B and L are the footing width and length, respectively, and q_{max} is the maximum stress applied to the foundations under the measured displacement.

1.4.6 Perspective of Shallow Foundations ULS Calibration

The preceding sections have outlined the available formats of factor development and a powerful implementation via robust databases. The established RFA was utilized in two extensive studies: one related to the ULS of deep foundations (NCHRP Project 24-17) and one related to the SLS of all foundations (NCHRP Project 12-66).

The complexity of the ULS of shallow foundations (to be discussed in the next section) requires a multifaceted approach in which combinations of calibrations are utilized for obtaining the desired factors. The method of approach is presented in Chapter 2 of this report. Mutiple approaches are needed for the ULS of shallow foundations because of the following:

1. The capacity of shallow foundations on granular soils under centric vertical load is calculated via a relatively simple model (the bearing capacity model without cohesion-related factors, modified by shape and depth factors only). This type of foundation and loading is commonly tested and, hence can be calibrated using a large database (the database is presented in Section 3.2).
2. Determination of the capacity of shallow foundations under combined loading conditions requires a multiparameter model. The differentiation between favorable and unfavor-
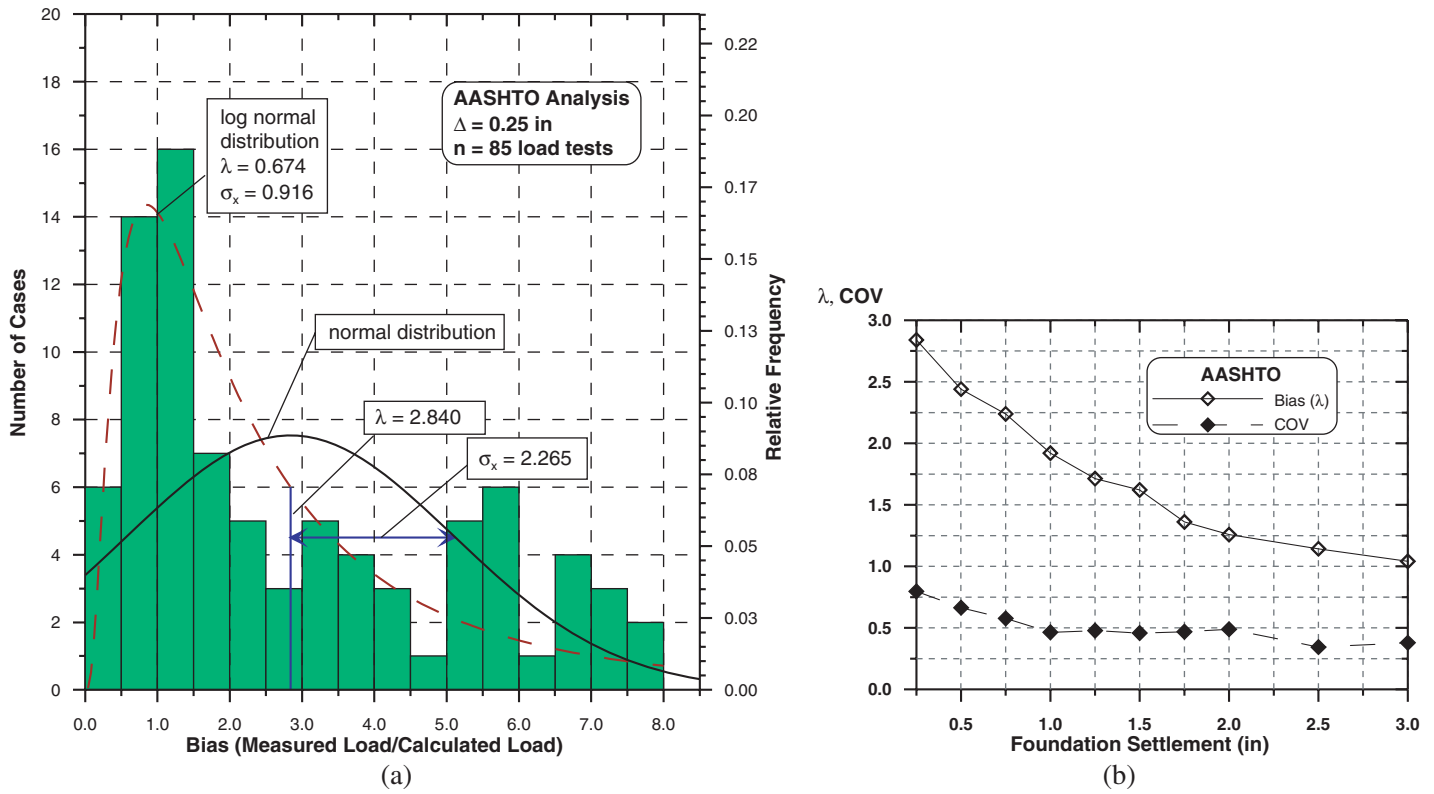
Figure 8. (a) Histogram and frequency distributions of measured over calculated loads for a settlement (Δ = 0.25 in) using AASHTO's analysis method for 85 shallow foundation cases, and (b) variation of the bias (λ) and uncertainty in the ratio between measured to calculated loads for shallow foundations on granular soils under displacements ranging from 0.25 to 3.00 in.

able loading conditions is quite complex due to coupled loads and resistances. ULS under combined loading requires both an attempt to calibrate the existing methodology and an examination of a different approach for design, as described in Section 1.5.

3. The capacity of shallow foundations on rock under all types of loading is highly dependent on the relative scale of the foundation width to the rock discontinuity spacing and on the nature of the rock and its discontinuities. No established bearing capacity theory exists for these cases. The calibration of such cases, both for ULS and SLS (not included in NCHRP Project 12-66), requires therefore establishing models, using sophisticated analysis methods for evaluating both strength and serviceability, and performing a probability evaluation of incomplete data and calibration.

1.5 Bearing Capacity of Shallow Foundations

1.5.1 Basic Formulation

Buismann (1940) and Terzaghi (1943) adopted the solution for metal punching proposed by Prandtl (1920, 1921) to the foundation bearing capacity problem. They defined a three-term bearing capacity equation by the superposition of the effects of soil cohesion, soil surcharge, and weight of soil, respectively. For a general case of centric vertical loading of a rigid strip footing (plain strain problem) on a cohesive-frictional soil surface with a uniform surcharge of q, the ultimate bearing capacity (q_u) is given as the following:

$$q_u = cN_c + qN_q + (1/2)\gamma BN_\gamma \tag{19}$$

where

- c = soil cohesion;
- γ = unit weight of the soil beneath the foundation;
- B = footing width;
- q = overburden pressure at the level of the footing base; and
- N_c, N_q, and N_γ are bearing capacity factors for cohesion, overburden, and self-weight of soil, respectively.

For weightless soil ($\gamma = 0$), Prandtl (1920) and Reissner (1924) developed the following formulas for N_c and N_q:

$$N_c = (N_q - 1)\cot\phi_f \tag{20}$$
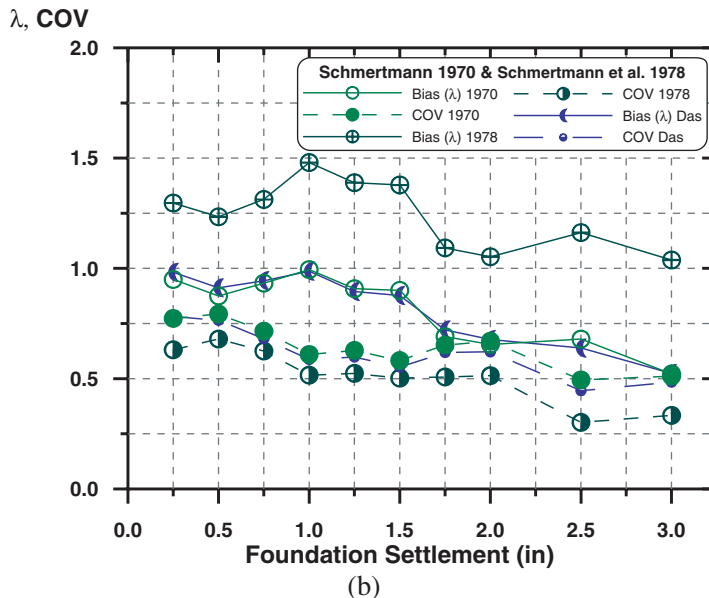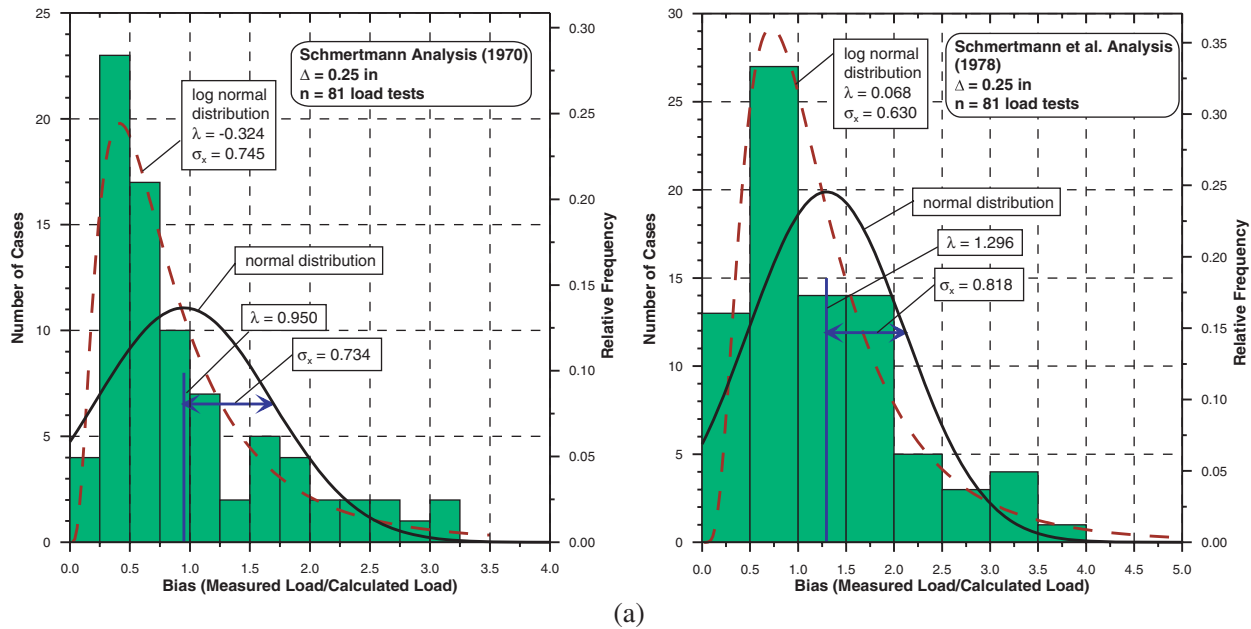
Figure 9. (a) Histogram and frequency distributions of measured over calculated loads for a settlement (Δ = 0.25 in) using Schmertmann (1970) and Schmertmann et al. (1978) analysis methods for 81 shallow foundation case, and (b) variation of the bias (λ) and uncertainty in the ratio between measured to calculated loads for shallow foundations on granular soils under displacements ranging from 0.25 to 3.00 in.

$$N_q = \exp\left(\pi \tan\phi_f\right) \tan^2\left(45° + \frac{\phi_f}{2}\right) \qquad (21)$$

where ϕ_f = friction angle.

The bearing capacity factor N_c is sometimes credited to Caquot and Kérisel (1953). These formulas are exact closed-form solutions based on Prandtl's assumption of rupture surfaces (see Figure 10) in which the downward movement of the active wedge (I) is resisted by the shear resistance along the slip surfaces CDE (along the transi-
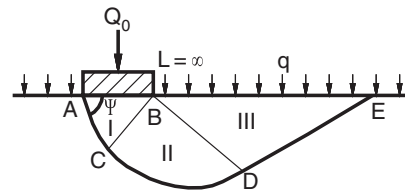
Figure 10. Assumed rupture surfaces by Prandtl (1920, 1921).

tion zone [II] and passive wedge [III]) and the overburden pressure, q.

1.5.2 The Factor N_γ

1.5.2.1 N_γ Formulations

A closed-form analytical solution for the bearing capacity problem including the effects of the unit weight of the soil beneath the footing via the factor N_γ is not possible. Different solutions for N_γ were developed based on empirical relations, analytical derivations, or numerical analyses. Some of these solutions are listed below and are presented in Figure 11 for comparison.

1.5.2.2 Formulas Based on Empirical Relations

Formulas based on empirical relations are the following:

Meyerhof (1963):

$$N_\gamma = (N_q - 1)\tan(1.4\phi_f) \tag{22}$$
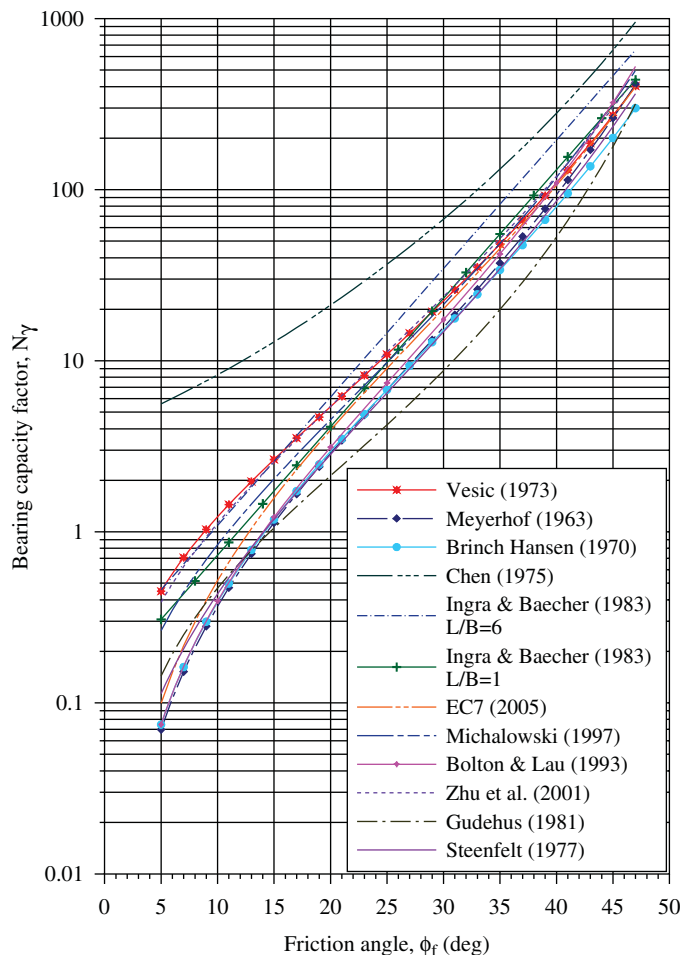
Figure 11. Bearing capacity factor N_γ versus friction angle (ϕ_f) according to different proposals.

Muhs and Weiss (1969) and Muhs (1971) adapted by Eurocode 7 (2005) and DIN 4017 (2006):

$$N_\gamma = 2(N_q - 1)\tan\phi_f \tag{23}$$

Brinch Hansen (1970):

$$N_\gamma = 1.5(N_q - 1)\tan\phi_f \tag{24}$$

Steenfelt (1977):

$$N_\gamma = \left(0.08705 + 0.3231\sin(2\phi_f) - 0.04836\sin^2(2\phi_f)\right)$$
$$\left[N_q \exp\left(\frac{\pi}{2}\tan\phi_f\right) - 1\right] \tag{25}$$

Gudehus (1981):

$$N_\gamma = \exp\left(5.19(\tan\phi_f)^{1.5}\right) - 1 \tag{26}$$

Ingra and Baecher (1983) for footings with $L/B = 6$:

$$N_\gamma = \exp(-1.646 + 0.173\phi_f) \tag{27}$$

Ingra and Baecher (1983) for square footings:

$$N_\gamma = \exp(-2.046 + 0.173\phi_f) \tag{28}$$

1.5.2.3 Formulas Based on Analytical Derivations

Formulas based on analytical derivations are the following:

Vesić (1973):

$$N_\gamma = 2(N_q + 1)\tan\phi_f \tag{29}$$

Chen (1975):

$$N_\gamma = 2(N_q + 1)\tan(45 + \phi_f/2) \tag{30}$$

Michalowski (1997) for a rough footing base:

$$N_\gamma = \exp(0.66 + 5.11\tan\phi_f)\tan\phi_f \tag{31}$$

Zhu et al. (2001):

$$N_\gamma = (2N_q + 1)\tan(1.07\phi_f) \tag{32}$$

1.5.2.4 Formulas Based on Numerical Analyses

There is one formula based on numerical analyses:

Bolton and Lau (1993):

$$N_\gamma = (N_q - 1)\tan(1.5\phi_f) \tag{33}$$

1.5.3 General Bearing Capacity Formulation

The basic equation by Terzaghi has been modified to account for the effects of the shape of the footing, load inclination, load eccentricity, and shear strength of the embedment depth on the ultimate bearing capacity. Some of these modifications were incorporated originally by Meyerhof (1953) and then further enhanced by Meyerhoff (1963), Brinch Hansen (1961, 1970), and Vesić (1973, 1975) to give what is known as the General Bearing Capacity Equation:

$$q_u = cN_c s_c d_c i_c + qN_q s_q d_q i_q + (1/2)\gamma B' N_\gamma s_\gamma d_\gamma i_\gamma \qquad (34)$$

where
s_i = shape factors,
i_i = load inclination factors,
d_i = depth factors, and
B' = is the effective (i.e., functional) width of the footing considering the effect of load eccentricity (see Equation 35).

Various approaches for the calculation of these factors including evaluation and critical review are presented in the following sections.

1.5.4 Eccentricity

The effect of eccentric loading on the bearing capacity is usually accounted for via Meyerhof's (1953) effective area consideration. Bearing capacity is calculated for the footings' effective dimensions by the following:

$$L' = L - 2 \cdot e_L$$

$$B' = B - 2 \cdot e_B \qquad \text{with } e_B = M_L/V \text{ and } e_L = M_B/V \qquad (35)$$

where
M, M_B and M_L = the moments loading in L and B directions, respectively;
V = the total vertical load; and
e_L and e_B = load eccentricities along footing length (L) and footing width (B), respectively.

In contrast, other approaches describe the decrease in the bearing capacity with the increase in the eccentricity of the load using reduction factors. These factors indicate the ratio of the average ultimate bearing capacity under eccentric loading, q_u, to that under the centric vertical loading, $q_{u,centric}$. The formulas are mostly based on small-scale model tests on cohesionless soils without embedment, i.e., embedment depth of the foundation (D_f) = 0 and c = 0. Some approaches are specified below, and their evaluations are presented in Figure 12. The approaches are the following:
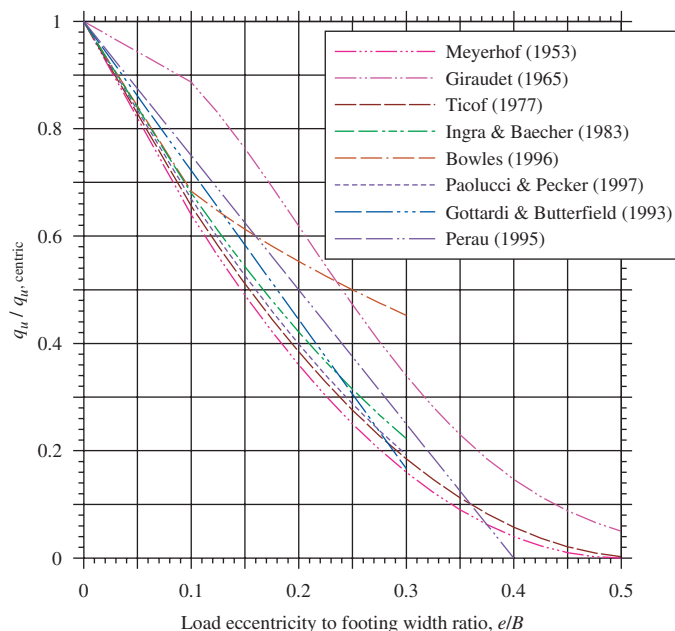
Figure 12. Reduction factors for shallow foundations under vertical-eccentric load.

Meyerhof (1953):

$$\frac{q_u}{q_{u,\,centric}} = \left(1 - 2\frac{e}{B}\right)^2 \qquad (36)$$

Giraudet (1965):

$$\frac{q_u}{q_{u,\,centric}} = \exp\left(-12\left(\frac{e}{B}\right)^2\right) \qquad (37)$$

Ticof (1977):

$$\frac{q_u}{q_{u,\,centric}} = \left(1 - 1.9\frac{e}{B}\right)^2 \qquad (38)$$

Bowles (1996):

$$\frac{q_u}{q_{u,\,centric}} = 1 - \sqrt{\frac{e}{B}} \qquad \text{for } 0 < \frac{e}{B} < 0.3 \qquad (39)$$

Paolucci and Pecker (1997):

$$\frac{q_u}{q_{u,\,centric}} = \left(1 - \frac{e}{0.5B}\right)^{1.8} \qquad \text{for } \frac{e}{B} < 0.3 \qquad (40)$$

Ingra and Baecher (1983):

$$\frac{q_u}{q_{u,\,centric}} = 1 - 3.5\left(\frac{e}{B}\right) + 3.03\left(\frac{e}{B}\right)^2 \qquad (41)$$

Gottardi and Butterfield (1993):

$$\frac{q_u}{q_{u, centric}} = 1 - \frac{e}{0.36B} \tag{42}$$

Perau (1995, 1997):

$$\frac{q_u}{q_{u, centric}} = 1 - 2.5\frac{e}{B} \tag{43}$$

Figure 12 presents the ratio of eccentric to centric load capacity versus the ratio of load eccentricity to the smaller footing width (B) of a strip footing. From the figure, it can be seen that the influence of load eccentricity in the approaches of Meyerhof (1953), Ticof (1977), and Ingra and Baecher (1983) is very similar. The curve according to Bowles (1996) shows a different progression, beyond an eccentricity of $e/B = 0.1$. Here, the decrease of the bearing capacity is less pronounced as compared to the three aforementioned approaches. In contrast, the approach by Giraudet (1965) shows a completely different progression and a much smaller reduction of bearing capacity for smaller load eccentricities. One cannot derive conclusions regarding the validity of the different approaches based on this figure alone. For example, it seems that Meyerhof's (1953) approach leads to a greater bearing capacity; however, this is not entirely so. The change in the shape factors because of the change in the footing size, as effective width and effective length, must be considered as well.

Figure 13 shows some of the reviewed approaches together with experimental results cited by Perau (1995). It can be seen that the three selected equations (Meyerhof, 1953; Ticof, 1977; and Ingra and Baecher, 1983) represent a lower boundary of the experimental results.

1.5.5 Shape Factors

The effect of a foundation shape other than a strip footing (plain strain condition) has to be considered with foundation shape factors. A footing is theoretically defined as a strip footing for the length to width ratios of $L/B > 10$. Practically, foundations possessing the ratio of $L/B > 5$ already behave as strip footings (Vesic, 1975). Due to the difficulties in obtaining mathematical solutions that consider the effect of a foundation shape, semi-empirical approaches have been formulated. Various relations proposed for shape factors, s_i, are listed in Table 4. For eccentrically loaded footings, the effective footing dimensions B' and L' have to be used to compute the shape factors (e.g., AASHTO, 2007; EC 7, 2005).

The presented shape factors in Table 4 are empirical except for the expressions by Zhu and Michalowski (2005) that have been derived from numerical simulations. For example, to determine the shape factor, s_γ footings with different length to
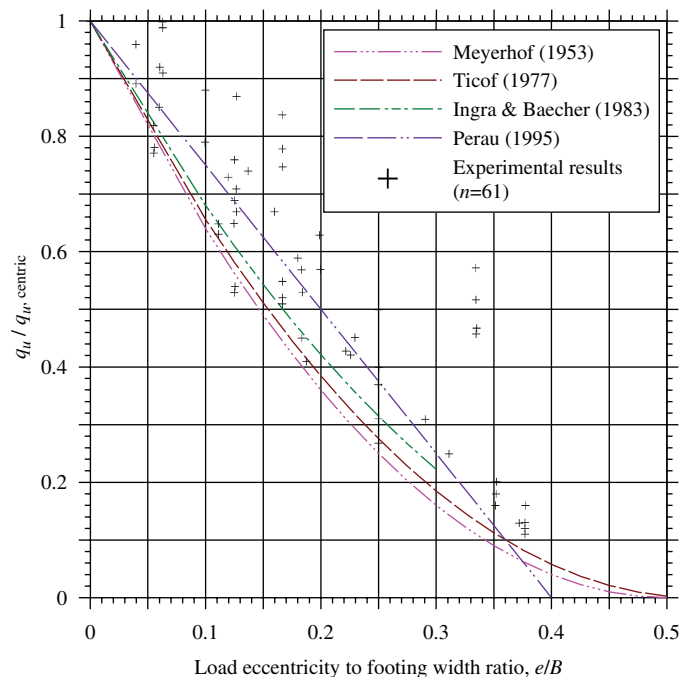
Figure 13. Reduction factors for shallow foundations under vertical-eccentric load compared with test results from different authors as presented by Perau (1995). The experimental results presented are from Ramelot and Vanderperre (1950) as cited by Döerken (1969) for B/L = 1; Meyerhof (1953) for B/L = 1, 1/6, and 6; Schultze (1952) for B/L = 2; Das (1981) for B/L = 1/3; Giraudet (1965) for B/L = 1/3.5; and Eastwood (1955) for B/L = 1/1.8, 1/2.25, and 1/3.

width (L/B) ratios under centric vertical loading and without embedment have been modeled and analyzed.

Figures 14 and 15 present the numerical values of the aforementioned shape factors s_γ and s_q, respectively, versus the foundation width to length ratios, B/L. Due to the fact that the bearing capacity of Equation 19 was developed for strip footings assuming plain strain conditions, the values of the shape factors approach unity for long footings (as $B/L \rightarrow 0$). Practically, the value of s_γ is within the range of 1 ± 0.05 for $L/B \geq 6.7$ ($B/L \leq 0.15$), and the value of s_q is within the same range for $L/B \geq 10.0$ ($B/L \leq 0.10$) for most cases.

For footings with dimension ratios close to unity (approaching equidimension), the deviations of the shape factors from the unity proposed by different authors show that very careful consideration is required in the choice of the shape factors. The values suggested by Meyerhof (1963) for s_γ (see Figure 14) are always greater than unity and increase with the decrease in the width to length ratio (B/L). In contrast, the values calculated with other equations decrease below unity as the ratio increases. The reason for this is that Meyerhof's (1963) values of N_γ for a strip footing ($B/L \rightarrow 0$) are smaller than those for a circle ($B/L = 1$), and the bearing capacities for the footing

Table 4. Shape factors proposed by different authors.

Reference	Footing base shape	s_c	s_q	s_γ
De Beer (1970) as modified by Vesic (1973)	Rectangle	$1+\dfrac{B'}{L'}\dfrac{N_q}{N_c}$	$1+\dfrac{B'}{L'}\cdot\tan\phi_f$	$1-0.4\dfrac{B'}{L'}$
	Circle and Square	$1+\dfrac{N_q}{N_c}$	$1+\tan\phi_f$	0.6
EC 7 (2005) and DIN 4017 (2006)	Rectangle	$\dfrac{\left(s_q\cdot N_q-1\right)}{N_q-1}$	$1+\dfrac{B'}{L'}\cdot\sin\phi_f$	$1-0.3\dfrac{B'}{L'}$
	Circle and Square	$\dfrac{\left(s_q\cdot N_q-1\right)}{N_q-1}$	$1+\sin\phi_f$	0.7
Meyerhof (1963)	Rectangle	$1+0.1\dfrac{B'}{L'}\cdot K_p$	$=1;\ \text{for }\phi_f=0$ $=1+0.1K_p(B'/L');$ $\text{for }\phi_f>10°$	$1+0.1\dfrac{B'}{L'}\cdot K_p;$ $K_p=\tan^2\left(45°+\dfrac{\phi_f}{2}\right)$
Perau (1995, 1997)	Rectangle	Not applicable	$1+1.6\tan\phi_f$ $\cdot\dfrac{B'/L'}{1+\left(\dfrac{B'}{L'}\right)^2}$	$\dfrac{1}{1+\dfrac{B'}{L'}}$
Zhu and Michalowski (2005)	Rectangle	Not applicable	Not applicable	$1+(0.6\sin^2\phi_f-0.25)B'/L'$ $\text{for }\phi_f\le30°;$ $1+(1.3\sin^2\phi_f-0.5)(L'/B')^{1.5}$ $\cdot\exp(-L'/B')$ $\text{for }\phi_f>30°$

with width to length ratios between $B/L\rightarrow0$ and $B/L=1$ are linearly interpolated values. Hence, a consistent set of equations for the bearing capacity factors and their modifications by the same author are recommended for use in the bearing capacity calculation. In summary, the foundation shape (varying between strip to equidimensional footing) and hence, the shape factor have an important influence on the ultimate bearing capacity.

1.5.6 Depth Factors

If the foundation is placed with a certain embedment depth, D_f, below the ground surface, the bearing capacity is affected in two ways: one, by the overburden pressure, $q=\gamma\cdot D_f$, and two, via the shear strength of the soil above the base level. Table 5 presents typically used expressions of the depth factors. Figure 16 presents the values of the depth factor d_q versus the friction angle for the different expressions provided in Table 5. In contrast to the factors proposed by Meyerhof (1963), the depth factor d_q according to Brinch Hansen (1970) decreases with the increase in the soil friction

angle. The depth factors proposed by Brinch Hansen are greater than those proposed by Meyerhof. The depth factors listed in AASHTO (2007) are also shown in Figure 16. These values lie between the expressions proposed by Meyerhof and Brinch Hansen.

1.5.7 Load Inclination Factors

An inclination in the applied load always results in a reduced bearing capacity, often of a considerable magnitude (Brinch Hansen, 1970). Meyerhof (1953) suggested that the vertical component of the bearing capacity under a load inclined at an angle α to the vertical is obtained using the following inclination factors:

$$i_c=i_q=\left(1-\alpha/90°\right)^2 \tag{44}$$

$$i_\gamma=\left(1-\alpha/\phi_f\right)^2 \tag{45}$$

These expressions were modified by Meyerhof and Koumoto (1987) and presented for cases of footings on a sand surface,
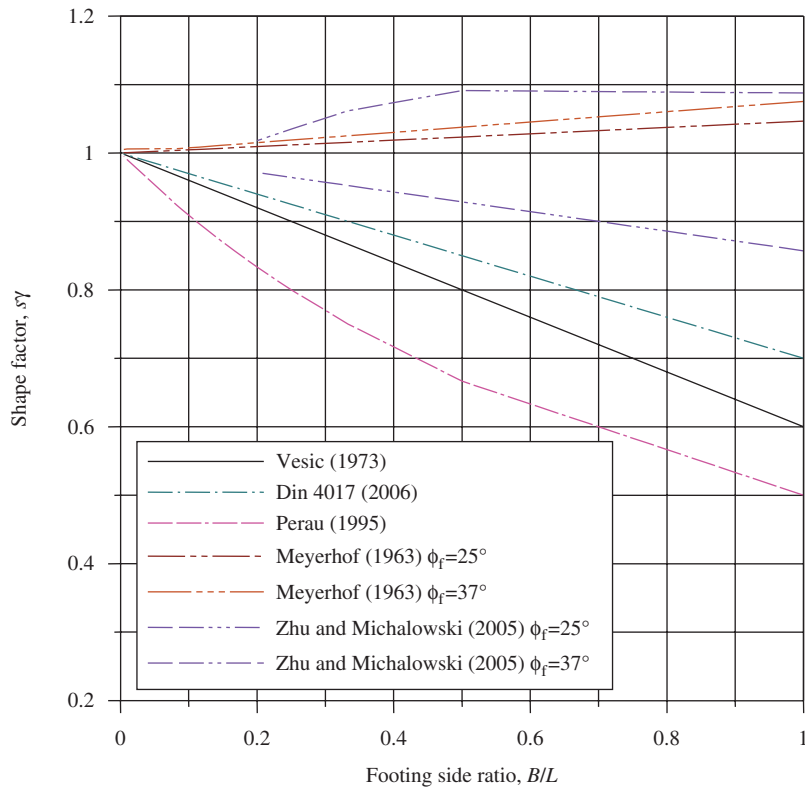
Figure 14. Shape factor s_γ proposed by different authors versus footing side ratio, B/L.
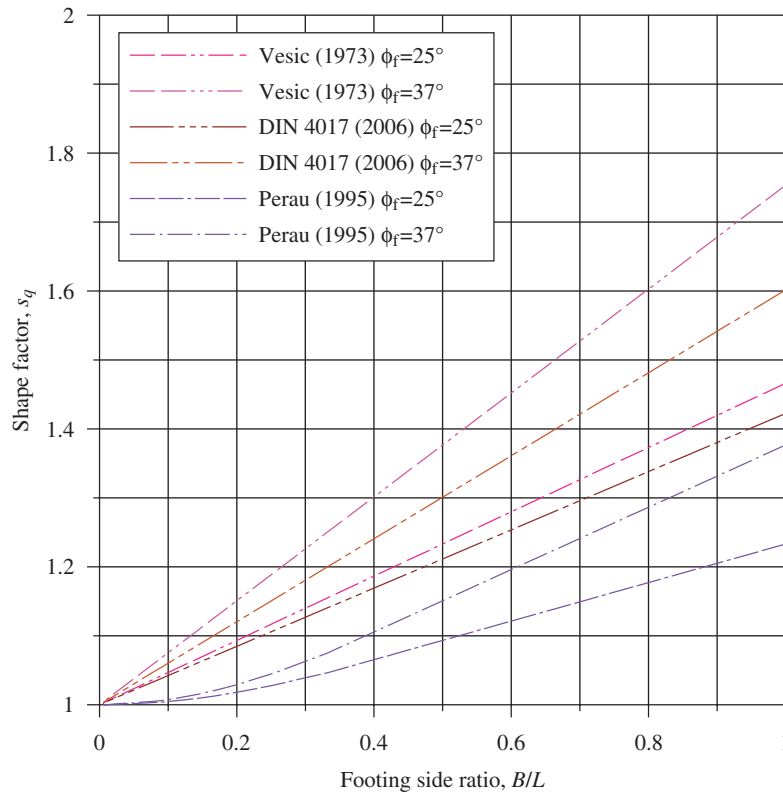
Figure 15. Shape factor s_q proposed by different authors versus footing side ratio, B/L.

Table 5. Depth factors proposed by different authors.

Author	d_c	d_q		d_γ
Meyerhof (1963)	$d_c = 1 + 0.2\sqrt{K_p} \cdot \dfrac{D_f}{B'}$	$d_q = 1 + 0.1\sqrt{K_p} \cdot \dfrac{D_f}{B'}$ for $\phi_f > 10$ $= 1$ for $\phi_f = 0$		$d_\gamma = d_q$
Brinch Hansen (1970) and Vesic (1973)	$d_c = d_q - \dfrac{1 - d_q}{N_C \cdot \tan\phi_f}$ $= d_q - \dfrac{1 - d_q}{N_q - 1}$	$D_f / B' \leq 1:$ $d_q = 1 + 2\tan\phi_f \cdot \left(1 - \sin\phi_f\right)^2 \cdot \left(D_f / B'\right)$		1
		$D_f / B' > 1:$ $d_q = 1 + 2\tan\phi_f \cdot \left(1 - \sin\phi_f\right)^2 arc\tan\left(D_f / B'\right)$		
where $K_p = \tan^2(45° + \phi_f / 2)$				

when the embedment ratio (D_f/B) is unity, and for footings on a clay surface, as shown in Equations 46 through 48. Assuming that a footing with a perfectly rough base on a sand surface starts to slide when the load inclination angle to the vertical is approximately equal to the soil's friction angle, the following expression was proposed:

$$i_\gamma = \cos\alpha\left(1 - \frac{\sin\alpha}{\sin\phi_f}\right) \quad \text{for } D_f/B' = 0, \quad c = 0 \quad (46)$$

For the case of footings with an embedment ratio equal to 1 in a soil with a friction angle greater than 30°, the inclination factor was expressed as the following:

$$i_\gamma = \cos\alpha\left(1 - \sin\alpha\right) \quad \text{for } \phi_f > 30°, D_f/B' = 1, \quad c = 0 \quad (47)$$

For footings on the surface of clay:

$$i_\gamma = \cos\alpha\left(1 - \sin\alpha\right) \quad \text{for } c_a = 0$$
$$= \cos\alpha\left(1 - 0.81\sin\alpha\right) \quad \text{for } c_a = c_n = \text{undrained shear strength of the clay} \quad (48)$$

where c_a = adhesion between the clay and the base of the footing.

Muhs and Weiss (1969) suggested, based on DEGEBO (Deutsche Forschungsgesellschaft für Bodenmechanik) tests with large-scale models of shallow footings on sands, that there is a distinct difference between load inclination effects when the inclination is in the direction of the longer side, L, and when the inclination is in the direction of the shorter side, B. Thus, the direction of load inclination as well as the
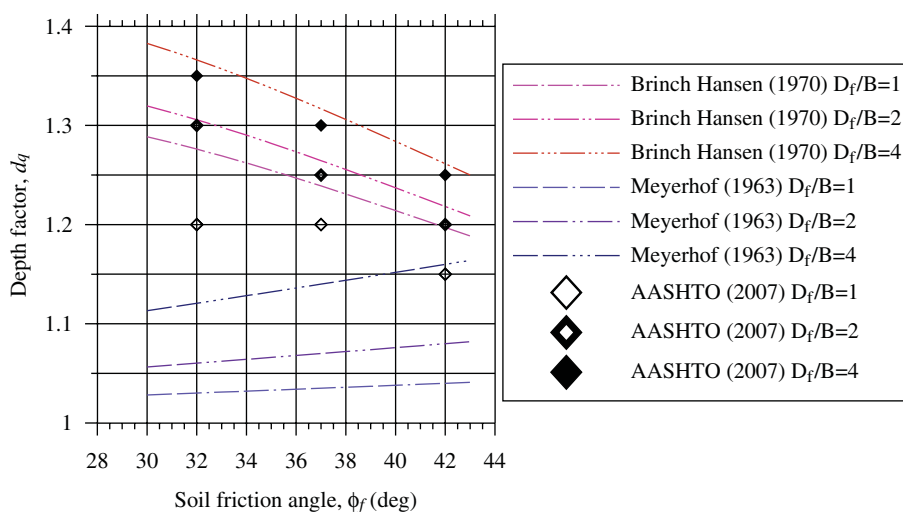
Figure 16. Depth factor d_q proposed by different sources versus soil friction angle, ϕ_f.

ratio B/L affect the inclination factor. Brinch Hansen (1970) incorporated the inclination effects as

$$i_q = \left(1 - \frac{0.5H}{\left(V + A'c\cot\phi_f\right)}\right)^5 \tag{49}$$

$$i_\gamma = \left(1 - \frac{0.7H}{\left(V + A'c\cot\phi_f\right)}\right)^5 \tag{50}$$

Vesic (1975) proposed the factors in the following forms:

$$i_q = \left(1 - \frac{H}{\left(V + A'c\cot\phi_f\right)}\right)^n \tag{51}$$

$$i_\gamma = \left(1 - \frac{H}{\left(V + A'c\cot\phi_f\right)}\right)^{n+1} \tag{52}$$

$$n = \left[\frac{\left(2 + L'/B'\right)}{\left(1 + L'/B'\right)}\right]\cos^2\theta + \left[\frac{\left(2 + B'/L'\right)}{\left(1 + B'/L'\right)}\right]\sin^2\theta \tag{53}$$

where

H and V = the horizontal and vertical components of the applied inclined load, P (see Figure 17);

θ = the projected direction of the load in the plane of the footing, measured from the side of length L in degrees;

A' = the effective area of the footing;

c = soil cohesion; and

L' and B' are as defined in Equation 35.

Figures 18 and 19 are graphical presentations of Equations 49 through 53 for load inclination factors i_q and i_γ, respectively.

Figure 18. Load inclination factor i_q versus load ratio, H/V, for $c = 0$, $\phi_f = 35°$, and any D_f/B.

The inclination factor i_c results from Caquot's theorem of corresponding stress states (De Beer and Ladanyi 1961 and Vesić 1973 as cited by Vesić 1975):

$$i_c = i_q - \frac{1 - i_q}{N_c\tan\phi_f} = i_q - \frac{1 - i_q}{N_q - 1} \qquad \text{for } \phi_f > 0 \tag{54a}$$

$$i_c = 1 - \frac{nH}{A'c\,N_c} \qquad \text{for } \phi_f = 0 \tag{54b}$$

where i_q is given by Equation 51.

Figure 17. Inclined load without eccentricity and the projected direction, θ.
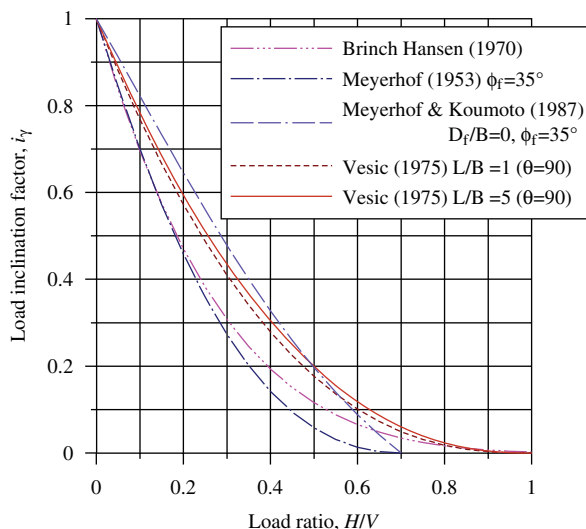
Figure 19. Load inclination factor i_γ versus load ratio, H/V, for $c = 0$, $\phi_f = 35°$, and $D_f/B = 0$.
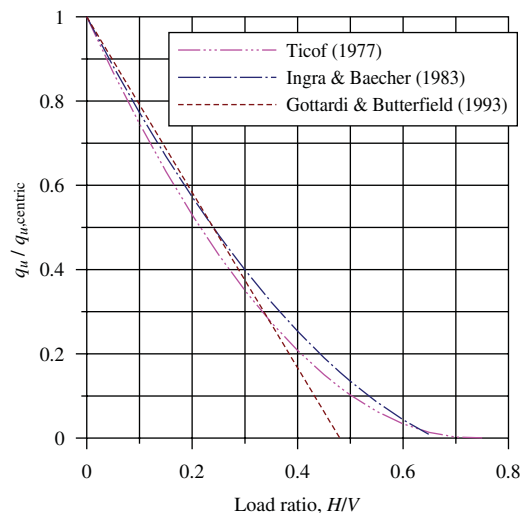
Figure 20. Reduction factors for shallow foundations under inclined loading (c = 0, D_f = 0).

Reduction factors for the case of a load inclination related to the case of centrically and vertically loaded footings can be found in Ticof (1977), Ingra and Baecher (1983), and Gottardi and Butterfield (1993) (see Figure 20). These expressions were determined based on model foundation test results on sand without embedment and as such are valid for the case of $D_f = 0$, $c = 0$:

Ticof (1977):

$$\frac{q_u}{q_{u,centric}} = \left(1 - 1.36\frac{H}{V}\right)^2 \tag{55}$$

Ingra and Baecher (1983):

$$\frac{q_u}{q_{u,centric}} = 1 - 2.41\left(\frac{H}{V}\right) + 1.36\left(\frac{H}{V}\right)^2 \tag{56}$$

Gottardi and Butterfield (1993):

$$\frac{q_u}{q_{u,centric}} = 1 - \frac{H}{0.48 \cdot V} \tag{57}$$

1.6 An Alternative Approach and Method of Analysis for Limit State Design of Shallow Foundations

1.6.1 Some Aspects of Stability and Safety of Shallow Foundations

1.6.1.1 Bearing Capacity and Sliding Limit States

Geotechnical resistances such as the bearing capacity of shallow foundations are entirely load dependent. The application of LRFD in cases of foundations under complex loading is, therefore, difficult as there is no strict separation between load and resistance. Furthermore, it is not always clear whether a load should be classified as favorable or unfavorable, which may have consequences for the calibration of safety factors. The difficulty in classification applies especially to the influence of the vertical load on the bearing capacity.

In order to illustrate this problem, Figure 21a shows the bearing capacity limit state and sliding limit state of a shallow foundation under inclined loading as a function of vertical and horizontal loads. In this so-called interaction diagram, the sliding limit state is illustrated as a simple straight line with an inclination tan δ_S representing the soil foundation interfacial shear resistance accounting for the roughness of the footing's base. The bearing capacity limit state is a closed curve in this illustration. The interaction diagram depicts the well-known physical phenomenon that the occurrence of horizontal loads reduces the bearing capacity of a shallow foundation, which is described by the inclination factors used in the traditional bearing capacity equation. A similar diagram can be generated for eccentric vertical loading or in the three-dimensional space for eccentric and inclined loading.

As the inclination factors depend on the characteristic load inclination H_k/V_k, the bearing capacity calculation implies a radial load path, which is the same for loading and resistance as indicated in Figure 21(a). However, only the vertical components of load and resistance are compared within the proof of stability. On the other hand, the sliding resistance calculation is based on the assumption of a step-like load path. For a given vertical load, the associated horizontal resistance is calculated, which itself is compared to the horizontal load component. The distances between design loads (H_d or V_d, respectively) and design resistances ($R_{h,d}$ or $R_{v,d}$, respectively) in Figure 21(a) represent the actual degree of mobilization.

In Figure 21(b), bearing capacity limit state and sliding limit state are referred to the maximum vertical resistance, V_{max} (i.e., under centric vertical loading only). Hence, the diagram shows the pure interaction of the load components without any other influences on the bearing capacity. In this illustration it is shown that a maximum horizontal load, H_{max}, can be applied for $V/V_{max} \approx 0.42$. Let us now consider a certain horizontal load, $H < H_{max}$. For this case, a minimum vertical load (min V) is required to carry the horizontal load. This means the load inclination is limited and the limit is provided either by the bearing capacity limit state or by the sliding limit state, whichever is more restrictive. With increasing vertical load, the resultant load inclination decreases and, hence, the bearing capacity of the system increases. However, because of the convex shape of the bearing capacity limit state, the degree of mobilization increases if $V/V_{max} > 0.42$, so the magnitude of the applicable vertical load is limited as well (max V).

Figure 21. Influence of load components on bearing resistance and sliding resistance utilizing interaction diagram.

Notes:

H	resultant horizontal load		V	resultant vertical load
H_{max}	max. horizontal load that can be carried by the system		min V	min. vertical load required for a certain applied horizontal load
H_d	design value of horizontal load		max V	max. vertical load possible for certain applied horizontal load
H_k/V_k	load inclination (characteristic values)		V_G	permanent vertical load
$R_{v,d}$	design value of bearing capacity		ΔV_G	additional permanent vertical load
$R_{v,k}$	characteristic value of bearing resistance (capacity)		V_k	characteristic vertical load
			V_d	design value of vertical load
$R_{h,d}$	design value of sliding resistance		V_{max}	bearing capacity under pure vertical loading, i.e., max. vertical load that can be carried by the system
$R_{h,k}$	characteristic sliding resistance			
γ_R	resistance factor		V/V_{max}	degree of utilization of maximum vertical load
δ_s	base friction angle			

1.6.1.2 Favorable and Unfavorable Load Actions

Now consider a given vertical load, e.g., the foundation dead load, V_G. In the ULS (i.e., the condition in which the bearing capacity is fully mobilized), this load is associated with one specific horizontal load. A larger horizontal load can only be applied if the vertical load is increased simultaneously, e.g., by increasing the dead weight applied to the footing. The vertical load acts favorably because an increase in the vertical load results in the possible increase of the horizontal load. These relationships are, however, valid only for $V/V_{max} < 0.42$. Larger vertical loads ($V_G + \Delta V_G$) act unfavorably because they reduce the maximum allowable horizontal load. In this situation, an arbitrary increase in the dead load applied to the footing would be counterproductive because it does not help to improve the performance of the system in resisting horizontal loads. These complex interrelations demonstrate that the role of the vertical load component is not unique. Hence, within the standard design procedure it is difficult to classify the vertical load as a favorable or unfavorable load. The use of the presented simple interaction diagrams may help, however, to better understand the complex interaction of the load components (Lesny, 2006).

1.6.1.3 Example

The favorable and unfavorable actions may affect the safety of the system as demonstrated by the following example of a vertical breakwater (Lesny and Kisse, 2004; Lesny, 2006). The breakwater is a structure supported by a strip footing of width B_C founded on sand and subjected to vertical, horizontal, and moment loading (see Figure 22). The basic parameters of the system are (Lesny et al., 2000; Oumeraci et al., 2001)

Caisson: $B_c = 17.5$ m, $h_c = 23$ m
Crushed stone layer: $\phi_f = 44.2°$, γ' (effective unit weight) = 10.4 kN/m³, $\tan\delta_s = 0.5$
Subsoil: $\phi_f = 38.2°$, $\gamma' = 10.2$ kN/m³
Water depth at still water level: $h_s = 15.5$ m

Notes:

h_s	water depth at still water level (SWL)	e_C	eccentricity of dead weight F_G of breakwater
h_r	height of rubble mound	$F_h(t)$	horizontal wave load
h^*	height of wave crest	$F_u(t)$	resultant of uplift water pressure due to wave loading
h_C	height of breakwater	$S(t)$	seepage force in rubble mound
B_C	width of breakwater		
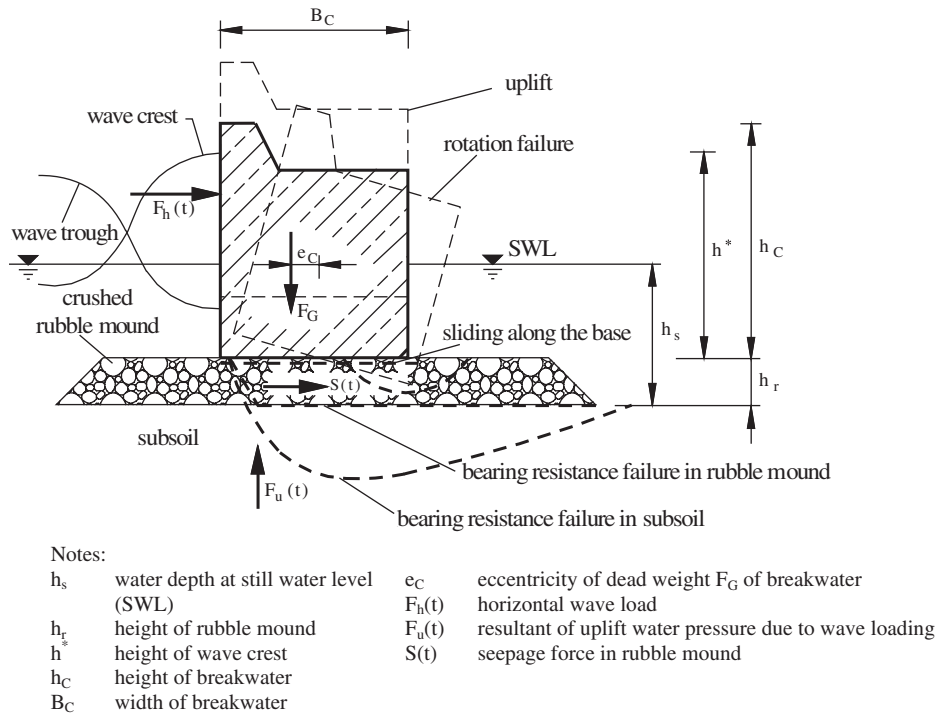
Figure 22. Breakwater, wave loading, and failure modes.

Figure 23 depicts the bearing capacity limit state and the sliding limit state of the breakwater for a fixed eccentricity of $e_k/B = 0.12$ in the V-H plane.

We assume a fictitious characteristic loading mainly due to dead weight and wave loading of

$H_{Q,k}$ (horizontal fictitious characteristic loading due to dead weight) = 2.55 MN

$V_{G,k}$ (vertical fictitious characteristic loading due to wave) = 15 MN

The factored design loads below were developed assuming vertical and horizontal load factors of $\gamma_G = 1.35$ and 1.00 for unfavorable and favorable permanent action, respectively, and $\gamma_Q = 1.50$ and 1.0 for unfavorable and favorable variable action, respectively. The factor γ_G is applied to the vertical loads only, and the factor γ_Q is applied to the horizontal loads. The horizontal and vertical factored design loads are the following:

$H_{Q,d} = 3.82$ MN
$V_{G,d} = 15$ MN (V favorable)
$V_{G,d} = 20.3$ MN (V unfavorable)

The safety of the system may be expressed here by the available resistance factor resulting from the characteristic resistance divided by the associated design load: $\gamma_R = R_k/L_d$. Hence, the safety for the sliding limit state is $\gamma_{R,h} = R_{h,k}/H_{Q,d} = 2.0$. For

the bearing capacity limit state, the safety is $\gamma_{R,v} = R_{v,k}/V_{G,d} = 2.7$ if V is favorable, but only $\gamma_{R,v} = 2.0$ if V is unfavorable. Under both conditions, the safety of the system seems to be sufficient.

These results do not represent, however, the actual safety of the foundation. In the interaction diagram of Figure 23, the actual safety is described by the closest distance of the loading to the resistance of the foundation as indicated by the arrows. Additional load components acting along this path are most hazardous. If arbitrary load paths are possible, only additional load components acting within the circles sketched in Figure 23 are admissible. Such a critical load situation is not artificial; it may occur if the wave height is higher than assumed for design, resulting in an increase of the horizontal load along with a decrease of the vertical load due to uplift forces.

The actual safety can be determined with the help of the factored design load vector $\vec{Q} = [V_{G,d}; H_{Q,d}]$ and the additional load vector $\Delta\vec{Q}$ in the V-H plane, which coincides with the radius of the circles in Figure 23 (Butterfield, 1993). For the design load components given above ($\vec{Q}$) the maximum additional loading is limited by the sliding limit state and amounts to $\Delta Q = 3.30$ MN (V favorable) or $\Delta Q = 5.68$ MN (V unfavorable), respectively. Thus, the actual safety of the system is the following:

$$\gamma_R = (Q + \Delta Q)/Q = \begin{cases} 1.21 & V \text{ favorable} \\ 1.28 & V \text{ unfavorable} \end{cases} \quad (58)$$

The actual safety in both cases is considerably smaller than the one calculated previously using the regular design proce-

H [kN]

safety: $\gamma_{R,h} = R_{h,k}/H_d = 2.0$

sliding resistance $R_{h,k}$

safety: $\gamma_{R,v} = R_{v,k}/V_d = 2.0$

V [kN]

safety: $\gamma_{R,v} = R_{v,k}/V_d = 2.7$

bearing resistance $R_{v,k}$

■ fictitious characteristic loading

◉ fictitious design loading (V favorable)

● fictitious design loading (V unfavorable)

Notes:

H	resultant horizontal load	V	resultant vertical load
H_d	design value of resultant horizontal load	V_d	design value of resultant vertical load
$R_{h,k}$	characteristic value of sliding resistance	$\gamma_{R,h}$	available resistance factor for sliding
$R_{v,k}$	characteristic value of bearing resistance	$\gamma_{R,v}$	available resistance factor for bearing resistance

Figure 23. Interaction diagram for stability analysis of a vertical breakwater.

dure. However, the safety for V when assumed to be unfavorable is greater than when V is favorable, as indicated also by the longer arrow in Figure 23. Not only is this result contradictory to the result of the regular safety calculation, but it is also inconsistent with the classification of V as unfavorable to begin with because this load actually improved the safety of the system.

The reason for these inconsistencies can be found in the convex shape of the resultant resistance. As a consequence, the safety of the system depends on the load path. This may be critical for design situations with large variable loads, especially if the vertical load is small.

1.6.1.4 Conclusions and Alternative Solution

The example given in Section 1.6.1.3 clearly demonstrates that the assumption of certain load paths within traditional design procedures may lead to a misinterpretation of the safety level. Hence, for the calibration of resistance factors, possible load combinations and the associated load paths have to be identified in advance for evaluation of their significance to the bearing capacity. For this purpose, the use of an interaction diagram for visualization and better understanding is helpful and may be necessary.

This problem can also be solved with an alternative design method, which directly considers the interaction of the differ-

ent load components without assuming specific load paths. This method is based on a consistent definition of the ULS of a shallow foundation by a unique limit state equation without the need for distinguishing between different failure modes. This model can also be extended to analyze the deformations of the foundation within the SLS. Such a model is introduced in the following section.

1.6.1.5 Note Concerning References of Related Work

The concept of an interaction diagram to describe the ULS of a shallow foundation was introduced by Butterfield and Ticof (1979). This concept was later utilized by Nova and Montrasio (1991), Montrasio and Nova (1997), Gottardi and Butterfield (1993, 1995), Martin and Houlsby (2000, 2001), and others. However, this work focused on the calculation of displacements and rotations dealing essentially with forces and moments acting on a single plane (one-way, inclined-eccentric loading). As a result, the failure condition played a minor role and was established by a pure curve fitting only. Work on arbitrary loading conditions (two-way lateral, eccentric, and torsional loading) was first developed by Lesny (2001) with the resulting influence parameters related to physical factors rather than curve fitting (see also Lesny and Richwien, 2002, and Lesny et al. 2002). Lesny used earlier experimental work conducted

by Perau (1995, 1997) at the Institute of Soil Mechanics and Foundation Engineering at the University of Duisburg-Essen (UDE), Essen, Germany. Recently, Byrne and Houlsby (2005) and Bienen et al. (2006) presented experimental work on shallow foundations on sand under arbitrary loading conditions as well. In this work, the failure or yield condition is defined by so-called swipe tests, in which the load path followed closely the failure or yield surface in the interaction diagram. However, the use of these data for the research project reported on herein (NCHRP Project 24-31) may be limited as the tests remain close to but below failure. In other words, failure loads for definite loading conditions are not directly available.

1.6.2 Alternative Design Method for Shallow Foundations

1.6.2.1 Overview

The alternative design method includes two components. The first component is a failure condition that describes the ULS of a shallow foundation without the need to distinguish between different failure modes. The second component is a displacement rule that reflects the complete load-displacement relation within the SLS before the system reaches its ULS.

The failure condition can be used independently of the displacement rule and may be combined with other methods for settlement analysis. It has been developed for foundations on granular soils with and without embedment, whereas the displacement rule is currently developed for foundations without embedment only. Please note that in the general definition of the failure condition and the displacement rule the notation of the load components is different from the notation used previously. An in-depth discussion of the subject and the normalization concept validation via small-scale testing is presented

in Appendix A. For more information, refer to Kisse and Lesny (2007) and Kisse (2008).

1.6.2.2 Failure Condition

In the general case, a single footing is loaded by a vertical load, F_1, horizontal load components F_2 and F_3, a torsional moment, M_1, and bending moment components, M_2 and M_3 (see Figure 24). The load components are summarized in the load vector $\vec{Q}$:

$$\vec{Q}^T = \left[F_1 F_2 F_3 M_1 M_2 M_3 \right] \tag{59}$$

For the basic case of a footing on non-cohesive soil without embedment, the geometry of the footing described by the side ratio ($\bar{b} = b_2/b_3$), weight (γ), the soil's shear strength ($\tan \phi_f$), and a quantity describing the roughness of the footing base (μ_s) have to be considered as well (see Figure 24). With these input parameters, the failure condition of the general form

$$F\left(\vec{Q}, \bar{b}, \gamma, \tan\phi_f, \mu_s\right) = 0 \tag{60}$$

is defined by the following expression:

$$\sqrt{\frac{F_2^2 + F_3^2}{\left(a_1 F_{10}\right)^2} + \frac{M_1^2}{\left(a_2\left(b_2 + b_3\right)F_{10}\right)^2} + \frac{M_2^2 + M_3^2}{\left(a_3 b_2 F_{10}\right)^2}} -$$

$$\frac{F_1}{F_{10}}\left(1 - \frac{F_1}{F_{10}}\right)^\alpha = 0 \tag{61}$$

In Equation 61, all load components are referred to as F_{10}, which is the resistance of a footing under pure vertical loading. This quantity is calculated using the traditional bearing capac-
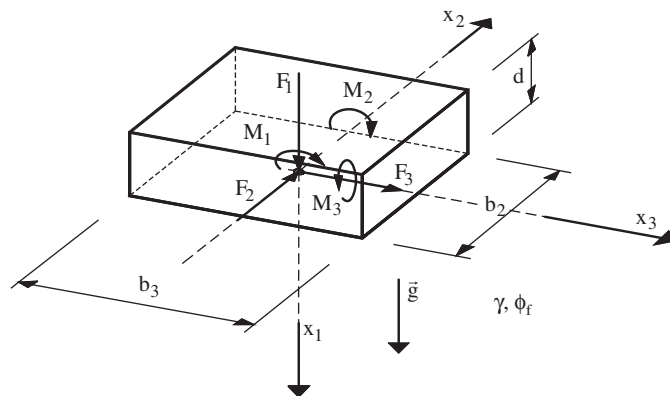
Notes:
b_2, b_3 length of the footing referred to x_2-, x_3- axis M_1, M_2, M_3 torsional and bending moments (referred to
d embedment depth x_1-, x_2-, x_3- axis)
F_1 vertical load γ unit weight of soil
F_2, F_3 horizontal load (referred to x_2-, x_3- axis) ϕ_f angle of internal friction

Figure 24. Geometry and loading.

ity formulae. The advantage of the formulation described in Equation 61 is that the complex interaction of the load components is considered directly without using reduction factors or the concept of the effective foundation area. Other influences on the bearing capacity are included in F_{10}. It should be noted that as F_{10} is the bearing capacity under vertical-centric loading only, the uncertainties of the calculation method are reduced to the bearing capacity factors and the shape and depth factors (if required) of the traditional bearing capacity calculations. Thus, no inclination factors or use of effective area are necessary. The use of such factors and the concept of effective area were the cause for difficulties in establishing the degree of conservatism and hence a source of ambivalent application of LRFD facing the existing AASHTO 2008 specifications.

In an interaction diagram like the ones in Figures 21 or 23, the failure condition spans a failure surface, which is the outer boundary of the admissible loading. The parameters $a_{1,2,3}$ govern the inclination of this failure surface for small vertical loading where the limit states of sliding and the restriction of the eccentricity to $\frac{1}{3}$ of the foundation width have previously been relevant (see Figure 25). These limit states are integrated by defining the parameters $a_{1,2,3}$ and α according to Equation 62:

$$a_1 = (\pi/2)\mu_s(\tan\phi_f)e^{(-\pi/3)\tan\phi_f},$$

$$a_2 = 0.098, \, a_3 = 0.42, \, \alpha = 1.3 \qquad (62)$$

The limit state uplift is already included in Equation 61 because only positive vertical loads are admissible. The parameters provided in Equation 62 have been derived from an analysis of numerous small-scale model tests conducted at the Institute of Soil Mechanics and Foundation Engineering at UDE. Figures 26 and 27 show the failure condition compared with the model test results for various load combinations.

In the case of footings embedded in the soil, the failure condition according to Equation 61 needs to be extended if the shearing resistance in the embedment zone is taken into account:

$$\sqrt{\frac{F_2^2 + F_3^2}{(a_1 F_{10})^2} + \frac{M_1^2}{(a_2(b_2+b_3)F_{10})^2} + \frac{M_2^2 + M_3^2}{(a_3 b_2 F_{10})^2}}$$

$$-\left[(1+f_z)\frac{F_1}{F_{10}} - f_z\right]\left[1-\left((1+f_z)\frac{F_1}{F_{10}} - f_z\right)\right]^\alpha = 0 \qquad (63a)$$

with
$$f_z = \frac{F_{1,min}/F_{10}}{1 - F_{1,min}/F_{10}} \qquad (63b)$$

In Equation 63b, $F_{1,min}$ is the bearing capacity due to pure vertical tension loading resulting from the shearing resistance in the embedment zone, which may be carefully calculated using an earth pressure model. F_{10} can be determined using the traditional bearing capacity equation taking into account depth factors provided by Brinch Hansen (1970). The increasing capacity for horizontal and moment loading is considered by the parameters a_i according to Equation 64, which requires additional verification at this stage:

$$a_1 = \left(\frac{\pi}{2}\right)\mu_{S,k}(\tan\phi_f)\left(e^{\left(-\frac{\pi}{3}\right)\tan\phi_f}\right)$$

$$\left[1+\left(2-\left(\frac{\pi}{2}\right)\tan\phi_f\right)\left(1-e^{(-\tan\phi_f)d/b_2}\right)\right]$$

$$a_2 = 0.098 \qquad (64)$$

$$a_3 = 0.42\left[1+0.5\left(1-\exp\left(-\pi\frac{d}{b_2}\right)\right)\right]$$

$$\alpha = 1.3$$
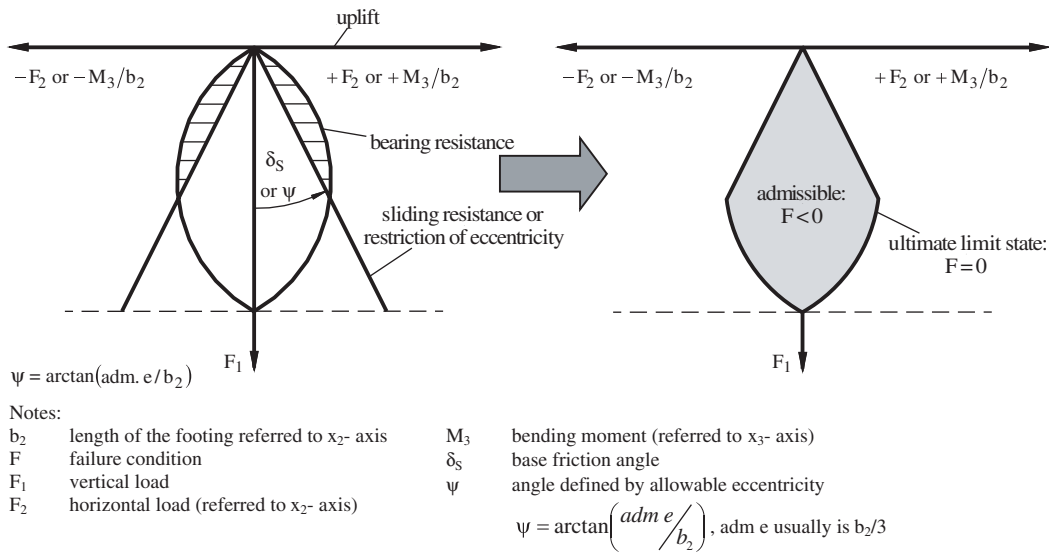
Figure 25. Isolated limit states (left) and failure condition (right).
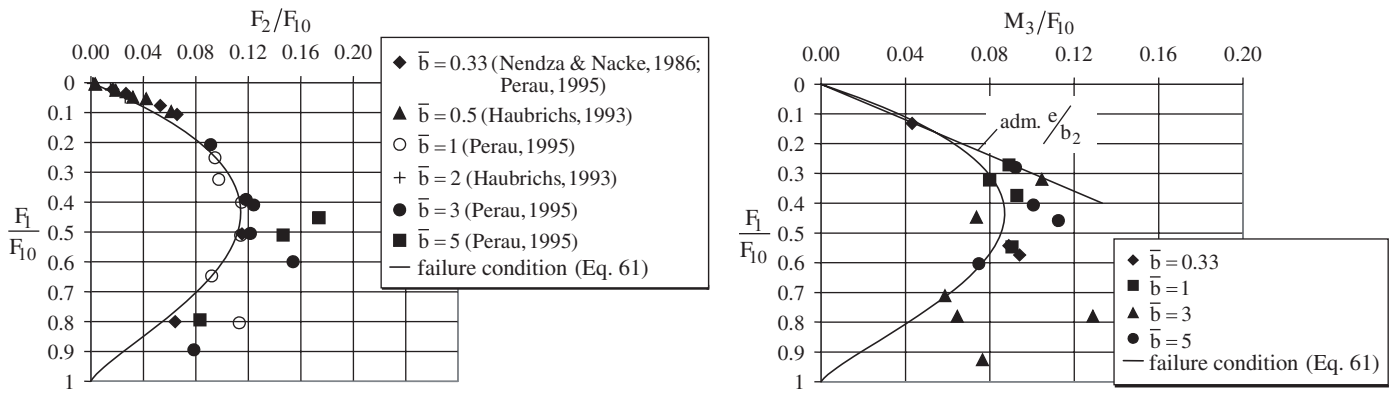
Notes:
F_1 vertical load
F_2 horizontal load
        (referred to x_2- axis)
$\bar{b}$ b_2/b_3 side ratio
F_{10} bearing capacity under pure vertical loading, i.e.,
        maximum vertical load that can be carried by the system
M_3 bending moment

Figure 26. Failure condition for inclined loading (left) and eccentric loading (right) versus failure loads from small-scale model tests.

where

$\mu_{S,k}$ = value of characteristic roughness of the foundation base.

1.6.2.3 Displacement Rule

The displacements and rotations of the foundation due to arbitrary loading inside the failure surface are described by the displacement rule. The displacements u_i and rotations ω_i are summarized in a displacement vector:

$$\vec{u}^T = \begin{bmatrix} u_1 & u_2 & u_3 & \omega_1 & \omega_2 & \omega_3 \end{bmatrix} \tag{65}$$

Due to the complex interaction of load components, displacements, and rotations, the displacement rule is formulated using the well-known strain hardening plasticity theory with

$$\sqrt{\frac{F_2^2 + F_3^2}{(a_1 \cdot F_{10})^2} + \frac{M_1^2}{(a_2 \cdot (b_2 + b_3) \cdot F_{10})^2} + \frac{M_2^2 + M_3^2}{(a_3 \cdot b_2 \cdot F_{10})^2}}$$
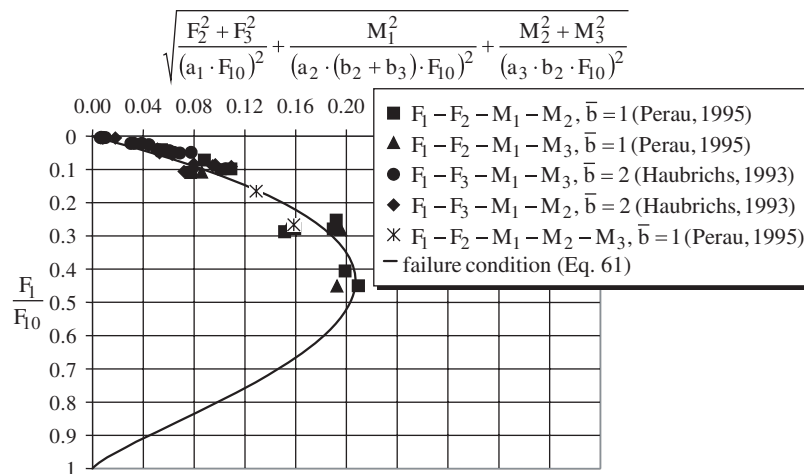
Notes:
b_2, b_3 length of the footing (referred to x_2-, x_3- axis)
$\bar{b}$ b_2/b_3 side ratio
F_1 vertical load
F_2, F_3 horizontal load (referred to x_2-, x_3- axis)
F_{10} bearing capacity under pure vertical loading, i.e., max. vertical load that can be carried by the system
M_1, M_2, M_3 torsional and bending moments (referred to x_1-, x_2-, x_3- axis)
a_1, a_2, a_3 parameters of failure condition according to (Eq. 61)

Figure 27. Failure condition for general loading versus failure loads from small-scale model tests.

isotropic hardening (e.g., Zienkiewicz, 2005). Hence, displacements and rotations are calculated according to Equation 66, assuming that all deformations are plastic:

$$d\vec{u} = \frac{1}{H}\left(\frac{\partial F}{\partial \vec{Q}}\right)^T \frac{\partial G}{\partial \vec{Q}} d\vec{Q} \tag{66}$$

The components of the displacement rule are a yield surface described by the yield condition, F, which is derived from the failure condition equation (Equation 61):

$$F(\vec{Q}, F_a) = \frac{F_2^2 + F_3^2}{(a_1 F_a)^2} + \frac{M_1^2}{(a_2(b_2 + b_3)F_a)^2} + \frac{M_2^2}{(a_3 b_3 F_a)^2} + \frac{M_3^2}{(a_3 b_2 F_a)^2}$$
$$- \left[\frac{F_1}{F_a}\left(1 - \frac{F_1}{F_a}\right)^a\right]^2 = 0 \tag{67}$$

with the parameters $a_{1,2,3}$ of Equation 62, a plastic potential, G:

$$G(\vec{Q}, F_b) = \frac{F_2^2 + F_3^2}{(c_1 F_b)^2} + \frac{M_1^2}{(c_2(b_2 + b_3)F_b)^2} + \frac{M_2^2}{(c_3 b_3 F_b)^2}$$
$$+ \frac{M_3^2}{(c_3 b_2 F_b)^2} - \left[\frac{F_1}{F_b}\left(1 - \frac{F_1}{F_b}\right)^\beta\right]^2 = 0 \tag{68}$$

and a hardening function, H:

$$H = -\frac{\partial F}{\partial F_a} \cdot \frac{\partial F_a}{\partial u_1} \cdot \frac{\partial G}{\partial F_1} \tag{69}$$

In Equation 68, F_b is the hardening function and c_1, c_2, and c_3 are the parameters of the plastic potential.

The yield surface according to Equation 67 expands due to isotropic hardening until the failure surface defined by Equation 61 is reached (see Figure 28). Thus, the parameters c_i and
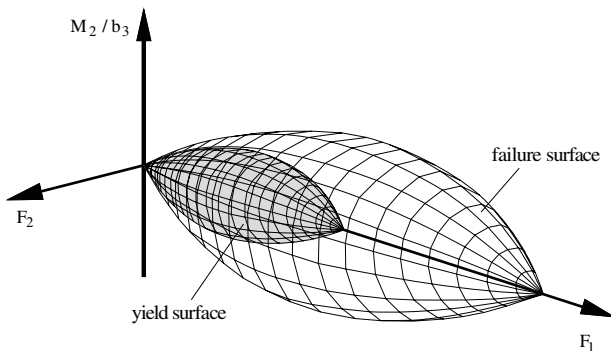
β in Equation 68 have to be determined as functions of a_i and α, respectively. The expansion of the yield surface depends mainly on the vertical displacement, u_1, which itself depends on the degree of mobilization of the maximum resistance, F_{10}. Hence, it is sufficient to define the hardening parameter, F_a, in Equation 67 as a function of these two quantities according to the following:

$$F_a = (F_{10} + k_f u_1)\left\{1 - \exp\left(\frac{-k_0 u_1}{F_{10} + k_f u_1}\right)\right\} \tag{70}$$

Many hardening laws (e.g., Nova and Montrasio, 1991) require small-scale model tests under centric vertical loading to determine the hardening parameter. Since this is not convenient for practical applications, the initial and final stiffness of the corresponding load-displacement curve, k_0 and k_f, respectively, may be determined using a method proposed by Mayne and Poulos (2001) in which the soil stiffness can be determined by any standard procedure.

Figure 29 shows the results of the proposed model applied to the example breakwater of Figure 22. Safety factors are not applied here. On the left side of Figure 29 the failure condition and the loading in the $F_1 - F_2$ plane and in the $F_1 - M_3/B_C$ plane are shown. Obviously, the stability of the breakwater is governed by the high horizontal loading. Only an increase in the vertical loading (i.e., of the breakwater weight) would lead to a sufficient safety. The right side of Figure 29 shows the vertical and horizontal displacements of the breakwater depending on the corresponding load components, F_1 and F_2. However, due to some conservative assumptions made in the current version of the proposed model, a breakwater width of 21.0 m instead of 17.5 m was required to reach stability.

1.6.2.4 Implementation of a Safety Concept

To implement a safety concept for the ULS based on load and resistance factors, the bearing capacity and loading for the characteristic input parameters shall be considered first. The bearing capacity defined by the failure condition is qualitatively shown again in the interaction diagram of Figure 30. Each load combination to be checked marks a point in the interaction diagram. Connecting all load points provides a polygon in the interaction diagram (see Figure 30). It can be shown that the corners of this polygon are represented by load combinations, which either consider live loads to the full extent or neglect them. Because of the convexity of the failure condition, it is sufficient to prove only these load combinations.

To get the design failure condition, F_d, the parameters a_i in Equations 61 and 62 are divided by the required resistance factor $\gamma_{R,i}$. Additionally, a resistance factor also has to be adapted to F_{10}. This procedure means that in practice the failure surface shrinks as depicted in Figure 30.

Notes:
b_3 length of the footing (referred to x_3-axis) F_2 horizontal load
F_1 vertical load M_2 bending moment (referred to x_2-axis)

Figure 28. Isotropic expansion of the yield surface in the loading space.

Notes:

B_c	width of breakwater	M_3	torsional and bending moments (referred to x_1-, x_2-, x_3-axis)
F_1	vertical load	u_1	vertical displacements (settlements)
F_2	horizontal load (referred to x_3-axis)	u_2	horizontal displacements

Figure 29. Failure condition (left) and load displacement curves (right) for the example breakwater.

The resistance factors are no longer distinguished according to different limit states but according to the possible load interactions. So at least resistance factors for pure vertical loading, inclined loading, torsional loading, and eccentric loading may be defined:

$\gamma_{R,pure\ vertical}$	for F_{10} (pure vertical loading)
$\gamma_{R,horizontal}$	for a_1 (inclined loading)
$\gamma_{R,torsional}$	for a_2 (torsional loading)
$\gamma_{R,eccentric}$	for a_3 (eccentric loading)

The case of inclined and eccentric load combinations may result in a coupled interaction of the resistance factors. These cases, like other aspects of this concept, require further analysis. The application of load factors means that load components are reduced if they work favorably and are increased if they work unfavorably regarding the bearing capacity of the foundation (considering the aspects that were discussed earlier). This may cause displacements and distortions of the load polygon in the interaction diagram.
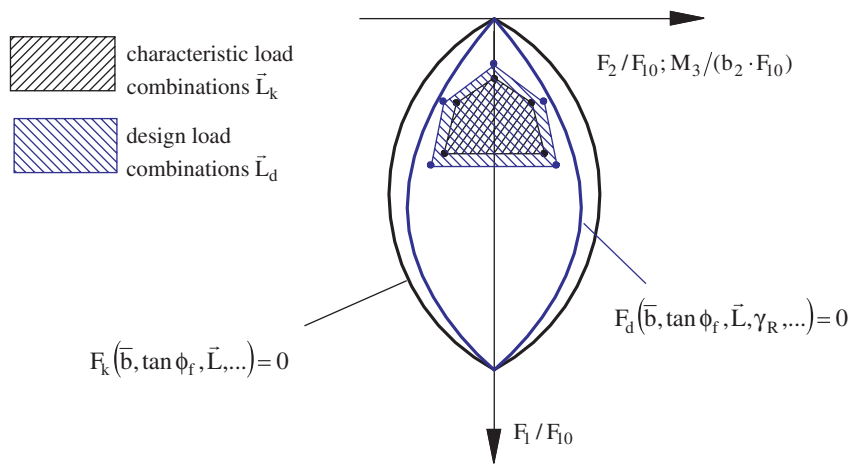
Notes:

b_2	length of the footing (referred to x_2-axis)	F_{10}	bearing capacity under pure vertical loading, i.e., maximum vertical load that can be carried by the system
$\bar{b}$	b_2/b_3 side ratio		
F_k	characteristic failure condition	$\vec{L}_k$	characteristic load combination
F_d	design failure condition	$\vec{L}_d$	design load combination
F_1	vertical load		
F_2	horizontal load	γ_R	resistance factor
M_3	bending moment	ϕ_f	angle of internal friction

Figure 30. Illustration of the safety concept principle.

For simplicity, it is assumed here that the load polygon in Figure 30 expands evenly.

Finally, the foundation stability is verified, if it can be shown that

$$\underset{\vec{L}_d \in L_d}{\forall} F\left(\ldots, \gamma_{R,i}, \vec{L}_d\right) < 0 \tag{71}$$

where $\vec{L}_d$ is one design load combination of the set of all design load combinations, L_d, which need to be checked. If the inequality (Equation 71) is fulfilled, all design load combinations are located inside the design failure surface.

1.7 Bearing Capacity of Shallow Foundations on Rock

1.7.1 Overview

The bearing capacity of foundations founded on rock masses depends mostly on the ratio of joint spacing to foundation width, as well as intact and rock mass qualities like joint orientation, joint condition (open or closed), rock type, and intact and mass rock strengths. Failure modes may consist of a combination of modes, some of which include bearing capacity failure. Limited review of the bearing capacity of foundations on rock, as well as the relationships among bearing capacity mechanisms, unconfined compressive strength (q_u), and other rock parameters is presented. Emphasis is placed on classifications and parameters already specified by AASHTO and methods of analysis utilized in this study for bearing capacity calibrations.

Loads on foundation elements are limited by the structural strength, the ultimate (geotechnical) limit state (strength), and the load associated with the serviceability limit state. The relationships among these limits when applied to foundations on rock are often vastly different than when they are applied to shallow foundations on soil. For typical concrete strengths in use today, the strength of the concrete member is significantly less than the bearing capacity of many rock masses. The structural design of the foundation element will dictate, therefore, the minimum element size and, consequently, the maximum contact stress on the rock. In other loading conditions—such as intensely loaded pile tips, concentrated loads of steel supports in tunnels, or the bearing capacity of highly fractured or softer homogeneous rocks (such as shale and sandstone)—the foundation's geotechnical limit state (bearing capacity) can be critical. While settlement (i.e., serviceability) is often the limit that controls the design load of shallow foundations on soil, for many rocks the load required to develop common acceptable settlement limits well exceeds the bearing capacity values. As such, both settlement

and capacity are important to quantify for the design of shallow foundations on both soil and rock. The research herein addresses, however, only the bearing capacity (i.e., the ULS of shallow foundations).

1.7.2 Failure Mechanisms of Foundations on Rock

Failure of foundations on rock may occur as the result of one of several mechanisms, as shown in Figure 31 (Franklin and Dusseault, 1989). The failure modes are described by the *Canadian Foundation Engineering Manual* (Canadian Geotechnical Society, 2006) in the following way:

1. Bearing capacity failures occur when soil foundations are overloaded (see Figures 31a and b). Such failures, although uncommon, may occur beneath heavily loaded footings on weak clay shales.
2. Consolidation failures, common in weathered rocks, occur where the footing is placed within the weathered profile (see Figures 31c and e). In this case, unweathered rock core-stones are pushed downward under the footing load because of a combination of low shear strength along clay-coated lateral joints and voids or compressible fillings in the horizontal joints.
3. A punching failure (see Figure 31d) may occur where the foundation rock comprises a porous rock type, such as shale, tuff, and porous limestone (chalk). The mechanism includes elastic distortion of the solid framework between the voids and the crushing of the rock where it is locally highly stressed (Sowers and Sowers, 1970). Following such a failure, the grains are in much closer contact. Continued leaching and weathering will weaken these rock types, resulting in further consolidation with time.
4. Slope failure may be induced by foundation loading of the ground surface adjacent to a depression or slope (see Figure 31f). In this case, the stress induced by the foundation is sufficient to overcome the strength of the slope material.
5. Subsidence of the ground surface may result from collapse of strata undercut by subsurface voids. Such voids may be natural or induced by mining. Natural voids can be formed by solution weathering of gypsum or rock salt and are commonly encountered in limestone terrain (see Figure 31g). When weathering is focused along intersecting vertical joints, a chimney-like opening called a pipe is formed, which may extend from the base of the soil overburden to a depth of many tens of meters. When pipes are covered by granular soils, the finer silt and sand components can wash downward into the pipes, leaving a coarse sand and gravel arch of limited stability, which may subsequently collapse (see Figure 31h).
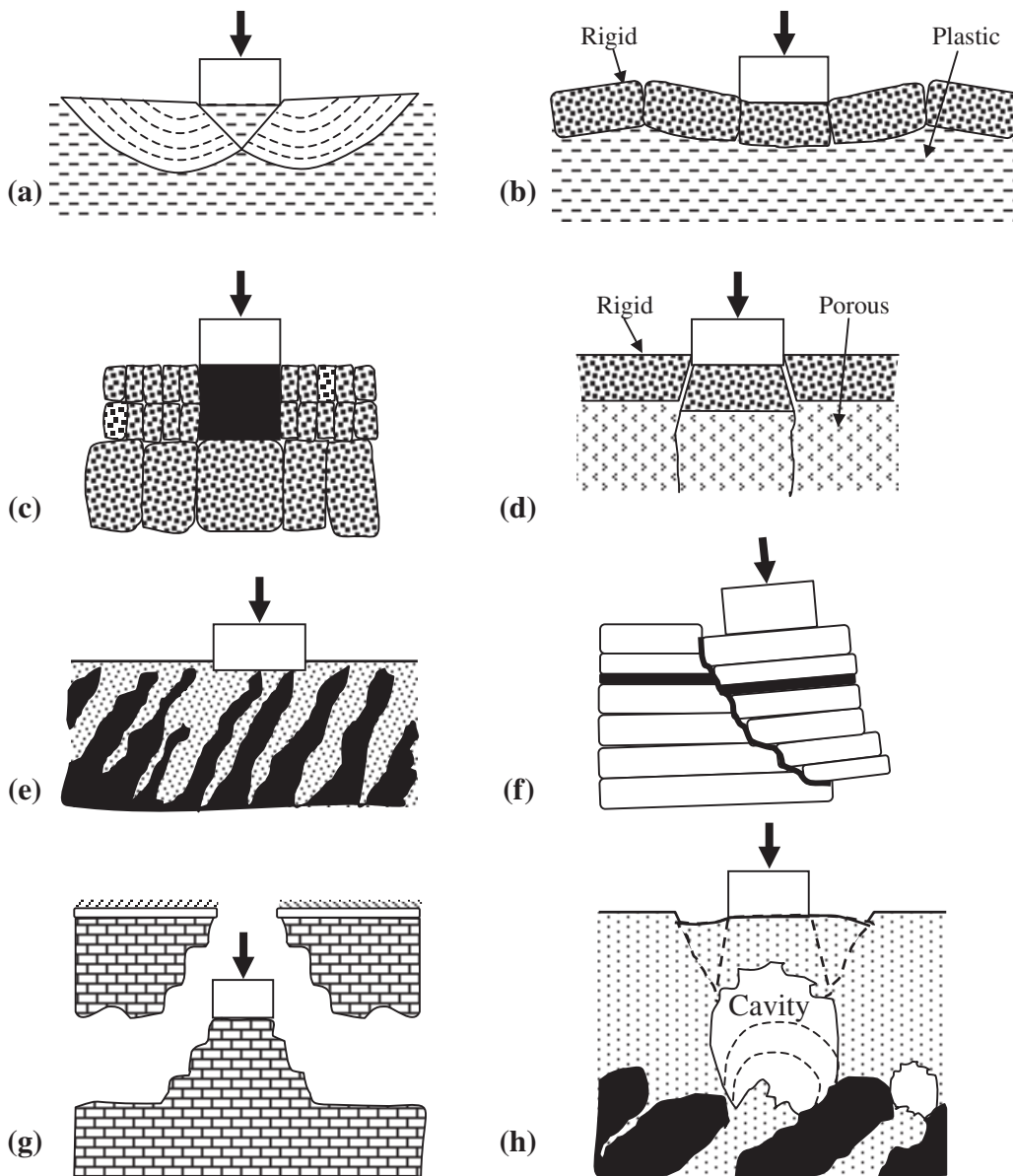
Figure 31. Mechanisms of foundation failure from Franklin and Dusseault (1989), adapted from Sowers (1979): (a) Prandtl-type shearing in weak rock, (b) shearing with superimposed brittle crust, (c) compression of weathered joints, (d) compression and punching of porous rock underlying a rigid crust, (e) breaking of pinnacles from a weathered rock surface, (f) slope failure caused by superimposed loading, (g) collapse of a shallow cave, and (h) sinkhole caused by soil erosion into solution cavities (Canadian Geotechnical Society, 2006).

1.7.3 Bearing Capacity Failure Mechanisms

Out of the various aforementioned possible failures of foundations on rock, this research is focused on those associated with bearing capacity mechanisms. The mechanism of potential failure in jointed rocks depends mostly on the size of the loaded area relative to the joint spacing, joint opening, and the location of the load. Figure 32 (a through c)

shows three simple possible analyses associated with the ratio of foundation width to joint spacing and the joint conditions.

1. Closed Spaced Open Joints: Figure 32a illustrates the condition where the joint spacing, s, is a fraction of B, and the joints are open. The foundation is supported by unconfined rock columns; hence, the ultimate bearing
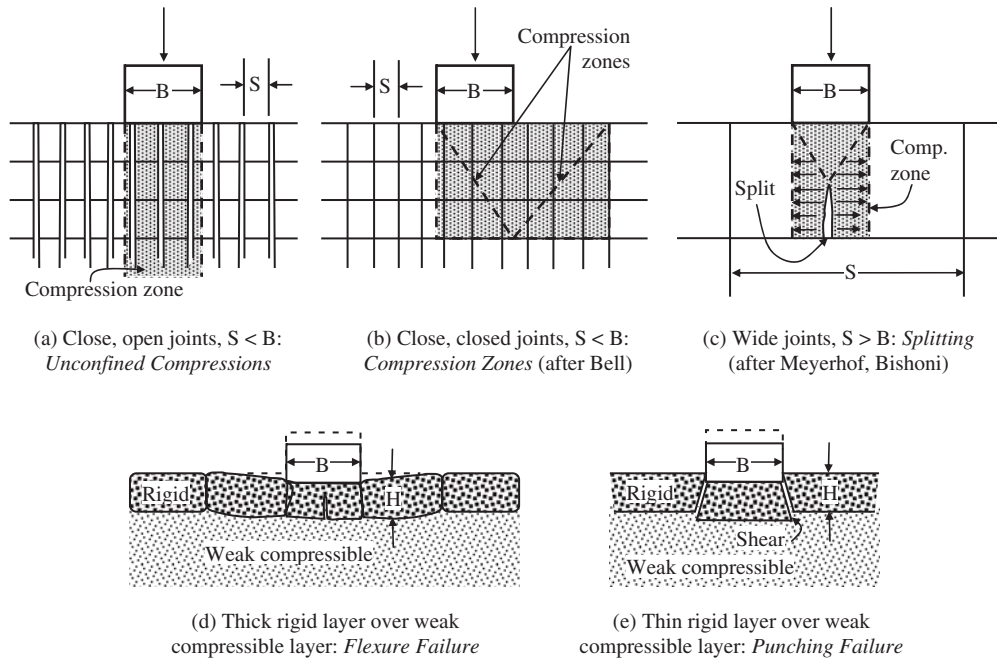
Figure 32. **Bearing capacity failure modes of rock (based on Sowers, 1979).**

capacity approaches the sum of the unconfined compressive strengths of each of the rock prisms. Because all rock columns do not have the same rigidity, some will fail before others reach their ultimate strength; hence, the total capacity is somewhat less than the sum of the prism strengths.

2. Closed Spaced Joints in Contact: The Bell-Terzaghi analysis is shown in Figure 32b. When $s < B$ and the joints are closed so that pressure can be transmitted across them without movement, the rock mass is essentially treated as a continuum, and the bearing capacity can be evaluated in the way shown in Figure 33 in which the major principal stress of Prism II (σ_{1-II}) is equal to the embedment confining stresses q_o, and the minor principal stress of Prism II (σ_{3-II}) is equal to the major principal stress of Prism I (σ_{1-I}) such that the bearing capacity is

the major principal stress of Prism I and is expressed in Equation 72:

$$q_{ult} = 2c \tan\left(45 + \frac{\phi_f}{2}\right) \tag{72}$$

where c is cohesion, and ϕ_f is friction angle of the rock mass.

3. Wide Joints: If the joint spacing is much greater than the foundation width, $s \gg B$ (see Figure 32c), the proposed failure mechanism is a cone-shaped zone forming below the foundation that splits the block of rock formed by the joints. Equation 73 can be used to approximate the bearing capacity assuming that the load is centered on the joint block and little pressure is transmitted across the joints:

$$q_{ult} \approx JcN_{cr} \tag{73}$$
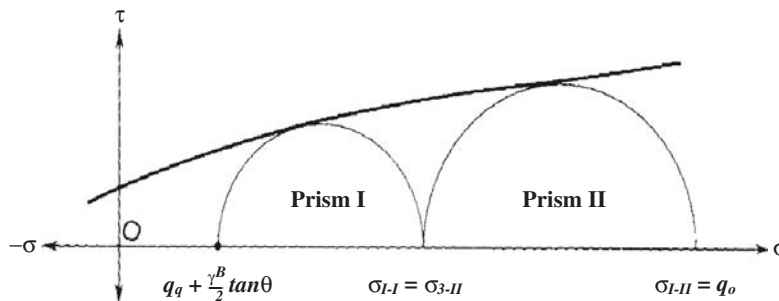
Figure 33. **Mohr Circle analysis of bearing capacity based on straight-line failure planes and prismatic zones of triaxial compression and shear (based on Sowers, 1979).**

For continuous strip foundations:

$$q_{ult} = \frac{JcN_{cr}}{\left(2.2 + 0.18\frac{L}{B}\right)} \tag{74}$$

where

B and L = width and length of the footing, respectively;

J = a correction factor dependent upon the thickness of the foundation rock below the footing and the width of the footing; and

N_{cr} = bearing capacity factor.

Based on laboratory test results and the N_{cr} solution by Bishoni (1968), J is estimated by the following:

$$\frac{H}{B} \leq 5 \quad J = 0.12\frac{H}{B} + 0.4 \tag{75a}$$

$$\frac{H}{B} > 5 \quad J = 1 \tag{75b}$$

where H is the average spacing between a pair of horizontal discontinuities.

Values of N_{cr} derived from models for splitting failure depend on the s/B ratio and ϕ_f, which will be discussed later. The values for square footings are 85% of the circular. Graphical solutions for the bearing capacity factor (N_{cr}) and correction factor (J) by Bishoni (1968) are provided in Figures 34a and 34b, respectively. The bearing capacity factor (N_{cr}) is given by Goodman (1980):

$$N_{cr} = \frac{2N_\phi^2}{1+N_\phi}(\cot\phi_f)\left(\frac{s}{B}\right)\left(1 - \frac{1}{N_\phi}\right)$$

$$- N_\phi(\cot\phi_f) + 2N_\phi^{1/2} \tag{76}$$

where

s = the spacing between a pair of vertical open discontinuities,

ϕ_f = the friction angle of intact rock, and

N_ϕ = the bearing capacity factor given by:

$$N_\phi = \tan^2\left(45 + \frac{\phi_f}{2}\right) \tag{77}$$

4. Thick and Thin Rigid Rock Layer over Weak Compressible Layer: As shown in Figures 31d, 32d, and 32e, depending on the ratio H/B and S/B and on the flexural strength of the rock stratum, two forms of failure occur when the rock formation consists of an extensive hard seam underlain by a weak compressible stratum. If the H/B ratio is large and the flexural strength is small, the rock failure occurs by flexure (see Figure 32d). If the H/B ratio is small, punching is more likely (see Figure 32e). The same analysis can also be used for designs with hard rock layers over voids. Bearing capacity calculations for flexural or punching failure are proposed by Lo and Hefny (2001) and by ASCE (Zhang and Einstein, 1998; Bishoni, 1968; Kulhawy, 1978).

1.7.4 The Canadian Foundation Engineering Manual

The bearing capacity methods for foundations on rock proposed by the *Canadian Foundation Engineering Manual* (Canadian Geotechnical Society, 2006) are described to be suitable for all ranges of rock quality, noting that the design bearing pressure is generally for SLSs not exceeding 25 mm (1 in.) settlement. The *Canadian Foundation Engineering Manual* (Canadian Geotechnical Society, 2006) considers a

(a) bearing capacity factors for circular foundation on jointed rock, with S/B > 1 and H/B > 8.

(b) correction factor J for rock layer thickness, H
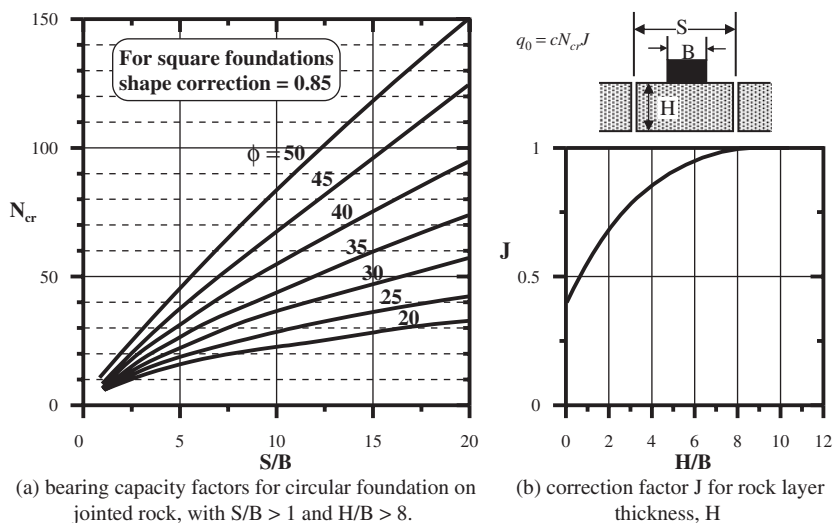
Figure 34. Bearing capacity factors for rock splitting (based on Bishoni, 1968).

Table 6. Coefficients of discontinuity spacing, K_{sp} (Canadian Geotechnical Society, 2006).

Discontinuity spacing		K_{sp}
Description	Distance m (ft)	
Moderately close	0.3 to 1 (1 to 3)	0.1
Wide	1 to 3 (3 to 10)	0.25
Very wide	> 3 (> 10)	0.4

rock to be sound when the spacing of discontinuities is in excess of 0.3 m (1 ft). When the rock is sound, the strength of the rock foundation is commonly in excess of the design requirements provided the discontinuities are closed and are favorably oriented with respect to the applied forces, i.e., the rock surface is perpendicular to the foundation, the load has no tangential component, and the rock mass has no open discontinuities. Under such conditions, the design bearing pressure may be estimated from the following approximate relation:

$$q_a = K_{sp} \times q_{u-core} \tag{78}$$

where

q_a = design bearing pressure;
q_{u-core} = average unconfined compressive strength of rock (as determined from ASTM D2938); and
K_{sp} = an empirical coefficient, which includes a factor of safety of 3 (in terms of WSD) and ranges from 0.1 to 0.4 (see Table 6 and Figure 35).

The factors influencing the magnitude of the coefficient are shown graphically in Figure 35. The relationship given in Figure 35 is valid for a rock mass with spacing of discontinuities greater than 300 mm (1 ft), aperture of discontinuities less than 5 mm (0.2 in.) (or less than 25 mm [1 in.] if filled with

soil or rock debris), and for a foundation width greater than 300 mm (1 ft). For sedimentary rocks, the strata must be horizontal or nearly so.

The bearing-pressure coefficient, K_{sp}, as given in Figure 35, takes into account the size effect and the presence of discontinuities and includes a nominal safety factor of 3 against the lower-bound bearing capacity of the rock foundation. The factor of safety against general bearing failure (ULSs) may be up to ten times higher. For a more detailed explanation, the *Canadian Foundation Engineering Manual* (Canadian Geotechnical Society, 2006) refers to Ladanyi et al. (1974) and Franklin and Gruspier (1983) who discuss a special case of foundations on shale. It is often useful to estimate a bearing pressure for preliminary design on the basis of the material description. Such values must be verified or treated with caution for final design. Table 7 presents presumed preliminary design bearing pressure for different types of soils and rocks.

1.7.5 Goodman (1989)

The considered mode of failure is shown in Figures 36a through 36c, in which a laterally expanding zone of crushed rock under a strip footing induces radial cracking of the rock on either side (Goodman, 1989). The strength of the crushed rock under the footing is described by the lower failure envelope (curve for Region A) in Figure 37, while the strength of the less fractured neighboring rock is being described by the upper curve in the same figure (curve for Region B). The largest horizontal confining pressure that can be mobilized to support the rock beneath the footing (Region A in Figure 37) is p_h, determined as the unconfined compressive strength of the adjacent rock (Region B of Figure 37). This pressure determines the lower limit of Mohr's circle tangent to the strength envelope of the crushed rock under the footing. Triaxial compression tests

$$K_{sp} = \frac{3 + \frac{c}{B}}{10\sqrt{1 + 300\frac{\delta}{c}}}$$

c = spacing of discontinuities
δ = aperture of discontinuities
B = footing width

Valid for 0.05 < c/B < 2.0
0 < δ/c < 0.02
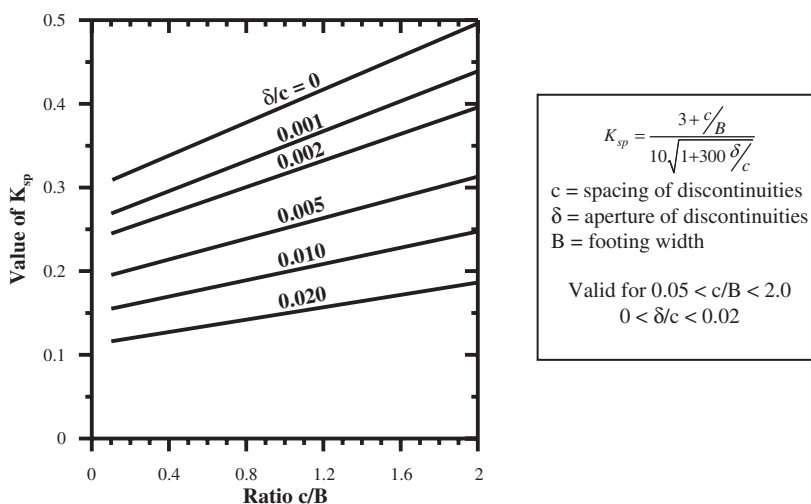
Figure 35. Bearing pressure coefficient (K_{sp}) (based on Canadian Geotechnical Society, 2006).

Table 7. Presumed preliminary design bearing pressure (Canadian Geotechnical Society, 2006).

Group	Types and conditions of rocks	Strength of rock material	Preliminary design bearing pressure [5] kPa (ksf)	Remarks
Rocks	Massive igneous and metamorphic rocks (granite, diorite, basalt, gneiss) in sound condition [2]	High-very high	10,000 (200)	These values are based on the assumption that the foundations are carried down to unweathered rock.
	Foliated metamorphic rocks (slate, schist) in sound condition [1] [2]	Medium-high	3,000 (60)	Not applicable
	Sedimentary rocks: cemented shale, siltstone, sandstone, limestone without cavities, thoroughly cemented in conglomerates, all in sound condition [1] [2]	Medium-high	1,000–4,000 (20–80)	Not applicable
	Compaction shale and other argillaceous rocks in sound condition [2][4]	Low-medium	500–1,000 (10–20) 1,000 (20)	Not applicable
	Broken rocks of any kind with moderately close spacing of discontinuities (0.3 m [11.8 in]) or greater), except argillaceous rocks (shale), limestone, sandstone, shale with closely spaced bedding	Not applicable	(See note 3)	Not applicable
	Heavily shattered or weathered rocks	Not applicable	(See note 3)	Not applicable

Notes:

1. The above values for sedimentary or foliated rocks apply where the strata or the foliation are level or nearly so, and, then, only if the area has ample lateral support. Tilted strata and their relation to nearby slopes or excavations should be assessed by a person knowledgeable in this field of work.
2. Sound rock conditions allow minor cracks at spacing not closer than 1 m (39.37 in).
3. To be assessed by examination in-situ, including test loading if necessary.
4. These rocks are apt to swell on release of stress, and on exposure to water they are apt to soften and swell.
5. The above values are preliminary estimates only and may need to be adjusted upwards or downwards in a specific case. No consideration has been made for the depth of embedment of the foundation. Reference should be made to other parts of the Manual when using this table.

on broken rock can define the latter strength envelope, and thus the bearing capacity can be found (Goodman, 1989).

Examination of Figure 37 leads to the conclusion that the bearing capacity of a homogeneous, discontinuous rock mass cannot be less than the unconfined compressive strength of the rock mass around the footing, and this can be taken as the lower bound. If the rock mass has a constant angle of internal friction (ϕ_f) and unconfined compressive strength (q_u) (Mohr-Coulomb material), the mechanism described in Figure 37 establishes the bearing capacity as

$$q_{ult} = q_u \left(N_\phi + 1 \right) \tag{79}$$

where N_ϕ is calculated using Equation (77).

Figure 38 depicts a footing resting on a portion of a single joint block created by orthogonal vertical joints each spaced distance s. Such a condition might arise, for example, in weathered granite (Goodman, 1989). If the footing width (B) is equal

to the joint spacing (s), the rock foundation can be compared to a column whose strength under axial load should be approximately equal to the unconfined compressive strength (q_u). If the footing contacts a smaller proportion of the joint block, the bearing capacity increases toward the maximum value consistent with the bearing capacity of homogeneous, discontinuous rock, obtained with the construction of the Mohr-Coulomb failure envelopes described in Figure 37 or from Equation 79, which takes into account the friction angle (ϕ_f) of the homogeneous discontinuous rock. This problem was studied by Bishoni (1968), who assumed that some load is transferred laterally across joints. Modifying this boundary condition for an open-jointed rock mass in which lateral stress transfer is zero, yields

$$q_{ult} = q_u \left\{ \frac{1}{N_\phi - 1} \left[N_\phi \left(\frac{S}{B} \right)^{(N_\phi - 1)/N_\phi} - 1 \right] \right\} \tag{80}$$

Cracking

(a)

Crushing

(b)

Wedging

(c)

Punching

(d)

Shear

(e)
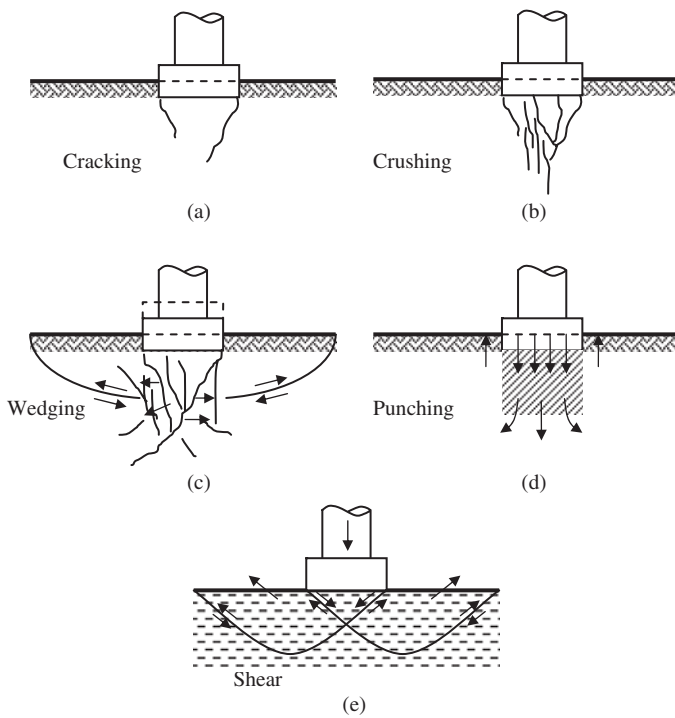
Figure 36. Modes of failure of a footing on rock including development of failure through crack propagation and crushing beneath the footing (a-c), punching through collapse of voids (d), and shear failure (e) (based on Goodman, 1989).

Strength of Rock Mass (region B)

Strength of Rock Mass (region A)

P_h q_f

q_f

Strip footing

B P_h B

A
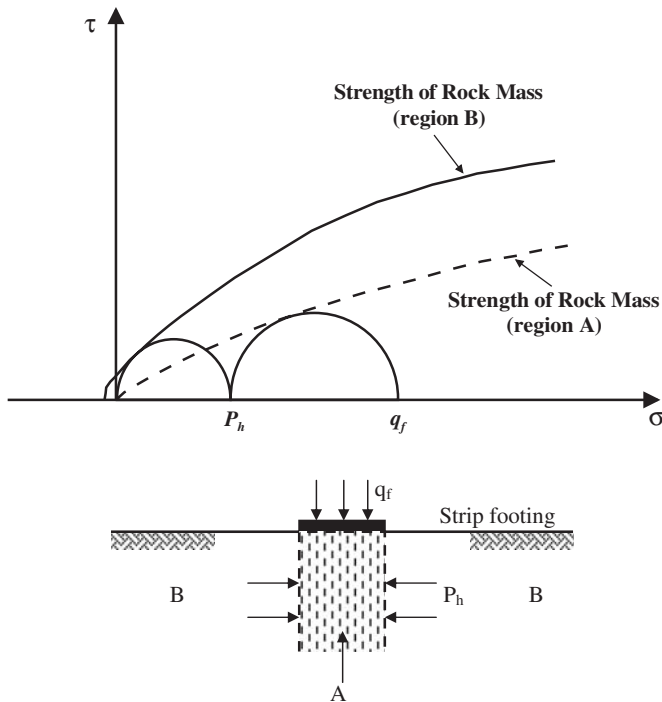
Figure 37. Analysis of bearing capacity on rock (based on Goodman, 1989).
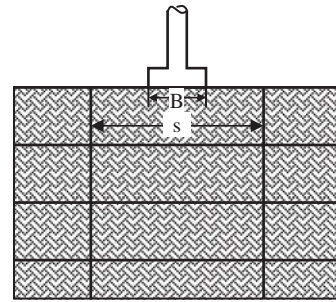
Figure 38. Footing on rock with open, vertical joints (based on Goodman, 1989).

Comparing the results of Goodman's (1989) computations with Equations 79 and 80 shows that open joints reduce the bearing capacity only when the ratio S/B is in the range from 1 to 5. The bearing capacity of footings on rock with open joints increases with increasing ϕ_f for any of the S/B ratios ranging from 1 to 5.

1.7.6 Carter and Kulhawy (1988)

Carter and Kulhawy (1988) suggested that the Hoek and Brown strength criterion for jointed rock masses (Hoek and Brown, 1980, see also Section 1.8.2.4) can be used in the evaluation of bearing capacity. The curved strength envelope for jointed rock mass can be expressed as

$$\sigma_1 = \sigma_3 + \left(mq_u\sigma_3 + sq_u^2\right)^{0.5} \tag{81}$$

where

σ_1 = major principal effective stress,
σ_3 = minor principal effective stress,
q_u = uniaxial compressive strength of the intact rock.
s and m = empirically determined strength parameters for the rock mass, which are to some degree analogous to c and ϕ_f of the Mohr-Coulomb failure criterion.

Carter and Kulhawy (1988) suggested that an analysis of the bearing capacity of a rock mass obeying this criterion can be made using the same approximate technique as used in the Bell (1915) solution. The details of this approach are described in Figure 39. A lower bound to the failure load was calculated by finding a stress field that satisfies both equilibrium and the failure criterion. For a strip footing, the rock mass beneath the foundation may be divided into two zones with homogeneous stress conditions at failure throughout each, as shown in Figure 39. The vertical stress in Zone I is assumed to be zero, while the horizontal stress is equal to the uniaxial compressive strength of the rock mass, given by Equation 81 as $s^{0.5}q_u$. For equilibrium, continuity of the horizontal stress
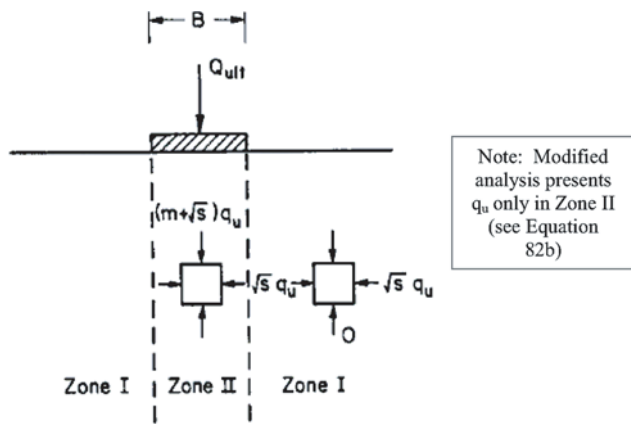
Rock Mass Failure Criterion: $\sigma_1 = \sigma_3 + \sqrt{(mq_u\,\sigma_3 + sq_u^2)}$

Figure 39. Lower bound solution for bearing capacity (Carter and Kulhawy, 1988).

across the interface must be maintained and therefore the bearing capacity of the strip footing may be evaluated from Equation 81 (with $\sigma_3 = s^{0.5}q_u$) as

$$q_{ult} = \left(m + \sqrt{s}\right)q_u \tag{82a}$$

In an errata to Carter and Kulhawy (1988), Equation (82a) was modified to the following:

$$q_{ult} = \left(\sqrt{s} + \left(m\sqrt{s} + s\right)^{0.5}\right)q_u \tag{82b}$$

A similar approach to the bearing capacity analysis of a strip footing was proposed by Carter and Kulhawy (1988) to be used for a circular foundation with an interface between the two zones that was a cylindrical surface of the same diameter as the foundation. In this axisymmetric case, the radial stress transmitted across the cylindrical surface at the point of collapse of the foundation may be greater than $q_u\sqrt{s}$, without necessarily violating either radial equilibrium or the failure criterion. However, because of the uncertainty of this value, the radial stress at the interface is also assumed to be $q_u\sqrt{s}$ for the case of a circular foundation. Therefore, the predicted (lower bound) bearing capacity is given by Equations 82a and 82b. The m and s constants are determined by the rock type and the conditions of the rock mass, and selecting an appropriate category is easier if either the Rock Mass Rating (RMR) system or the Geological Strength Index (GSI) classification data are available as outlined below. Both bearing capacity formulations expressed in Equations 82a and 82b were investigated in this study.

1.8 Rock Classification and Properties

1.8.1 Overview

A rock mass comprises blocks of intact rock that are separated by discontinuities such as cleavage, bedding planes, joints, and faults. Table 8 provides a summary of rock mass discontinuity definitions and characteristics. These naturally formed discontinuities create weakness surfaces within the rock mass, thereby reducing the material strength. As previously discussed, the influence of the discontinuities upon the material strength depends upon the scale of the foundation relative to the position and frequency of the discontinuities (Canadian Foundation Geotechnical Society, 2006).

This section provides a short review of rock mass classification/characterization systems and rock properties that are relevant to the methods selected for bearing capacity evaluation. Methods allowing engineering classification of rock mass are reviewed including the Rock Mass index (RMi) system, RMR system and the Hoek-Brown GSI.

1.8.2 Engineering Rock Mass Classification

1.8.2.1 Classification Methods

A number of classification systems have been developed to provide the basis for engineering characterization of rock masses. A comprehensive overview of this subject is provided by Hoek et al. (1995). Most of the classification systems incorporating various parameters were derived from civil engineering case histories in which all components of the engineering geological parameters of the rock mass were considered (Wickham et al., 1972; Bieniawski, 1973, 1979, 1989; Barton et al., 1974). More recently, the systems have been modified to account for the conditions affecting rock mass stability in underground mining. While no single classification system has been developed for or applied to foundation design, the type of information collected for the two more common civil engineering classification schemes—the Q system (Barton et al., 1974), used in tunnel design, and RMR (Bieniawski, 1989), used in tunnel and foundation design—are often considered. These techniques have been applied to empirical design situations, where previous experience greatly affects the design of the excavation in the rock mass. Table 9 outlines the many classification systems and their uses. Detailed descriptions of the different systems and the engineering properties associated with them are beyond the scope of this work and are restricted to the methods relevant to the current research.

The two most commonly used rock mass classification systems today are RMR, developed by Bieniawski (1973) and

Table 8. Rock mass discontinuity descriptions (Hunt, 1986).

Discontinuity	Definition	Characteristics
Fracture	A separation in the rock mass, a break.	Signifies joints, faults, slickensides, foliations, and cleavage.
Joint	A fracture or crack in rock not accompanied by dislocation.	Most common defect encountered. Present in most formations in some geometric pattern related to rock type and stress field. Open joints allow free movement of water, increasing decomposition rate of mass. Tight joints resist weathering and the mass decomposes uniformly.
Fault	A fracture along which there has been an observable amount of displacement.	Fault zones usually consist of crushed and sheared rock through which water can move relatively freely, increasing weathering. Faults generally occur as parallel to sub-parallel sets of fractures along which movement has taken place to a greater or lesser degree.
Slickenside	A smooth often striated surface produced on rock by movement along a fault or a subsidiary fracture.	Shiny, polished surfaces with striations. Often the weakest elements in a mass, since strength is often near residual.
Foliation Plane	Continuous foliation surface results from orientation of mineral grains during metamorphism.	Can be present as open joints or merely orientations without openings. Strength and deformation relate to the orientation of applied stress to the foliations.
Cleavage	The quality of a crystallized substance or rock of splitting along definite planes.	A fragment obtained by splitting along preferred planes of weakness, e.g., diamond.
Bedding Plane	Any of the division planes which separate the individual strata or beds in sedimentary or stratified.	Often are zones containing weak materials such as lignite or montmorillonite clays.
Mylonite	A fine-grained laminated rock formed by the shifting of rock layers along faults.	Fine-grained rock formed in shear zones.
Cavities	Openings in soluble rocks resulting from groundwater movement or in igneous rocks from gas pockets.	In limestone, range from caverns to tubes. In rhyolite and other igneous rocks, range from voids of various sizes to tubes.

adopted by the South African Council of Scientific and Industrial Research (CSIR), and the Norwegian Geotechnical Institute index (NGI-index or Q-system) (Barton et al., 1974). Both classification systems include Rock Quality Designation (RQD). In this study, the RMR geomechanics classification system was adopted because (1) the overwhelming majority of states evaluate RQD and utilize the RMR system (this information is based on a questionnaire presented in Chapter 3) and (2) it was favored by the available rock property data of the case histories. The Geological Strength Index (GSI), based on the RMR system and the tables from the latest versions of the Hoek-Brown failure criterion (e.g., Hoek et al., 2002), was used.

The systems presented in this report and utilized in the calibration (1) give a numerical value (have a numerical form), (2) present a result that can be used to determine/estimate the strength, (3) have been successfully used in the past, and (4) are applicable to hard rock masses. The parameters included in the classification systems resulting in a numerical value are presented in Table 10. The most commonly used parameters are the intact rock strength, joint strength, joint distance, and ground water condition. It has often been suggested that when using rock classification schemes—such as the RQD, RMR, and Q-system—only the natural discontinuities, which are of geological or geomorphic origin, should be taken into account. However, it is often difficult, if not impossible, to judge whether a discontinuity is natural or artificial after activities such as drilling, blasting, and excavation.

1.8.2.2 Rock Quality Designation (RQD)

In 1964, D. U. Deere introduced an index to assess rock quality quantitatively called RQD. RQD is a core recovery percentage that is associated with the number of fractures and the amount of softening in the rock mass that is observed from the drill cores. Only the intact pieces with a length greater than 100 mm (4 in.) are summed and divided by the total length of the core run (Deere, 1968).

$$RQD = \frac{\sum Length\ of\ core\ pieces \geq 10\ cm}{total\ core\ length} 100\,(\%) \qquad (83)$$

Table 9. Major rock classification/characterization systems (Edelbro, 2004, modified after Palström, 1995).

Name of classification	Author and first version	Country of origin	Application	Form and type [1]	Remarks
Rock Load Theory	Terzaghi, 1946	USA	Tunnels with steel supports	Descriptive F, Behavior F, Functional T	Unsuitable for modern tunneling
Stand Up Time	Lauffer, 1958	Austria	Tunneling	Descriptive F, General T	Conservative
New Austrian Tunneling Method (NATM)	Rabcewicz, 1964/65 and 1975	Austria	Tunneling in incompetent (overstressed) ground	Descriptive F, Behavioristic F, Tunneling concept	Utilized in squeezing ground conditions
Rock Quality Designation (RQD)	Deere et al., 1966	USA	Core logging tunneling	Numerical F, General T	Sensitive to orientation effects. In Deere, 1968
A Recommended Rock Classification for Rock Mechanical Purposes	Coates and Patching, 1968		For input in rock mechanics	Descriptive F, General T	
The Unified Classification of Soils and Rocks	Deere et al., 1966	USA	Based on particles and blocks for communication	Descriptive F, General T	In Deere and Deere, 1988
Rock Structure Rating (RSR) Concept[2]	Wickham et al., 1972	USA	Tunnels with steel supports	Numerical F, Functional T	Not useful with steel fiber shotcrete
Rock Mass Rating (RMR)-System, Council of Scientific and Industrial Research (CSIR)	Bieniawski, 1974	South Africa	Tunnels, mines, foundations, etc.	Numerical F, Functional T	Unpublished base case records
Q-System	Barton et al., 1974	Norway	Tunnels, large chambers	Numerical F, Functional T	
Mining RMR (MRMR)	Laubscher, 1975		Mining	Numerical F, Functional T	In Laubscher, 1977
The Typological Classification	Matula and Holzer, 1978		For use in communication	Descriptive F, General T	
[3]The Unified Rock Classification System (URCS)	Williamson, 1980	USA	For use in communication	Descriptive F, General T	In Williamson, 1984
Basic Geotechnical Description (BGD)	ISRM, 1981		For general use	Descriptive F, General T	
Rock Mass Strength (RMS)	Stille et al., 1982	Sweden		Numerical F, Functional T	Modified RMR
Modified Basic RMR (MBR)	Cummings et al., 1982		Mining	Numerical F, Functional T	
Simplified Rock Mass Rating	Brook and Dharmaratne, 1985		Mines and tunnels	Numerical F, Functional T	Modified RMR and MRMR
Slope Mass Rating (SMR)	Romana, 1985	Spain	Slopes	Numerical F, Functional T	
Ramamurthy/Arora	Ramamurthy and Arora, 1993	India	For intact and jointed rocks	Numerical F, Functional T	Modified Deere and Miller approach
Geological Strength Index (GSI)	Hoek et al., 1995		Mines, tunnels	Numerical F, Functional T	
Rock Mass Number (N)	Goel et al., 1995	India		Numerical F, Functional T	Stress-free Q-system
Rock Mass Index (RMi)	Palmström, 1995	Norway	Rock engineering communication, characterization	Numerical F, Functional T	

[1]Descriptive F = Descriptive Form: the input to the system is mainly based on descriptions. Numerical F = Numerical Form: the input parameters are given numerical ratings according to their character. Behavioristic F = Behavioristic Form: the input is based on the behavior of the rock mass in tunnel. General T = General Type: the system is worked out to serve as a general characterization. Functional T = Functional Type: the system is structured for a special application (for example, for rock support) (Palmström, 1995).

[2]RSR was a forerunner to the RMR system, although they both give numerical ratings to the input parameters and summarize them to a total value connected to the suggested support.

[3]The Unified Rock Classification System (URCS) is associated with Casagrande's classification system for soils in 1948.

Table 10. Parameters included in different classification systems resulting in a numerical value (Edelbro, 2004).

Parameters	RQD	RSR	RMR	Q	MRMR	RMS	MBR	SRMR*	SMR	**RAC	GSI	N	RMi
Block size	–	–	–	–	–	–	X	–	–	–	–	–	X
Joint orientation	–	–	X	–	–	–	X	–	–	–	–	–	X
Number of joint sets	–	–	–	X	–	X	–	–	–	–	–	X	X
Joint length	–	–	–	–	–	–	–	–	–	–	–	–	X
Joint spacing	X	X	X	X	X	X	X	X	X	X	X	X	X
Joint strength	–	X	X	X	X	X	X	X	X	X	X	X	X
Rock type	–	X	–	–	–	–	–	–	–	–	–	–	–
State of stress	–	–	–	X	X	–	X	–	–	–	–	–	–
Groundwater condition	–	X	X	X	X	X	X	X	X	–	–	X	–
Strength of intact rock	–	–	X	X	X	X	X	X	X	X	X	X	X
Blast damage	–	–	–	–	X	–	X	X	–	–	X	–	–

*SRMR = Simplified Rock Mass Rating
* *RAC - Ramamurthy and Arora Classification

RQD is used as a standard quantity in drill core logging, and its greatest value is perhaps its simplicity, low cost, and quick determination. RQD is simply a measurement of the percentage of "good" rock recovered from an interval of a borehole. The procedure for measuring RQD is illustrated in Figure 40. The recommended procedure for measuring the core length is to measure it along the centerline of the core. Core breaks caused by the drilling process should be fitted together and counted as one piece. The relationship between the numerical value of RQD and the engineering quality of the rock mass as proposed by Deere (1968) is given in Table 11.

When no cores are available, one can estimate RQD from relevant information, for instance, joint spacing (Brady and Brown, 1985). Priest and Hudson (1976) found that an estimate of RQD could be obtained from joint spacing (λ [number of joints per meter]) measurements made on an exposure by using the following:

$$RQD = 100e^{-0.1\lambda}(0.1\lambda + 1) \tag{84}$$

For $\lambda = 6$ to 16 joints/meter, the following simplified equation can be used (Priest and Hudson, 1976):

$$RQD = -3.68\lambda + 110.4 \tag{85}$$

Equations 84 and 85 are probably the simplest ways of determining RQD, when no cores are available. Palmström

(1982) presented the relationship between J_v and RQD in a clay free rock mass along a tunnel as the following:

$$RQD = 115 - 3.3 J_v \tag{86}$$

where J_v is the volumetric joint count and the sum of the number of joints per unit length for all joint sets in a clay-free rock mass. For $J_v < 4.5$, RQD = 100.

The RQD is not scale dependent and is not a good measure of the rock mass quality in the case of a rock mass with joint spacing near 100 mm. If the spacing between continuous joints is 105 mm (core length), the RQD value will be 100%. If the spacing between continuous joints is 95 mm, the RQD value will be 0%. For large-sized tunnels, RQD is of questionable value. It is, as mentioned by Douglas and Mostyn (1999), unlikely that all defects found in the boreholes would be of significance to the rock mass stability.

1.8.2.3 Rock Mass Rating (RMR)

In 1973, Bieniawski introduced RMR as a basis for geomechanics classification. The rating system was based on Bieniawski's experience in shallow tunnels in sedimentary rocks. Originally, the RMR system involved 49 unpublished case histories. Since then, the classification system has undergone several significant changes. In 1974, there was a reduction of parameters from eight to six, and, in 1975, there was an adjustment of ratings and a reduction of recommended support requirements.
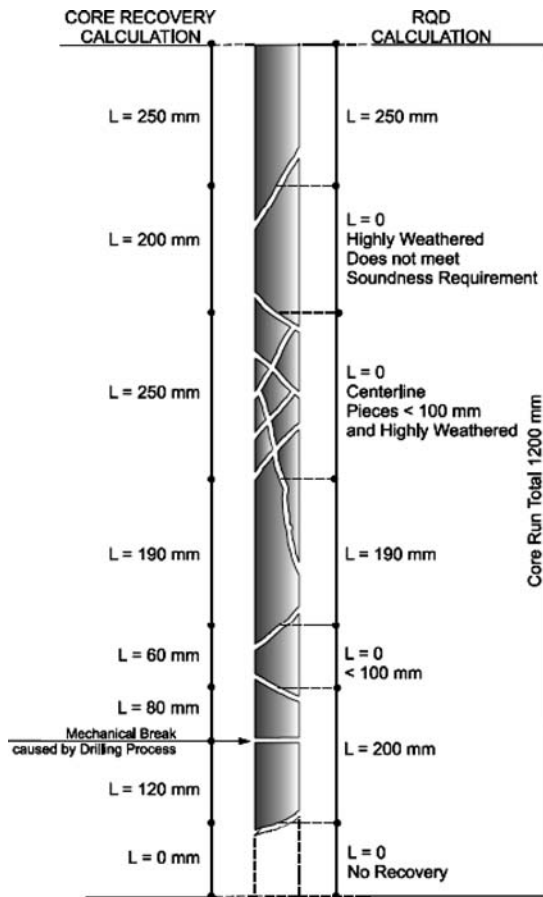
Figure 40. Procedure for measurement and calculation of rock quality designation (Sabatini et al., 2002).

In 1976, a modification of rating class boundaries (as a result of 64 new case histories) to even multiples of 20 took place, and, in 1979, there was an adoption of the International Society for Rock Mechanics (ISRM) rock mass description. The newest version of RMR is from 1989, when Bieniawski published guidelines for selecting rock reinforcement. In this version, Bieniawski suggested that the user could interpolate the RMR values between different classes and not just use discrete values. Therefore, it is important to state which version is used when RMR values are quoted. When applying this classification system, one divides the rock mass into a number of structural regions and classifies each region separately.

The RMR system uses six parameters, which are rated. The ratings are added to obtain a total RMR value. The six parameters are the following:

1. Unconfined compressive strength of intact rock material (q_u),
2. RQD,
3. Joint or discontinuity spacing (s),
4. Joint condition,
5. Ground water condition, and
6. Joint orientation.

The first five parameters represent the RMR basic parameters (RMR$_{basic}$) in the classification system. The sixth parameter is treated separately because the influence of discontinuity orientations depends upon the engineering application. Each of these parameters is given a rating that symbolizes the RQD. The first five parameters of all the ratings are algebraically summed and can be adjusted, depending on the joint and tunnel orientation, by the sixth parameter as shown in Equations 87a and 87b.

$$RMR = RMR_{basic} + \text{adjustment for joint orientation} \qquad (87a)$$

Table 11. Correlation between RQD and rock mass quality (Deere, 1968).

RQD %	Rock quality
< 25	Very Poor
25–50	Poor
50–75	Fair
75–90	Good
90–100	Excellent

Table 12. Meaning of rock mass classes and rock mass classes determined from total ratings (Bieniawski, 1978).

Parameter/properties of rock mass	Rock mass rating (rock class)				
Ratings	100–81	80–61	60–41	40–21	<20
Classification of rock mass	Very Good	Good	Fair	Poor	Very Poor
Average stand-up time	10 years for 15 m span	6 months for 8 m span	1 week for 5 m span	10 hours for 2.5 m span	30 minutes for 1 m span
Cohesion of the rock mass kPa (ksf)	> 400 (> 90)	300–400 (67.44–90)	200–300 (45–67.44)	100–200 (22.48–45)	< 100 (< 22.48)
Friction angle of the rock mass	> 45°	35°–45°	25°–35°	15°–25°	< 15°

$$\text{RMR}_{basic} = \sum \text{parameters} \left(1+2+3+4+5\right) \tag{87b}$$

The final RMR value is grouped into five rock mass classes (see Table 12 and the relevant Table 10.4.6.4-3 in the AASHTO [2008] specifications). The various parameters in the system are not equally important for the overall classification of the rock mass, since they have been given different ratings. Higher RMA indicates better rock mass condition/quality. The RMR system is very simple to use, and the classification parameters are easily obtained from either borehole data or underground mapping. Most of the applications of RMR have been in the field of tunneling, but RMR has also been applied in the stability analysis of slopes and shallow foundations, caverns, and different mining openings.

1.8.2.4 Geological Strength Index (GSI)

Hoek et al. (1995) introduced the GSI as a complement to their generalized rock failure criterion and as a way to estimate the material constants *s, a,* and m_b in the Hoek-Brown failure criterion. GSI estimates the reduction in rock mass strength for different geological conditions. The GSI has been updated for weak rock masses several times (1998, 2000, and 2001) (Hoek et al., 2002). The aim of the GSI system is to determine the properties of the undisturbed rock mass. For disturbed rock masses, compensation must be made for the lower GSI values obtained from such locations.

The strength of the rock mass depends on factors such as the shear strength of the surfaces of the blocks defined by discontinuities, their continuous length, and their alignment relative to the load direction (Wyllie, 1992). If the loads are great enough to extend fractures and break intact rock or if the rock mass can dilate, resulting in loss of interlock between the blocks, then the rock mass strength may be diminished significantly from that of the in situ rock. Where foundations contain potentially unstable blocks that may slide from the foundation, the shear strength parameters of the discontinuities should be used in design, rather than the rock mass strength.

If rock masses contain many discontinuities or are heavily jointed with discontinuities having similar strength characteristics, they can be treated as an isotropic continuum, and their strength can be estimated using methods based on a continuum approach. The strength and deformation properties of jointed rock masses can, therefore, be estimated using the Hoek-Brown failure criterion (Hoek and Brown, 1997) from three parameters (Hoek and Marinos, 2000; Marinos and Hoek, 2001):

- The unconfined compressive strength of the intact rock elements contained within the rock mass.
- A constant, m_i, which defines the frictional characteristics of the component minerals within each intact rock element.
- The GSI, which relates the properties of the intact rock elements to those of the overall rock mass (see Table 13) (Canadian Geotechnical Society, 2006).

The generalized Hoek-Brown failure criterion is defined as the following:
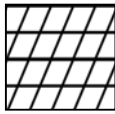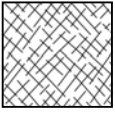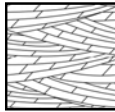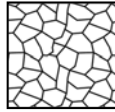
$$\sigma_1' = \sigma_3' + q_u \left(m_b \frac{\sigma_3'}{q_u} + s \right)^a \tag{88}$$

where

σ_1' and σ_3' = the principal effective stresses at failure;

q_u = the unconfined compressive strength of the intact rock pieces;

m_b = the value of the Hoek-Brown constant m for the rock mass, and $m_b = m_1 \exp\left(\frac{GSI-100}{28}\right)$;

m_i = the Hoek-Brown constant for the intact rock (see Table 14) (Canadian Geotechnical Society, 2006); and

s and a = constants that depend upon the rock mass characteristics.

For GSI > 25, $a = 0.5$, and $s = \exp\left(\frac{GSI-100}{9}\right)$. For GSI < 25, $s = 0$, and $a = 0.65 - \frac{GSI}{200}$.

L R F D   D e s i g n   a n d   C o n s t r u c t i o n   o f   S h a l l o w   F o u n d a t i o n s   f o r   H i g h w a y   B r i d g e   S t r u c t u r e

46

Table 13. GSI estimates for rock masses (Hoek and Marinos, 2000).

Geological Strength Index From the letter codes describing the structure and surface of the rock mass, select the appropriate box in this chart. Estimate the average value of the geological strength index (GSI) from the contours. Do not attempt to be too precise, i.e., quoting a range of GSI from 36 to 42 is more realistic than stating that GSI=38.	**VERY GOOD** Very rough, fresh unweathered surfaces	**GOOD** Rough, slightly weathered, iron stained surfaces	**Fair** Smooth, moderately weathered or altered surfaces	**POOR** Slickensided, highly weathered surfaces with compact coatings or fillings of angular fragments	**VERY POOR** Slickensided, highly weathered surfaces with soft clay coatings or fillings
STRUCTURE	Decreasing Surface Quality →				
BLOCKY – very well interlocked undisturbed rock mass consisting of cubical blocks formed by three orthogonal discontinuity sets.	80 / 70				
VERY BLOCKY – interlocked, partially disturbed rock mass with multifaceted angular blocks formed by four or more discontinuity sets.		60 / 50			
BLOCKY/DISTURBED – folded and/or faulted with angular blocks formed by many intersecting discontinuity sets.			40	30	
DISINTEGRATED – poorly interlocked, heavily broken rock mass with a mixture of angular and rounded rock pieces.				20	10

Decreasing Interlocking of Rock Pieces ↓

The Hoek-Brown constant (m_i) can be determined from triaxial testing of core samples using the procedure discussed by Hoek et al. (1995) or can be determined from the values given in Table 14 (Canadian Geotechnical Society, 2006). Most of the values provided in Table 14 have been derived from triaxial testing on intact core samples. The ranges of values shown reflect the natural variability in the strength of earth materials and depend upon the accuracy of the lithological description of the rock. For example, Marinos and Hoek (2001) note that the term "granite" describes a clearly defined rock type that exhibits very similar mechanical characteristics, independent of origin. As a result, m_i for granite is defined as 32±3. On the other hand, volcanic breccia is not very precise in terms of mineral composition, with the result that m_i is given as 19±5, denoting a higher level of uncertainty (Canadian Geo-

technical Society, 2006). The ranges of values depend upon the granularity and interlocking of the crystal structure. Higher values are associated with tightly interlocked and more frictional characteristics.

1.8.3 Current AASHTO (2008) Practice

The strength of intact rock material is determined using the results of unconfined compression tests on intact rock cores, splitting tensile tests on intact rock cores, or point load strength tests on intact specimens of rock. The rock is classified using the RMR system as described in Table 15. For each of the five parameters in Table 15, the relative rating based on the ranges of values provided is to be evaluated. The RMR is

Table 14. Values of the Hoek-Brown Constant (m_i) for intact rock by rock group (Marinos and Hoek, 2001).

					Silstone (7±2) Greywacke (18±3)	Claystone (4±2) Shale (6±2) Marl (7±2)
Sedimentary	Clastic		Conglomerate Breccia[1]	Sandstone (17±4)		
	Non-clastic	Carbonates	Crystalline Limestone (12±3)	Spartic Limestone (10±2)	Micritic Limestone (9±2)	Dolomite (9±3)
		Evaporites		Gypsum (8±2)	Anhydrite (12±2)	
		Organic				Chalk (7±2)
Metamorphic	Non-foliated		Marble (9±3)	Hornfels (19±4) Meta Sandstone (19±3)	Quartzite (20±3)	
	Slightly foliated		Migmatite (29±3)	Amphibolite (26±6)	Gneiss (28±5)	
	Foliated[2]			Schist (12±3)	Phyllite (7±3)	Slate (7±4)
Igneous	Plutonic	Light	Granite (32±3) Granodiorite (29±3)	Diorite (25±5)		
		Dark	Gabbro (27±3) Norite (20±5)	Dolerite (16±5)		
	Hypabyssal		Porphyry (20±5)		Diabase (15±5)	Peridotite (25±5)
	Volcanic	Lava		Ryolite (25±5) Andesite (25±5)	Dacite (25±3) Basalt (25±5)	
		Pyroclastic	Agglomerate (19±3)	Breccia (19±5)	Tuff (13±5)	

Notes:

Values in parentheses are estimates.

[1] Conglomerates and breccias may have a wide range of values, depending on the nature of the cementing material and the degree of cementation. Values range between those of sandstone and those of fine-grained sediments.

[2] These values are for intact rock specimens tested normal to bedding or foliation. Values of m_i will be significantly different if failure occurs along a weakness plane.

determined as the sum of all five relative ratings. The RMR should be adjusted in accordance with the criteria in Table 16. The rock classification should be determined in accordance with Table 17. Emphasis is placed on visual assessment of the rock and the rock mass because of the importance of the discontinuities in rock. The geomechanics classification can be used to estimate the value of GSI for cases where RMR is greater than 23, as follows:

$$GSI = RMR_{89} - 5 \tag{89}$$

where RMR_{89} = RMR according to Bieniawski (1989) as presented in Table 17. For RMR_{89} values less than 23, the modified Tunneling Quality Index (Q') is used to estimate the value of GSI:

$$Q' = \frac{RQD}{J_n} \times \frac{J_r}{J_a} \tag{90}$$

where

J_n = number of sets of discontinuities,

J_r = roughness of discontinuities, and

J_a = discontinuity condition and infilling.

$$GSI = 9 \log_e Q' + 44 \tag{91}$$

Table 18 gives the values of the parameters used to evaluate Q' in Equation 90.

The determination of the shear strength of fractured rock masses is essential in foundation design analyses. The Hoek and Brown criteria can be used to evaluate the shear strength of fractured rock masses in which the shear strength is represented as a curved envelope that is a function of the unconfined compressive strength of the intact rock, q_u, and two dimensionless constants, m and s. The values of m and s as defined in Table 19 should be used. The shear strength of the rock mass should be determined using the method

Table 15. Geomechanics classification of rock masses (AASHTO, 2008, Table 10.4.6.4-1).

	PARAMETER		RANGES OF VALUES						
1	Strength of intact rock material	Point load strength index	>175 ksf	85–175 ksf	45–85 ksf	20–45 ksf	For this low range, unconfined compressive test is preferred		
		Unconfined compressive strength	>4,320 ksf	2,160–4,320 ksf	1,080–2,160 ksf	520–1,080 ksf	215–520 ksf	70–215 ksf	20–70 ksf
	Relative Rating		15	12	7	4	2	1	0
2	Drill core quality RQD		90% to 100%		75% to 90%	50% to 75%	25% to 50%		<25%
	Relative Rating		20		17	13	8		3
3	Spacing of joints		>10 ft		3–10 ft	1–3 ft	2 in–1 ft		<2 in
	Relative Rating		30		25	20	10		5
4	Condition of joints		• Very rough surfaces • Not continuous • No separation • Hard joint wall rock		• Slightly rough surfaces • Separation <0.05 in • Hard joint wall rock	• Slightly rough surfaces • Separation <0.05 in • Soft joint wall rock	• Slicken-sided surfaces or • Gouge <0.2 in thick or • Joints open 0.05–0.2 in • Continuous joints		• Soft gouge >0.2 in thick or • Joints open >0.2 in • Continuous joints
	Relative Rating		25		20	12	6		0
5	Ground water conditions (use one of the three evaluation criteria as appropriate to the method of exploration)	Inflow per 30 ft tunnel length	None		<400 gal/hr		400–2,000 gal/hr		>2,000 gal/hr
		Ratio = joint water pressure/ major principal stress	0		0.0–0.2		0.2–0.5		>0.5
		General Conditions	Completely Dry		Moist only (interstitial water)		Water under moderate pressure		Severe water problems
	Relative Rating		10		7		4		0

Table 16. Geomechanics rating adjustment for joint orientations (AASHTO, 2008, Table 10.4.6.4-2).

Strike and dip orientations of joints		Very favorable	Favorable	Fair	Unfavorable	Very unfavorable
Ratings	Tunnels	0	–2	–5	–10	–12
	Foundations	0	–2	–7	–15	–25
	Slopes	0	–5	–25	–50	–60

Table 17. Geomechanics rock mass classes determined from total ratings (AASHTO, 2008, Table 10.4.6.4-3).

RMR rating	100–81	80–61	60–41	40–21	<20
Class No.	I	II	III	IV	V
Description	Very good rock	Good rock	Fair rock	Poor rock	Very poor rock

developed by Hoek (1983) and Hoek and Brown (1988, 1997) as follows:

$$\tau = (\cot\phi_i' - \cos\phi_i')m\frac{q_u}{8} \qquad (92)$$

where

τ = the shear strength of the rock mass (ksf),

q_u = average unconfined compressive strength of rock core (ksf),

m, s = constants from Table 19,

σ_n' = effective normal stress (ksf), and

ϕ_i' = the instantaneous friction angle of the rock mass (degrees):

$$\phi_i' = \tan^{-1}\left\{4h\cos^2\left[30+0.33\sin^{-1}\left(h^{\frac{-3}{2}}\right)\right]-1\right\}^{\frac{-1}{2}}$$

$$h = 1 + \frac{16(m\sigma_n' + sq_u)}{3m^2 q_u}$$

When a major discontinuity with a significant thickness of infilling is to be investigated, the shear strength is governed by the strength of the infilling material and the past and expected future displacement of the discontinuity. The elastic modulus of a rock mass (E_m) is taken as the lesser of the intact modulus

of a sample of rock core (E_i) or the modulus determined from one of the following equations:

$$E_m = 145\left(10^{\frac{RMR-10}{40}}\right) \qquad (93)$$

where

E_m = elastic modulus of the rock mass (ksi),

$E_m \le E_i$,

E_i = elastic modulus of intact rock from tests (ksi), and

RMR = rock mass rating.

or

$$E_m = \left(\frac{E_m}{E_i}\right)E_i \qquad (94)$$

where E_m is the elastic modulus of the rock mass (ksi), and E_m/E_i is a reduction factor based on RQD determined from Table 20 (dim.).

For critical or large structures, determination of rock mass modulus (E_m) using in situ tests may be warranted. It is extremely important to use the elastic modulus of the rock mass for computation of displacements of rock materials under applied loads. Use of the intact modulus will result in unrealistic and unconservative estimates. Poisson's ratio for

Table 18. Joint parameters used to determine Q' (Barton et al., 1974).

1. No. of sets of discontinuities = J_n	
Massive	0.5
One set	2
Two sets	4
Three sets	9
Four or more sets	15
Crushed rock	20

2. Roughness of Discontinuities = J_r	
Noncontinuous joints	4
Rough, wavy	3
Smooth, wavy	2
Rough, planar	1.5
Smooth, planar	1
Slick and planar	0.5
Filled discontinuities	1

3. Discontinuity condition and infilling = J_a	
3.1 Unfilled cases	
Healed	0.75
Stained, no alteration	1
Silty or sandy coating	3
Clay coating	4
3.2 Filled discontinuities	
Sand or crushed rock infill	4
Stiff clay infilling < 5 mm	6
Soft clay infill < 5 mm thick	8
Swelling clay < 5 mm	12
Stiff clay infill > 5 mm thick	10
Soft clay infill > 5 mm thick	15
Swelling clay > 5 mm	20

Note: Add + 1 if mean joint spacing > 3 m.

Table 19. Approximate relationship between rock mass quality and material constants used in defining nonlinear strength (Hoek and Brown, 1988; AASHTO, 2008, Table 10.4.6.4-4).

Rock quality	Constants	Rock type A = Carbonate rocks with well developed crystal cleavage— *dolomite, limestone, and marble* B = Lithified argrillaceous rocks—*mudstone, siltstone, shale, and slate (normal to cleavage)* C = Arenaceous rocks with strong crystals and poorly developed crystal cleavage—*sandstone and quartzite* D = Fine grained polyminerallic igneous crystalline rocks— *andesite, dolerite, diabase, and rhyolite* E = Coarse-grained polyminerallic igneous and metamorphic crystalline rocks—*amphibolite, gabbro, gneiss, granite, norite, quartz-diorite*				
		A	B	C	D	E
INTACT ROCK SAMPLES Laboratory size specimens free from discontinuities. CSIR rating: *RMR* = 100	m s	7.00 1.00	10.00 1.00	15.00 1.00	17.00 1.00	25.00 1.00
VERY GOOD QUALITY ROCK MASS Tightly interlocking undisturbed rock with unweathered joints at 3–10 ft. CSIR rating: *RMR* = 85	m s	2.40 0.082	3.43 0.082	5.14 0.082	5.82 0.082	8.567 0.082
GOOD QUALITY ROCK MASS Fresh to slightly weathered rock, slightly disturbed with joints at 3–10 ft. CSIR rating: *RMR* = 65	m s	0.575 0.00293	0.821 0.00293	1.231 0.00293	1.395 0.00293	2.052 0.00293
FAIR QUALITY ROCK MASS Several sets of moderately weathered joints spaced at 1–3 ft. CSIR rating: *RMR* = 44	m s	0.128 0.00009	0.183 0.00009	0.275 0.00009	0.311 0.00009	0.458 0.00009
POOR QUALITY ROCK MASS Numerous weathered joints at 2 to 12 in; some gouge. Clean compacted waste rock. CSIR rating: *RMR* = 23	m s	0.029 3×10^{-6}	0.041 3×10^{-6}	0.061 3×10^{-6}	0.069 3×10^{-6}	0.102 3×10^{-6}
VERY POOR QUALITY ROCK MASS Numerous heavily weathered joints spaced < 2 in with gouge. Waste rock with fines. CSIR rating: *RMR* = 3	m s	0.007 1×10^{-7}	0.010 1×10^{-7}	0.015 1×10^{-7}	0.017 1×10^{-7}	0.025 1×10^{-7}

rock is determined from tests on intact rock core. Where tests on rock core are not practical, Poisson's ratio may be estimated from Table 21.

1.8.4 Summary

A common way of determining the rock mass strength is by using a failure criterion. The existing rock mass failure criteria are stress dependent and often include one or several parameters that describe the rock mass properties. These parameters are usually based on classification or characterization systems. The unconfined compressive strength, block size and shape, joint strength, and a scale factor are the most important parameters that should be used when estimating the rock mass strength. Based on findings, selected systems and criteria have been discussed in this chapter. These include RMR, GSI, and the Hoek-Brown criterion. GSI is similar to RMR, but incorporates newer versions of Bieniawski's original system (Bieniawski 1976, 1989). The Hoek-Brown criterion is the most widely used failure criterion for estimating the strength of jointed rock masses despite its lack of a theoretical basis and the limited amount of experimental data that went into the first development of the criterion (Sjöberg, 1997).

Table 20. Estimation of E_m based on RQD (O'Neill and Reese, 1999; AASHTO, 2008, Table 10.4.6.5-1).

RQD (percent)	E_m/E_i	
	Closed joints	Open joints
100	1.00	0.60
70	0.70	0.10
50	0.15	0.10
20	0.05	0.05

Table 21. Summary of Poisson's Ratio for intact rock (AASHTO, 2008, Table C10.4.6.5-2, modified after Kulhawy, 1978).

Rock type	No. of values	No. of rock types	Poisson's Ratio, ν			Standard deviation
			Minimum	Maximum	Mean	
Granite	22	22	0.39	0.09	0.2	0.08
Gabbro	3	3	0.2	0.16	0.18	0.02
Diabase	6	6	0.38	0.2	0.29	0.06
Basalt	11	11	0.32	0.16	0.23	0.05
Quartzite	6	6	0.22	0.08	0.14	0.05
Marble	5	5	0.4	0.17	0.28	0.08
Gneiss	11	11	0.4	0.09	0.22	0.09
Schist	12	11	0.31	0.02	0.12	0.08
Sandstone	12	9	0.46	0.08	0.2	0.11
Siltstone	3	3	0.23	0.09	0.18	0.06
Shale	3	3	0.18	0.03	0.09	0.06
Limestone	19	19	0.33	0.12	0.23	0.06
Dolostone	5	5	0.35	0.14	0.29	0.08

C H A P T E R   2

Research Approach

2.1 Scope and Structure

NCHRP Project 24-31 was structured under two major units, each leading to a key requirement in the accomplishment of the final objective. This section describes the conceptual method of approach behind each of the units. Flow charts merging the various activities are provided to elucidate the interrelations of the activities.

2.1.1 Unit I

Unit I involved assembly and assessment of knowledge and data with the final goal of establishing (1) databases, (2) design methods and alternative design methods, (3) typical structures and case histories, and (4) expected load ranges and their distributions.

Figure 41 provides a flow chart of Unit I(a) outlining the research plan for establishing the state of practice in design and construction as well as case histories and loading. Figure 42 provides a flow chart of Unit I(b), addressing the establishment of databases allowing for the statistical parameters required for the calibrations that are addressed in Unit II. The material required for the statistical parameters for the calibration was assembled in Unit I. In the direct Resistance Factor Approach (RFA) implemented in this research, the focus is on the uncertainty of the model (to be discussed further in the following section); hence, the parameters required for calibration are obtained from analysis of databases of case histories. The utilization of the data and knowledge assembled in Unit I along the bearing capacity evaluation for the calibration of the design methods is addressed in Unit II.

2.1.2 Unit II

The data and methods established in Unit I are analyzed in Unit II with the following goals: (1) establishment of the uncertainty of the methods and parameters including the inves-

tigation of their sources, (2) development of resistance factors and examination of them in design cases, (3) development of final resistance factors and the conditions for their implementation, and (4) development of the specifications.

Unit II was subdivided along the geotechnical challenges considering the design of shallow foundations on soil and rock. Unit II(a) addresses the effort required for the development of resistance factors for shallow foundations constructed on granular soils, outlined in Figure 43. A separation is made between foundations subjected to centric vertical loads only and foundations subjected to inclined and/or eccentric loads. This separation is associated with the nature of the databases, the parameters that can be obtained in each case, and the complexity of inclined/eccentric loading discussed in Section 1.6 of this report. Unit II(b) addresses the effort required for the development of resistance factors for shallow foundations on rock as outlined in Figure 44.

2.1.3 Additional Topics

The outlined method of approach addresses the conditions and difficulties associated with the prevailing design and construction practices of shallow foundations for bridges and their systematic adaptation to LRFD. The presented scope reflects budget restrictions and needs in addressing the most urgent issues as directed by the research panel. Topics such as foundations on cohesive soils or friction-cohesive soils (ϕ'-c materials) materials will require, therefore, additional effort. Other pertinent conditions like foundation sliding, footings on slopes, and two-layer soil systems were addressed in various detail depending on importance and the available information.

2.2 Methodology

Section 1.4 reviewed the format for the design factors. The resistance factor approach (RFA) was adopted in this study following previous NCHRP deep foundation LRFD database

Existing AASHTO Specifications and FHWA Manuals
- AASHTO (2006)
- FHWA Reference Manual, Munfakh et al., 2001
- FHWA GEC No. 6, Kimmerling, 2002
- FHWA Spread Footings of Highway Bridges, Gifford et al., 1987
- FHWA Soils & Foundations Workshop Manual, Cheney & Chassie, 1982

Available Questionnaires of Foundations Design Methods and Construction Practices
NCHRP Report 507, Paikowsky et al., 2004
NCHRP Project 12-66, Paikowsky et al., 2005

Review Design Cases Used in NCHRP Project 12-66

Examination of Lateral Loads Data on Structures

Design Cases in Manuals
- FHWA GEC No. 6, Kimmerling, 2002
- FHWA Soils & Foundation Workshop Manual, Cheney & Chassie, 1982
- FHWA RD-86/185, Gifford et al., 1987

NCHRP Project 24-31 Questionnaire Determination of DOT Design Methods and Construction Practices of Shallow Foundations

Examination of Load Ranges and Statistics of Horizontal and Vertical Loading for the Typical Design Examples and Case Histories

UDE Institute of Soil Mechanics & Foundation Engineering

Determination of Alternative Design Methods

- Gifu Univ., Japan
- Japan Geotech. Soc.
- International Society of Soil Mechanics and Foundation Engineering

Established:
- AASHTO/FHWA and DOTs' Design Methods
- Complementary and/or Alternative Design Methods
- Typical Structures under Common Construction Practices
- Design Cases
- Load Ranges and their Distributions

Figure 41. Flowchart outlining the research plan for Unit I(a) establishing design methods, construction practices, design cases, and loads.

Literature Identifying Additional Shallow Foundation Load Tests

- 31 Data Cases Collected at Cornell (Prakoso, 2002)
- 39 Data Cases Collected at MIT (Zhang and Einstein, 1998)

Institute of Soil Mechanics & Foundation Engineering UDE Germany Load Testing Program

Existing UML/GTR Shallow Foundation Database
329 Load Test Cases

Database III
Loading of Shallow Foundations on Rock

Database II
Vertical Inclined & Eccentric Loading of Shallow Foundations on Granular Soils

Database I
Vertical-Centric Loading of Shallow Foundations on Granular Soils

Data Solicitation from DOTs across the USA

Figure 42. Flowchart outlining the research plan for Unit I(b) establishing databases for shallow foundation load tests.

Figure 43. Flowchart outlining the research plan for Unit II(a) to develop LRFD parameters for the ULS design of shallow foundations on granular soils.

calibrations (Paikowsky et al., 2004). Figures 45 and 46 illustrate the sources of uncertainty and principal differences between probability-based design (PBD) application to the design of a structural element of the superstructure and to a geotechnical design of a foundation in the substructure. If one considers a bridge girder as a simple supported beam under the assumption of a homogenous cross-section, a horizontal symmetry line, and beam height, h, one can accurately calculate moments (hence, stresses) and deflections in the beam. The major source of uncertainty is the loading (especially the live and extreme event loading on the bridge); the material properties and physical dimensions present relatively less
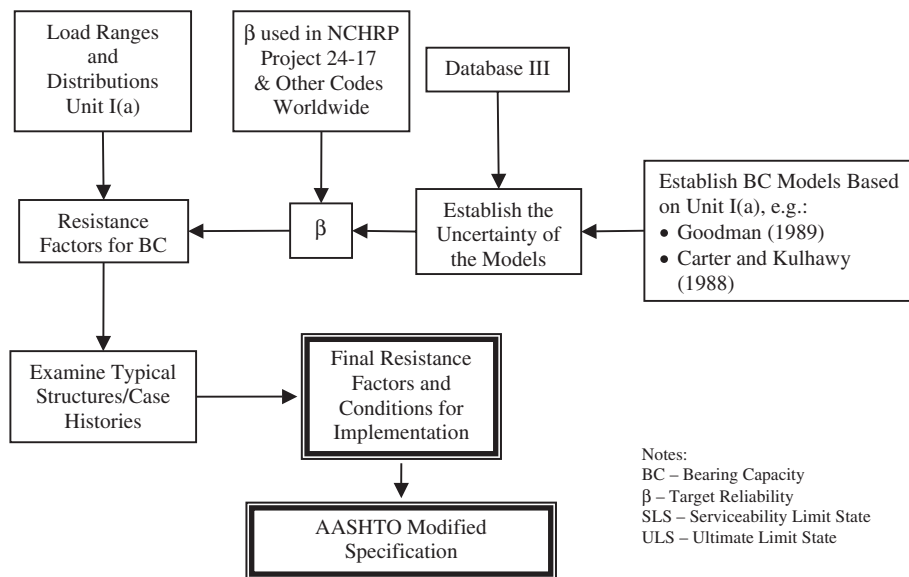
Figure 44. Flow chart outlining the research plan for Unit II(b) to develop LRFD parameters for the ULS of shallow foundations on rock.

loading

$A = B = \dfrac{ql}{2}$ shear

Sources of Uncertainty
- Loading (q)
- Dimensions/Geometry (l, h, I)
- Material Properties (E)

moment

$M_{max} = \dfrac{ql^2}{8}$

Most Noticeable:
1. No uncertainty in the model—under given loading conditions the uncertainty in the material properties dictates the uncertainty in strength and deflection
2. Largest uncertainty in the loading, source, magnitude, and distribution (in case of bridges)

deflection

y

$y_{max} = \dfrac{5}{384}\dfrac{ql^4}{EI} = \dfrac{5}{24}\dfrac{\sigma_{max}}{E}\dfrac{l^2}{h}$

(Assuming homogenous cross-section, horizontal symmetry line, and beam height, h)

Figure 45. Simplified example of a beam design and associated sources of uncertainty.

Soil sampling and testing for engineering material parameters

Analysis model

Assumed Failure Pattern under Foundations

Method of Approach
- **LOAD** Use the load uncertainty from the structures (until better research is done)

- **RESISTANCE** Establish the uncertainty of the "complete" foundation resistance (capacity) analysis (including established procedures for parameters) by comparing a design procedure to measured resistance (failure)

Uncertainty in the assumptions made in the model development leaves unknown analysis versus actual performance

Uncertainty due to site, material and testing variability, and estimation of parameters

Loading

Code of practice

AASHTO LRFD Bridge Design Specifications
Customary U.S. Units
4th Edition
2007

FOUNDATION DESIGN

Traditional design, although developed over many years and used as a benchmark, has undocumented, unknown uncertainty

Sources of Uncertainty
- Material properties and strength parameters
- Resistance model
- Loading

Figure 46. Components of foundation design and sources of uncertainty.

uncertainty. Figure 46 (borrowing from the concept presented by Ovesen, 1989) demonstrates the higher degree of uncertainty associated with the design of a foundation. The material properties are based on subsurface investigation and direct or indirect parameter evaluation. The loading of the foundation and its distribution is mostly unknown as only limited information has ever been gathered on loading at the foundation level. Because of this, the loading uncertainty is assumed as that attributed to the design of the structural element. The main difficulty associated with the design of a foundation in comparison with the design of a structural element remains with the analysis model. While the calculation model in the structural element is explicit (although becoming extremely complex and less definite as the element evolves in geometry and composition and requires the interaction with other units), the analysis model for the evaluation of the soil resistance (i.e., bearing capacity) is extremely uncertain due to the assumptions made during its establishment and the empirical data on which it is based. As such, the uncertainty of the geotechnical resistance model controls the resistance evaluation of the foundation.

The concept adopted in this research (similar to that adopted by Paikowsky et al., 2004, for deep foundations) focused, therefore, on the calibration of selected bearing capacity (resistance) models as a complete unit while reducing other associated sources of uncertainty by following specific procedures, e.g., soil parameter establishment. This approach is discussed in Section 1.4, and demonstrated in the examples presented in Sections 1.4.4 and 1.4.5. The systematic analysis of many case histories via a selected resistance model and their comparison to measured resistance provided the uncertainty of the model application, but also included in it the influence of the different sites from which the data were obtained as well as the uncertainty associated with the "measured" resistance.
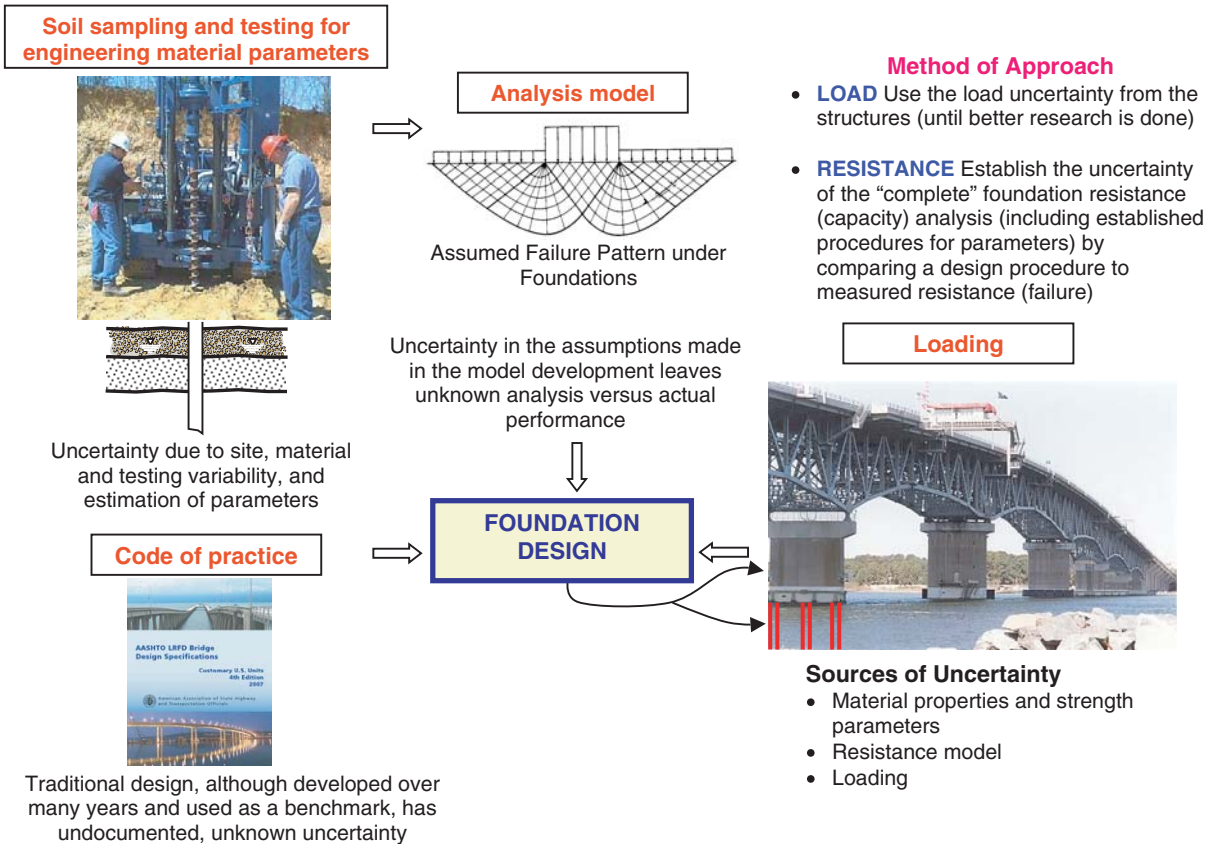
The assumption that the uncertainty obtained by the process discussed above represents the variability of the model application for a specific foundation analysis (i.e., the resistance variability as depicted in Figures 1 and 3) is reasonable and has proven successful although it may contain some conservatism, depending on the quality and reliability of the database cases. The calibration, referring to soil type, specific model, and pile type combination as applied previously to deep foundations, has proven extremely effective compared to arbitrary selection of parameters or WSD back-calculated values that defeat the PBD principles as demonstrated in Section 1.4.4. The present calibration is composed mostly of adopting the vertical load statistics established in NCHRP Project 24-17 (Paikowsky et al., 2004) and new development of horizontal load statistics and resistance for design methodologies based on the state of practice established as outlined above.

The detailed calibration methodology and process are presented in Section 4.3.

2.3 Execution and Presentation

1. The execution of Unit I(a) (see Section 2.1, Figure 41) resulted in the selection of the bearing capacity equations to be analyzed, i.e., established the (calculated) limit state equations to be evaluated. Section 3.1 outlines the findings for establishing the state of practice in design and construction leading to Section 3.4 presenting the selected bearing capacity methodology for soils and Section 3.8 the bearing capacity methodology for foundations on rock.
2. The execution of Unit I(b) (see Section 2.1, Figure 42) resulted in the development of case history databases, presented in Section 3.2. Examination and determination of the measured strength limit state in these database case histories are described in Sections 3.3, 3.6, and 3.7. Comparison of the calculated strength limit state (defined in Item 1 above) to the measured strength limit state resulted in the statistical parameters of the resistance distribution functions. These are described in Sections 3.5, 3.6, and 3.7. The distribution functions of the loads are defined and established in Section 4.2.
3. Selection of target reliability is described in Section 4.3.2.
4. The development of resistance factors is described in Chapter 4 with summaries presented in Sections 4.10 and 4.13 for foundations in/on granular soil and rock, respectively.

C H A P T E R   3

Findings

3.1 Design and Construction State of Practice

3.1.1 Questionnaire and Interviews

Code development requires examining the state of practice in design and construction in order to address the needs, research the performance, and examine alternatives. The identification of current design and construction methodologies was carried out via a questionnaire. A six-page questionnaire concerning the design and construction practices of highway departments was developed and distributed in June 2007 to 161 state highway officials, TRB representatives, state and FHWA bridge engineers, and bridge engineers from Canadian Provinces. Appendix C provides a copy of the questionnaire.

3.1.2 Summary of the Questionnaire Response

A total of 40 surveys was returned and analyzed (39 states and 1 Canadian province, see Table C-1 in Appendix C). The survey elicited information concerning foundation alternatives and shallow foundation design. The questionnaire was followed by telephone interviews with geotechnical engineers of selected states determined based on information gathered in the responses. Appendix C provides a summary of the responses obtained for the questionnaire in the form of two summary tables and a summary of the responses. The original form was used as a basis for the summary encompassing all responses. The percent (%) values provided relate to the arithmetic average of the responding states and province (Alberta, Canada) for the specific item.

3.1.3 Summary of Major Findings— Foundation Alternatives

Among survey respondents, the use of foundations by type was the following: shallow foundations were used by 17%, driven piles were used by 59%, and drilled foundations were used by 24%. The use of shallow foundations was not changed overall relative to the last survey (conducted under NCHRP Project 12-66). There is a consistent trend, however, in the decrease of the use of driven piles—75%, 62%, and 59% for 1999, 2004, and 2007, respectively—and the increase of the use of drilled foundations—11%, 21%, and 24% for 1999, 2004, and 2007, respectively (1999 data from Paikowsky et al., 2004; 2004 data from NCHRP Project 12-66). There is some discrepancy between the total foundation use and the percentage of use specifically addressing piers and abutments. Some of this discrepancy can be attributed to the fact that all foundations include non-bridge structures like buildings, posts, and sound barriers. The average use presented above changes significantly across the country as shown in Table C-2 that relates to bridge foundations only (with average use of 17.7% for abutments and piers). The use of shallow foundations in the Northeast exceeds by far the use of shallow foundations in all other regions of the United States—40% in New York, New Jersey, and Maine; 47% in New Hampshire; 50% in Vermont; 53% in Massachusetts; 65% in Pennsylvania; and 67% in Connecticut. Other "heavy users" are Tennessee (63%), Washington (30%), Nevada (25%), and Idaho (20%). In contrast, out of the 39 responding states, 6 states do not use shallow foundations for bridges at all, and an additional 8 states use shallow foundations in 5% or less of highway bridge foundations.

3.1.4 Summary of Findings—Subsurface Conditions for Shallow Foundations

The summary provided in Appendix C indicates that 55.8% of shallow foundations are built on rock (average of piers and abutments) with an additional 16.8% on Intermediate Geomaterial (IGM); hence, 72.6% of foundations are built on rock or cemented soils and only 27.4% are built on soils (24.2% are built on granular soils and 3.2% are built on clay

or silt). A further breakdown is presented in Table C-2, allowing clarification of the practices of the different states. For example, Michigan indicated that 50% of its shallow foundations at the piers' location are built on fine-grained soils; however, Michigan is using only 5% of its pier foundations on shallow foundations; hence, only 2.5% of the pier foundations are built on clay or silt. Examining all the states this way suggests that the state leading in building bridge foundations on clay is Washington (6%) followed by Vermont (5%), Idaho (4%), and Michigan and Nevada (3.75%) each. Further examination of these facts (in a telephone interview) revealed that Washington's use of foundations on silt and clay refers to highly densified glacial soils with SPT N values exceeding 30 for silts and between 40 to 100 for the clays.

Twenty-eight states (out of 39) do not build shallow foundations for bridges on cohesive soils at all; hence, only 0.8% of all bridge shallow foundations are built on clay or silt (including Washington), in comparison to 16.9% on rock, 5.4% on IGM, and 12.2% on frictional soils. The survey also suggests that only about 60% of the foundations on clay were built without ground improvement measures; hence, only about 0.48% of the bridges were actually built on shallow foundations on cohesive soils, practically a marginal number considering the state of these soils as described by Washington State Department of Transportation (WSDOT).

3.1.5 Summary of Findings—Design Considerations

3.1.5.1 Foundations on Rock

Findings for foundations on rock are the following:

1. About 90% of the states using foundations on rock obtain rock cores, evaluate RQD, and conduct uniaxial (unconfined) compressive strength tests.
2. About 19% of the states using foundations on rock use presumptive values alone, 22% use engineering analyses alone, and 59% use both when evaluating bearing capacity.
3. Fifty-three percent (53%) of the states use AASHTO's presumptive values. Other states use or consult the *Canadian Foundation Engineering Manual* (2006), NY Building Code (International Code Council, 2008), or NAVFAC (1986), or base their capacity values on local experience (e.g., South Dakota, Wisconsin, Oregon, Kansas, Iowa, and Arkansas).
4. Seventy percent (70%) of the responding states would like to see a specific analytical method presented for the evaluation of the bearing capacity of foundations on rock. Twenty-five percent (25%) use the Kulhawy and Goodman (1987) analytical method and 33% use the Carter and Kulhawy (1988) semi-empirical design method. Others use Kulhawy and Goodman (1980), Hoek-Brown (1997),

and Hoek and Marinos (2000). Two states commented on using GSI instead of RMR.

5. Sixty percent (60%) evaluate failure by sliding for footings on rock. Seven states do not evaluate sliding because of a requirement to "wedge" the foundation into the rock either by a key (Alabama—1 to 2 ft, Alaska—1.5 to 2.0 ft, North Carolina) or some other method (Iowa—notched in rock, Minnesota—using dowels, Pennsylvania—footings embedded 1 ft below top of rock, and Maryland—"seat" footings in the rock). Those that evaluate sliding use various methods and margins of safety (ϕ): Idaho—$\phi = 0.5$, Ohio and Indiana—factor of safety = 1.5, New Hampshire—F.S. = 1.5 and $\phi = 0.8$, Washington—F.S. = 1.5 and $\phi = 0.67$, Alberta Canada—$\phi = 0.8$ (friction) and $\phi = 0.6$ (cohesion). Maine specified that sliding for Strength I is done by using minimum vertical load and maximum horizontal load and $\phi = 0.8$ (based on footings on sand). Nevada specified that they use the limit equilibrium method per FHWA "Rock Slopes" with superimposed foundation loading. F.S. = 1.5 for static conditions and F.S. = 1.1 for seismic.
6. Seventy percent (70%) of the states do not analyze lateral displacement of shallow foundations on rock because they use limiting measures (key way, dowling, etc.) as described above. New York specifies geologic inspection during construction to ensure rock quality, and key way or dowelling is ordered if necessary.
7. Seventy-five percent (75%) of the responding states limit the eccentricity of footings on rock. Most of the states follow AASHTO recommendations for $e/B \leq \frac{3}{8}$. Some (Idaho, Iowa, Michigan, North Carolina, Ohio, Wisconsin, and Massachusetts) use $e/B \leq \frac{1}{4}$ based on the FHWA "Soils and Foundations Manual" that also meets the AASHTO standards specification. Wyoming, South Dakota, and Alberta (Canada) use $e/B \leq \frac{1}{6}$, with Alberta specifying that either eccentricity is maintained within limits or an effective foundation size is used in which the dimensions are reduced by twice the eccentricity (e.g., $B' = B - 2e$).
8. Seventy percent (70%) of the states do not analyze settlement of footings on rock as it is not seen as an issue of importance and the settlement is limited to 0.5 in. Twenty-eight percent (28%) use AASHTO procedures for broken/jointed rock, with Nevada also using Kulhawy and Goodman (1987) and the Army EM 110-1-2908 (1994).

3.1.5.2 Foundations on Soil

Findings for foundations on soil are the following:

1. All states using shallow foundations on soils follow either AASHTO's LRFD or ASD guidelines. Only a small number of responders use presumptive values. Fifty-eight percent (58%) use the theoretical general bearing capacity equation.

2. Fifty-three percent (53%) of the responders find it reasonable to omit the load inclination factors and 63% limit the eccentricity of the footing mostly with $e/B \leq \frac{1}{6}$ to $\frac{1}{4}$ (standard specifications $e/B = \frac{1}{6}$, LRFD specifications $e/B = \frac{1}{4}$). Massachusetts responded that load inclination factors must be used in the final design of the footing. Pennsylvania commented that when inclination factors were considered together with factored loads, it resulted in an increased footing size; hence, unfactored loads are used.

3. Forty-five percent (45%) do not decrease the soil's strength parameters considering punching shear, while 23% do so. Seven states commented that punching shear is not a viable option as foundations are not built on loose soil conditions or, alternatively, settlement criteria prevail, especially under such conditions.

4. Fifty-eight (58%) use the AASHTO procedures presented for footings on a slope. Nevada, Idaho, and Michigan commented that the charts are not clear and need to be improved. Washington and North Carolina commented on the use of Meyerhoff's method, also presented by the Navy Design Manual (NAVFAC, 1986), essentially identical to the AASHTO presentation. Oregon commented that the provided foundations on slope analysis result in a reasonable approach (somewhat conservative) while Pennsylvania commented that experience shows that sometimes this analysis results in a drastically larger footing.

5. Thirty percent (30%) of the responding states do not use the AASHTO procedures for footings on a layered soil, while 38% of the responders do use these procedures. Eighteen states commented on the procedures. Idaho, Michigan, Vermont, and Wisconsin commented that they calculate the bearing capacity for the layer with the lower strength. Iowa and Oregon commented that under such conditions alternative foundation solutions are examined.

6. Only 28% (with 40% responding "No") of the responders use the semi-empirical procedures described in Section 10.6.3.1.3 of AASHTO's LRFD Bridge Specifications for evaluation of bearing capacity. The majority of the states that commented on the procedure expressed the opinion that the method is used for a rough evaluation, only as an initial estimation and/or in comparison to other methods. Oregon commented that the SPT method usually yields higher capacity and settlement controls the design.

7. Nineteen states responded when asked for comments about the currently existing resistance factors being all about the same value. Some states stated that they don't have enough experience with LRFD to judge the resistance factor values. North Carolina and New Hampshire suggested combining all resistance factors to be 0.45, while Oregon, Pennsylvania, Vermont, and Washington com-

mented that the resistance factors are in line with the factor of safety range (2.5 to 3.0) used in the ASD methodology and hence result in a design similar to that obtained using ASD.

8. Seventy percent (70%) evaluate failure by sliding, with about half (33%) using the full foundation area and 30% using the effective foundation area.

9. Only 13% consider passive resistance for the lateral resistance of the shallow foundations and all utilize a limited value due to a limited displacement. Many responding states expressed concern with a long-term reliance on a passive resistance. Washington commented that it is rarely used to meet the sliding criterion of extreme events, and Minnesota commented it is used in front of shear keys only.

10. Traditionally no safety margin is provided to settlement analysis although it typically controls the size of shallow foundations. When asked about it, 35% answered that the issue should not be of concern and 25% answered that it should. Of those who responded, some recognized that safety margin needs to be researched (Connecticut, Michigan, and Tennessee) while others hold the notion that a safety margin on bearing capacity already addresses the issue (Hawaii, Maine, New Jersey, North Carolina, and Washington) or that settlement calculations are conservative to begin with (New Hampshire and North Carolina).

11. Only two states stated that they conduct plate load tests: one state (Connecticut) referred to tests from over 20 years ago, and the other state referred to three recent tests (Massachusetts).

12. When asked to comment on any related subject, 13 states responded. A major concern expressed by Michigan was written by a bridge designer referring to the difficulties in using effective width for bearing capacity calculations as it requires iterations for each load case for service and strength. Moreover, the division of responsibilities between the geotechnical section (providing allowable pressure) and structural section (examining the final design iteratively) is a source for problems. The engineer proposes allowable contact stresses for service and strength based on gross footing width and eccentricity limited to $B/6$. (The issue of "allowable" to ULS is not so clear and the engineer was contacted.)

3.1.6 Telephone Interviews

3.1.6.1 Overview

Engineers of seven states were interviewed to obtain complementary information and enhance understanding of the state of practice of shallow foundation design and construction. All the interviewed states were selected due to their extensive use of shallow foundations and/or specific usage that

required further investigation. Six of the interviews are summarized below.

3.1.6.2 Connecticut—Interview with Leo Fontaine, Transportation Principal Engineer

Connecticut is the leading state among the responding states (39) in the use of shallow foundations (66% of bridge foundations). This fact was attributed by Transportation Principal Engineer, Leo Fontaine, to the longstanding high-quality engineering traditions established by Phillip Keene and Lyle Moulton that, along with sound economics, lead to the prevailing use of shallow foundations. Connecticut design practice for foundations on rock include unconfined rock testing, RQD evaluation, and bearing capacity calculations followed by the use of predominantly presumptive values (typically 5 to 6 tsf), mostly due to lack of confidence in the rock variability. Hence, Fontaine sees a great need for the calibration of the design methods based on a database.

Connecticut's design practice for foundations on soil refers mostly to frictional soils as the construction schedule prevents building foundations on soft soils using the conventional approach (e.g., preloading), and the use of ground improvement techniques was found to be less attractive than the use of deep foundations in such cases. The design process of the shallow foundations mostly includes SPT, internal friction angle, bearing capacity analysis without inclination factors, and then settlement evaluation that controls the foundation size. The procedure is completed by checking bearing capacity again with the foundation size dictated by the settlement analysis. For settlement analysis, service load is used without a safety margin, and based on past performance, Connecticut feels comfortable with the process.

3.1.6.3 Massachusetts—Interview with Nabil Hourani, Chief Geotechnical Engineer

Massachusetts is one of three states using the highest portion of shallow foundations in bridge structures (53%), along with Connecticut (66%) and Pennsylvania (65%). When designing foundations on rock, Massachusetts uses Goodman's method, which according to the accumulated experience, correlates well with both test results, unconfined and point load tests. Massachusetts does not use presumptive values and would like to see the uncertainty of the design methodology (i.e., Goodman) evaluated and calibrated for LRFD.

Foundation design follows the AASHTO recommendations for the range of eccentricity limitation. The values, according to Nabil Hourani, Chief Geotechnical Engineer, were obtained from the load factor design methodology as presented in *NCHRP Report 343* (Barker et al., 1991, Part 3 [Kim et al., 1991],

Chapter 5, Figures 5.2 to 5.4). No settlement on rock is evaluated; anchors and dowels are being used but not keys.

3.1.6.4 Pennsylvania—Interview with Beverly Miller, Bureau of Design

The extensive use of shallow foundations in Pennsylvania (65%) is attributed to the combination of subsurface conditions (rock or stiff soil at a shallow depth) and economic competitiveness. The design is commonly based on an in-house design manual (Pennsylvania DOT, Publication Number 15M, April 2000 edition, Part 4, Volume 1 of 2) and a software package (ABLRFD by PDT and Ibsen & Assoc., Inc.).

About 60% of shallow foundations are built into rock, embedded 1 ft into the rock. As a result, it is not required that sliding be checked. About 33% of the foundations are built on granular material with no shallow foundations being built on cohesive soils. Cohesive soils would be either excavated (approximate depth of up to 10 ft) or penetrated by piles. The bearing capacity of foundations on rock is calculated utilizing Goodman (1989) and Carter & Kulhawy (1988) with $\phi = 0.55$, relying on good past experience with both methods. Pennsylvania, according to Beverly Miller at the Bureau of Design, would very much like to see the methods being calibrated. Presumptive values are rarely used and only used for comparison. Inclination factors are not used, and the design is based on unfactored loads because the use of factored loads resulted in unreasonably large foundations compared to past experience. Pennsylvania makes use of shallow foundations in water using protective measures. Abutments are built below construction scour, and piers are built below construction scour and use rip rap to mitigate for half of the local scour.

3.1.6.5 Tennessee—Interview with Edward Wasserman (Director of Structures Division), Len Oliver, and Vanessa Bateman (Soils and Foundations)

A large portion of Tennessee has relatively shallow soil depth to rock. Similar to Pennsylvania, the practice in Tennessee is to excavate foundations to a depth of about 10 ft and use end bearing piles for soil depths exceeding 12 ft.

The practice in Tennessee is to use capacity analysis on rock based on AASHTO's *Standard Specifications for Highway Bridges* (1997), utilizing unconfined test results and being sensitive to the large variation in limestone strength and possible karst phenomena. Presumptive values are used in locations where good data are not available (e.g., drilling is not possible) or the tests are inconclusive. The Navy Design Manual (NAVAC, 1986) values are then used, being overall similar to AASHTO's values. When the rock is highly fractured such that it controls the strength, shallow foundations are not

used. Very often the foundation size is restricted by the strength of the concrete, which is a limiting value (10 to 15 tsf) compared with the rock's strength. Inclination factors are not used because no load details are available from the structures group at the time of the design. When designing foundations for retaining wall, the maximum eccentricity is assumed.

3.1.6.6 Washington—Interview with Jim Cuthbertson, Chief Foundations Engineer

Washington's questionnaire response indicated a relatively common use of shallow foundations on silts and clay (6%), the highest of all responders. It was clarified that those soils are glacier, compacted, highly densified soils, with silts having SPT N values of 30 to 40 and clays having SPT N values of 40 to 100. These materials are in some ways IGMs and, hence, skew the statistics presented of foundations on silt/clay. When calculating bearing capacity, cohesion is neglected and only a frictional component is assumed. Foundations on rock and IGM are common (about 30%) and the use of the classical bearing capacity analysis leads to unrealistically high values, which are then limited to about 80 tsf ultimate capacity based on experience.

Similar to the problem presented by Tennessee, in Washington the geotechnical analysis is carried out before eccentricity values are available. This is resolved by providing foundation dimensions (width and length) that are required to be maintained as effective foundation sizes. When the final design accounts for eccentricity, it results in foundation sizes that, after being reduced for eccentricity, end with the originally provided effective foundation sizes. This effective foundation width is used for settlement analysis calculations and sliding resistance. As the foundations are cast on grade, a full mobilization of the friction angle is assumed.

3.1.6.7 Maine—Interview with Laura Krusinski, Senior Geotechnical Engineer

The extensive use of shallow foundations in Maine can be attributed to rock close to the ground surface (especially in coastal areas) and economic considerations. The foundations are sized first based on presumptive values and then are checked against the factored resistance. Maine is making an effort to obtain the references mentioned in the code and study them as no details are provided in the specifications. Laura Krusinski, Senior Geotechnical Engineer, finds it useful to provide details of recommended design methods and calibrate them against a database. As with other states, in Maine the foundation design is carried out before loading details are available; hence, eccentricity is assumed not to exist. However, the foundation is later checked as part of the structural design. Krusinski also sees a need for guidelines for footing embedment in 100-year and 500-year scour events.

3.1.7 Major Conclusions

Major conclusions are the following:

1. In many states, the geotechnical aspects of the foundation design (bearing capacity, settlement, and sliding) are being evaluated *before* all the loading details are available. As such, load inclination and/or eccentricity cannot be directly accounted for. Several approaches are taken to resolve the situation including (1) providing effective foundation sizes so that final design sizes will include the eccentricity effect (i.e., $B = B' + 2e$); (2) assuming highest eccentricity; and (3) providing unit bearing values, nominal and factored.
2. The vast majority of the shallow foundations used to support bridges are founded on rock. Only various references are currently available in the specification. A need for specific, detailed methodology and its calibration was advocated by most states and all those interviewed.
3. Although most states do not use inclination factors in design, they examine the resistance to sliding, and once the final foundation size is established (after settlement consideration), they check again for bearing capacity with or without inclination factor (depending on the state).
4. New foundations on soft, cohesive soils are rarely being constructed. Some of the statistics in that regard were skewed due to referencing highly compacted cohesive soils (which border on being IGM) as regular cohesive soils.

3.2 Assembled Databases

3.2.1 Overview

Section 2.1 presents the research plan for establishing databases for shallow foundation load tests. Two major databases were established:

- UML-GTR ShalFound07, which incorporates Databases I and II. This database is based on a database originally assembled for NCHRP Project 12-66 and in its current scope contains 549 case histories of which 409 would conform to what is described as Database I and 140 case histories would conform to Database II. UML-GTR ShalFound07 will be discussed in Section 3.2.2.
- UML-GTR RockFound07, which is presented as Database III and contains 122 case histories, 119 of which were used in the calibration. UML-GTR RockFound07 will be discussed in Section 3.2.3.

A summary of the major attributes of each database is presented below. Additional statistics are presented for relevant analyses (e.g., see Section 3.5 for centric vertical loading on shallow foundations in/on granular materials).

3.2.2 UML-GTR ShalFound07

The UML-GTR ShalFound07 database was expanded from its original format of 329 cases (developed for NCHRP Project 12-66) to contain 549 load test cases for shallow foundations, mostly on granular soils, and concentrating on load tests to failure and/or loading other than centric vertical loads. The database was constructed in Microsoft Access 2003 format. The bulk of the cases was collected and assembled from four sources: (1) ShalDB Ver5.1 (updated version of Briaud and Gibbens, 1997), (2) *Settlement of Shallow Foundations on Granular Soils,* a report to the Massachusetts Highway Department by Lutenegger and DeGroot (1995), (3) a German test database compiled by DEGEBO (Deutsche Forschungsgesellschaft für Bodenmechanik) in a set of volumes, and (4) tests carried out at or compiled by the University of Duisburg-Essen, Germany. Table 22 lists the countries in which the tests were carried out and the number of related cases. The majority of cases were tests carried out in Germany, the United States, France, and Italy.

Table 23 summarizes the database by classification based on the foundation type, predominant soil type below the footing base, and country. The foundation type was classified based on the footing width, which follows the convention utilized by Lutenegger and DeGroot (1995). The tests on footing widths less than or equal to 1 m (3.3 ft) were classified as plate load tests, widths between 1 m and 3 m (9.8 ft) were classified as small footings, widths between 3 m and 6 m (19.7 ft) were classified as large footings, and widths greater than 6 m were classified as rafts and mats. "Mixed" refers to soil containing alternating layers of sand or gravel and clay or silt. "Others" refers to cases with either unknown soil type or with materials like loamy scoria. The majority of the tests in the database are plate load tests on granular soils.

Table 22. Countries in which tests were conducted and number of test cases conducted in each country.

Country	No. of cases
Australia	1
Brazil	19
Colombia	1
Croatia	1
France	60
Germany	254
India	6
Italy	56
Jamaica	1
Japan	9
Kuwait	10
Nigeria	3
Northern Ireland	1
Portugal	6
South Africa	1
Sweden	11
UK	14
USA	84
Others	11
Total	**549**

A detailed list of input parameters in the database is presented in Appendix D (see Table D-1). See Figure 47 for the site condition (e.g., a footing tested in an excavation or a footing on a slope, etc.) and Figure 48 for the conventions of footing dimensions and loading. Figures D-1 through D-13 in Appendix D contain screen images of the UML-GTR ShalFound07 database in Microsoft Access. SearchModify, listed under Forms, allows the user to easily search/modify a footing case in the database.

Table 23. Summary of UML-GTR ShalFound07 database.

Foundation type	Predominant soil type					Total	Country	
	Sand	Gravel	Cohesive	Mixed	Others		Germany	Others
Plate load tests B ≤3.3 ft (1m)	346	46	--	2	72	**466**	253	213
Small footings 3.3 ft < B ≤9.8 ft (3m)	26	2	--	4	1	**33**	--	33
Large footings 9.8 ft< B ≤19.7 ft (6m)	30	--	--	1	--	**31**	--	31
Rafts & Mats B > 19.7 ft	13	--	--	5	1	**19**	1	18
Total	**415**	**48**	**0**	**12**	**74**	**549**	**254**	**295**

Note:
  "Mixed" are cases with alternating layers of sand or gravel and clay or silt
  "Others" are cases with either unknown soil types or with other granular materials like Loamy Scoria
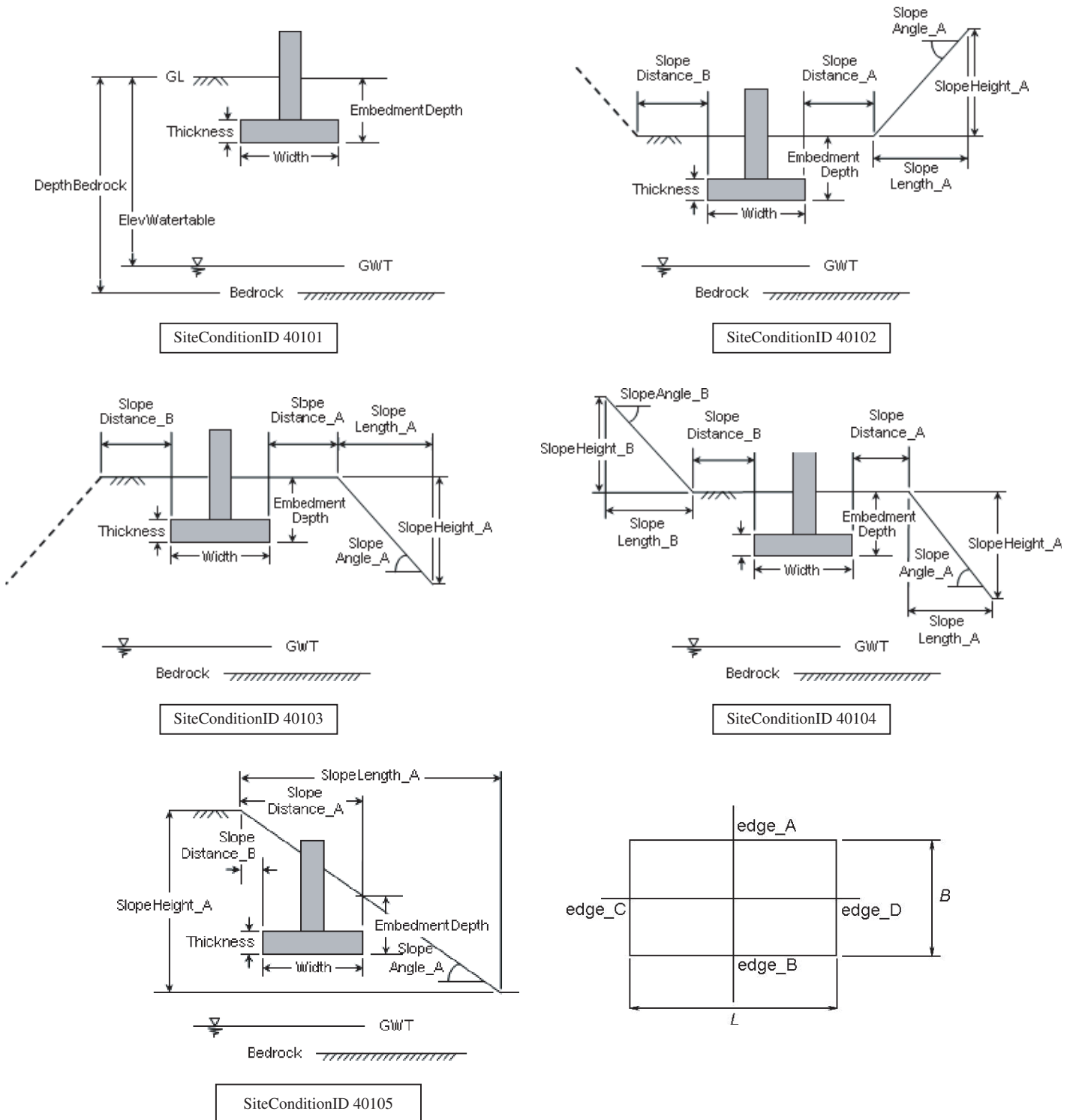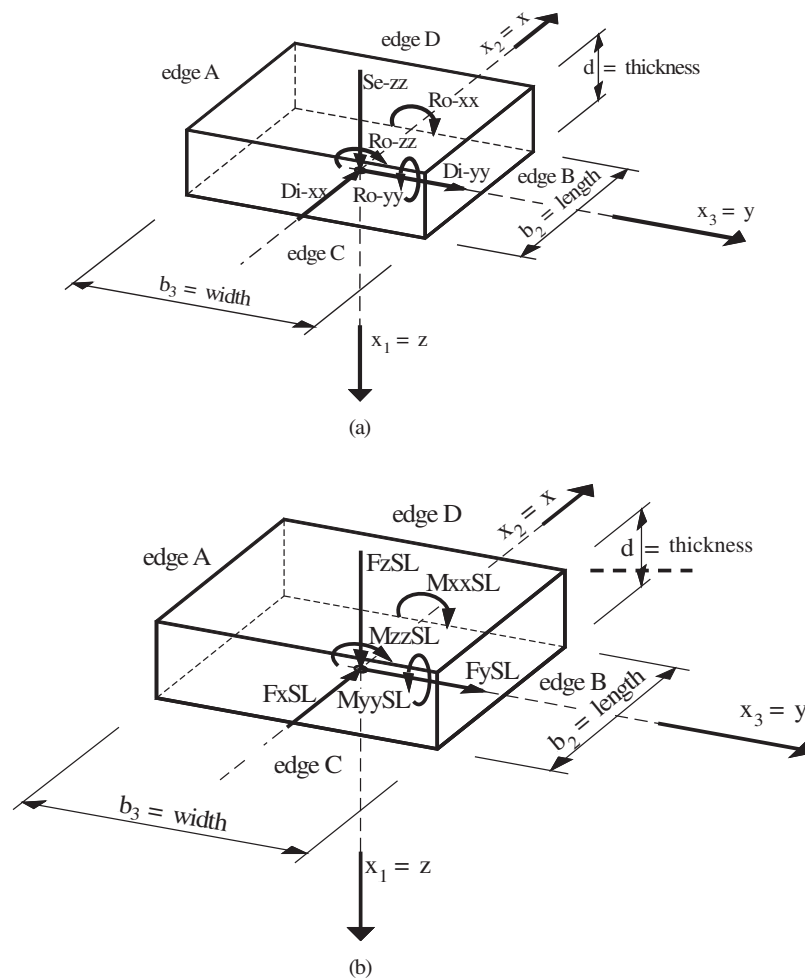 1m ≈ 3.3 ft

Figure 47. Footing dimensions and site details along with the associated SiteConditionID employed in database UML-GTR ShalFound07.

*Figure 48. Conventions for footing dimensions (a) and applied loads (b).*

3.2.3 UML-GTR RockFound07

A database consisting of rock loading by small size indentation, shallow foundations, and drilled shafts (for which the tip load-displacement relations were measured) was assembled. The database is composed of a total of 122 case histories from 10 different countries. Thirty-nine of the cases were obtained from a study by Zhang and Einstein (1998), and 31 cases were obtained from a study by Prakoso (2002) whereas the remaining cases were searched for and found in the literature. In a final review, three of the footing cases were found to be tested over a rock that contained a clay seam and, hence, were excluded from the statistics used in the calibrations. The database developed for the study included footing field load tests conducted in pseudo rock, hardpan, fine-grained sedimentary and igneous or volcanic rocks. The shallow foundation case histories were subcategorized according to their embedment, differentiating between embedded (embedment depth $D > 0$) and non-embedded ($D = 0$) footings with circular

and/or square shapes. A majority of the circular footings are plates. All the rock sockets in the database are circular for which the end bearing capacity (tip resistance) could be isolated, separating it from the shaft resistance of the rock sockets.

Figures 49 to 52 present the distributions of the foundation sizes for all cases—non-embedded and embedded footings and rock sockets, respectively. Table 24 presents a summary of the database cases used for the determination of the uncertainty of the bearing capacity analyses of foundations on rock. Appendix E presents in detail the references that were used to build the rock foundation database along with the rock details and the foundation type. All 122 original cases are presented in Appendix E with the three foundations omitted clearly marked. The database has 30 non-embedded shallow foundations, 28 embedded shallow foundations, and 61 rock sockets. Only four of the shallow foundations have square shapes; the others are circular. All 61 rock sockets are circular. The width or diameter (B) of the shallow foundations range from 0.07 to 23 ft with an average (B_{avg}) of 1.98 ft. The Rock Sockets have a
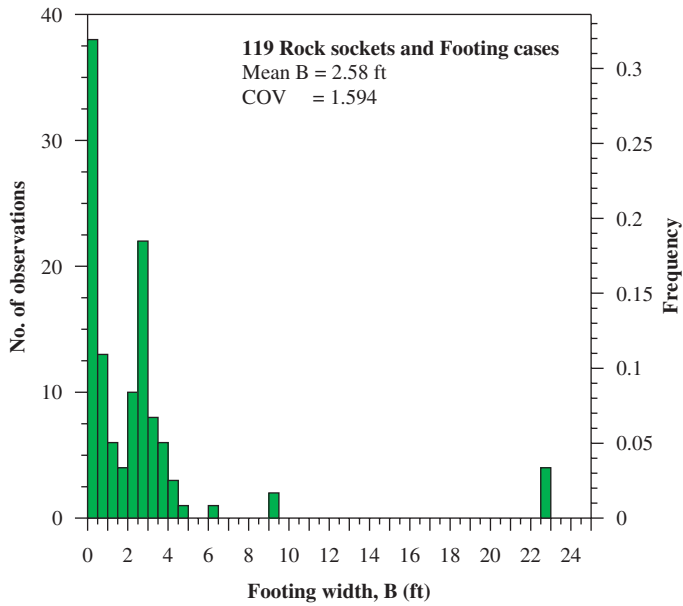
Figure 49. Distribution of B (ft) for 119 case histories in database UML-GTR RockFound07.
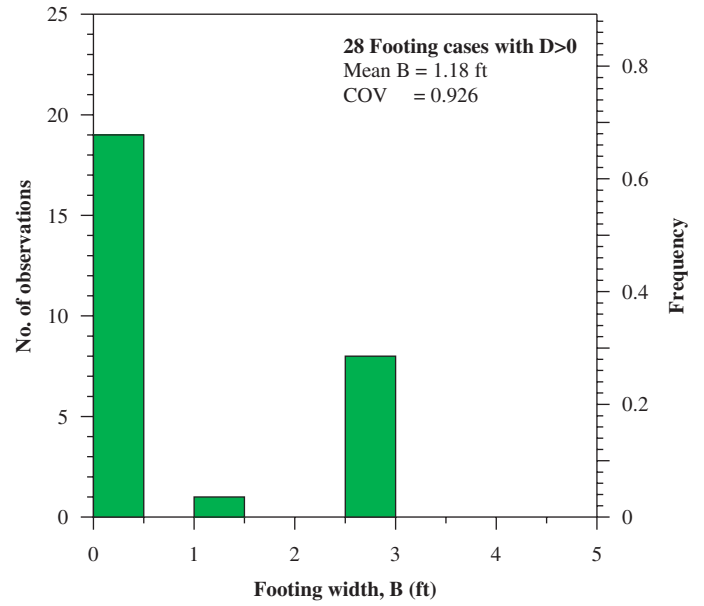
Figure 51. Distribution of B (ft) for 28 embedded footing case histories in database UML-GTR RockFound07.

Figure 50. Distribution of B (ft) for 30 non-embedded footing case histories in database UML-GTR RockFound07.
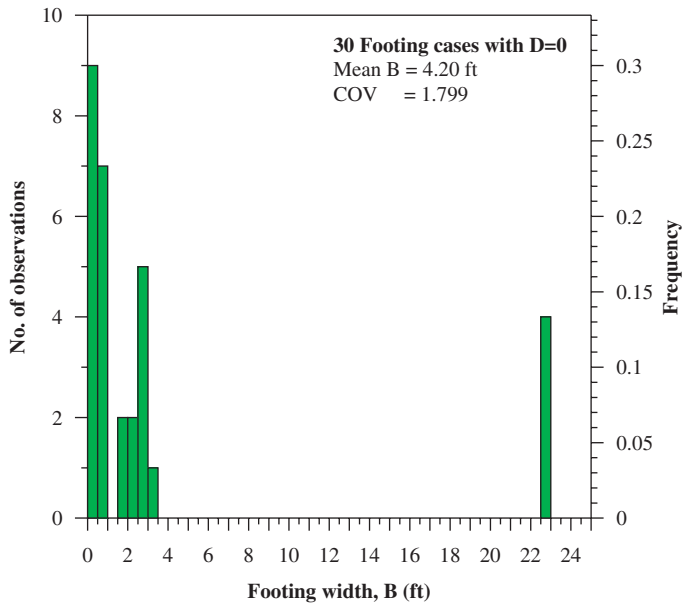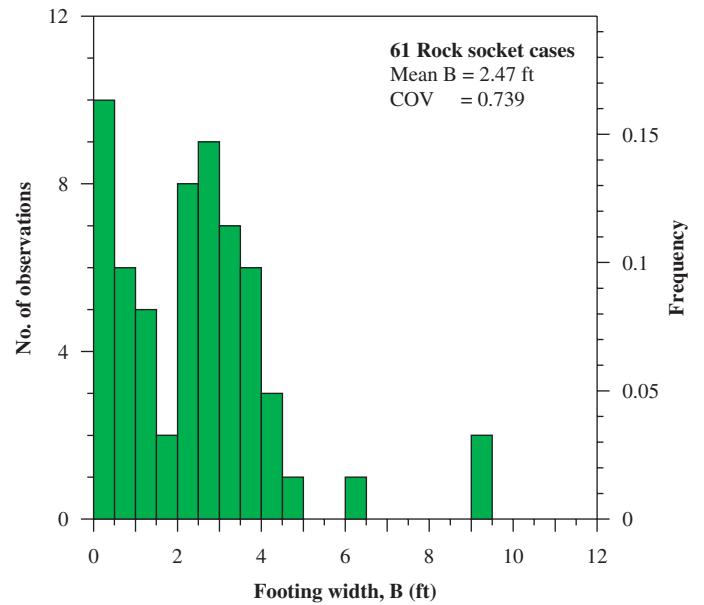

Figure 52. Distribution of B (ft) for 61 rock socket case histories in database UML-GTR RockFound07.

Table 24. Summary of database UML-GTR RockFound07 cases used for foundation capacity evaluation.

Foundation type	No. of cases	No. of sites	No. of rock types	Shape	Size range (ft)	Location									
						USA	Canada	Italy	UK	Australia	Taiwan	Japan	Singapore	Russia	South Africa
Shallow Foundations (D = 0)	33[1]	22	10	Square 4 Circular 29	$0.07 \leq B \leq 23$ $B_{avg} = 2.76$	2	1	1	3	13	0	1	0	1	0
Shallow Foundations (D > 0)	28	8	2	Circular 28	$0.23 \leq B \leq 3$ $B_{avg} = 1.18$	0	0	0	8	0	0	0	0	0	0
Rock Sockets	61	49	14	Circular 61	$0.33 \leq B \leq 9$ $B_{avg} = 2.59$	19	4	1	0	21	1	0	1	0	2

[1]Three (3) cases had been omitted in the final statistics due to a clay seam in the rock.

diameter (B) ranging from 0.33 ft to 9 ft with an average (B_{avg}) of 2.59 ft. Table 24 presents a summary of the database case histories breakdown based on foundation type, embedment, sites, size and country. It can be inferred from Table 24 that most of the shallow foundation and rock socket data were obtained from load tests carried out in Australia and the United States, respectively.

3.3 Determination of the Measured Strength Limit State for Foundations Under Vertical-Centric Loading

3.3.1 Overview

The strength limit state of a foundation may address two kinds of failure: (1) structural failure of the foundation material itself and (2) bearing capacity failure of the supporting soils. While both need to be examined, this research addresses the ULSs of the soil's failure. The ULS consists of exceeding the load-carrying capacity of the ground supporting the foundation, sliding, uplift, overturning, and loss of overall stability. In order to quantify the uncertainty of an analysis, one needs to find the ratio of the measured ("actual") capacity to the calculated capacity for a given case history. The measured strength limit state (i.e., the capacity) of each case needs, therefore, to be identified.

Depending on the footing displacements, one may define (1) allowable bearing stress, (2) bearing capacity, (3) bearing stress causing local shear failure, and (4) ultimate bearing capacity (Lambe and Whitman, 1969). Allowable bearing stress is the contact pressure for which the footing movements are within the permissible limits for safety against instability and functionality, hence defined by SLS. Bearing capacity is that contact pressure at which settlements become very large and unpredictable because of shear failure. Bearing stress causing local shear failure is the stress at which the first major non-linearity appears in a load-settlement curve, and generally the

bearing capacity is taken as equal to this stress. Ultimate bearing capacity is the stress at which sudden catastrophic settlement of a foundation occurs. Bearing capacity and ultimate bearing capacity define the ULS and differ only in the foundation response to load. Appendix F presents a review of foundation modes of failure and suggests that the terms "bearing capacity" and "ultimate bearing capacity" should be used interchangeably to define the maximum loading (capacity) of the ground, depending on the mode of failure.

3.3.2 Failure (Ultimate Load) Criteria

3.3.2.1 Overview—Shallow Foundations on Soils

The strength limit state is a "failure" load or the ultimate capacity of the foundation. The bearing capacity (failure) can be estimated from the curve of vertical displacement of the footing against the applied load. A clear failure, known as a general failure, is indicated by an abrupt increase in settlement under a very small additional load. Most often, however (other than for small scale plate load tests in dense soils), test load-settlement curves do not show clear indications of bearing capacity failures. Depending on the mode of failure, a clear peak or an asymptote value may not exist at all, and the failure or ultimate load capacity of the footing has to be interpreted. Appendix F provides categorization of failure modes followed by common failure criteria. The interpretation of the failure or ultimate load from a load test is made more complex by the fact that the soil type or state alone does not determine the mode of failure (Vesić, 1975). For example, a footing on very dense sand can also fail in punching shear if the footing is placed at a greater depth, or if loaded by a transient, dynamic load. The same footing will fail in punching shear if the very dense sand is underlain by a compressible stratum such as loose sand or soft clay. It is clear from the above discussion that the failure load of a footing is clearly defined only for the case of general shear; for cases of local and punching shear, it is often difficult to establish a unique failure load.

Criteria proposed by different authors for the failure load interpretation are presented in Appendix F, while only the selected criterion is presented in the following section. Such interpretation requires that the load test be carried to very large displacements, which constrains the availability of test data, in particular for larger footing sizes.

3.3.2.2 Minimum Slope Failure (Ultimate) Load Criteria, Vesić (1963)

Based on the load-settlement curves, a versatile ultimate load criterion is recommended to define the ultimate load at the point where the slope of the load-settlement curve first reaches zero or a steady, minimum value. The interpreted ultimate loads for different tests are shown as black dots in Figure 53 for soils with different relative densities, D_r. For footings on the surface of, or embedded in, soils with higher relative densities, there is a higher possibility of failure in general shear mode, and the failure load can be clearly identified for Test Number 61 in Figure 53. For footings in soils with lower relative densities, however, the failure mode could be local shear or punching shear, with the identified failure location being arbitrary at times (e.g., see Test Number 64). A semi-log scale plot with the base pressure (or load) in logarithmic scale can be used as an alternative to the linear scale plot if it facilitates the identification of the starting of minimum slope and hence the failure load.

3.3.2.3 The Uncertainty in the Minimum Slope Failure Criterion Interpretation

In order to examine the uncertainty in the method selected for defining the bearing capacity of shallow foundations on soils, the following failure criteria (described in detail in Appendix F) were used to interpret the failure load from the load-settlement curves of footings subjected to centric vertical loading on granular soils (measured capacity): (a) minimum slope criterion (Vesić, 1963), (b) limited settlement criterion of 0.1B (Vesić, 1975), (c) log-log failure criterion (De Beer, 1967), and (d) two-slope criterion (shape of curve).

Examples F1 and F2 in Appendix F demonstrate the application of the four examined criteria to the database UML-GTR ShalFound07. The measured bearing capacity could be interpreted for 196 cases using the minimum slope criterion (Vesić, 1963) and 119 cases using the log-log failure criterion (De Beer, 1967). Most of the footings failed before reaching a settlement of 10% of footing width (the limited settlement criterion of 0.1B [Vesić, 1975] could therefore only be applied to 19 cases). A single "representative" value of the relevant measured capacity was then assigned to each footing case. This was done by taking an average of the measured capacities interpreted using the minimum slope criterion, the limited settlement criterion of 0.1B (Vesić, 1975), the log-log failure criterion, and the two-slope criterion (shape of curve).
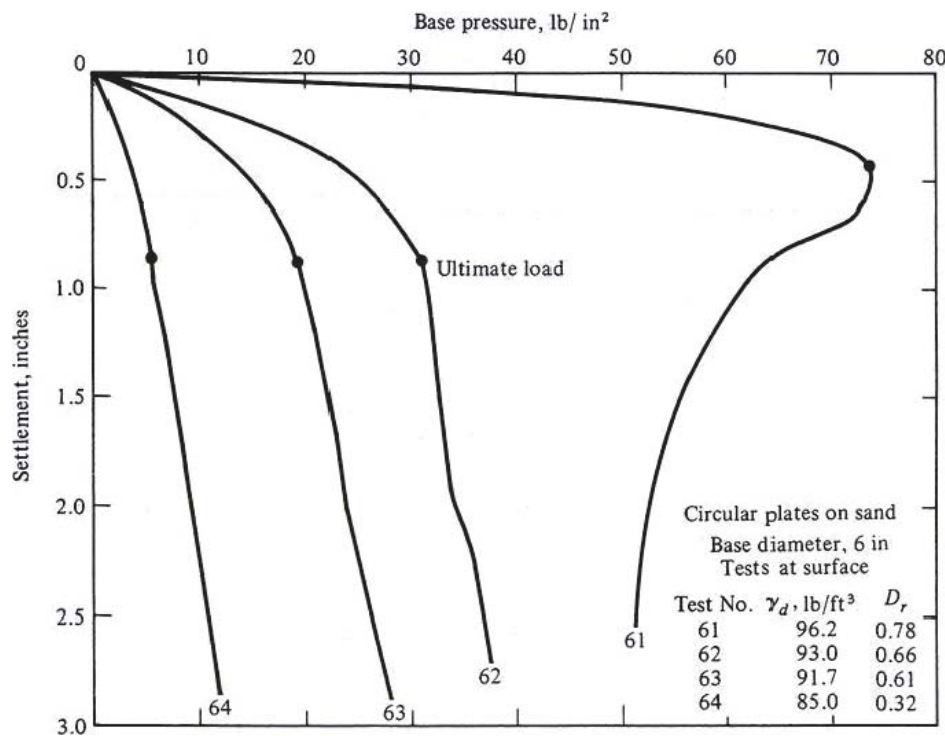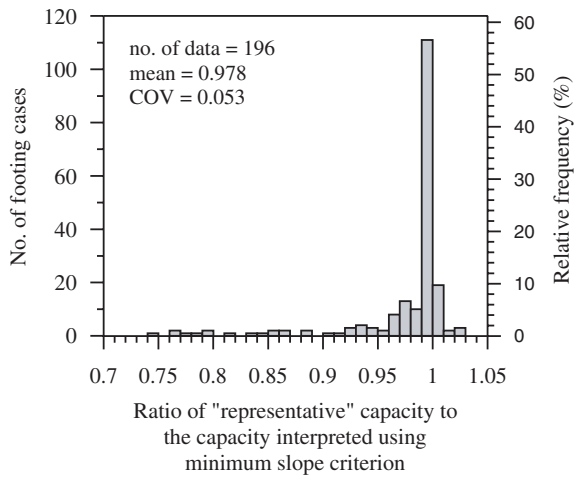

Figure 53. Ultimate load criterion based on minimum slope of load-settlement curve (Vesić, 1963).
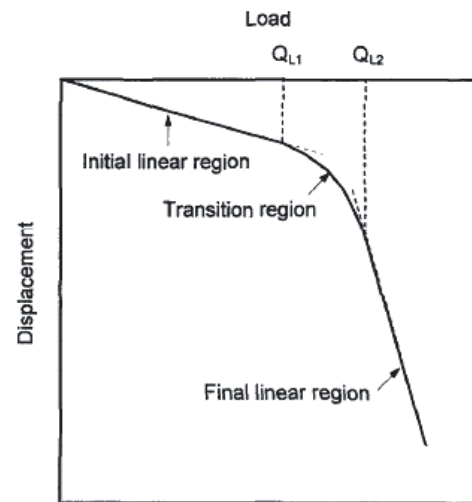
Figure 54. Histogram for the ratio of representative measured capacity to interpreted capacity using the minimum slope criterion for 196 footing cases in granular soils under centric vertical loading.

Figure 55. Example of L_1-L_2 method for capacity of foundations on rocks showing the regions of the load-displacement curve and interpreted limited loads (Hirany and Kulhawy, 1988).

The statistics of the ratios of this representative value over the interpreted capacity using the minimum slope criterion and the log-log failure criterion were comparable with the mean of the ratio for the minimum slope criterion being 0.98 versus that for the limited settlement criterion being 0.99. Due to the simplicity and versatility of its application, the minimum slope criterion was selected as the failure interpretation criterion to be used for all cases of footing, including those with combined loadings. Figure 54 shows the histogram for the ratio of the representative measured capacity to the interpreted capacity using the minimum slope criterion. Figure 54 presents the uncertainty associated with the use of the selected criterion, suggesting that the measured capacity interpreted using the minimum slope criterion has a slight overprediction.

3.3.3 Failure Criterion for Footings on Rock

The bearing capacity interpretation of loaded rock can become complex due to the presence of discontinuities in the rock mass. In a rock mass with vertical open discontinuities, where the discontinuity spacing is less than or equal to the footing width, the likely failure mode is uniaxial compression of rock columns (Sowers, 1979). For a rock mass with closely spaced, closed discontinuities, the likely failure mode is the general wedge occurring when the rock is normally intact. For a mass with vertical open discontinuities spaced wider than the footing width, the likely failure mode is splitting of the rock mass and is followed by a general shear failure. For the interpretation of ultimate load capacities from the load-settlement

curves, the L_1-L_2 method proposed by Hirany and Kulhawy (1988) was adopted.

A typical load-displacement curve for foundations on rock is presented in Figure 55. Initially, linear elastic load-displacement relations take place; the load defining the end of this region is interpreted as Q_{L1}. If a unique peak or asymptote in the curve exists, this asymptote or peak value is defined as Q_{L2}. There is a nonlinear transition between loads Q_{L1} and Q_{L2}. If a linear region exists after the transition, as in Figure 55, the load at the start of the final linear region is defined as Q_{L2}. In either case, Q_{L2} is the interpreted failure load. This criterion is similar to the aforementioned minimum slope failure proposed by Vesić for foundations in soil. The selection of the ultimate load using this criterion is demonstrated in Example F3 of Appendix F using a case history from the UML-GTR RockFound07 database. It can be noted that the axes aspect ratios (scales of axes relative to each other) in the plot of the load-settlement curve changes the curve shape, and thus could affect the interpretation of the ultimate load capacity. However, unlike the interpretation of ultimate capacity from pile load tests, which utilizes the elastic compression line of the pile, there is no generalization of what the scales of the axes should be relative to each other for the shallow foundation load tests. It can only be said that depending on the shape of the load-settlement curve, a "favorable" axes aspect ratio needs to be fixed. This should be done on a case-by-case basis, using judgment, so that the region of interest (e.g., if the minimum slope criterion is used, the region where the change in the curve slope occurs) is clear. The L_1-L_2 method was applied to all cases for which

the load-settlement curve was available with sufficient detail and extent to be employed. For all other cases, the reported failure was adopted as the foundation's capacity.

3.4 Determination of the Calculated Strength Limit States for the Case Histories (Foundations on Soils)

3.4.1 Equations for Bearing Capacity (Resistance) Estimation

The bearing capacity equation specified in AASHTO (2008) with minimal necessary adjustment has been used to calculate the bearing capacity of a footing (q_n) of length L and width B' and supported by a soil with cohesion, c, average friction angle, ϕ_f, and average unit weights, γ_1 and γ_2, above and below the footing base, respectively. The format presented in Equation 95 is based on the general bearing capacity formulation used by Vesić (1975) as presented in Section 1.5.3 (see Equation 34). The numbering in parentheses represents the proposed numbering for the modified AASHTO specifications.

$$q_n = c \cdot N_{cm} + \gamma_1 \cdot D_f \cdot N_{qm} + 0.5 \cdot \gamma_2 \cdot B \cdot N_{\gamma m}$$

$$(10.6.3.1.3a - 1) \quad (95)$$

in which:

$$N_{cm} = N_c s_c d_c i_c \qquad (10.6.3.1.3a - 2) \quad (96)$$

$$N_{qm} = N_q s_q d_q i_q \qquad (10.6.3.1.3a - 3) \quad (97)$$

$$N_{\gamma m} = N_\gamma s_\gamma d_\gamma i_\gamma \qquad (10.6.3.1.3a - 4) \quad (98)$$

where

c = cohesion, taken as undrained shear strength c_u in total stress analysis or as cohesion c' in effective stress analysis (ksf);

N_c = cohesion term bearing capacity factor as specified in Tables 25 and 26 (dim.);

N_q = surcharge (embedment) term bearing capacity factor as specified in Tables 25 and 26 (dim.);

N_γ = unit weight (footing width) term bearing capacity factor as specified in Tables 25 and 26 (dim.);

γ_1 = moist or submerged unit weight of soil above the bearing depth of the footing (kcf);

γ_2 = moist or submerged unit weight of soil below the bearing depth of the footing (kcf);

D_f = footing embedment depth (ft);

B = footing width (ft), equal to the physical footing width (B) in the case of centric loading or effective footing width (B') in the case of eccentric loading;

s_c, s_γ, s_q = footing shape correction factors as specified in Table 27 (dim.);

d_c, d_γ, d_q = depth correction factors to account for the shearing resistance along the failure surface passing through the soil above the bearing elevation as specified in Table 28 (dim.); and

i_c, i_γ, i_q = load inclination factors as specified in Table 29 (dim.).

The effective vertical stress calculated at the base of the footing $\sum_0^{D_f} \gamma_i (D_{i+1} - D_i)$ should be used (where γ_i and D_i are effective unit weight and depth to the ith layer up to a depth of D_f) or alternatively, an average weighted soil unit weight (γ_1) should be used above the base. Below the base an average soil unit weight (γ_2) should be used within a zone of 1.5B. The highest anticipated groundwater level should be used in design.

In Tables 27 through 29, B and L are the physical footing dimensions (in the case of centric loading), or they have to be substituted with the effective footing dimensions, B' and L' (in the case of eccentric loading).

In Table 29, H and V are the unfactored horizontal and vertical loads (kips), respectively. The angle θ is the projected direction of load in the plane of the footing, measured from the side of the footing length, L (deg.). Figure 17 (similar to AASHTO Figure 10.6.3.1.3a-1) shows the conventions for determining θ. The parameter n is defined according to Equation 99:

$$n = \left[\frac{(2 + L'/B')}{(1 + L'/B')} \right] \cos^2\theta + \left[\frac{(2 + B'/L')}{(1 + B'/L')} \right] \sin^2\theta$$

$$(10.6.3.1.3a - 5) \quad (99)$$

Table 25. Bearing capacity factors N_c (Prandtl, 1921), N_q (Reissner, 1924), and N_γ (Vesic, 1975) (AASHTO Table 10.6.3.1.3a-1).

Factor	Friction angle	Cohesion term (N_c)	Unit weight term (N_γ)	Surcharge term (N_q)
Bearing Capacity Factors N_c, N_γ, N_q	$\phi_f = 0$	$2 + \pi$	0.0	1.0
	$\phi_f > 0$	$(N_q - 1) \cdot \cot \phi_f$	$2 \cdot (N_q + 1) \cdot \tan \phi_f$	$\exp(\pi \cdot \tan \phi_f) \cdot \tan^2 \left(45 + \frac{\phi_f}{2} \right)$

Table 26. Bearing capacity factors N_c (Prandtl, 1921), N_q (Reissner, 1924), and N_γ (Vesic, 1975) (AASHTO Table 10.6.3.1.3a-2).

ϕ_f	N_c	N_q	N_γ	ϕ_f	N_c	N_q	N_γ
0	5.14	1.0	0.0	23	18.1	8.7	8.2
1	5.4	1.1	0.1	24	19.3	9.6	9.4
2	5.6	1.2	0.2	25	20.7	10.7	10.9
3	5.9	1.3	0.2	26	22.3	11.9	12.5
4	6.2	1.4	0.3	27	23.9	13.2	14.5
5	6.5	1.6	0.5	28	25.8	14.7	16.7
6	6.8	1.7	0.6	29	27.9	16.4	19.3
7	7.2	1.9	0.7	30	30.1	18.4	22.4
8	7.5	2.1	0.9	31	32.7	20.6	26.0
9	7.9	2.3	1.0	32	35.5	23.2	30.2
10	8.4	2.5	1.2	33	38.6	26.1	35.2
11	8.8	2.7	1.4	34	42.2	29.4	41.1
12	9.3	3.0	1.7	35	46.1	33.3	48.0
13	9.8	3.3	2.0	36	50.6	37.8	56.3
14	10.4	3.6	2.3	37	55.6	42.9	66.2
15	11.0	3.9	2.7	38	61.4	48.9	78.0
16	11.6	4.3	3.1	39	67.9	56.0	92.3
17	12.3	4.8	3.5	40	75.3	64.2	109.4
18	13.1	5.3	4.1	41	83.9	73.9	130.2
19	13.9	5.8	4.7	42	93.7	85.4	155.6
20	14.8	6.4	5.4	43	105.1	99.0	186.5
21	15.8	7.1	6.2	44	118.4	115.3	224.6
22	16.9	7.8	7.1	45	133.9	134.9	271.8

Table 27. Shape correction factors s_c, s_γ, s_q (Vesić, 1975) (AASHTO Table 10.6.3.1.3a-3).

Factor	Friction angle	Cohesion term (s_c)	Unit weight term (s_γ)	Surcharge term (s_q)
Shape Factors s_c, s_γ, s_q	$\phi_f = 0$	$1 + 0.2 \cdot \dfrac{B}{L}$	1.0	1.0
	$\phi_f > 0$	$1 + \dfrac{B}{L} \cdot \dfrac{N_q}{N_c}$	$1 - 0.4 \cdot \dfrac{B}{L}$	$1 + \dfrac{B}{L} \cdot \tan \phi_f$

Table 28. Depth correction factors d_c, d_γ, d_q (Brinch Hansen, 1970) (AASHTO Table 10.6.3.1.3a-4).

Factor	Friction angle	Cohesion term (d_c)	Unit weight term (d_γ)	Surcharge term (d_q)
Depth Correction Factors d_c, d_γ, d_q	$\phi_f = 0$	for $D_f \le B$: $1 + 0.4 \cdot \dfrac{D_f}{B}$ for $D_f > B$: $1 + 0.4 \cdot \arctan\left(\dfrac{D_f}{B}\right)$	1.0	1.0
	$\phi_f > 0$	$d_q - \dfrac{1 - d_q}{N_q - 1}$	1.0	for $D_f \le B$: $1 + 2 \cdot \tan \phi_f \cdot (1 - \sin \phi_f)^2 \cdot \dfrac{D_f}{B}$ for $D_f > B$: $1 + 2 \cdot \tan \phi_f \cdot (1 - \sin \phi_f)^2 \cdot \arctan\left(\dfrac{D_f}{B}\right)$

Table 29. Load inclination factors i_c, i_γ, i_q (Vesić, 1975) (AASHTO Table 10.6.3.1.3a-5).

Factor	Friction angle	Cohesion term (i_c)	Unit weight term (i_γ)	Surcharge term (i_q)
Load Inclination Factors i_c, i_γ, i_q	$\phi_f = 0$	$1 - \dfrac{n \cdot H}{c \cdot B \cdot L \cdot N_c}$	1.0	1.0
	$\phi_f > 0$	$i_q - \dfrac{1 - i_q}{N_q - 1}$	$\left[1 - \dfrac{H}{V + c \cdot B \cdot L \cdot \cot \phi_f}\right]^{(n+1)}$	$\left[1 - \dfrac{H}{V + c \cdot B \cdot L \cdot \cot \phi_f}\right]^{n}$

Table 30. Summary of equations correlating internal friction angle (ϕ_f) to corrected SPT N value ($N_1)_{60}$.

Reference	Correlation equation	Equation no.
Peck, Hanson, and Thornburn (PHT) (1974) as mentioned in Kulhawy and Mayne (1990)	$\phi_f \approx 54 - 27.6034 \cdot \exp\left(-0.014\left(N_1\right)_{60}\right)$	(100)
Hatanaka and Uchida (1996)	$\phi_f = \sqrt{20\left(N_1\right)_{60}} + 20$ for $3.5 \leq \left(N_1\right)_{60} \leq 30$	(101)
PHT (1974) as mentioned by Wolff (1989)	$\phi_f = 27.1 + 0.3\left(N_1\right)_{60} - 0.00054\left(N_1\right)_{60}^{2}$	(102)
Mayne et al. (2001) based on data from Hatanaka and Uchida (1996)	$\phi_f = \sqrt{15.4\left(N_1\right)_{60}} + 20$	(103)
Specifications for Highway Bridges (SHB) Japan, JRA (1996)	$\phi_f = \sqrt{15(N_1)_{60}} + 15$ for $\left(N_1\right)_{60} > 5$ and $\phi_f \leq 45°$	(104)

Note: p_a is the atmospheric pressure and σ'_v is effective overburden pressure in the same units. For English units, $p_a = 1$ and σ'_v is expressed in tsf at the depth N_{60} is observed. $(N_1)_{60}$ is the corrected SPT N value corrected using the correction given by Liao and Whitman (1986):

$$(N_1)_{60} = \sqrt{\frac{p_a}{\sigma'_v}} \cdot N_{60} \qquad (105)$$

The depth correction factor should be used only when the soils above the footing bearing elevation are competent and there is no danger of their removal over the foundation's lifetime; otherwise, the depth correction factor should be taken as 1.0, or D_f should be reduced to include the competent, secured depth only.

The depth correction factors presented in Table 28 refer, when applicable, to the effective foundation width B'. Some design practices use the physical footing width (B) for evaluating the depth factors under eccentric loading as well. The calibration presented in this study was conducted using B'. The use of B in the depth factor expressions results in a more conservative evaluation as discussed by Paikowsky et al. (2009a).

3.4.2 Estimation of Soil Parameters Based on Correlations

3.4.2.1 Correlations Between Internal Friction Angle (ϕ_f) and SPT N

Table 30 summarizes various correlations between SPT N and the soil's internal friction angle (see Equations 100 to 105).
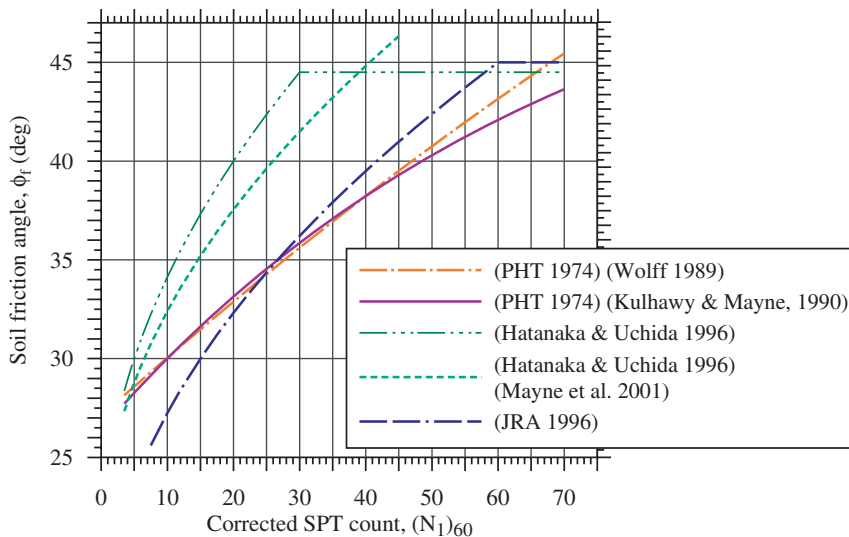
Figure 56. Comparison of various correlations between granular soil friction angle and corrected SPT blow counts using the overburden correction proposed by Liao and Whitman (1986).

Figure 56 presents a comparison of the different correlations listed in Table 30. The graph in Figure 56 suggests that in the range of about $(N_1)_{60}$ = 27 to 70, the Peck, Hanson, and Thornburn (PHT) (1974) correlation (modified by Kulhawy and Mayne, 1990, see Equation 100) provides the most conservative yet realistic estimate of the soil's friction angle.

The use of Equations 100 and 101 is examined in Figure 57, where the bias (measured over calculated bearing capacity) when using both equations is presented. The use of Equation 100 resulted in the increase of the bias mean from 0.32 to 0.97 and COV improved from 0.454 to 0.362 compared to that when using Equation 101. Using Equation 101, the bias mean was 0.32 and the COV was 0.454; however, using Equation 100, the bias mean increased to 0.97 and the COV improved, becoming 0.32. For example, for the footing cases with Footing IDs (FOTIDs) of #46, #49, and #77, the friction angles obtained using Equation 101 are 41.0°, 33.9°, and 35.9°, and those using Equation 100 are 33.75°, 29.8°, and 32.3°. The resulting biases were found to be 0.41, 0.39, and 0.77, in the previous case, and 1.20, 0.69, and 1.30 in the latter, respectively.

The correlation proposed by PHT (1974) as modified by Kulhawy and Mayne (1990) was adopted for the friction angle evaluation. The PHT (1974) correlation has been found to give more reasonable soil friction angles based on SPT N counts than other correlations. The same correlation was also used in NCHRP Project 24-17 (published as *NCHRP Report 507: Load and Resistance Factor Design (LRFD) for Deep Foundations*) and NCHRP Project 12-66 "AASHTO LRFD Specifications for Serviceability in the Design of Bridge Foundations." The friction angle of the soils for the footings for which SPT N was available (typically field tests, categorized in later sections as "natural soil condition" cases) was therefore evaluated using the Equation 100 relationship.

3.4.2.2 Correlations Between γ and SPT N

The following equation was established by Paikowsky et al. (1995) for estimation of the unit weight of granular soils from SPT blow counts:

$$\gamma = 0.88(N_1)_{60} + 99 \, (\text{pcf}) \qquad \text{for } \gamma \leq 146 \text{pcf} \tag{106}$$

The unit weights for the footing cases (for which soil unit weight was not specified and SPT blow counts are available) have been estimated through an iteration process, as shown in the flowchart presented in Figure 58. For an *i*th layer of thickness $(D_{i+1} - D_i)$, as shown, the unit weight of soil is estimated through an iteration until a precision of a small error (ε) is obtained.

3.4.2.3 Correlation Between ϕ_f and γ

For the unique set of tests conducted at the University of Duisburg-Essen (UDE), soil friction angles were estimated using locally developed correlation with soil bulk density. The soil friction angle used in these laboratory tests was extensively tested, and Figure 59 shows the results of 52 direct shear tests carried out on dry Essen sand with a dry unit weight in the range of $15.46 \leq \gamma \leq 17.54$ kN/m³ ($98.5 \leq \gamma \leq 111.75$ pcf). The tests were carried out with normal stresses between $50 \leq \sigma \leq 200$ kPa ($0.52 \leq \sigma \leq 2.09$ tsf). Essen sand is a medium-to-coarse, sharp-edged silica sand. The sand has a specific gravity of $G_s \approx 2.693 \pm 0.004$ and minimum and maximum porosities of $n_{\min} \approx 0.330 \pm 0.012$ and $n_{\max} \approx 0.443 \pm 0.006$, respectively.

The correlation was revised after identifying outlier(s). The best fit lines are as shown in Figure 59. Perau (1995) used all 52 test data. The revised correlation is the best fit line obtained from linear regression on 51 samples, with the circled test result considered as an outlier.

The correlation given by Perau (1995) is the following:

$$\phi_f = 3.9482\gamma - 23.492 \, (n = 52, \, R^2 = 0.771) \tag{107}$$

The revised correlation is the following:

$$\phi_f = 3.824\gamma - 21.527 \, (n = 51, \, R^2 = 0.804) \tag{108}$$

It was found that the difference between the ultimate bearing capacities obtained for a square footing (1.0 m²) using the friction angles obtained from the original correlation, Equation 107 (Perau, 1995), and the revised correlation (Equation 108) is 10% to 18% for the range of friction angles between 40° and 47°.
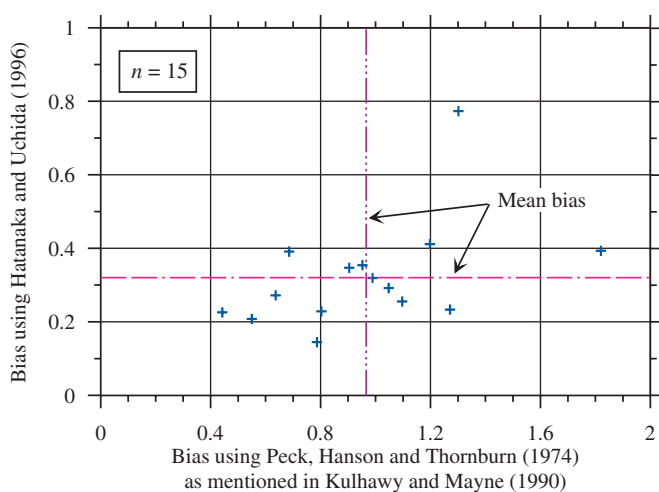
Figure 57. Comparison of biases for the cases in natural soil conditions when using Equations 100 and 101.
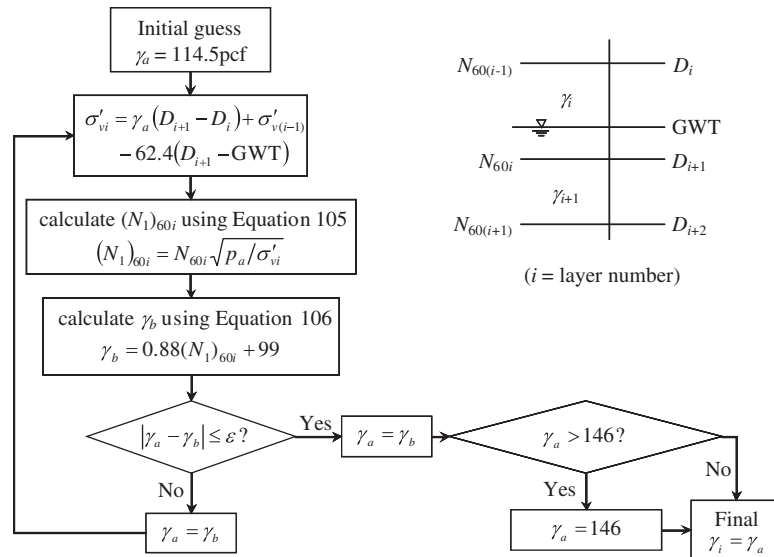
Figure 58. Flow chart showing iteration for the estimation of soil unit weight.

3.5 Uncertainty in the Bearing Capacity of Footings in/on Granular Soils Subjected to Vertical-Centric Loading

3.5.1 Scope of Case Histories

In 172 load test cases of the UML-GTR ShalFound07 database, the foundations were subjected to vertical-centric loadings, and the load test results could be interpreted employ-

ing the minimum slope failure criterion. The soil friction angles for these cases ranged from $30.5°(\pm0.5)$ to $45°$ (±0.5).

3.5.2 Summary of Mean Bias Statistics

Of the 172 cases, 14 foundations were tested in *natural soil conditions* and the remaining 158 in *controlled soil conditions.* The cases for which SPT N blow count observations are available have been categorized as the cases in natural soil

Figure 59. Revised correlation for angle of internal friction and dry unit weight of Essen sand.

Figure 60. Summary of bias (measured over calculated bearing capacity) for vertical-centric loading cases (Database I) (0.1 m = 3.94 in, 1 m = 3.28 ft).

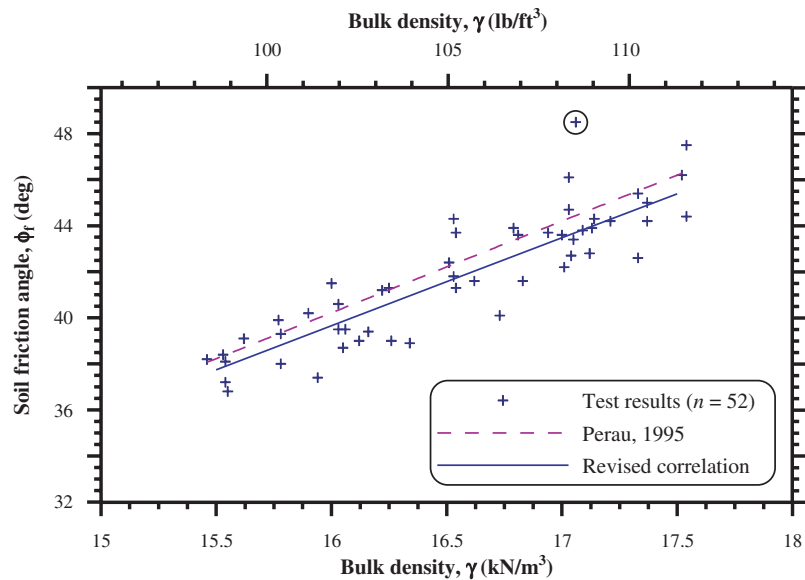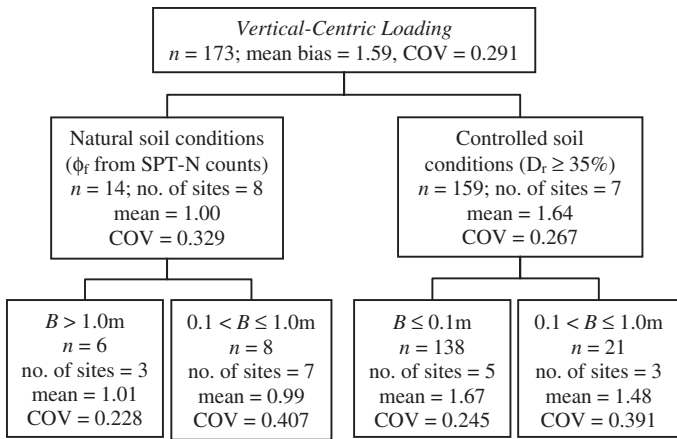conditions, while those tested in laboratories using soils of known particle size and controlled compaction have been categorized as the cases in controlled soil conditions. Each of the cases was analyzed to obtain the measured failure from the load-settlement curve and the calculated bearing capacity following the equations and correlations presented in Section 3.4. The relation of the two (i.e., measured failure over calculated capacity) constitutes the bias of the case. Appendix G presents examples for bias calculations for the

case histories. Section G.1 presents the bias calculations for footing ID (FOTID) #35 of database UML-GTR ShalFound07 related to vertical-centric loading. Figure 60 presents a flow-chart summary of the mean bias for vertical-centric loading cases grouped by soil conditions and footing widths. Figures 61 to 63 present the bias histograms and probability density functions as well as measured versus calculated bearing capacity relations for all the cases and the subcategorization of natural versus controlled soil conditions. The data in Figures 60 to 63 represent all available cases without giving consideration to outliers, which will be addressed in Chapter 4.

The mean bias value for the footings in natural soil conditions was found to be around 1.0, regardless of the footing sizes (the largest footing tested was about 10 ft wide). In contrast, for the footings in controlled soil conditions the mean bias value changed from about 1.5 for larger footings to 1.7 for smaller footings. The variation in the mean bias with the footing width is further discussed in Chapter 4. Compared to the biases for the tests in controlled soil conditions, the biases for the tests in natural soil conditions have higher variation, even when the number of sites is comparable. One may conclude that as the controlled soil conditions more correctly represent the accurate soil parameters, the higher mean bias reflects conservatism (under-prediction) in the calculation model (i.e., the bearing capacity equation). The layer variation in soil conditions and the integrated parameters from the SPT
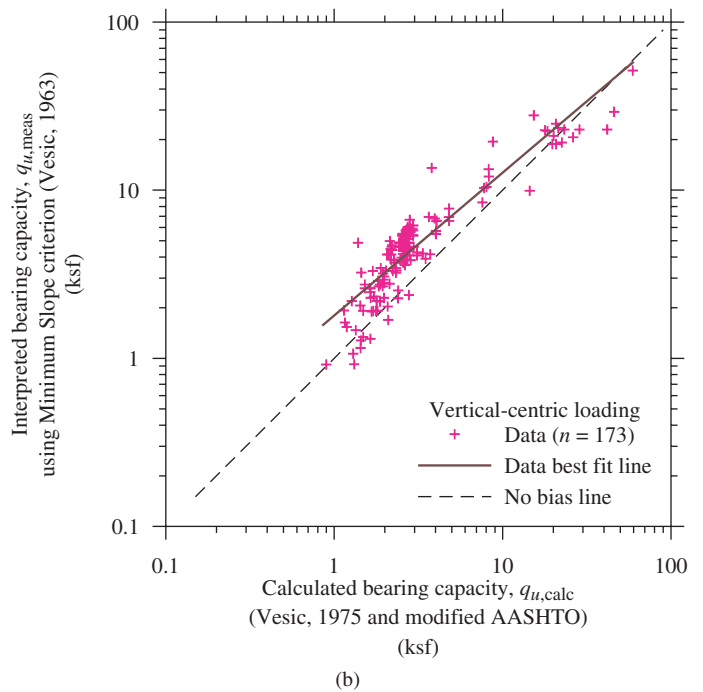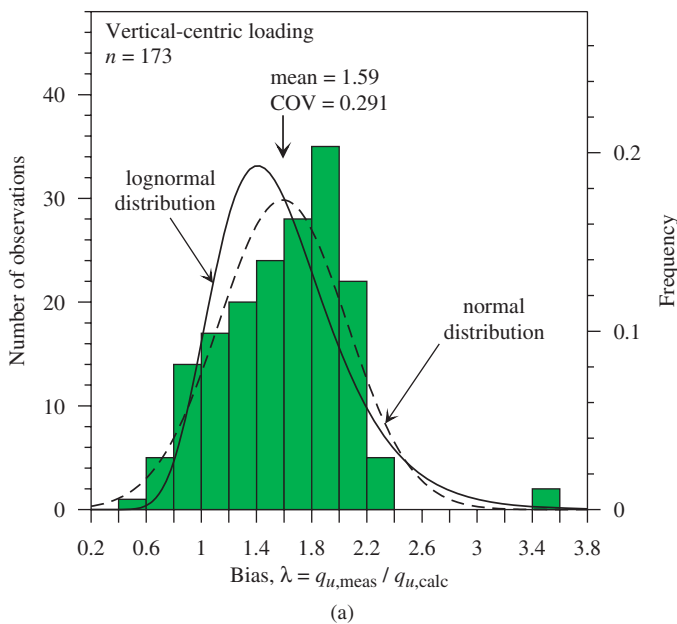
Figure 61. (a) Histogram and probability density functions of the bias and (b) relationship between measured and calculated bearing capacity for all cases of shallow foundations under vertical-centric loading.
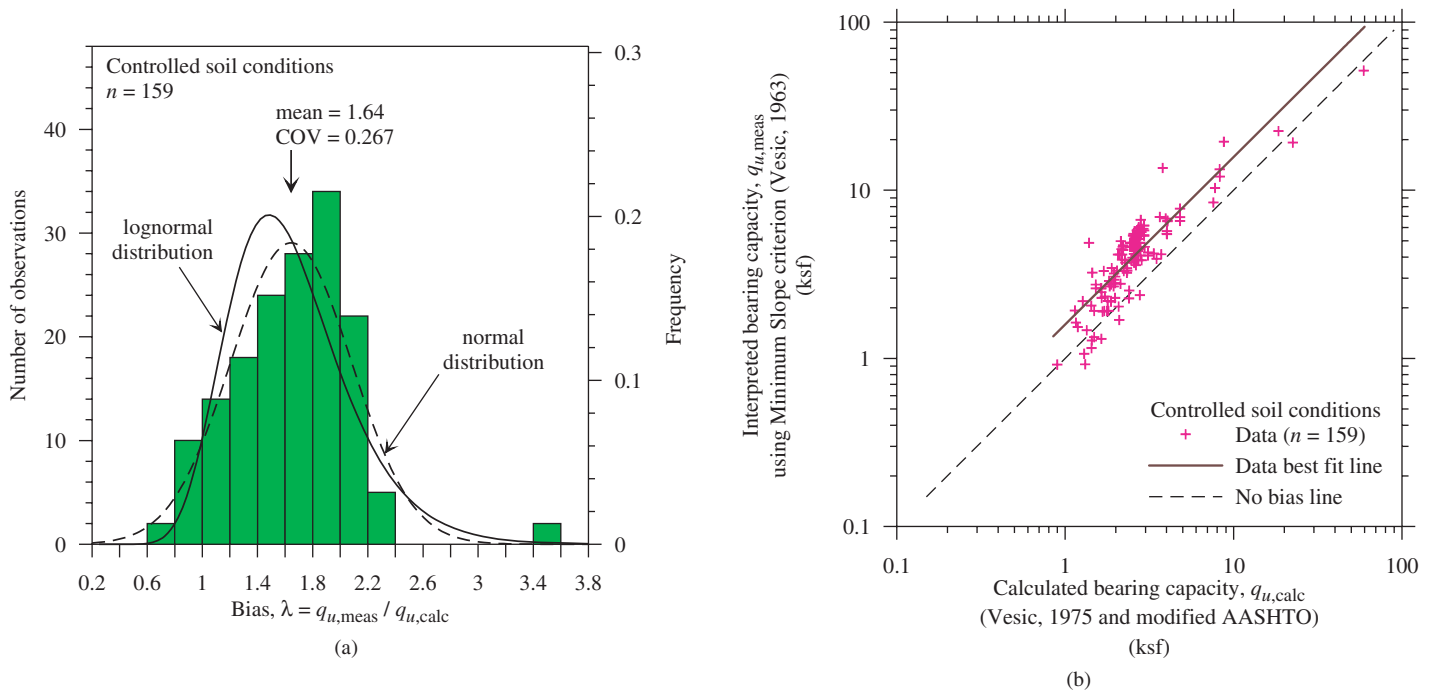
Figure 62. (a) Histogram and probability density functions of the bias and (b) relationship between measured and calculated bearing capacity for vertical, centrically loaded shallow foundations on controlled soil conditions.
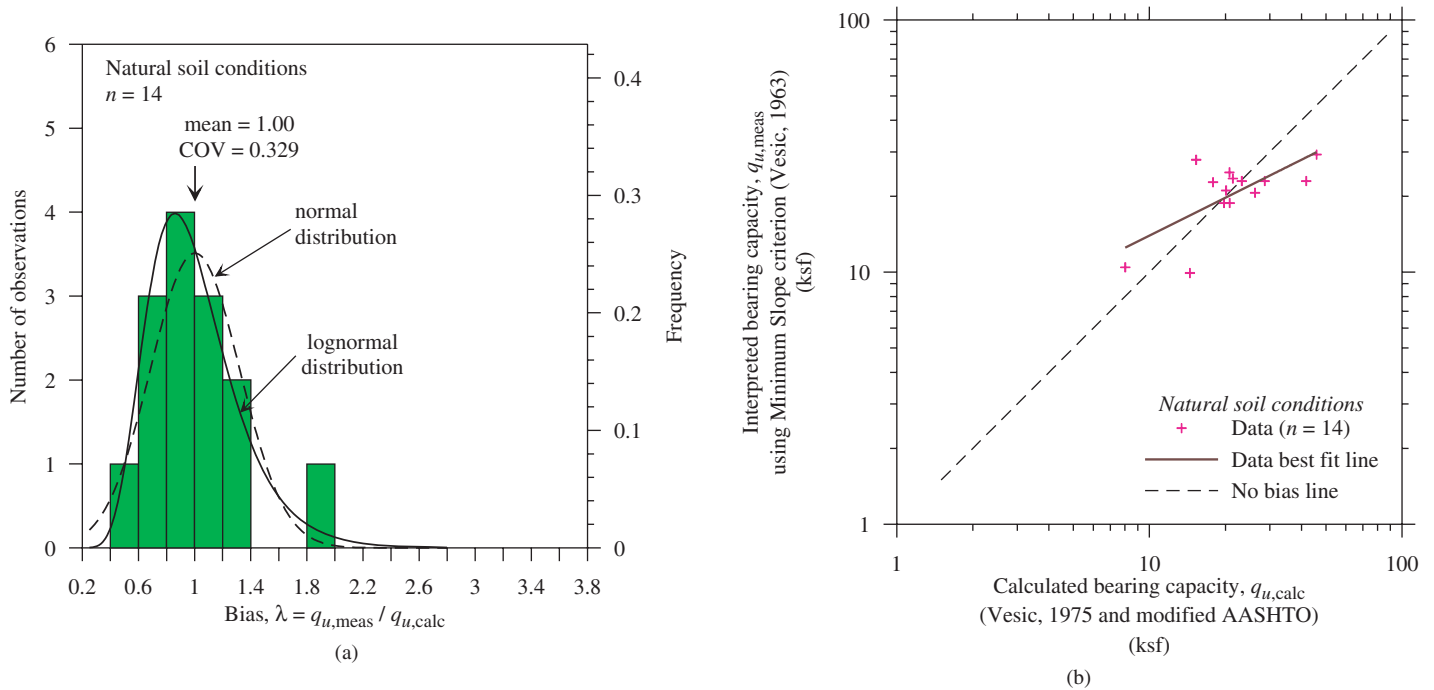
Figure 63. (a) Histogram and probability density functions of the bias and (b) relationship between measured and calculated bearing capacity for vertical, centrically loaded shallow foundations on natural soil conditions.

when analyzing data for natural soil deposits result in layer variation (as expressed by the COV) and reduction in the mean bias. Further investigation as to the source of the obtained bias is presented in Section 4.4.

3.6 Uncertainty in the Bearing Capacity of Footings in/on Granular Soils Subjected to Vertical-Eccentric, Inclined-Centric, and Inclined-Eccentric Loading

3.6.1 Scope and Loading Procedures of the Case Histories

The analysis of failure under vertical-eccentric, inclined-centric, and inclined-eccentric loading is based on test results from DEGEBO, Perau (1995), Montrasio (1994), and Gottardi (1992). The test conditions of the various data sources are summarized in Table 31. The following analysis is based on the loading convention shown in Figure 64(a).

The application of loadings in the tests varied. In the tests with *radial load paths,* both the vertical and the horizontal loads were increased up to failure, maintaining a constant ratio of F_3/F_1 during the test, i.e., the load inclination (δ) was constant (see Figure 64(b)). The same applies to the tests with eccentric loading; the eccentricity, $e = M_2/F_1$, was maintained constant during the test, because the vertical load was applied eccentrically at one location. On the other hand, in the tests with *step-like load paths,* the vertical load was increased up to a certain level and then kept constant while the horizontal load was increased up to failure (see Figure 64(c)).

This means that the load inclination was no longer constant during the test but varied from zero up to the maximum load inclination at failure, δ_{ult}. The step-like load paths were applied in tests under inclined-centric and inclined-eccentric loadings only.

3.6.2 Determination of the Measured Strength Limit State for Foundations Under Inclined Loading

The procedure to determine the failure loads from the model tests depends on the load paths applied in the tests. The analysis shows that in the case of a test with a radial load path it is sufficient to consider only the vertical load versus vertical displacement curve. This curve already includes the unfavorable effect that a horizontal load or a bending moment has on the bearing capacity of a shallow foundation, leading to smaller vertical failure loads compared to the case of centric vertical loading.

Figure 65 provides an example using test results with inclined loading performed by Montrasio (1994) under different load inclination angles. Both vertical load/vertical displacement and horizontal load/horizontal displacement curves are shown for each test with inclined load. The load displacement relationship in Figure 65 indicates that the vertical failure load, $F_{1,ult}$, decreases with the increase of the load inclination.

Applying the minimum slope criterion to the centric vertical load test results ($\delta = 0°$, MoA2.1) provides the failure load $F_{10,ult} = 0.956$ kip (4.25kN). The failure loads for the tests with inclined loading decrease to $F_{1,ult} = 0.738$kip (3.28kN) for a load inclination angle of $\delta = 3°$ (MoD2.1) and $F_{1,ult} = 0.677$ kip (3.01kN) for $\delta = 8°$ (MoD2.2) and further

Table 31. Test data used for failure analysis.

Source	Soil conditions	Footing size ft² (m²)	Footing base	Loading[1]	Load application[1]
DEGEBO	Fine to medium sand, loose to medium dense, dense; gravel, medium dense, dense	1.6×6.6 (0.5×2.0) 3.3×3.3 (1.0×1.0) 3.3×9.8 (1.0×3.0) 2.0×6.9 (0.6×2.09)	medium rough (prefabricated)	Eccentric	radial load path
				Inclined	radial load path
				Inclined-eccentric	radial load path
Perau (1995)	Medium to coarse sand, dense to very dense	0.3×0.3 (0.09×0.09) 0.2×0.2 (0.05×0.15)	rough (base glued with sand)	Eccentric	radial load path
				Inclined	step-like load path
				Inclined-eccentric	F_1-M_2: radial load path F_1-F_3: step-like load path
Montrasio (1994)	Medium to coarse sand (Ticino Sand), dense	0.3×0.3 (0.08×0.08) 0.5×0.3 (0.16×0.08) 0.8×0.3 (0.24×0.08)	rough (base glued with sand)	Eccentric	radial load path
				Inclined	radial load path
				Inclined-eccentric	F_1-F_3: step-like load path F_3-M_2: radial load path
Gottardi (1992)	Medium to coarse sand (Adige Sand), dense	1.6×0.3 (0.5×0.1)	rough (base glued with sand)	Eccentric	radial load path
				Inclined	radial or step-like load path
				Inclined-eccentric	F_1-M_2: radial load path F_1-F_3: radial or step-like load path

[1] See Figure 64 for details

(a) Loading convention

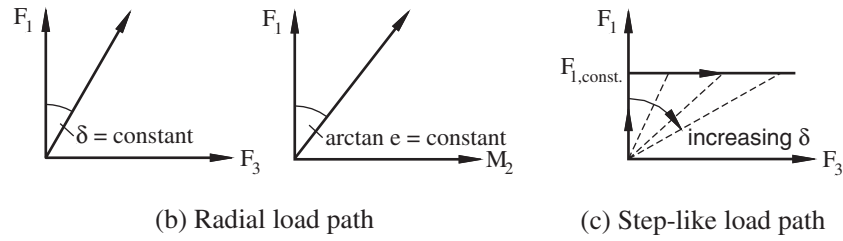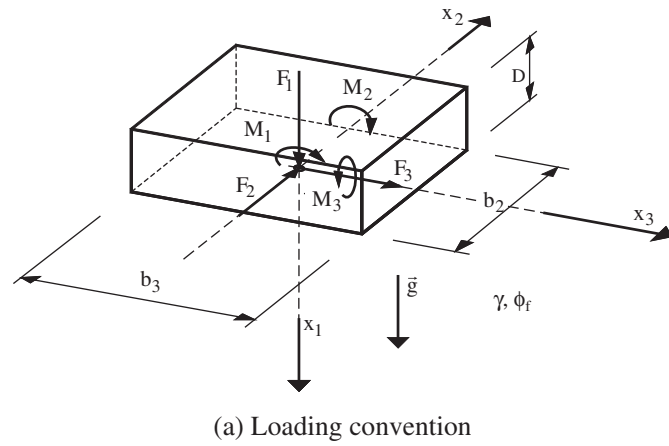(b) Radial load path

(c) Step-like load path

Figure 64. Loading convention and load paths used during tests.
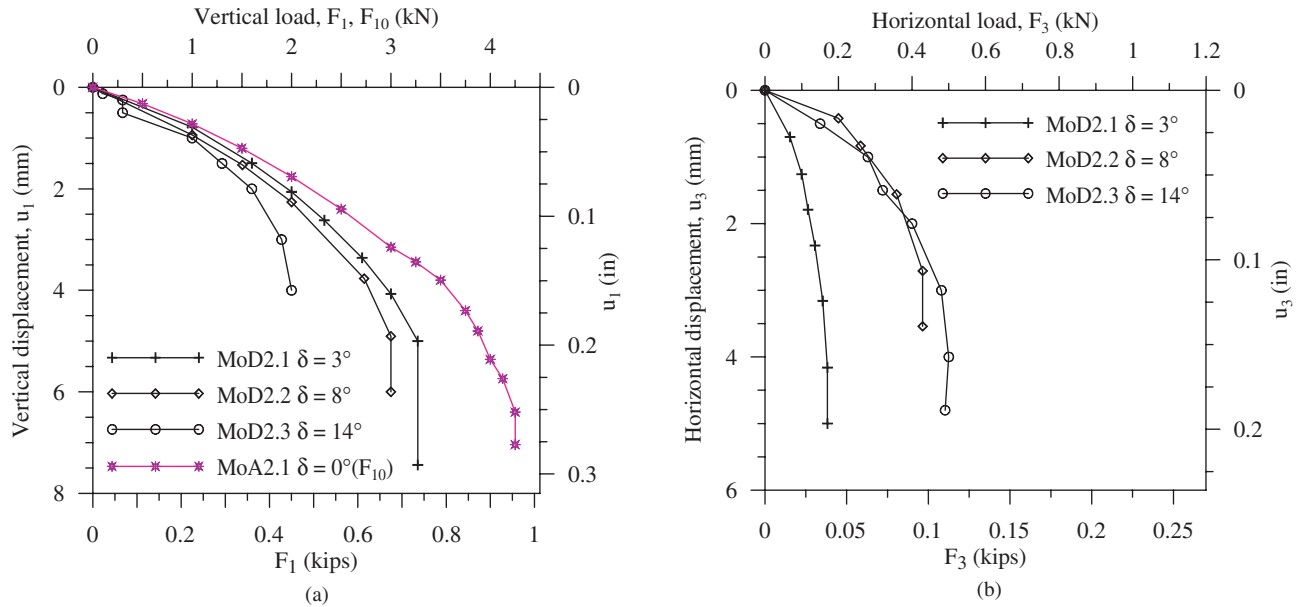

Figure 65. Load–displacement curves for model tests conducted by Montrasio (1994) with varying load inclination: (a) vertical load versus vertical displacement and (b) horizontal load versus horizontal displacement.

decreases to $F_{1,ult} = 0.425$kip (1.89kN) when the load inclination increases to $\delta = 14°$ (MoD2.3). Consequently, the corresponding horizontal component of the failure load, $F_{3,ult}$, increases with the increase in the load inclination. Overall, the horizontal loads are significantly smaller than the vertical failure loads due to limited soil-foundation frictional resistance. This procedure results in vertical failure loads ($F_{1,ult}$) that can be directly related to the theoretical failure loads determined by the calculation model for the relevant load inclination, hence making it possible to obtain the bias of the model for the bearing capacity of foundations under inclined loads.

In the case of a step-like load path, a different procedure has to be applied. In these tests, the vertical load was kept constant up to failure, hence the vertical load/vertical displacement curves are not meaningful. The failure is analyzed on the basis of the horizontal load/horizontal displacement curves resulting in horizontal failure loads, $F_{3,ult}$. The vertical failure loads, $F_{1,ult}$, are the ones corresponding to the horizontal failure loads, $F_{3,ult}$, and coincide with the constant vertical load in each test. As the load inclination is increased during the test, the maximum load inclination reached is the load inclination at failure, $\tan \delta_{ult} = F_{3,ult}/F_{1,ult}$. The theoretical (vertical) failure load is then calculated for the load inclination at failure, δ_{ult}, and compared to the measured vertical failure load, $F_{1,ult}$, to determine the bias. Additionally, the theoretical horizontal failure loads are calculated using the respective load inclination at failure and the theoretical vertical failure loads. It can be shown that the resulting biases of the horizontal failure loads coincide with the biases of the vertical failure loads and confirm this procedure.

In both procedures, the minimum slope criterion and the two-slope criterion were examined for the failure load interpretation. In most cases, the results were found to be comparable. However, in some cases, the two-slope criterion was not applicable (FOTIDs #251 and #266, DEGEBO tests on eccentric loading, FOTIDs #301 and #317, and DEGEBO tests on inclined loading) while the minimum slope criterion could always be used and therefore seemed to have a distinct advantage.

3.6.3 Summary of Mean Bias Statistics for Vertical-Eccentric Loading

Table 32 presents a summary of the statistics of the bias for the footings under vertical-eccentric loading. Section G.2 in Appendix G presents the details of the bias calculation for a single relevant case history (ID #471) of database UML-GTR ShalFound07. The total number of cases under vertical-eccentric loading from all sources was 43, including all outliers to be addressed in Chapter 4. Seventeen cases from DEGEBO, 14 cases from Montrasio (1994) and Gottardi (1992) and 12 cases from Perau (1995) could be analyzed. Figure 66 presents a histogram and a PDF of the bias as well as the relationship between measured and calculated bearing capacities for all vertical, eccentrically loaded foundation cases summarized in Table 32. DEGEBO results show the highest mean and COV of the bias when using any of the failure criteria. Table 33 summarizes the statistics of the bias associated with bearing capacity calculations when using the full geometrical size of the foundation width (B). Table 33 was added in order to gain perspective on the bias in cases where the influence of the effective width is neglected.

Comparing Tables 32 and 33, it can be seen that the mean bias of the ultimate strength estimation decreases and the COV of the bias increases when full footing geometry (B) is used instead of the effective footing dimensions (B'). This is an expected outcome considering the larger B would result in a higher bearing capacity (and hence decreased bias) while the methodology is incorrect, contributing to the increased uncertainty (being represented by the COV). The decreased bias and increased COV would necessitate a significant increase in the resistance to ensure a specified safety, i.e., utilizing lower resistance factors. For example, considering all cases, the resistance factor obtained is 0.60 when B' is used and 0.30

Table 32. Summary of the statistics for biases of the test results for vertical-eccentric loading when using effective foundation width (B').

Tests	No. of cases	Minimum slope criterion			Two-slope criterion		
		Mean	Std. dev.	COV	Mean	Std. dev.	COV
DEGEBO – radial load path	17 (15)[1]	2.22	0.754	0.340	2.04	0.668	0.328
Montrasio (1994)/Gottardi (1992) – radial load path	14	1.71	0.399	0.234	1.52	0.478	0.313
Perau (1995)– radial load path	12	1.43	0.337	0.263	1.19	0.470	0.396
All cases	43 (41)[1]	1.83	0.644	0.351	1.61	0.645	0.400

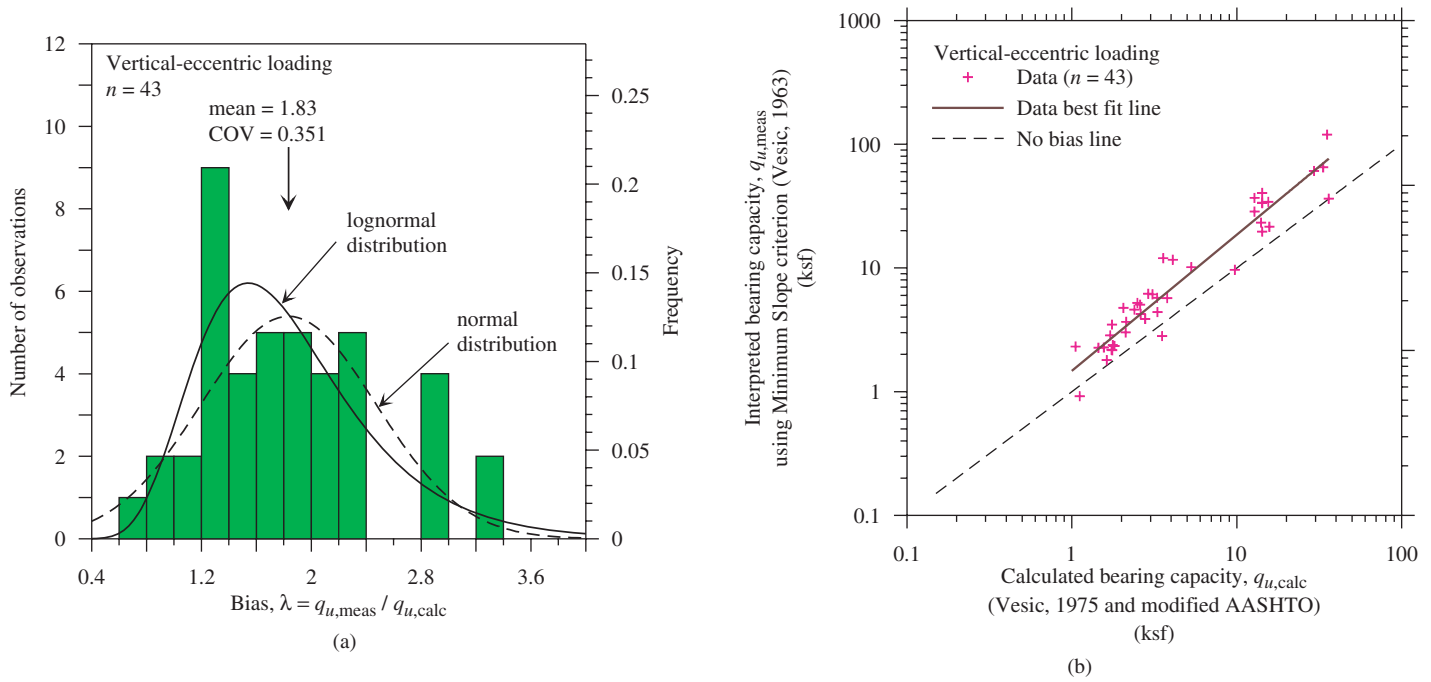[1] Number of cases for two-slope criterion

Figure 66. (a) Histogram and probability density function of the bias and (b) relationship between measured and calculated bearing capacity for all vertical, eccentrically loaded shallow foundations.

when B is used. Thus, Tables 32 and 33 indicate that the bearing capacity obtained using the full footing width (B) is unsafe when compared to the bearing capacity obtained when using the effective width (B').

3.6.4 Summary of Mean Bias Statistics for Inclined-Centric Loading

The mean and standard deviation of the calculated biases in the case of inclined loading are summarized in Table 34 for the two failure criteria. Section G.3 of Appendix G presents the details of the bias calculations for a single relevant case history (ID #547) of database UML-GTR ShalFound07. Figure 67

presents a histogram and PDF of the bias as well as the relationship between measured and calculated bearing capacity for all inclined, centrically loaded shallow foundations.

There are no differences in the biases obtained from the two-slope and the minimum slope failure criteria for the cases of step-like load paths. Gottardi's tests with radial load paths sometimes seem to result in smaller biases than the other tests, but overall, no significant differences exist in the biases of the step-like and radial load path tests. The biases determined for the DEGEBO tests are also in the same order of magnitude as the ones from the small-scale model tests although they were carried out on foundations significantly larger in size. DEGEBO tests were carried out on foundations of 1.6 ft × 3.3 ft

Table 33. Summary of the statistics for biases of the test results for vertical-eccentric loading when using the full foundation width (B).

Tests	No. of cases	Minimum slope criterion			Two-slope criterion		
		Mean	Std. dev.	COV	Mean	Std. dev.	COV
DEGEBO – radial load path	17 (15)[1]	1.30	0.464	0.358	1.20	0.425	0.355
Montrasio (1994)/Gottardi (1992) – radial load path	14	0.97	0.369	0.380	0.86	0.339	0.396
Perau (1995) – radial load path	12	0.79	0.302	0.383	0.64	0.296	0.465
All cases	43 (41)[1]	1.05	0.441	0.420	0.92	0.423	0.461

[1] Number of cases for two-slope criterion

Table 34. Summary of the statistics for biases of the test results for inclined-centric loading when using foundation width (*B*).

Tests	No. of cases	Minimum slope criterion			Two-slope criterion		
		Mean	Std. dev.	COV	Mean	Std. dev.	COV
DEGEBO/ Montrasio (1994)/Gottardi (1992) – radial load path	26 (24)[1]	1.56	0.346	0.222	1.35	0.452	0.334
Perau (1995)/Gottardi (1992) – step-like load path	13	1.17	0.537	0.459	1.17	0.537	0.459
All cases	39 (37)[1]	1.43	0.422	0.295	1.29	0.455	0.353

[1] Number of cases for two-slope criterion

(0.5 m × 1.0 m) to 3.3 ft × 9.8 ft (1 m × 3 m) versus the small scale models having foundation sizes of 2 in. × 6 in. (5 cm × 15 cm) to 4 in. × 20 in. (10 cm × 50 cm).

3.6.5 Summary of Mean Bias Statistics for Inclined-Eccentric Loading

Table 35 presents a summary of the statistics of the bias for footings subjected to inclined-eccentric loadings, with both radial and step-like load paths and including the effective foundation width, B'. Figure 68 presents a histogram and PDF of the bias as well as the relationship between measured and calculated bearing capacity for all inclined, eccentrically loaded

shallow foundation cases. As in the inclined-centric loading cases, there is no significant difference in the tests results between the radial and the step-like load paths. The bearing capacity calculations of these case histories were noticeably affected by using the effective foundation width (B') versus the geometrical actual foundation width (B). Table 36 summarizes the statistics associated with the bearing capacity calculations using the full geometrical foundation width (B) in order to gain perspective on the bias in cases where the influence of the effective width is neglected. The biases presented in Table 36 indicate that for the examined case histories the calculated bearing capacity using the effective width resulted in a bias about two times larger (i.e., a bearing capacity two times
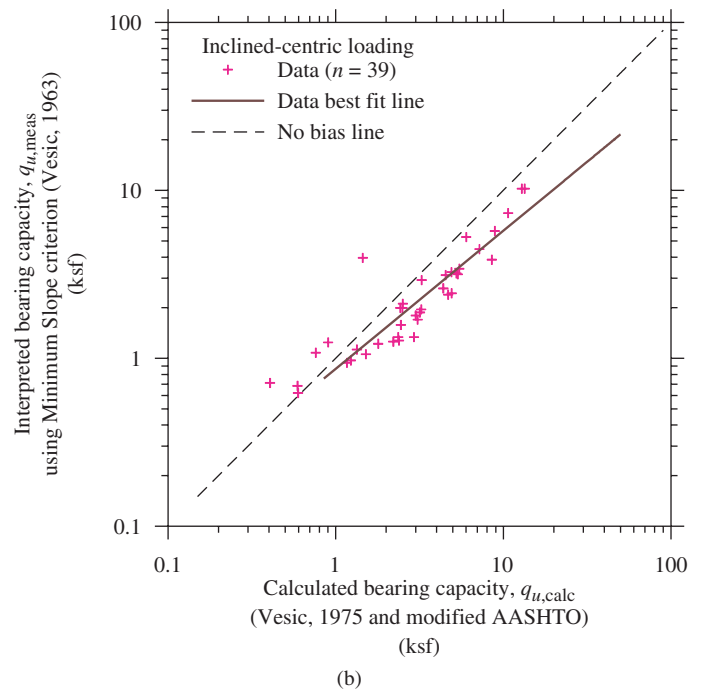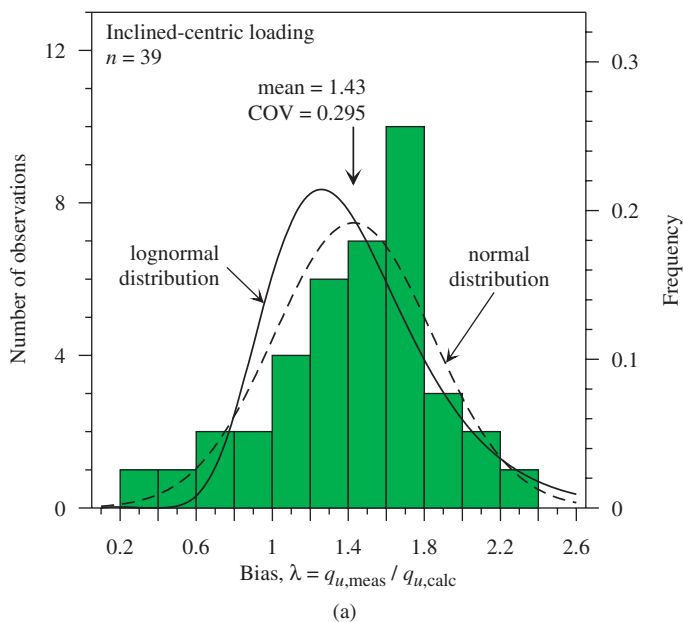
Figure 67. (a) Histogram and probability density function of the bias and (b) relationship between measured and calculated bearing capacity for all inclined, centrically loaded shallow foundations.

Table 35. Summary of the statistics for biases of the test results for inclined-eccentric loading when using effective foundation width (B′).

Tests		No. of cases	Minimum slope criterion			Two-slope criterion		
			Mean	Std. dev.	COV	Mean	Std. dev.	COV
DEGEBO/Gottardi (1992) – radial load path		8	2.06	0.813	0.394	1.78	0.552	0. 310
Step-like load path	Montrasio (1994)/ Gottardi (1992)	6	2.13	0.496	0.234	2.12	0.495	0.233
	Perau (1995) – positive eccentricity	8	2.16	1.092	0.506	2.15	1.073	0.500
	Perau (1995) – negative eccentricity	7	3.43	1.792	0.523	3.39	1.739	0.513
	All step-like load cases	21	2.57	1.352	0.526	2.56	1.319	0.516
All cases		29	2.43	1.234	0.508	2.34	1.201	0.513

Figure 68. (a) Histogram and probability density function of the bias and (b) relationship between measured and calculated bearing capacity for all inclined, eccentrically loaded shallow foundations.

Table 36. Summary of the statistics for biases of the test results for inclined-eccentric loading when using foundation width (B).

Tests		No. of cases	Minimum slope criterion			Two-slope criterion		
			Mean	Std. dev.	COV	Mean	Std. dev.	COV
DEGEBO/Gottardi (1992) – radial load path		8	1.07	0.448	0.417	0.94	0.365	0. 387
Step-like load path	Montrasio (1994)/ Gottardi (1992)	6	1.18	0.126	0.106	1.18	0.125	0.106
	Perau (1995)– positive eccentricity	8	0.70	0.136	0.194	0.70	0.135	0.194
	Perau (1995) – negative eccentricity	7	1.09	0.208	0.191	1.08	0.208	0.193
	All step-like load cases	21	0.97	0.267	0.276	0.96	0.267	0.277
All cases		29	1.00	0.322	0.323	0.96	0.290	0.303

smaller) than that obtained using the full geometrical width of the foundation. The ramifications of these findings are relevant to design practices in which the loading details are not known at the time of the design. This issue was touched upon in Section 3.1.7 and will be further discussed in Chapter 4. The change in variability between the two cases as well as the mean bias are greatly affected by a few outliers and will be further discussed in Chapter 4. The effects of the moment direction (or load eccentricity) with respect to the horizontal load, noted in Tables 35 and 36 as positive and negative moments for tests conducted by Perau (1995), are discussed in the following sections.

3.7 Loading Direction Effect for Inclined-Eccentric Loading

The loading direction in the case of inclined-eccentric loading affects the failure loads. Figure 69 presents the definitions established for the loading direction along the footing width (a) and along the footing length (b) (see also Butterfield et al., 1996) depending on the eccentricity direction in relation to the direction of the applied lateral load. The footing in the upper part of Figure 69 (a) and (b) is loaded by a horizontal load and

Moment acting in direction opposite to the lateral loading – negative eccentricity

Moment acting in the same direction as the lateral loading – positive eccentricity

Moment acting in direction opposite to the lateral loading – negative eccentricity

Moment acting in the same direction as the lateral loading – positive eccentricity

Figure 69. Loading directions for the case of inclined-eccentric loadings: (a) along footing width and (b) along footing length.

an eccentric vertical load with "negative" eccentricity. The resultant moment, which is negative in case of loading eccentricity along footing width b_3 (a) and positive in case of loading eccentricity along footing length b_2 (b)(refer to Figure 69 for sign conventions), then acts in the opposite direction to the horizontal load. The induced rotations counteract the displacements forced by the horizontal load, leading to a higher resistance of the footing compared with the inclined-centric load case and, thus, to higher failure loads. In contrast, the footing in the lower part of Figure 69 is loaded by an eccentric vertical load with "positive" eccentricity. This leads to a positive moment in the case of loading eccentricity along footing width b_3 (a), and a negative moment in the case of loading eccentricity along footing length b_2 (b), which acts in the same direction as the horizontal load. The induced rotations enforce the horizontal displacements; hence, the footing resistance is smaller than in the case of inclined-centric loading, leading to smaller failure loads.

In a different approach, when the moment is in the "opposite" direction, it induces higher contact stresses between the foundation and the soil in the "front" of the foundation where the lateral load is applied. As the foundation-soil friction is progressive, the higher contact stress results in a higher friction resistance and, hence, the overall layer capacity. In contrast, when the moment acts in the "same" direction, the contact stress at the "front" of the footing decreases, thereby reducing the friction and resulting in a decrease in the total foundation resistance (bearing capacity). The effect of the loading direction expressed in Tables 35 and 36 is demonstrated in a graphical format in Figures 70 and 71. Figures 70 and 71 present a histogram and PDF of the bias as well as the relationship between measured and calculated bearing capacity for inclined-eccentric loading under positive and negative moments, respectively. A comparison of Figures 70 and 71 shows an increase of the bias for the negative moment cases.

The effect of loading direction is further demonstrated by the results of two tests carried out by Gottardi (1992) and shown in Figure 72. The failure loads in the case of loading in the same direction (positive loading eccentricity) are significantly smaller than the failure loads in the case of opposite loading direction (negative loading direction). The influence on the bias is substantial—0.37 versus 0.64 for the two-slope criterion and 0.37 versus 0.66 for the minimum slope criterion. Hence, it appears that this difference cannot be neglected and needs to be considered.

Figure 73 shows the load-displacement curves for two double tests (positive and negative loading eccentricity) conducted by Perau (1995) and one double test by Montrasio (1994), applying different loading directions at the same level of vertical loading. The results of Perau's and Montrasio's tests show a similar trend. Montrasio's test leads to a bias of 1.86 versus 1.97 (positive versus negative loading eccentricity),
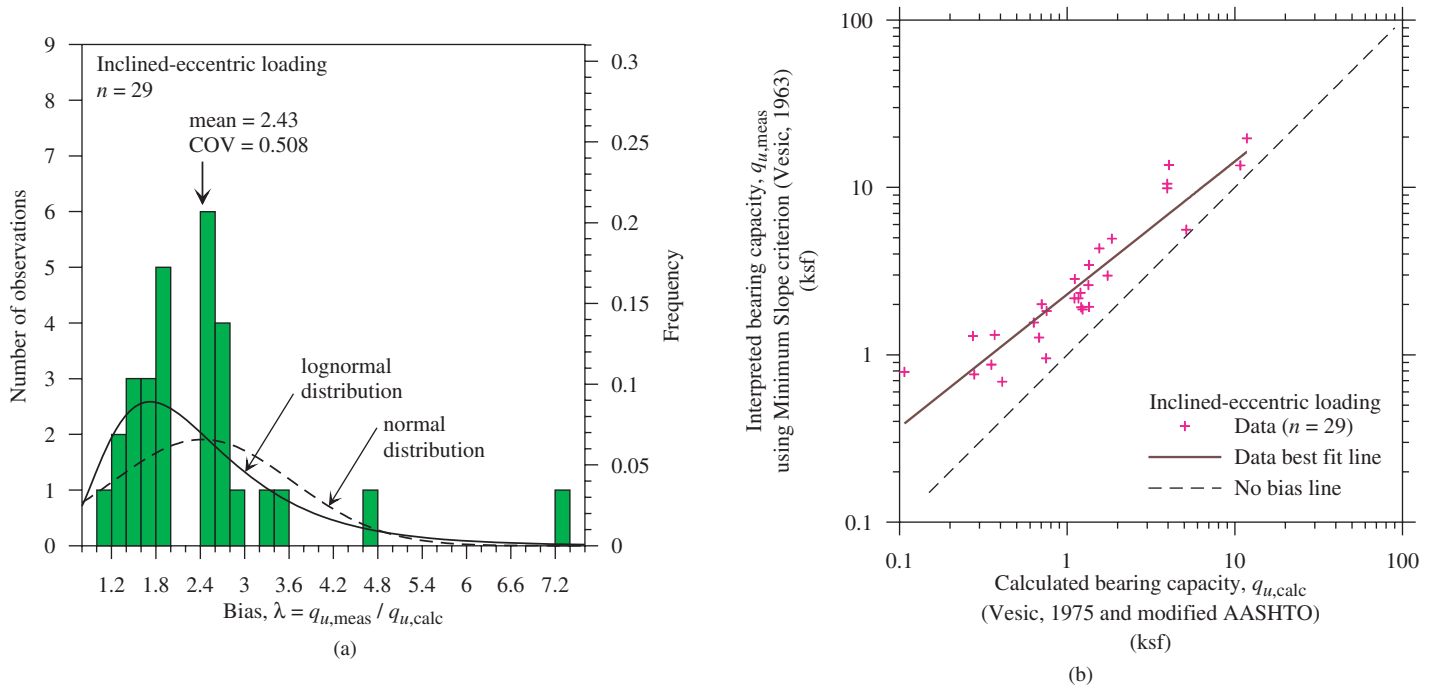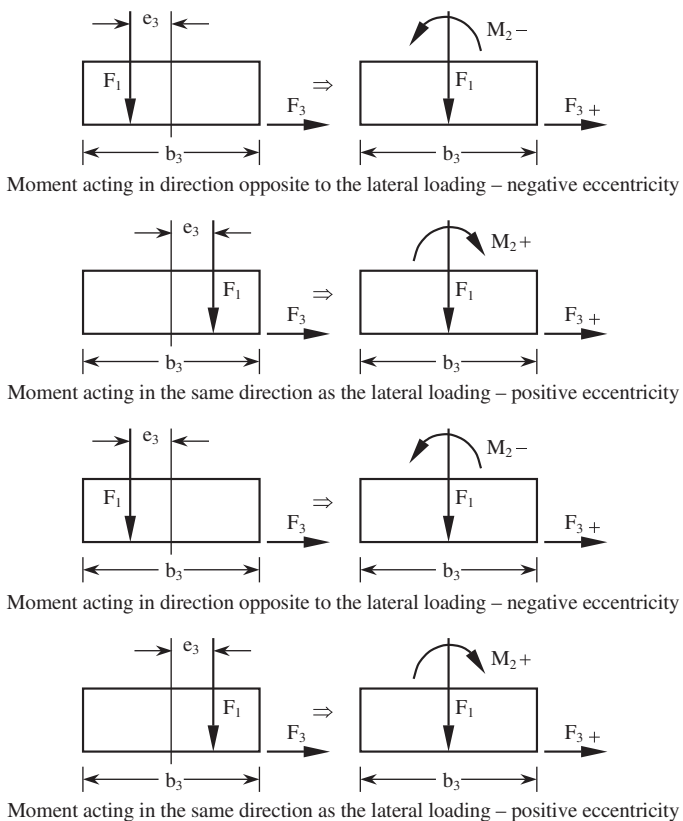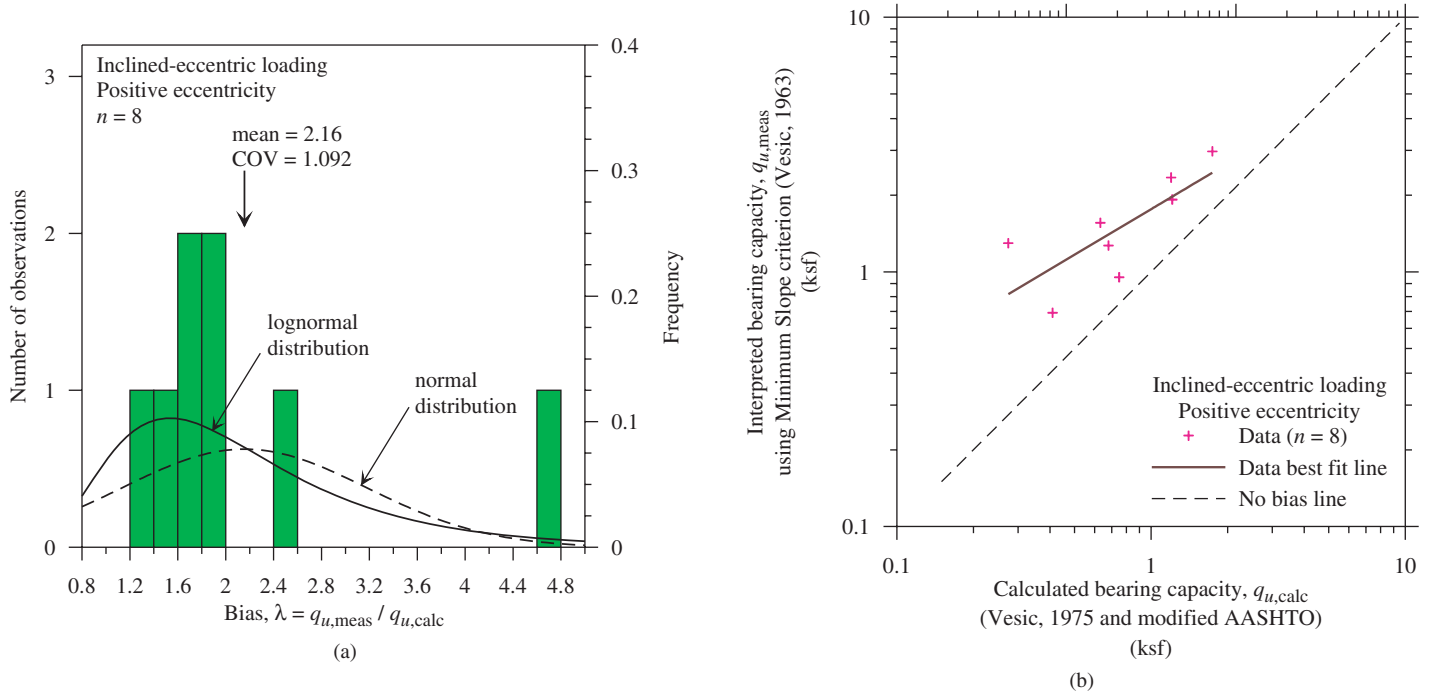
Figure 70. (a) Histogram and probability density function of the bias and (b) relationship between measured and calculated bearing capacity for all inclined, eccentrically loaded shallow foundations under positive moment.
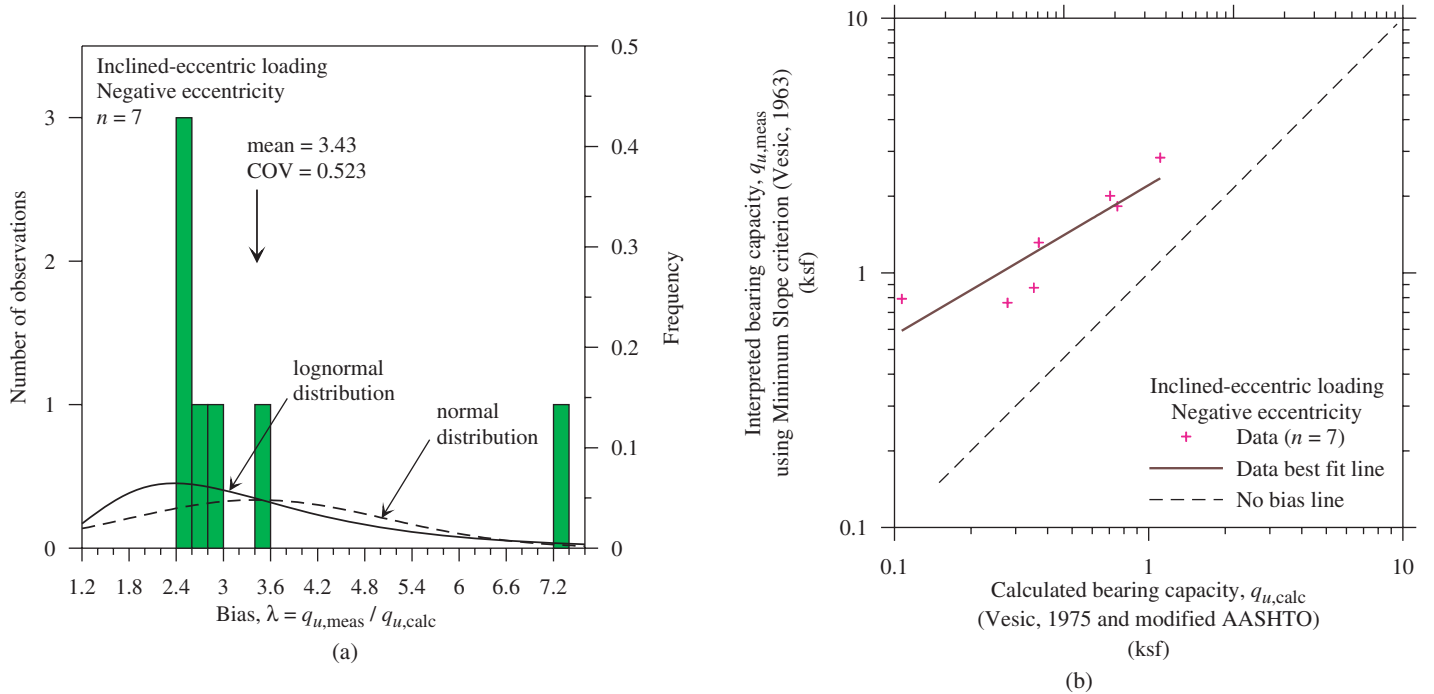
Figure 71. (a) Histogram and probability density function of the bias and (b) relationship between measured and calculated bearing capacity for all inclined, eccentrically loaded shallow foundations under negative moment.
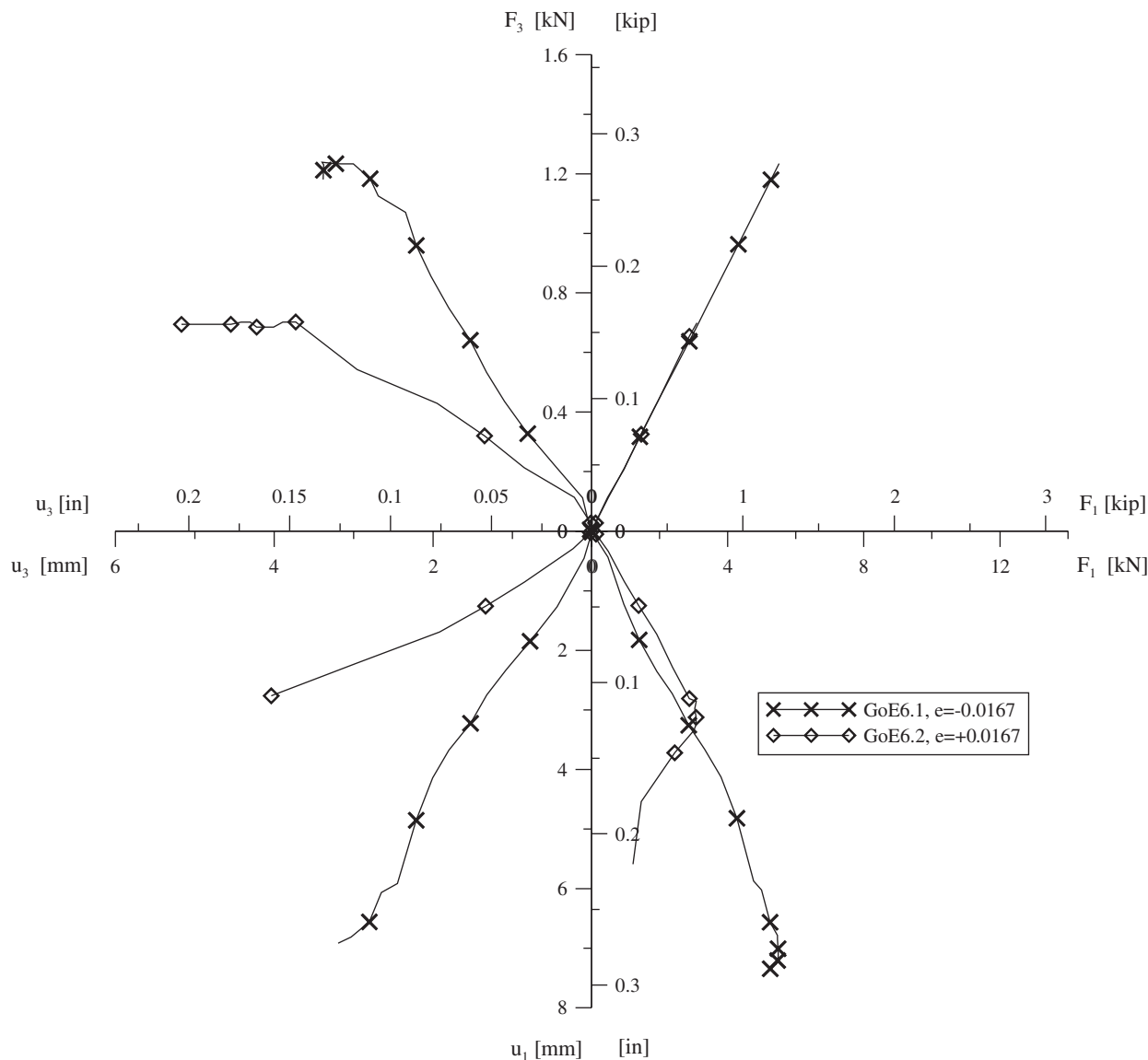
Figure 72. Load–displacement curves for inclined-eccentric loading with different loading directions utilizing data from Gottardi (1992).

indicating a minor effect of the loading direction. However, this effect is more significant in Perau's tests, where the evaluation of the failure loads leads to a mean bias of 1.79 (COV 0.206) for a horizontal load and moment acting in the same direction (positive loading eccentricity) and 2.76 (COV 0.152) for a moment in an opposite loading direction (negative loading eccentricity).

In general, it can be stated that the effect of the loading direction is less pronounced if the vertical load (F_1) is relatively high (i.e., the load inclination is relatively small) because this effect is predominantly determined by the load inclination and not by the load eccentricity. The level of the vertical load (F_1) can properly be expressed by relating it to the failure load for centric vertical loading (F_{10}). The notation F_{10} has been adopted in order to differentiate the failure load of vertical-centric loading from the vertical component F_1 of the inclined failure loads (refer to Figure 65 and Section 3.6.2). In this context, small load inclinations coincide with relatively high vertical load levels. Figure 74 shows an evaluation of the bearing capacity in the $F_2/F_{10} - M_3/(F_{10} \cdot b_2)$ plane performed by Lesny (2001) using Perau's (1995) test results. In reference to Figure 64, F_2 is the horizontal component of the inclined load and b_2 is the footing length in the same direction. Different loading directions and different load levels have been analyzed in Figure 74, resulting in distorted trend lines due to the existence of a higher capacity if horizontal load and moment act in the opposite direction (i.e., both load components are positive and the loading eccentricity is negative). However,
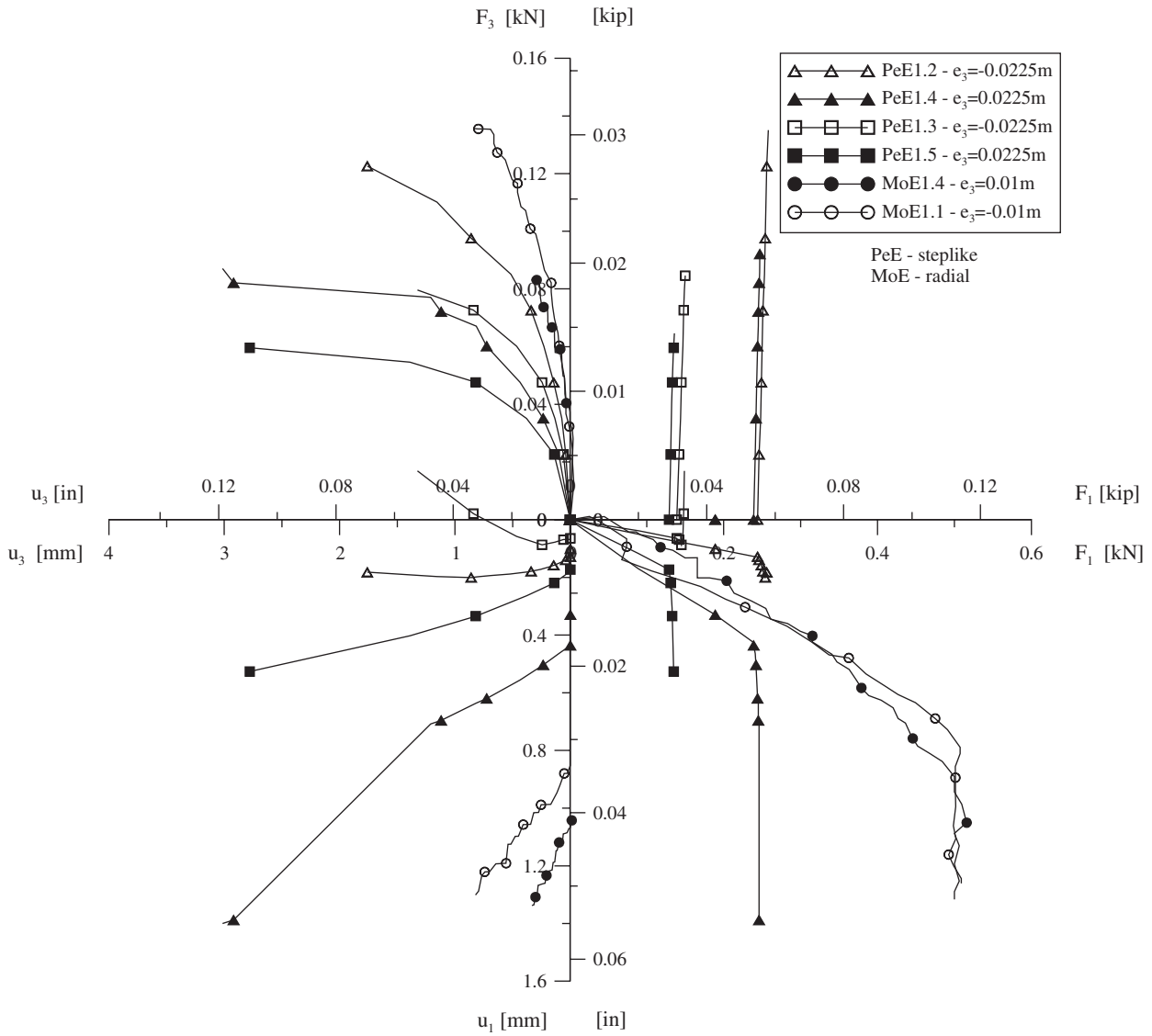
Figure 73. Load–displacement curves for inclined-eccentric loading with different loading directions utilizing data from Perau (1995) and Montrasio (1994).

the analysis also reveals that the gain of capacity is relatively small, and, for vertical load levels greater than or equal to 0.3, the effect of loading direction is negligible.

3.8 Uncertainty in the Bearing Capacity of Footings in/on Rock

3.8.1 Overview

The ratio of the measured/interpreted bearing capacity to the calculated shallow foundation bearing capacity (the bias λ) was used to assess the uncertainty of the selected design methods for the 119 case histories of database GTR-UML RockFound07. Section 1.7 details the methods of analysis selected for the bearing capacity calculations. Appendix G provides detailed examples for the calculations performed for each analysis. Sections G.5 and G.6 relate to the utilization of Goodman's (1989) method, and Section G.7 relates to the utilization of Carter and Kulhawy's (1988) method in the traditional way (i.e., using Equation 82a). This section summarizes the results of the analyses for the examined methods: the semi-empirical mass parameters procedure developed by Carter and Kulhawy (1988) and the analytical method proposed by Goodman (1989).

The consistency of the rocks in the database, the types of foundation, and the level of knowledge of the rock were categorized, when applicable, while examining their influence on the bias. In addition, histograms and PDFs of the bias obtained by the different methods are presented and discussed.
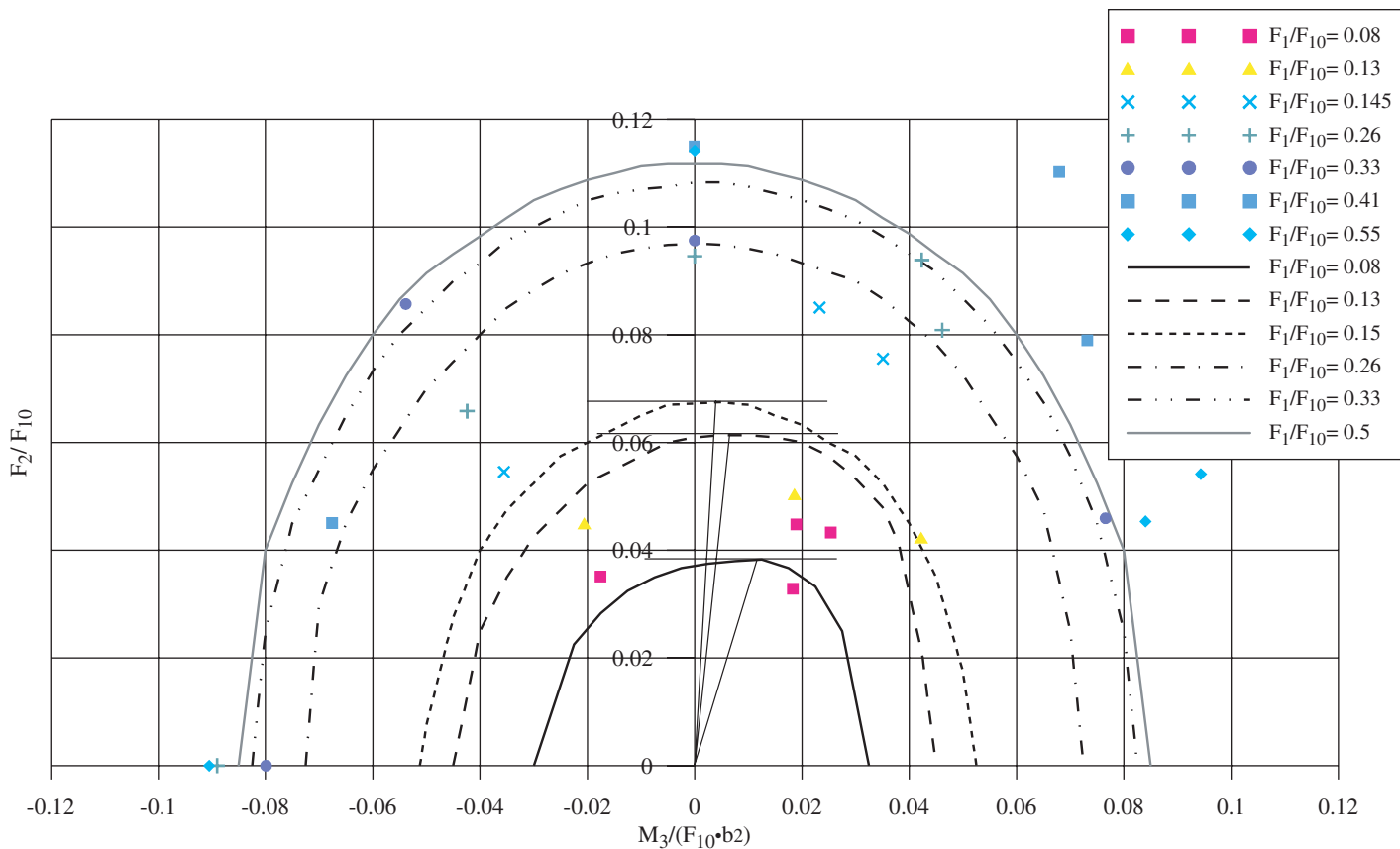
Figure 74. Influence of loading direction on capacity in the case of inclined-eccentric loading (Lesny, 2001).

3.8.2 Carter and Kulhawy's (1988) Semi-Empirical Bearing Capacity Method

3.8.2.1 Presentation of Findings

Carter and Kulhawy's (1988) method is described in Section 1.7.6 and its application is demonstrated in Section G.7 in Appendix G. Table E-2 of Appendix E presents the calculated bearing capacity values and the associated bias for each of the 119 case histories of database UML-GTR RockFound07 (Table E-2 includes all 122 original cases and the excluded 3 cases as noted). The relationships between the bearing capacities (q_{ult}) calculated using the two Carter and Kulhawy (1988) semi-empirical procedures (Equation 82a and the revised relations given by Equation 82b) and the interpreted bearing capacity (q_{L2}) are presented in Figure 75. Equation 109a provides the best fit line generated using regression analysis of all data using Equation 82a and results in a coefficient of determination (R^2) of 0.921. Equation 109b represents the best fit line generated using regression analysis of all data using Equation 82b for calculating the bearing capacity and results in a coefficient of determination (R^2) of 0.917.
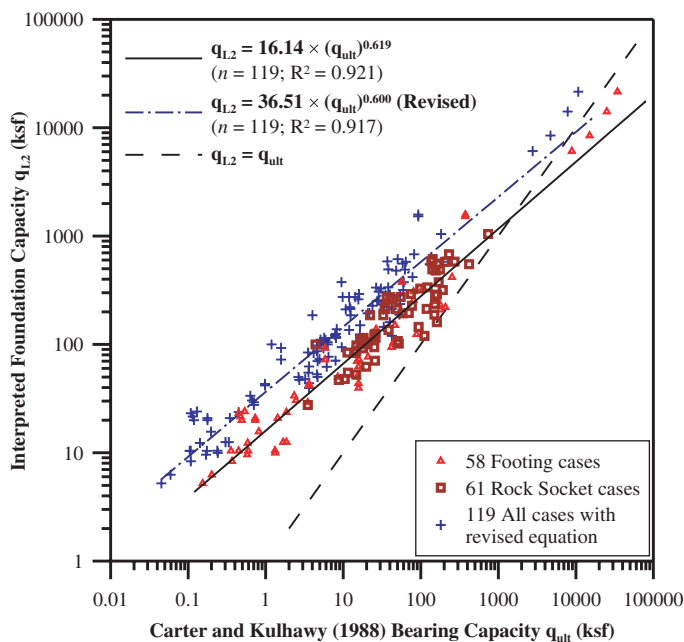
Figure 75. Relationship between calculated bearing capacity (q_{ult}) using two versions of Carter and Kulhawy (1988) and interpreted bearing capacity (q_{L2}).

Table 37. Summary of the statistics for the ratio of measured (q_{L2}) to calculated bearing capacity (q_{ult}) for all foundations on rock using the Carter and Kulhawy (1988) method.

Cases	n	No. of sites	m_λ	σ_λ	COV
All (measured q_u)	119	78	8.00	9.92	1.240
Measured discontinuity spacing (s′)	83	48	8.03	10.27	1.279
Fractured with measured discontinuity spacing (s′)	20	9	4.05	2.42	0.596
All non-fractured	99	60	8.80	1066	1.211
Non-fractured with measured discontinuity spacing (s′)	63	39	9.29	11.44	1.232
Non-fractured with s′ based on AASHTO (2007)	36	21	7.94	9.22	1.161

n = number of case histories, m_λ = mean of biases, σ_λ = standard deviation, COV = coefficient of variation
Calculated capacity based on Equation 82a

$$q_{L2} = 16.14 \left(q_{ult} \right)^{0.619} \tag{109a}$$

$$q_{L2} = 36.51 \left(q_{ult} \right)^{0.600} \tag{109b}$$

It can be observed in Figure 75 (and in Equations 109a and 109b) that the revised expression provided by Equation 82b gives systematically higher resistance biases than those biases obtained using Equation 82a. The bias mean and COV obtained using Equation 82b for all data ($n = 119$) are found to be 30.29 and 1.322, respectively, versus 8.00 and 1.240, respectively, obtained using Equation 82a. Both relations provide close to parallel lines when compared to the measured capacities. Equations 109a and 109b suggest that Equation 82b roughly predicts half the capacity of Equation 82a as its multiplier to match the measured capacity is about double. As the relations provided by Equation 82a are already consistently conservative, Equation 82a is preferred over Equation 82b, and the results processed and analyzed are those obtained using Equation 82a.

Statistical analyses were performed to investigate the effect of the joint or discontinuity spacing (s′) either measured or determined based on AASHTO (2008) tables (see Section 1.8.3) and the effect of the friction angle (ϕ_f) of the rock on the calculated bearing capacity. Statistics for the ratio of the bias

(measured bearing capacity, q_{L2}, to calculated bearing capacity, q_{ult}) using Carter and Kulhawy's (1988) semi-empirical method are summarized in Table 37. In Table 37, the statistics are categorized according to the joint spacing and the source of the data (i.e., measured discontinuity spacing versus spacing assumed based on the specifications). In Table 38, the data are subcategorized according to type of foundation (footings versus rock sockets) and the source of the joint spacing data. Table 39 is a summary of the statistics for the ratio of the measured bearing capacity (q_{L2}) to calculated bearing capacity (q_{ult}) categorized according to foundation type and rock quality ranges for each type and all types combined.

The distribution of the ratio of the interpreted bearing capacity to the calculated bearing capacity (the bias λ) for the 119 case histories (detailed in Table E-2 of Appendix E) is presented in Figure 76. The distribution of the bias λ has a mean (m_λ) of 8.00 and a COV$_\lambda$ of 1.240 and resembles a lognormal random variable. The distribution of the bias λ for foundations on fractured rock only (20 cases) is presented in Figure 77 and has an m_λ of 4.05 and a COV$_\lambda$ of 0.596. The distribution of the bias λ for the foundations on fractured rock resembles a lognormal random variable and has less scatter, reflected by the smaller COV when compared with the distribution of λ for all 119 case histories.

Table 38. Summary of the statistics for the ratio of measured (q_{L2}) to calculated bearing capacity (q_{ult}) of rock sockets and footings on rock using the Carter and Kulhawy (1988) method.

Cases	n	No. of sites	m_λ	σ_λ	COV
All rock sockets	61	49	4.29	3.08	0.716
All rock sockets on fractured rock	11	6	5.26	1.54	0.294
All rock sockets on non-fractured rock	50	43	4.08	3.29	0.807
Rock sockets on non-fractured rock with measured discontinuity spacing (s′)	34	14	3.95	3.75	0.949
Rock sockets on non-fractured rock with s′ based on AASHTO (2007)	16	13	4.36	2.09	0.480
All footings	58	29	11.90	12.794	1.075
All footings on fractured rock	9	3	2.58	2.54	0.985
All footings on non-fractured rock	49	26	13.62	13.19	0.969
Footings on non-fractured rock with measured discontinuity spacing (s′)	29	11	15.55	14.08	0.905
Footings on non-fractured rock with s′ based on AASHTO (2007)	20	11	10.81	11.56	1.069

n = number of case histories, m_λ = mean of biases, σ_λ = standard deviation, COV = coefficient of variation
Calculated capacity based on Equation 82a

Table 39. Summary of the statistics for the ratio of measured (q_{L2}) to calculated bearing capacity (q_{ult}) using the Carter and Kulhawy (1988) method categorized by the rock quality and foundation type.

Foundation Type	Cases	n	No. of sites	m_λ	σ_λ	COV
All	RMR ≥ 85	23	23	2.93	1.908	0.651
	65 ≤ RMR < 85	57	36	3.78	1.749	0.463
	44 ≤ RMR < 65	17	10	8.83	5.744	0.651
	3 ≤ RMR < 44	22	9	23.62	13.550	0.574
Rock Sockets	RMR ≥ 85	16	16	3.42	1.893	0.554
	65 ≤ RMR < 85	35	24	3.93	1.769	0.451
	44 ≤ RMR < 65	9	8	6.82	6.285	0.921
	3 ≤ RMR < 44	1	1	8.39	--	--
Footings	RMR ≥ 85	7	7	1.81	1.509	0.835
	65 ≤ RMR < 85	22	13	3.54	1.732	0.489
	44 ≤ RMR < 65	8	5	11.09	4.391	0.396
	3 ≤ RMR < 44	21	8	24.34	13.440	0.552

n = number of case histories, m_λ = mean of biases, σ_λ = standard deviation, COV = coefficient of variation
Calculated capacity based on Equation 82a

3.8.2.2 Observations

The presented findings of Carter and Kulhawy's (1988) methods for the prediction of bearing capacity suggest the following:

1. The bias of the estimated bearing resistances obtained using the revised equation (Equation 82b) are systematically higher than those obtained using Equation 82a, with very similar COVs. As both equations are by and large conservative, only the traditional equation (Equation 82a) was used for further analysis and method evaluation.

2. The method (Equation 82a) substantially underpredicts (on the safe side) for the range of capacities typically lower than 700 ksf. The bias increases as the bearing capacity decreases. This provides a logical trend in which founda-
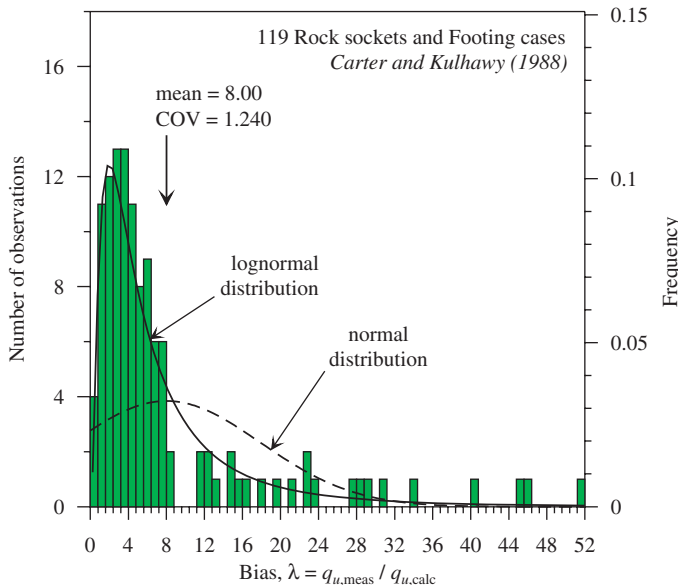
Figure 76. Distribution of the ratio of the interpreted bearing capacity (q_{L2}) to the bearing capacity (q_{ult}) calculated using Carter and Kulhawy's (1988) method (Equation 82a) for the rock sockets and footings in database UML-GTR RockFound07.
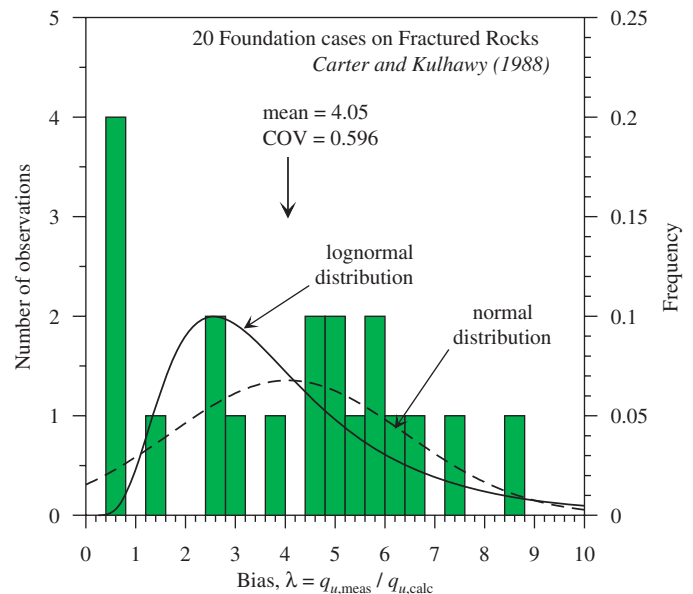
Figure 77. Distribution of the ratio of the interpreted bearing capacity (q_{L2}) to the bearing capacity (q_{ult}) calculated using Carter and Kulhawy's (1988) method (Equation 82a) for foundations on fractured rock in database UML-GTR RockFound07.

tions on lower bearing capacity materials are provided with a higher margin of safety while for foundations on harder rock with higher bearing capacities, the bias is smaller than one (1.0) (i.e., measured capacities are lower than calculated capacities). The bearing capacity values on the higher capacity sides are controlled by the strength of the foundation material (i.e., concrete), and, therefore, the results in that range are not necessarily translated into unsafe practice.

3. Comparison of the statistics obtained for shallow foundations ($n = 58$, $m_\lambda = 11.90$, $COV_\lambda = 1.075$ and number of sites = 29) with the statistics obtained for rock sockets ($n = 61$, $m_\lambda = 4.29$, $COV_\lambda = 0.716$ and number of sites = 49) may suggest that the method better predicts the capacity of rock sockets than the capacity of footings. This observation might also suggest that the use of load-displacement relations for the tip of a loaded rock socket is not analogous to the use of load-displacement relations for a shallow foundation constructed below surface; hence, the data related to the tip of a rock socket should not be employed for shallow foundation analyses. This observation must be re-examined in light of the varied bias of the method with the rock strength, as is evident in Figure 75 and detailed in Table 39. The varying bias of the method, as observed in Figure 75 and described in Number 2 above, results in a relatively high scatter (COV = 1.240 for all cases). When the evaluation is categorized based on rock quality, the scatter (COV) systematically decreases to be between about 0.5 to 0.6, as detailed in Table 39. However, the changes in the mean of the bias with rock quality for the footings are much more pronounced than the changes for the rock sockets because most of the footings were tested on rock that was of lower quality than the rock existing at the tip of the rock sockets. For example, of the 22 cases of the lowest rock quality ($3 \leq RMR < 44$), 21 cases involved a shallow foundation and 1 case involved a rock socket. In contrast, of the 23 cases of the highest quality rock ($RMR \geq 85$), only 7 cases involve footings and 16 cases involve rock sockets. The conclusion, therefore, is that the variation in the method application is more associated with the rock type/strength and its influence on the method's prediction than the foundation type. This conclusion is further confirmed by examination of the Goodman (1989) method, in which the bias is not affected by rock quality and, hence, similar statistics are obtained for the rock socket and the footing cases.

4. No significant differences exist between the cases for which discontinuity spacing (s') was measured in the field and the cases for which the spacing was determined based on generic tables utilizing rock description (Tables 37 and 38).

3.8.3 Goodman's (1989) Analytical Bearing Capacity

3.8.3.1 Presentation of Findings

Goodman's (1989) method is described in Section 1.7.5 and its application is demonstrated in Sections G.5 and G.6 of Appendix G. Table E-3 of Appendix E presents the calculated bearing capacity values for each of the 119 case histories. The relationship between the bearing capacity calculated using Goodman's (1989) analytical procedure (q_{ult}) and the interpreted bearing capacity (q_{L2}) is presented in Figure 78. Equation 110 represents the best fit line that was generated using regression analysis and resulted in a coefficient of determination (R^2) of 0.897.

$$q_{L2} = 2.63 \left(q_{ult} \right)^{0.824} \tag{110}$$

Statistical analyses were performed to investigate the effect of the measured and AASHTO-based joint (2007) or discontinuity spacing (s') and friction angle (ϕ_f) of the rock on the bearing capacity calculations. Table 40 summarizes the statistics for the ratio of the measured bearing capacity (q_{L2}) to calculated bearing capacity (q_{ult}) using Goodman's (1989) analytical method for the entire database. Table 41 provides the statistics for subcategorization based on foundation type and available information. Table 42 is a summary of the statistics for the ratio of the measured bearing capacity (q_{L2}) to the calculated bearing capacity (q_{ult}) categorized according to foundation type and rock quality ranges for each type.
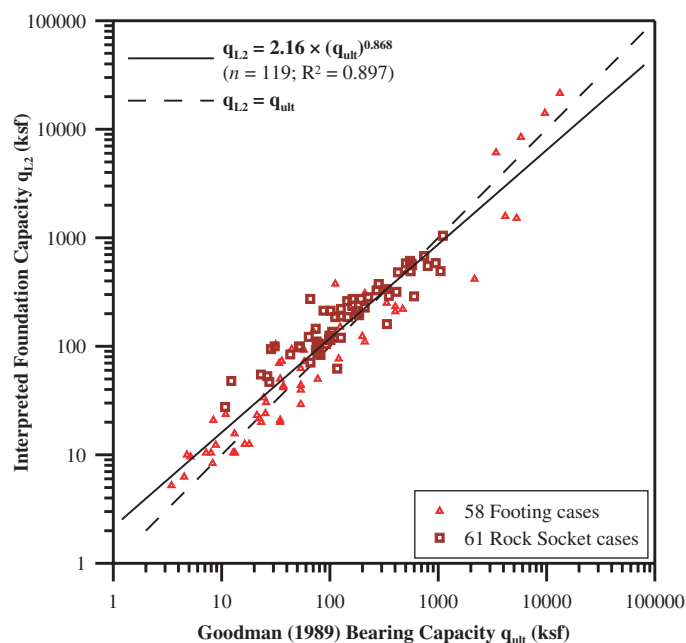
Figure 78. Relationship between Goodman's (1989) calculated bearing capacity (q_{ult}) and the interpreted bearing capacity (q_{L2})

Table 40. Summary of the statistics for the ratio of measured (q_{L2}) to calculated bearing capacity (q_{ult}) of rock sockets and footings on rock subcategorized by data quality using the Goodman (1989) method.

Cases	n	No. of sites	m_λ	σ_λ	COV
All	119	78	1.35	0.72	0.535
Measured discontinuity spacing (s′) and friction angle (ϕ_f)	67	43	1.51	0.69	0.459
Measured discontinuity spacing (s′)	83	48	1.43	0.66	0.461
Measured friction angle (ϕ_f)	98	71	1.41	0.76	0.541
Fractured	20	9	1.24	0.34	0.276
Fractured with measured friction angle (ϕ_f)	12	7	1.33	0.25	0.189
Non-fractured	99	60	1.37	0.77	0.565
Non-fractured with measured s′ and measured ϕ_f	55	37	1.55	0.75	0.485
Non-fractured with measured discontinuity spacing (s′)	63	39	1.49	0.72	0.485
Non-fractured with measured friction angle (ϕ_f)	86	64	1.42	0.81	0.569
Spacing s′ and ϕ_f, both based on AASHTO (2007)	5	3	0.89	0.33	0.368
Discontinuity spacing (s′) based on AASHTO (2007)	36	21	1.16	0.83	0.712
Friction angle (ϕ_f) based on AASHTO (2007)	21	7	1.06	0.37	0.346

n = number of case histories, m_λ = mean of biases, σ_λ = standard deviation, COV = coefficient of variation

The distribution of the ratio of the interpreted measured bearing capacity to the calculated bearing capacity (λ) for the 119 case histories in Table E-3 of database UML-GTR RockFound07 is presented in Figure 79. The distribution of λ has a mean (m_λ) of 1.35 and a COV$_\lambda$ of 0.535 and resembles a lognormal random variable. The distribution of λ for only the foundations on fractured rock is presented in Figure 80 and has an m_λ of 1.24 and a COV$_\lambda$ of 0.276.

3.8.3.2 Observations

The presented findings of Goodman's (1989) method for the prediction of bearing capacity suggest the following:

1. The method is systematically accurate, as demonstrated by the proximity of the best fit line to the perfect match line (measured q_{L2} = predicted q_u) presented in Figure 78

Table 41. Summary of the statistics for the ratio of measured (q_{L2}) to calculated bearing capacity (q_{ult}) of rock sockets and footings on rock subcategorized by foundation type and data quality using the Goodman (1989) method.

Cases	n	No. of sites	m_λ	σ_λ	COV
All rock sockets	61	49	1.52	0.82	0.541
Rock sockets with measured friction angle (ϕ_f)	46	48	1.64	0.90	0.547
All rock sockets on fractured rock	11	6	1.29	0.26	0.202
Rock sockets on fractured rock with measured friction angle (ϕ_f)	7	5	1.23	0.18	0.144
All rock sockets on non-fractured rock	50	43	1.58	0.90	0.569
Rock sockets on non-fractured rock with measured s′ and measured ϕ_f	26	26	1.58	0.79	0.497
Rock sockets on non-fractured rock with measured discontinuity spacing (s′)	34	14	1.49	0.71	0.477
Rock sockets on non-fractured rock with measured friction angle (ϕ_f)	39	43	1.72	0.96	0.557
Rock sockets on non-fractured rock with discontinuity spacing (s′) based on AASHTO (2007) and measured friction angle (ϕ_f)	13	12	1.99	1.22	0.614
Rock sockets on non-fractured rock with measured discontinuity spacing (s′) and friction angle (ϕ_f) based on AASHTO (2007)	8	3	1.19	0.21	0.176
Rock sockets on non-fractured rock with discontinuity spacing (s′) based on AASHTO (2007) and friction angle (ϕ_f) based on AASHTO (2007)	3	2	0.75	0.36	0.483
All footings	58	29	1.23	0.66	0.539
Footings with measured friction angle (ϕ_f)	52	23	1.27	0.69	0.542
All footings on fractured rock	9	3	1.18	0.43	0.366
Footings on fractured rock with measured friction angle (ϕ_f)	5	2	1.47	0.29	0.200
All footings on non-fractured rock	49	26	1.24	0.70	0.565
Footings on non-fractured rock with measured s′ and measured ϕ_f	29	11	1.51	0.73	0.481
Footings on non-fractured rock with measured discontinuity spacing (s′)	29	11	1.51	073	0.481
Footings on non-fractured rock with measured friction angle (ϕ_f)	47	21	1.25	0.72	0.573
Footings on non-fractured rock with discontinuity spacing (s′) based on AASHTO (2007) and measured friction angle (ϕ_f)	18	10	0.82	0.45	0.543
Footings on non-fractured rock with discontinuity spacing (s′) based on AASHTO (2007) and friction angle (ϕ_f) based on AASHTO (2007)	2	1	1.10	0.13	0.115

n = number of case histories, m_λ = mean of biases, σ_λ = standard deviation, COV = coefficient of variation

Table 42. Summary of the statistics for the ratio of measured (q_{L2}) to calculated bearing capacity (q_{ult}) using the Goodman (1989) method categorized by rock quality and foundation type.

Foundation type	Cases	n	No. of sites	m_λ	σ_λ	COV
All	RMR $\geq$ 85	23	23	1.55	0.679	0.438
	65 $\leq$ RMR < 85	57	36	1.33	0.791	0.595
	44 $\leq$ RMR < 65	17	10	1.27	0.746	0.586
	3 $\leq$ RMR < 44	22	9	1.24	0.529	0.426
Rock Sockets	RMR $\geq$ 85	16	16	1.59	0.809	0.509
	65 $\leq$ RMR < 85	35	24	1.40	0.722	0.515
	44 $\leq$ RMR < 65	9	8	1.47	0.916	0.624
	3 $\leq$ RMR < 44	1	1	1.27	--	--
Footings	RMR $\geq$ 85	7	7	1.46	0.204	0.140
	65 $\leq$ RMR < 85	22	13	1.22	0.896	0.738
	44 $\leq$ RMR < 65	8	5	1.06	0.461	0.437
	3 $\leq$ RMR < 44	21	8	1.24	0.542	0.437

n = number of case histories, m_λ = mean of biases, σ_λ = standard deviation, COV = coefficient of variation

and the bias of about 1.2 to 1.5 for all types of major subcategorization.

2. The consistently reliable performance of the method for all ranges of rock strength (and hence RMR) provides a COV of 0.535 for all cases. The variation of the bias mean and COV with rock quality is essentially absent, as can be observed in Table 42. This is in contrast to the performance of Carter and Kulhawy's (1988) method, in which the variation of bias with rock strength resulted in a similar COV only when each range of rock strength was examined separately. This observation enforces the notion of incorporating rock quality categorization (e.g., RMR) within the bearing capacity predictive methodology when necessary.

3. Similar statistics were obtained for shallow foundations ($n = 58$, $m_\lambda = 1.23$, $COV_\lambda = 0.539$) and rock sockets ($n = 61$, $m_\lambda = 1.52$, $COV_\lambda = 0.541$). These observations suggest that
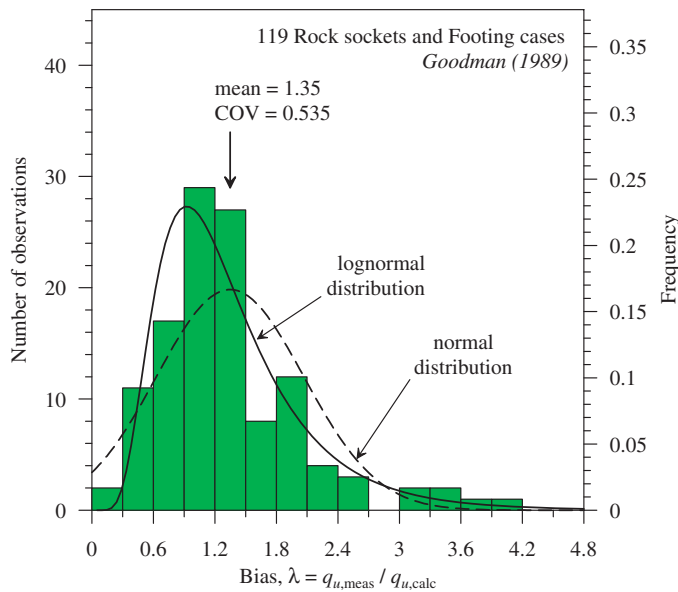
Figure 79. Distribution of the ratio of the interpreted bearing capacity (q_{L2}) to the bearing capacity (q_{ult}) calculated using Goodman's (1989) method for the rock sockets and footings in database UML-GTR RockFound07.
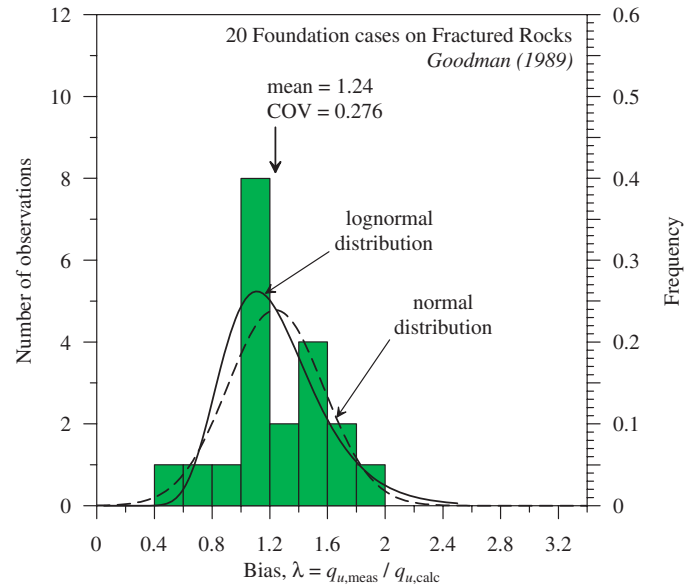
Figure 80. Distribution of the ratio of the interpreted bearing capacity (q_{L2}) to the bearing capacity (q_{ult}) calculated using Goodman's (1989) method for foundations on fractured rock in database UML-GTR RockFound07.

the use of load-displacement relations for the tip of a loaded rock socket is analogous to the load-displacement relations of a shallow foundation constructed below surface.

4. The scatter of the method is significantly improved when measured discontinuity spacing (s') is applied to the analysis. A COV value of 0.461 for 83 cases is obtained when the spacing is known. A COV value of 0.712 for 36 cases was exhibited by the analyses when using a discontinuity spacing (s') based on the generic rock description provided by *LRFD Bridge Design Specifications Section 10: Foundations* (AASHTO 2007).

5. A significant reduction in the mean and the bias was systematically observed for foundations (both footings and rock sockets) on fractured rock. This observation is limited, however, to a small number of cases—20 for 9 sites as compared to 99 for 60 sites for all other cases.

3.9 Uncertainties in the Friction Along the Soil-Structure Interface

3.9.1 Overview

The solid-soil interfacial friction is an important factor affecting soil-structure interaction. In the context of the ULS of shallow foundation design, one needs to address the possibility of shallow foundation sliding when subjected to lateral loading, often encountered in bridge abutments. The issue of foundation-rock sliding was not investigated as the state of practice suggested common use of keys and dowels and therefore the subject is more related in design to rock or concrete controlled strength. The issue of footings resting on granular soil is mostly confined to the possibilities of prefabricated versus cast-in-place foundations on soil. A general discussion of the soil-structure interfacial friction is presented. The uncertainties in the interfacial friction angle of solid-structure interfaces of various "roughness" subjected to inclined loads have been evaluated based on three sources of data:

- Results of research using a dual interface apparatus to establish mechanisms and provide a framework (Paikowsky et al., 1995),
- Results of tests on foundations cast on soil (Horn, 1970), and
- Results of tests on precast foundations (Vollpracht and Weiss, 1975).

Additional sources are used to examine the data listed above including friction limits under inclined loads. A practical summary and appropriate resistance factors are further discussed and presented in Chapter 4.

3.9.2 Experimental Results Using a Dual Interface Apparatus (DIA)

3.9.2.1 Background

Paikowsky et al. (1995) developed a dual interface shear apparatus to evaluate the distribution and magnitude of friction between granular materials and solid inextensible surfaces. The dual interface apparatus (DIA) facilitates the evaluation of boundary conditions (effects) and interfacial shearing modes including unrestricted interfacial shear unaffected by the boundaries. Such measurements allow comparisons to test results from a modified direct shear (MDS) box commonly used for measuring soil-solid interfacial friction (by replacing the lower part of the shear box with a solid surface). Ideal and natural granular materials were sheared along controlled and random solid surface interfaces and compared to direct shear test results.

The tests are designed based on a micro-mechanical model approach describing the interface friction mechanism (Paikowsky, 1989) and making use of the term "normalized roughness" (R_n) as defined by Uesugi and Kishida (1986) and illustrated in Figure 81:

$$R_n = \frac{R_{max}\left(L = D_{50}\right)}{D_{50}} \tag{111}$$

where R_{max} is the maximum surface roughness measured along a distance L equal to the mean grain size of the soil particle D_{50}.

Three zones of R_n associated with the interfacial shear mechanism reflecting different shear strength levels were identified and presented (see Figure 82): Zone I for a "smooth" interface, Zone II for an "intermediate" interface roughness and Zone III for a "rough" interface, respectively. In Zone I, shear failure occurs by sliding particles along the soil-solid body
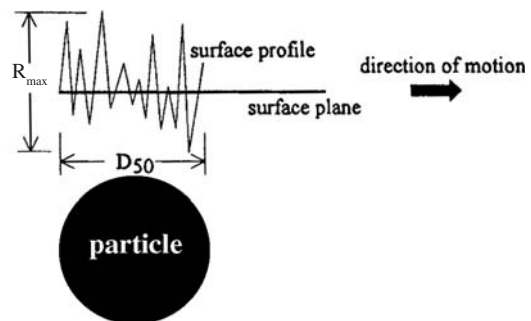
Figure 81. Solid surface topography representation through normalized roughness.
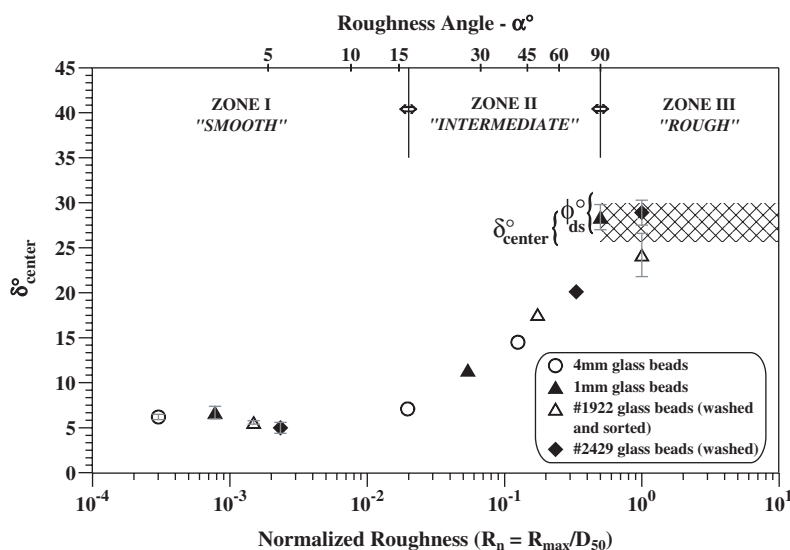
Figure 82. Interfacial characterization according to zones identified through the relations existing between average unrestricted interfacial friction angles (measured along the central section) of glass beads and normalized roughness (Paikowsky et al., 1995).

interface for all granular materials, while in Zone III shear failure occurs within the granular mass, mobilizing its full shear strength. In Zone II, the interaction between the solid surface and the soil allows only partial mobilization of the soil's shear strength, depending on normalized roughness and several other factors, primarily the granular material particle shape. The data in Figure 82 relate to tests with glass beads varying in size from fine to coarse (related to sand) and uniform grain shape (round). The use of natural sand sheared along an interface results in the same three-zone characterization, differentiated only by the absolute magnitude of the friction angles.

3.9.2.2 Experimental Results Using DIA

Soil-solid body interfaces with different normalized roughness and round particles have been tested. The interface friction angles along the unrestricted zone at the center of the solid surfaces, δ_{center}, were obtained as follows, expressed as the mean (± 1 standard deviation):

- Zone I—Smooth interface (14 test results): 6.0 ($\pm 0.8°$)
- Zone II—Intermediate interface roughness: δ_{center} increases from about 8° to 25° with an increase in the logarithm of the normalized roughness (R_n)
- Zone III—Rough interface (6 test results): 28.7 ($\pm 1.3°$)

The friction angle of the granular materials used in the experiments was established to be residual $\phi_f = 31.6$ (± 1.0)° from the direct shear tests of 17 samples. As a result, the ratio

of the friction coefficients, $\tan(\delta_{center})/\tan(\phi_f)$, were obtained as 0.171 for Zone I, 0.890 for Zone III, and therefore 0.171 to 0.890 (increasing with R_n) for Zone II.

3.9.2.3 DIA Results versus MDS Results

Figure 83 presents the relationship between the unrestricted friction angles (δ_{center}) to friction angles measured using a direct shear box modified for interfacial testing with a solid surface of the same roughness (δ_{MDS}). The observations of the results obtained from the DIA and the MDS tests indicate that if the shearing mechanism takes place along the soil-solid surface interface, the test results are markedly influenced by the resisting stresses developing on the boundary walls of the direct shear box (for detailed measurements on the boundary walls, see Paikowsky and Hajduk, 1997; Paikowsky et al., 1996). The shearing resistances measured over the center interfacial area in the DIA tests, which is related to δ_{center}, represent unrestricted friction conditions since this location is not within the boundaries' zone of influence in the shear box. Paikowsky et al. (1995) found that the ratios of δ_{MDS} to δ_{center} for sand and glass beads in different zones of interface roughness are the following:

- Zone I—1.50,
- Zone II—1.20, and
- Zone III—1.10.

These results clearly indicate the inadequacy of the small-size direct shear box for interfacial friction measurements and
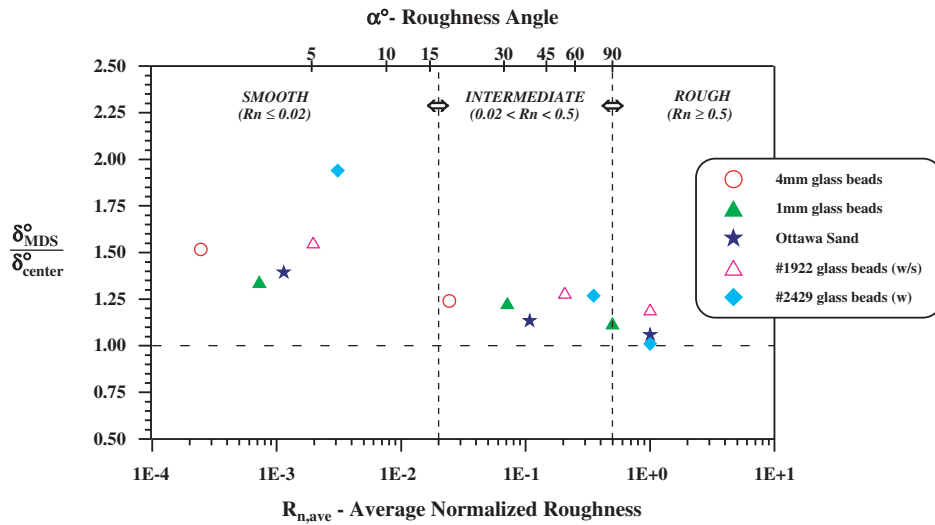
Figure 83. *The ratio of modified direct shear box to unrestricted (central section) interfacial friction angles versus average normalized roughness (Paikowsky et al., 1995).*

the need to be aware of the biased measurements. For the smooth and intermediate zones of normalized roughness, a significant bias exists when applying direct shear test results, namely 0.67 (Zone I) and 0.83 (Zone II). The ranges of the interface friction angles based on δ_{center} are presented in Table 43, along with the corresponding friction coefficient ratios obtained from the DIA tests. The ratio of δ_{MDS} to δ_{center} is represented by the multiplier m. The bias of the typical measured (by a direct shear box) interfacial friction angle (δ_{MDS}) is $1/m$. The values of m are used to obtain the converted friction coefficient ratios, $\tan \delta / \tan \phi$, resulting in 0.25 for Zone I, 1.00 for Zone III, and increasing from 0.25 to 1.00 for Zone II.

3.9.3 Experimental Results of Footings Cast in Place (Horn, 1970)

Horn (1970) presented experimental results of sliding resistance tests for 44 concrete footings of 3.3 ft × 3.3 ft × 1.6 ft (H) (1 m × 1 m × 0.5 m [H]) cast in place on sandy-gravel fill. The soil contained 15% gravel with stones greater than 2.5 in. (63 mm) and maximum stone size (d_{max}) of 7.9 in. (200 mm),

porosity of 0.22, and material friction angle $\phi_f = 33.5°$ obtained from direct shear tests. Figure 84 presents the ratio of the interface friction coefficient ($\tan \delta_s$) and the soil's internal friction coefficient ($\tan \phi_f$) as a function of the applied normal stress on the foundation. Both friction angle values were corrected by Horn, applying the so-called energy correction proposed by Hvorslev (1937) as reported in Schofield and Wroth (1968). The mean and COV of the friction coefficient ratio, $\tan(\delta_{center})/\tan(\phi_f)$, of the 44 tests were found to be 0.99 and 0.091, respectively. The mean of the friction coefficient ratio and the corresponding range of interface friction angles of $33.3 \pm 3.5°$ correspond to those for Zone III (rough interface) in Table 43.

3.9.4 Uncertainties in the Interface Friction Coefficient Ratio

The uncertainties in the interface friction coefficient ratio ($\tan \delta_s / \tan \phi_f$) are directly related to the uncertainties in the interface friction and the soil friction angles. If the uncertainties in these angles are known, the statistics of the friction coefficient

Table 43. Ranges of soil-solid body interface friction angles for different interface roughness zones, based on DIA tests (based on Paikowsky et al., 1995).

Roughness zone	δ_{center}	Friction coefficient ratio from DIA	Multiplier m ($=\delta_{MDS}/\delta_{center}$)	δ_{MDS} ($= \delta_{center} \times m$)	Converted friction coefficient ratio
Zone I	6.0 ± 0.8	0.17	1.50	9.0 ± 1.2	0.25
Zone II	8.0 to 25.0	0.17 to 0.90	1.20	9.5 to 30.0	0.25 to 1.00
Zone III	28.7 ± 1.3	0.90	1.10	31.5 ± 1.4	1.00

Note: Material friction angle obtained from direct shear test = 31.6° (±1.0°).
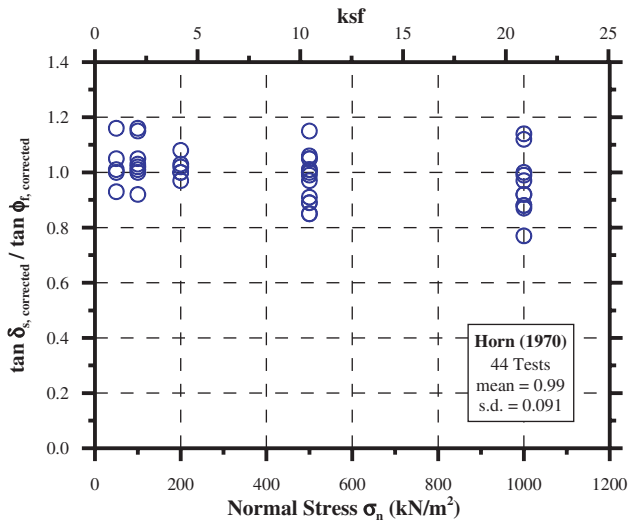
Figure 84. Ratio of measured friction coefficients of cast-in-place footings (rough base) to the soil's internal friction coefficient versus applied normal stress (Horn, 1970).

ratio can be computed as follows. If the distributions followed by both friction angles are normal, the corresponding friction coefficients and, thereby, the friction coefficient ratio, also follow normal distributions. For simplicity in notation, let the interface and material friction coefficients be X_1 and X_2, respectively.

Hence, for mean m_{Xi} and standard deviation σ_{Xi},

$$X_1 \sim N\left(m_{X1}, \sigma_{X1}^2\right)$$

$$X_2 \sim N\left(m_{X2}, \sigma_{X2}^2\right)$$

If the friction coefficient ratio is g, then

$$g = X_1/X_2 \Rightarrow \ln(g) = \ln(X_1) - \ln(X_2)$$

i.e., $m_{\ln(g)} = m_{\ln(X_1)} - m_{\ln(X_2)}$, and

$$\sigma_{\ln(g)}^2 = \sigma_{\ln(X_1)}^2 + \sigma_{\ln(X_2)}^2$$

where the mean and the variance of $\ln(X_i)$ are given by

$$m_{\ln(X_i)} = \ln\left(m_{X_i}\right) - 0.5\sigma_{\ln(X_i)}^2$$

$$\sigma_{\ln(X_i)}^2 = \ln\left(1 + \left(\frac{\sigma_{X_i}^2}{m_{X_i}^2}\right)\right)$$

Then the mean and variance of g, m_g and σ_g^2 are given by

$$m_g = \exp\left(m_{\ln(g)} + 0.5\sigma_{\ln(g)}^2\right)$$

$$\sigma_g^2 = m_g\left(\exp\left(\sigma_{\ln(g)}^2\right) - 1\right)$$

(112)

Table 44. Variations in the estimated soil friction angle (ϕ_f).

| ϕ_f Obtained from | ϕ_f for Granular soils | | | |
| | D'Appolonia & University of Michigan, 2004[1] | | Used for study | |
	Bias	COV	Bias	COV
SPT	1.00 to 1.20	0.15 to 0.20	1.00	0.20
CPT	1.00 to 1.15	0.10 to 0.15	1.00	0.15
Lab test	1.00 to 1.13	0.05 to 0.10	1.00	0.10

[1]Unpublished material based on Phoon et al., 1995.

Table 44 presents the uncertainties in the estimation of the soil friction angle (based on Phoon et al., 1995; NCHRP Project 12-55, 2004). Hence, for a given soil friction angle, say 31.6°, obtained from correlations to SPT N counts, the standard deviation is 6.32°. Using Equation 112, the COV of the friction coefficient ratio is 0.444 for Zone I and 0.201 for Zone III. The friction coefficient ratio uncertainties in Zones I and III are presented in Table 45 for material friction angles obtained from various tests.

Comparing the results for Zone III (rough interface) in Table 45 with the experimental results by Horn (1970), it can be seen that the COV of the friction coefficient ratio in Table 45 corresponds to that obtained by Horn for Zone III and ϕ_f from lab tests. It can thus be concluded that for a rough foundation base (e.g., resulting from a direct pour on the soil), the interface roughness in Zone III is relevant and, further, that the uncertainties in the sliding friction coefficient ratio (tan δ_s/tan ϕ_f) directly correspond to those existing in the method by which the soil friction angle is being defined (i.e., lab test, SPT, and so forth). Based on these observations, the uncertainties in the interface friction coefficient ratio to be used for calibration purposes can be recommended as presented in Table 46,

Table 45. Uncertainties in friction coefficient ratio obtained using Equation 112, based on data in Tables 43 and 44.

ϕ_f Obtained from	Friction coefficient ratio (tanδ_s/tanϕ_f)	
	Zone I (Smooth)	Zone III (Rough)
	tanδ_s/tanϕ_f = 0.25	tanδ_s/tanϕ_f = 1.00
	COV	COV
SPT	0.444	0.201
CPT	0.374	0.158
Lab test	0.312	0.109

Table 46. Uncertainties in interface friction coefficient ratio according to interface roughness and the determination of the soil friction angle.

ϕ_f Obtained from	Friction coefficient ratio ($\tan\delta_s/\tan\phi_f$)		
	Smooth	Intermediate	Rough
	Bias = 0.67	Bias = 0.83	Bias = 0.91
	COV	COV	COV
SPT	0.45	0.45 to 0.20	0.20
CPT	0.38	0.38 to 0.15	0.15
Lab test	0.31	0.31 to 0.10	0.10

where the bias of the friction coefficient ratio estimation is assumed to be that of the direct shear test interfacial testing (bias = $1/m$) and that of Table 44 for the estimation of ϕ_f (bias = 1.0).

The interpretation of smooth, intermediate, and rough interfaces has been illustrated in Table 47, based on friction angles provided by the NAVFAC (1986) for different dissimilar materials used in geotechnical construction. The COV to be used depends on the range of roughness (as defined in Table 47). The resistance factors associated with the uncertainties discussed above and a rationale for their use is discussed in Chapter 4.

Table 47. Friction coefficients (NAVFAC, 1986b) and interface roughness of dissimilar materials.

Interface Materials			tan δ_s	Friction (degrees)	Interface roughness
Mass concrete on the following foundation materials:	Clean sound rock		0.70	35	Rough
	Clean gravel, gravel-sand mixtures, coarse sand		0.55 to 0.60	29 to 31	Intermediate-Rough
	Clean fine to medium sand, silty medium to coarse sand, silty or clayey gravel		0.45 to 0.55	24 to 29	Intermediate-Rough
	Clean fine sand, silty or clayey fine to medium sand		0.35 to 0.45	19 to 24	Intermediate
	Fine sandy silt, nonplastic silt		0.30 to 0.35	17 to 19	Intermediate
	Very stiff and hard residual or preconsolidated clay		0.40 to 0.50	22 to 26	Intermediate-Rough
	Medium stiff and stiff clay and silty clay (Masonry on foundation materials has same friction factors.)		0.30 to 0.35	17 to 19	Intermediate
Steel sheet piles against the following soils:	Clean gravel, gravel-sand mixtures, well-graded rock fill with spalls		0.40	22	Intermediate
	Clean sand, silty sand-gravel mixture, single size hard rock fill		0.30	17	Intermediate
	Silty sand, gravel or sand mixed with silt or clay		0.25	14	Intermediate-Smooth
	Fine sandy silt, nonplastic silt		0.20	11	Intermediate-Smooth
Formed concrete or concrete sheet piling against the following soils:	Clean gravel, gravel-sand mixture, well-graded rock fill with spalls		0.40 to 0.50	22 to 26	Intermediate-Rough
	Clean sand, silty sand-gravel mixture, single size hard rock fill		0.30 to 0.40	17 to 22	Intermediate
	Silty sand, gravel or sand mixed with silt or clay		0.30	17	Intermediate
	Fine sandy silt, nonplastic silt		0.25	14	Intermediate
Various structural materials:	Masonry on masonry, igneous and metamorphic rocks:	Dressed soft rock on dressed soft rock	0.70	35	Rough
		Dressed hard rock on dressed soft rock	0.65	33	Rough
		Dressed hard rock on dressed hard rock	0.55	29	Intermediate-Rough
	Masonry on wood (cross grain)		0.50	26	Intermediate-Rough
	Steel on steel at sheet pile interlocks		0.30	17	Intermediate

3.9.5 Experimental Results of Precast Footings (Vollpracht and Weiss, 1975)

Vollpracht and Weiss (1975) presented experimental results of sliding resistance tests for 10 precast concrete footings of 1.6 ft × 6.6 ft × 2.6 ft (H) (0.5 m × 2.0 m × 0.8 m [H]) on sandy gravel fill. The soil interfacial friction angle was 39°, void ratio e was 0.395, and relative density was 61%. The mean soil-foundation interface friction angle of the 10 tests was found to be 23.2° (±4.08°). Figure 85 presents the ratio of the inter-face friction coefficient ($\tan \delta_s$) and the soil's internal friction coefficient ($\tan \phi_f$) as a function of the applied normal stress on the foundation. The mean of the 10 tests was found to be 0.53±0.102 (± 1 standard deviation). This range clearly identified the precast concrete–sand interfacial shear as having the intermediate roughness of Zone II. The scatter of the data can be attributed to the different ratios of horizontal to vertical loads, as will be further discussed below.

3.9.6 Summary of Relevant Results

Table 48 summarizes the uncertainties in interface friction coefficient ratios according to type of foundation construction—cast-in-place or precast concrete—utilizing the aforementioned data.

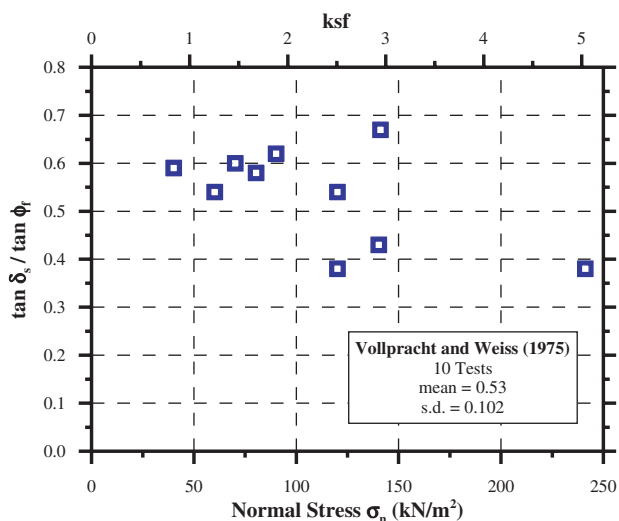### 3.9.7 Examination of Load Inclination and Other Factors Influencing Footings Interfacial Friction

Different tests were carried out to examine the bearing capacity of foundations under inclined loading. These tests were analyzed in Sections 3.6 and 3.7 for bearing capacity purposes, and some tests are re-evaluated here for interfacial friction purposes.

Tests were carried out by Foik (1984) on foundations under inclined loads ranging in size from 2.9 in. × 5.4 in. (7.4 cm × 13.7 cm) to 46 in. × 26 in. (117 cm × 65 cm). The foundations' base had a rough contact surface made of glued coarse sand or fine gravel. Figure 86 presents the relationship between the soil's unit weight and the internal friction angle. Figure 87 presents the relationship between the soil's unit weight and the measured friction coefficient ratios of the footings. Figure 88 presents the relationship between the load inclination (expressed as inter-facial friction coefficient, $\tan \delta_s$) and the internal friction angle coefficient (expressed as internal friction coefficient, $\tan \phi_f$), and Figure 89 presents the relationship between the load

Table 48. Uncertainties in interface friction coefficients of foundations on granular soils according to the foundation's construction method and the determination of the soil friction angle.

ϕ_f Obtained from	Friction coefficient ratio ($\tan\delta_s/\tan\phi_f$)	
	Cast in place	Prefabricated
	Bias = 0.91	Bias = 0.53
	COV	COV
SPT	0.20	0.34
CPT	0.15	0.30
Lab test	0.10	0.26

Figure 85. Ratio of measured friction coefficients of precast footings to the soil's internal friction coefficient versus applied normal stress (Vollpracht and Weiss, 1975).
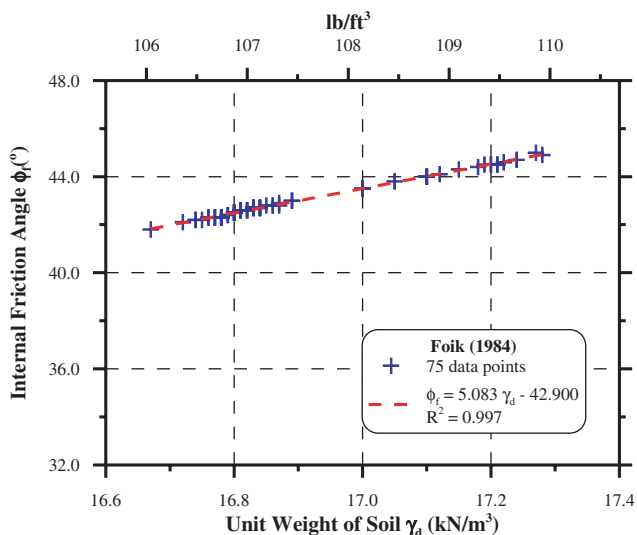
Figure 86. Relationship of soil unit weight and the internal friction angle used by Foik (1984) in test results interpretation.
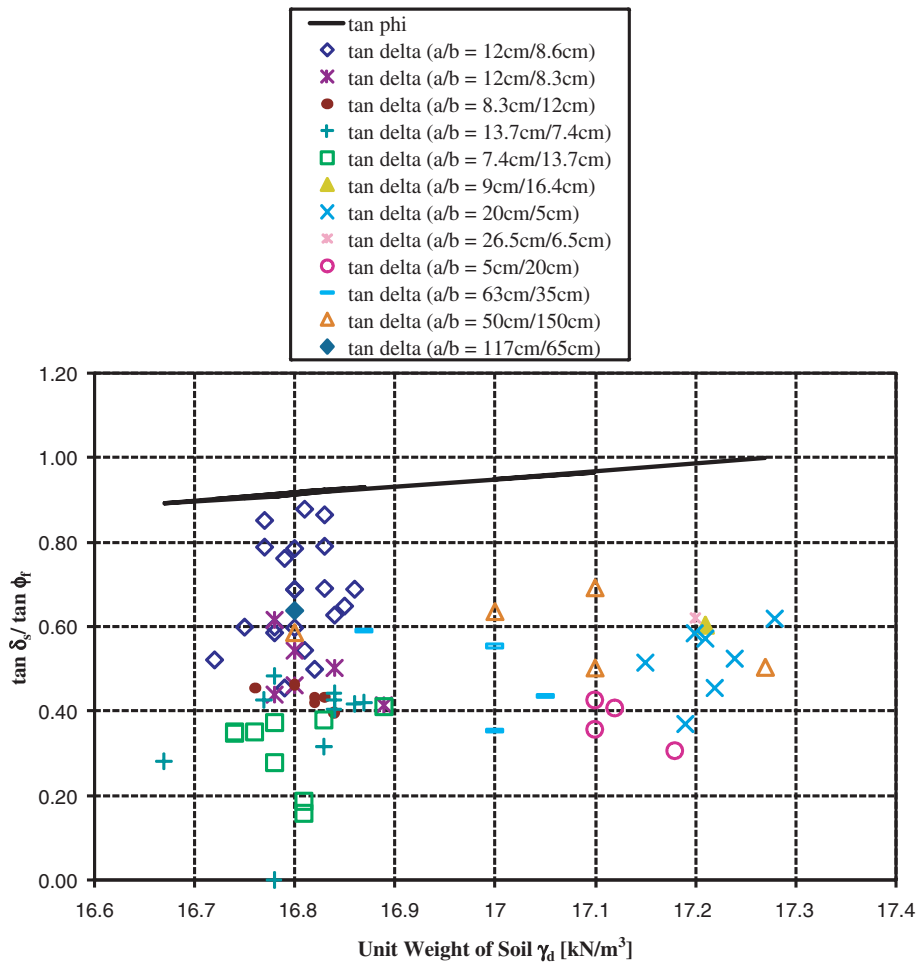
Figure 87. Ratio of measured footing friction coefficient ratios to the soil's internal friction coefficient versus soil unit weight (Foik, 1984).
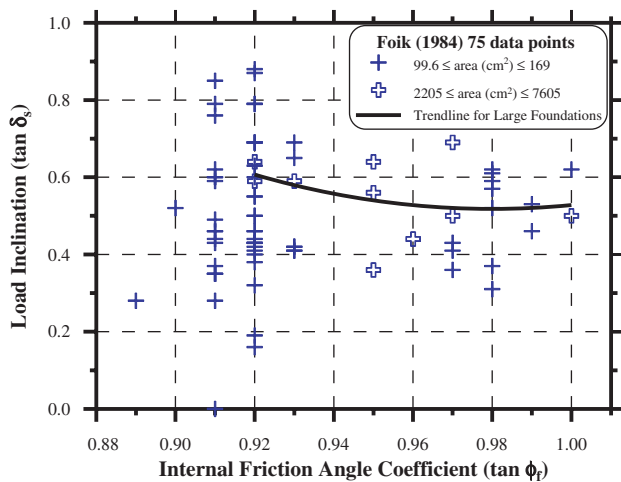
Figure 88. Load inclination (tan δ_s) versus the internal friction angle coefficient (tan ϕ_f) (Foik, 1984).
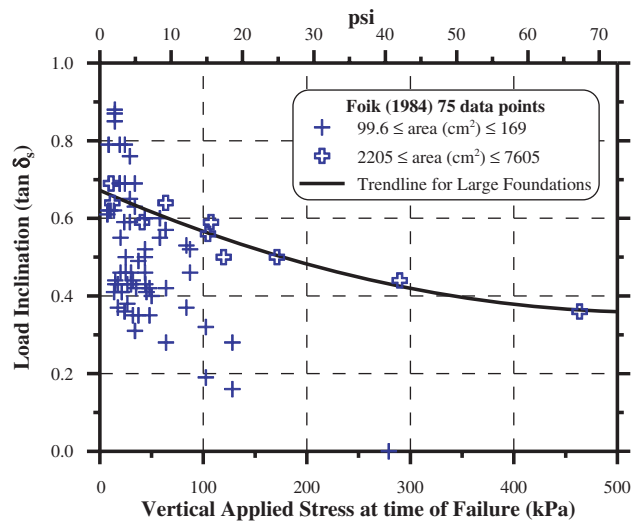
Figure 89. Load inclination (tan δ_s) versus vertical applied stress at the time of failure ($V_B/a \times b$) (Foik, 1984).

inclination ($\tan \delta_s$) and the vertical applied stress at the time of failure ($V_B / a \times b$).

The data in Figures 86 to 89 suggest the following:

1. Large variation exists in the ratio of the foundation's friction coefficient to the soil's internal friction coefficient. The data in Figure 87 do not indicate on a clear factor that controls this variation, but in all cases $\tan \delta_s < \tan \phi_f$.

2. Figures 88 and 89, which show the interface friction coefficient as a function of the soil's internal friction coefficient and the vertical applied stress (respectively) suggest that the scatter in the data is significantly smaller for the larger footing sizes. This may be explained by the physical difficulties of applying loads and conducting tests on small footings.

3. The interface friction coefficient (equal to the load inclination at failure) is clearly affected by the size of the vertical load, as shown in Figure 89. The sliding of the footing under small vertical loads is eliminated and large loads can be applied, which, again, seems to be associated with the physical limitations of conducting tests.

CHAPTER 4

Interpretations and Appraisal

4.1 Overview

Chapter 3 presents an analysis of available data that was mostly limited to direct correlations between the loading conditions (e.g., centric, eccentric, and so forth) and the performance of the bearing capacity calculation methods. The interpretation of the findings in the case of shallow foundations is more complex than the interpretation of the findings in the case of deep foundations, as presented, for example, in *NCHRP Report 507* (Paikowsky et al., 2004). The reason is that many more parameters can contribute to the trend provided by the data than may be apparent in the first evaluation. For example, Section 3.8.2 of this report examined the performance of Carter and Kulhawy's (1988) equation for the bearing capacity of foundations on rock. The database consisting of tests on shallow foundations and drilled shaft tips suggested large variations between the performances of the two. The natural conclusion could have been that the load-displacement relations of the tip of a rock socket cannot be applied to the examination of bearing capacity theory. However, further examination of the data suggested that the investigated method (i.e., Carter and Kulhawy) has a bias depending on the rock quality. As the two examined case history databases (i.e., shallow foundations and rock sockets) varied by the rock quality that predominated in each, it was possible to explain the difference in the performance based on rock quality rather than on the type of test. Similarly, the investigation of vertical loading of shallow foundations on natural soils as compared to vertical loading of shallow foundations on controlled soils, presented in Section 3.5, suggested large variations between the two groups. Earlier interpretations of the data (e.g., Paikowsky et al., 2008; Paikowsky et al., 2009b; Amatya et al., 2009) naturally followed these findings, distinguishing between the groups based on soil placement only (i.e., natural versus controlled). Further investigation revealed that part of the reason for variation was the difference in the friction angle of the soils in the investigated groups and the bias of the bearing capacity factor N_γ and its dependence on the magnitude of the internal friction angle.

This chapter addresses, therefore, the following issues:

1. Completion of loads and parameters required to carry out the calibration. The distribution functions of the lateral load were previously developed. These are developed to allow for calibrations of sliding resistances. Target reliability is also established to allow for the calibration of the resistance factors.
2. Investigation and interpretation of the data and findings presented in Chapter 3 of this report including sources of uncertainty, size effect, natural versus controlled soil, and the probabilistic approach to missing information.
3. Final determination of recommended resistance factors.

4.2 Uncertainty in Vertical and Lateral Loading

4.2.1 Overview

The following discussion presents the chosen characteristics for vertical and lateral loads, dead and live, acting on bridge foundations. Although the subject is beyond the scope of the present research, establishing the lateral load distributions and factors became a necessity for the calibration process and is therefore presented. It is expected that future experimental, analytical, and probabilistic work will enable better analysis and more reliable selection of load distributions.

4.2.2 Vertical Loads

NCHRP Report 507 (Paikowsky et al., 2004) established the load distributions and factors used for the ULS and SLS of deep and shallow foundations under vertical loads. These values are based on Table F-1 of *NCHRP Report 368,* which provides a range for live load (Nowak, 1999). The bias of live load has been taken as the mean of the range provided (1.10–1.20), and the COV is taken as 0.20 instead of 0.18, as presented in *NCHRP Report 368.* The load factors are from Tables 3.4.1-1

Table 49. Load factors and uncertainties in vertical live load and dead load.

Load type	Load factor[1]	Bias[2]	COV[2]
Live Load (LL)	$\gamma_L = 1.75$	1.15[3]	0.20[4]
Dead Load (DL)	$\gamma_D = 1.25$	1.05	0.10

[1] Tables 3.4.1-1 and 3.4.1-2 (AASHTO, 2007)
[2] Table F-1 of *NCHRP Report 368* (Nowak, 1999)
[3] Mean of the range 1.10 to 1.20
[4] COV of 0.18 rounded to 0.20

and 3.4.1-2 of *LRFD Bridge Design Specifications Section 10: Foundations* (AASHTO, 2007). These load factors are listed in Table 49.

4.2.3 Horizontal Loads

4.2.3.1 Horizontal Earth Pressure (Dead Load)

The sources of uncertainties in the horizontal earth pressures due to soil and surcharge are the variations in soil unit weight and the soil friction angle. Based on the study by Phoon et al. (1995), the final report for NCHRP Project 12-55 (D'Appolonia and the University of Michigan 2004) suggests the variation in soil unit weight as the following:

- Bias of soil unit weight = 1.00
- COV of 0.10 for in situ (natural) soil conditions
- COV of 0.08 for engineered backfill (controlled)
- Distribution followed = Normal

Also, based on the study by Phoon et al. (1995), the final report for NCHRP Project 12-55 (2004) lists the variation in the estimation of the soil friction angle (ϕ_f) as the following:

- ϕ_f from SPT:
  Bias = 1.00 to 1.20, COV = 0.15 to 0.20
- ϕ_f from cone penetration test (CPT) (Kulhawy and Mayne, 1990):
  Bias = 1.00 to 1.15, COV = 0.10 to 0.15
- ϕ_f from Lab test:
  Bias = 1.00 to 1.13, COV = 0.05 to 0.10
- Distribution followed = Lognormal
- Reasonable estimate of bias taken as 1.00

At-Rest Earth Pressure Coefficient, K_0. Based on the data summarized by Mayne and Kulhawy (1982) for drained and undrained at-rest earth pressure coefficient K_0, it was found that the COV of the corresponding transformation, using Jaky's equation given below (Jaky, 1944), was 0.18 (NCHRP Project 12-55, 2004). K_{0nc} represents K_0 for normally consolidated cohesionless soil.

Table 50. Ranges of COV of K_{0nc} for ranges of variation in soil friction angle (D'Appolonia and the University of Michigan, 2004).

Soil friction angle, ϕ_f	COV of K_{0nc}		
	COV of ϕ_f		
	0.05–0.10	0.10–0.15	0.15–0.20
	ϕ_f from Lab Test	ϕ_f from CPT	ϕ_f from SPT
30	0.186–0.202	0.202–0.227	0.227–0.260
35	0.189–0.217	0.217–0.257	0.257–0.303
40	0.195–0.237	0.237–0.295	0.295–0.364

$$K_{0nc} = 1 - \sin\phi_f \tag{113}$$

Table 50 summarizes the variation in K_{0nc} for cohesionless soils, which includes the transformation uncertainty, based on the final report for NCHRP Project 12-55 (D'Appolonia and the University of Michigan, 2004).

Rankine Active Earth Pressure Coefficient, K_a. The Rankine active earth pressure coefficient is given by the following:

$$K_a = \frac{1 - \sin\phi_f}{1 + \sin\phi_f} = \tan^2\left(45° - \frac{\phi_f}{2}\right) \tag{114}$$

The variation of the Rankine active earth pressure coefficient with the variation in the soil friction angle is presented in Table 51. The coefficients of variation for earth pressure coefficients in Table 51 were obtained by generating 1,000 samples of soil friction angle following lognormal distribution, with COVs of 0.10, 0.15, 0.20, and 0.25, respectively, and limiting maximum soil friction angle to 47°. In Table 51, these COVs are presented under "COV sim"; "COV calc" was obtained using the first order approximation in the calculation of COV, as mentioned in the final report for NCHRP Project 12-55 (2004). It can be seen that the difference between the estimated COV using the simulation and the first order approximation increases with the increase in the soil friction angle COV.

Rankine and Coulomb Passive Earth Pressure Coefficients, K_p. The Rankine passive earth pressure coefficient assumes no friction between the wall and the soil and therefore results in a conservative estimate of the passive earth pressure coefficient, which for frictional material is given by the following:

$$K_p = \frac{1 + \sin\phi_f}{1 - \sin\phi_f} = \tan^2\left(45° + \frac{\phi_f}{2}\right) \tag{115}$$

Table 51. COV of lateral earth pressure coefficients for different COVs and soil friction angles.

Soil friction angle, ϕ_f		Rankine active, K_a		Rankine passive, K_p		Coulomb passive, K_p						
						$\delta/\phi_f = 2/3$	$\delta/\phi_f = 0.5$	$\delta/\phi_f = 0.4$	$\delta/\phi_f = 0.3$	$\delta/\phi_f = 0.2$	$\delta/\phi_f = 0.1$	$\delta/\phi_f = 0.0$
Mean	COV	COV sim	COV calc	COV sim	COV calc	COV sim	COV sim	COV sim	COV sim	COV sim	COV sim	COV sim
25	0.10	0.09	0.10	0.10	0.09	0.20	0.17	0.15	0.14	0.12	0.11	0.10
	0.15	0.14	0.15	0.15	0.13	0.34	0.27	0.24	0.21	0.19	0.17	0.15
	0.20	0.19	0.21	0.22	0.17	0.64	0.45	0.38	0.33	0.28	0.25	0.22
	0.25	0.22	0.27	0.27	0.21	1.04	0.61	0.49	0.41	0.35	0.31	0.27
30	0.10	0.12	0.13	0.13	0.11	0.36	0.27	0.23	0.20	0.17	0.15	0.13
	0.15	0.17	0.19	0.19	0.16	0.70	0.43	0.35	0.30	0.26	0.22	0.19
	0.20	0.23	0.27	0.26	0.21	1.05	0.63	0.50	0.42	0.35	0.30	0.26
	0.25	0.27	0.34	0.33	0.25	1.39	0.84	0.67	0.55	0.46	0.39	0.33
35	0.10	0.15	0.16	0.16	0.14	0.58	0.37	0.30	0.25	0.22	0.18	0.16
	0.15	0.22	0.24	0.24	0.20	0.97	0.59	0.48	0.39	0.33	0.28	0.24
	0.20	0.28	0.33	0.30	0.25	1.13	0.73	0.59	0.49	0.42	0.35	0.30
	0.25	0.31	0.43	0.34	0.30	1.19	0.80	0.65	0.55	0.46	0.39	0.34
37	0.10	0.16	0.17	0.17	0.15	0.67	0.42	0.34	0.28	0.24	0.20	0.17
	0.15	0.22	0.26	0.24	0.21	0.97	0.61	0.49	0.40	0.34	0.28	0.24
	0.20	0.27	0.36	0.29	0.27	1.07	0.69	0.56	0.47	0.39	0.34	0.29
	0.25	0.32	0.47	0.33	0.32	1.09	0.75	0.62	0.52	0.44	0.38	0.33
40	0.10	0.17	0.19	0.17	0.16	0.68	0.42	0.34	0.28	0.24	0.20	0.17
	0.15	0.23	0.30	0.23	0.23	0.84	0.55	0.45	0.37	0.32	0.27	0.23
	0.20	0.28	0.41	0.27	0.29	0.91	0.63	0.52	0.44	0.37	0.32	0.27
	0.25	0.33	0.53	0.30	0.35	0.93	0.66	0.55	0.47	0.40	0.35	0.30

Notes:

   * "COV sim" of earth pressure coefficients calculated from 1000 samples of friction angles assumed to follow lognormal distribution

   * ϕ_f is limited to a maximum of 47degrees

   * COV calc: First order COV of earth pressure coefficients estimated as (D'Appolonia and the University of Michigan, 2004):

$$\frac{\left|K(\overline{\phi_f}) - K(\overline{\phi_f} - \sigma)\right|}{K(\overline{\phi_f})} \quad \text{where } \overline{\phi_f} \text{ and } \sigma \text{ are the mean and standard deviation of } \phi_f$$

The Coulomb passive earth pressure coefficient is used more commonly and is given by the following:

$$K_p = \frac{\sin^2(\beta - \phi_f)}{\sin^2\beta \cdot \sin(\beta + \delta)\left[1 - \sqrt{\frac{\sin(\phi_f + \delta) \cdot \sin(\phi_f + \alpha)}{\sin(\beta + \delta) \cdot \sin(\beta + \alpha)}}\right]^2} \quad (116)$$

where

  β = angle of wall/interface surface to soil with vertical,

  δ = friction angle between wall/interface and soil, and

  α = angle of soil backfill surcharge with the horizontal.

Table 51 presents variations in active and passive earth pressures for a range of soil friction angles and their COVs.

Coulomb passive earth pressure has been presented for $\beta = 90°$ and $\alpha = 0°$, i.e., vertical wall and level backfill.

Table 52 summarizes the COV results presented in Tables 50 and 51 for lateral earth pressure coefficients; these COVs can be used for at-rest and Rankine active and passive earth pressure coefficients.

For the Coulomb passive earth pressure coefficient, one can choose a reasonable COV, as has been presented in Table 52, for each ratio of interface friction angle to soil friction angle. For example, for a granular fill material with the ratio of interface friction angle to soil friction angle of about ⅔, when the soil friction angle is estimated from SPT readings, the COV lies in the range of 0.70 to about 1.1. One may choose a reasonable COV as 0.85. It should be noted that in Table 51 the maximum conceivable soil friction angle is assumed to be 47°,

Table 52. Summary of COVs of earth pressure coefficients.

	COV					
$30 < \phi_f \le 40$	K_{0nc}		Rankine K_a		Rankine K_p	
	Range	Reasonable	Range	Reasonable	Range	Reasonable
ϕ_f from Lab Test	0.20–0.22	0.20	0.12–0.17	0.15	0.12–0.17	0.15
ϕ_f from CPT	0.22–0.26	0.25	0.17–0.23	0.20	0.19–0.23	0.20
ϕ_f from SPT	0.25–0.33	0.30	0.23–0.28	0.25	0.23–0.28	0.25

hence, there is a drop in the COV calculated for a higher friction angle (40°).

The topic of lateral passive earth pressure is complex as it is often associated with the limiting displacement that controls the development of the pressure rather than the theoretical pressures associated with the coefficient. As such, the discussion in this section is limited in its scope and addresses solely the current limited needs.

With the reasonable estimates of the COVs of soil unit weight and earth pressure coefficients, the lateral pressure due to, for example, active earth pressure can be calculated as

$$E_a = 0.5h\gamma \cdot K_a$$

(where E_a is active earth pressure and h is height of soil) with a bias of 1.00. This implies that the combined statistics for the mean and standard deviation are the following:

$$\mu_{Ea} = 0.5h \cdot \mu_\gamma \mu_{Ka} \text{ and}$$

$$\sigma_{Ea}^2 \approx \sigma_\gamma^2 \left(0.5h \cdot K_a\right)^2 + \sigma_{Ka}^2 \left(0.5h \cdot \gamma\right)^2$$

Hence

$$COV_{Ea} = \sqrt{COV_\gamma^2 + COV_{Ka}^2} \qquad (117)$$

When soil friction angles are based on SPT readings, COVs of the horizontal dead load due to at-rest (K_0) or active earth pressure (K_a) can be calculated as 0.27 to 0.35. As such, a practical use of a bias of 1.00 and COV of 0.30 is a reasonable representation of a large range of possibilities for lateral dead load due to earth pressure and can be considered to follow a lognormal distribution.

Earth Pressure Due to Compaction. A typical distribution of residual earth pressure after compaction of backfill behind an unyielding wall with depth is given in Figure 90. A particular example of granular soil with ϕ_f of 35°, γ of 125 pcf, and roller load of 500lb/in. compacting a lift thickness of 6 in. when at a distance of 6 in. away from the wall has been presented. It can be seen that the residual earth pressure increases rapidly with depth, with a maximum pressure at around 5 ft below the compacted surface for this example. Table 53 summarizes the variation of the multiplier factor R_ϕ with the COV of a soil friction angle ϕ_f of 35°, specifically for one standard deviation change in ϕ_f. This range of multiplier (adjustment) factors was based on the tables of adjustment factors by Williams et al. (1987). It is to be noted that these adjustment factors themselves are empirical in nature and are approximate representations of test results with large scatters.

From Figure 90, it can be seen that the lateral earth pressure after compaction (residual lateral stress) is 800 psf at a
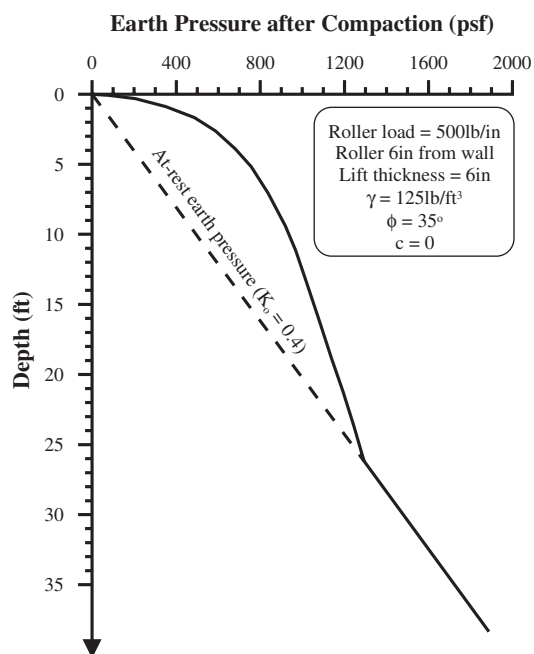

Figure 90. Residual earth pressure after compaction of backfill behind an unyielding wall (based on Clough and Duncan, 1991).

depth of 5 ft. When the measured soil friction angle has a COV of 0.20, based on the multiplier factors in Table 53, this residual stress can vary from 704 psf (800×0.88) to 952 psf (800×1.19).

To estimate the uncertainty in the establishment of the residual lateral pressure curve obtained based on a solution proposed by Duncan and Seed (1986) and shown in Figure 90, the bias of the measured lateral earth pressure versus the calculated lateral earth pressure was studied (see Figure 91). The measured earth pressures are from the experimental study by Carder et al. (1977). The residual earth pressures on a concrete retaining wall due to compaction of sand backfill were measured at different depths. The calculated earth pressures are, as presented by Duncan and Seed (1986), based on an "incremental solution."

Table 53. Range of multiplier factor R_ϕ for the estimation of earth pressure due to compaction at a depth of 5 ft of compacted soil for $\phi_f = 35°$, $\gamma = 125$ pcf, roller load = 500 lb/in, distance from wall = 6 in, lift thickness = 6 in, mean of $R_\phi = 1.00$.

$\phi_f = 35$	Range of R_ϕ at 5 ft depth for a variation of 1 s.d. in ϕ_f	
COV	Roller	Vibrator plates/ rammers
0.10	0.94 – 1.10	0.97 – 1.05
0.15	0.91 – 1.14	0.96 – 1.09
0.20	0.88 – 1.19	0.95 – 1.17
0.25	0.85 – 1.24	0.94 – 1.24
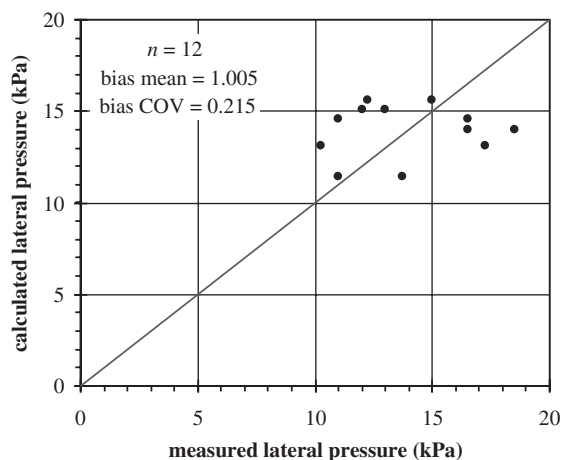
Figure 91. Measured versus calculated residual earth pressures. Measured earth pressures at Transport and Road Research Laboratory experimental concrete retaining wall by Carder et al. (1977) and calculated earth pressure using the incremental solution proposed by Duncan and Seed (1986) (bias = measured/calculated).

The mean of the bias was found to be 1.005 and the bias COV was 0.215.

Based on the results obtained in Table 53, it can be concluded that for the compaction case presented in Figure 90, the worst-case calculated COV of multiplier factor R_ϕ approaches the COV of the friction angle. Incorporating the effect of the result obtained in Figure 91, the combined COV for the estimation of residual lateral earth pressure due to compaction is approximately $0.35 \left(= \sqrt{0.20^2 + 0.20^2 + 0.215^2} \right)$ using the COVs of $\phi_f = 0.20$, $R_\phi = 0.20$ and residual earth pressure estimator = 0.215, respectively. Using COVs of ϕ_f and R_ϕ as 0.15 and 0.09 results in a combined COV of 0.27. The range of COV is thus 0.27 to 0.35. Hence, it may be said that a bias of 1.00 and COV of 0.30 would provide a reasonable estimate of the residual earth pressure due to compaction.

4.2.3.2 Lateral Pressure from Live Loads

In order to assess the horizontal lateral pressure due to live load, uncertainties in different components of the live load must be assessed (A.S. Nowak, personal communication, 2006). ACI 318 (Szerszen and Nowak, 2003) lists the following:

Wind (50-year maximum)	bias = 0.78	COV = 0.37
Snow	bias = 0.82	COV = 0.26
Earthquake	bias = 0.66	COV = 0.56

In 1983, the Ontario Ministry of Transport used the following for the assessment of lateral forces for the Toronto subway (OHBDC, 1979, 1983, 1993):

Temperature	bias = 1.00	COV = 0.25
Shrinkage and creep	bias = 0.90	COV = 0.20
Wind (75-year maximum)	bias = 0.85	COV = 0.25
Braking force (railways)	bias = 1.00	COV = 0.10

There are no exact measurements available, but wind load is similar to other forces and a limited parametric study seems to be reasonable. Experts (A.S. Nowak, personal communication) suggest that a bias of 1.00 and COV of 0.15 should be used for the lateral pressure due to live loads.

4.2.3.3 Summary of Horizontal Loads

Assuming that lateral loading due to dead load (LFD: lateral force due to dead load) is mostly due to soil and surcharge, possibly compacted, the following load distribution and load factors (load factors from AASHTO, 2007, Table 3.4.1-2) have been chosen for at-rest and active earth pressures:

λ_{LFD} = bias of lateral loading due to dead load = 1.00, $COV_{LFD} = 0.30$ and is assumed to follow lognormal distribution with the following distribution in soil unit weight γ (assumed to follow normal distribution):

λ_γ = bias of soil weight = 1.00, $COV_\gamma = 0.10$ for in-situ (natural) soil conditions,

$COV_\gamma = 0.08$ for engineered backfill (controlled soil condition)

Load factor for at-rest earth pressure, $\gamma_{EH0} = 1.35$, and load factor for active earth pressure, $\gamma_{EHa} = 1.50$.

Assuming the lateral loading due to live load (LFL: lateral force due to live load) is mostly shear loads from wind, temperature variation, and creep and shrinkage transferred via the bearing pads, the following distributions and load factors have been chosen:

$\lambda_{LFL} = 1.00$, $COV_{LFL} = 0.15$ and assumed to follow lognormal distribution

Load factor for lateral live load, $\gamma_{LFL} = 1.00$ (assumed)

4.3 Calibration Methodology

4.3.1 Overview of Calibration Procedures

Probability-based limit state designs are presently carried out using methods categorized into three levels (Thoft-Christensen and Baker, 1982):

• Level 3 includes methods of reliability analysis utilizing full probabilistic descriptions of design variables and the true nature of the failure domains (limit states) to calculate the exact failure probability, for example, using MCS techniques. Safety is expressed in terms of failure probability.

- Level 2 involves a simplification of Level 3 methods by expressing the uncertainties of the design variables in terms of mean, standard deviation, and/or COV and may involve either approximate iterative procedures (e.g., FOSM, FORM and SORM analyses) or more accurate techniques like MCS to evaluate the limit states. Safety is expressed in terms of a reliability index.
- Level 1 is more of a limit state design than a reliability analysis. Partial safety factors are applied to the predefined nominal values of the design variables (namely the loads and resistance(s) in LRFD); however, the partial safety factors are derived using Level 2 or Level 3 methods. Safety is measured in terms of safety factors.

Regardless of the probabilistic design levels described above, the following steps are involved in the LRFD calibration process:

1. Establish the limit state equation to be evaluated.
2. Define the statistical parameters of the basic random variables or the related distribution functions.
3. Select a target failure probability or reliability value.
4. Determine load and resistance factors consistent with the target value using reliability theory. More applicable to an AASHTO LRFD geotechnical application is a variation in which structural selected load factors are utilized to determine resistance factors for a given target value.

Chapter 1 of this report reviewed the limit state equations to be evaluated, and Chapter 2 developed their evaluation to establish the statistical parameters to be used. The statistical parameters to be used are further investigated in the following sections of this chapter to finally establish the parameters to be used in the calibration. The load characteristics were developed and presented in Section 4.2. The following section outlines the selected target reliability and develops the resistance factors based on the methodology presented in Sections 1.3.5 and 1.4.

4.3.2 Target Reliability

4.3.2.1 Methods of Establishing Target Reliability

As has been pointed out in *NCHRP Report 507* (Paikowsky et al., 2004), in general, two methods are used to generate target reliability levels: (1) basing them on the reliability levels implicit in current WSD codes and (2) using cost-benefit analysis with optimum reliability proposed on the basis of minimum total cost, which includes the cost of economic losses and consequences due to failure.

In establishing a target reliability level using the first method, the reliability levels implied in the current design practice are calculated. The target level is usually taken as the mean of the reliability levels of representative designs. Such target reliability can be thought of as related to the acceptable risks in current practice and hence an acceptable starting point for code revision. The second method is based on the concept that safety measures are associated with cost; therefore, "safety essentially is a matter not only of risk and consensus about acceptable risks, but also of cost" (Schneider, 2000). Even though attempts have been made to determine the cost of failure (Kanda and Shah, 1997), it is hard to assign the cost of failure, especially when it incorporates human injury or loss of life.

4.3.2.2 Target Reliability Based on Current WSD

It has been found that the reliability levels of foundations designed using WSD factors of safety can vary considerably (e.g., Phoon and Kulhawy, 2002; Honjo and Amatya, 2005). Hence, the recommendation of a target reliability index based on the reliability levels implied in the current WSD practice requires some judgment.

A literature survey shows that very few authors have dealt with the determination of the target reliability of shallow foundations. Phoon and Kulhawy (2002) calculated the reliability indexes for different COVs in the operative horizontal stress coefficient of soil. Taking the soil property variability into account, it was shown that reliability indexes lie in an approximate range of 2.6 to 3.7, with an average of 3.15. Designs for square footings with embedment depth ratios (ratio of embedment depth to footing width) of 1 and 3 and 50-year return period wind loads of 50% and 33.33% of the uplift capacity of the footings were evaluated. A target level of 3.2 was decided for ULS. However, this target level is specific only for footings subject to uplift loads.

In *NCHRP Report 343* (Barker et al., 1991), which forms a basis for the resistance factor in the current edition of AASHTO LRFD Bridge Design Specifications, it was found that the reliability indexes obtained using "Rational Theory" varied from 1.3 to 4.5 for the bearing capacity of footings on sand and from 2.7 to 5.7 for footings on clay (Allen, 2005). They concluded that a target reliability of 3.5 should be used for footings (for the reference, the resistance component was taken equal to the factor of safety times the summation of the effect of load combination and the reliability indexes calculated for a ratio of dead load to live load of 3).

A target level of 3.5 was used for the code calibration for foundations in the National Building Code of Canada (NRC, 1995). Becker (1996) mentions that this target reliability was the average of the range of 3.0 to 4.0 obtained using a semi-analytical approach to fit WSD for the typical load combinations in Canadian structural design, with ductile behavior and normal consequence of failure. This range of reliability level matches with the range obtained from an updated

database included in the final report for NCHRP Project 20-7/Task 186 (Kulicki et al., 2007)—for a majority (about 120) of the 124 bridges analyzed, the reliability index for superstructures was between 3 and 4. A target reliability level of 3.5 is taken in the current *AASHTO LRFD Bridge Design Specifications* (1994) (for the structural system) for the most common load combination, dead load and maximum 75-year live load (Strength I).

Further, a range of 2.5 to 3.0 for drilled shafts and 2.0 to 2.5 for a redundant foundation system such as a pile group of more than four piles was suggested by Barker et al. (1991). Paikowsky et al. (2004) suggested a target reliability of 3.0 for a nonredundant deep foundation system (system with four or less piles) and, along with the study by Zhang et al. (2001), suggested 2.33 for a redundant deep foundation system.

4.3.2.3 Recommended Target Reliability

General Considerations. It would be logical and convenient to assign at the present stage a target level for foundations equal to that assigned for superstructures. In order to fulfill one of the main goals of the LRFD, the reliability level of the foundation system should be comparable to that of the structural system. However, the actual resulting reliability level of the combined system of super- and sub-structures (including soil-structure interaction) is unknown, even though a target level equal to that obtained for the superstructure is assigned for substructures.

It may also be of interest to note that due consideration should be given to applying structural safety concepts to geotechnical designs (Phoon and Kulhawy, 2002) for two reasons. First, it is unrealistic to assign a single "typical" variation (of COV) to each soil parameter, even those obtained from direct measurements taking into consideration the inherent soil variability, measurement errors, and transformation uncertainties. Usually, a range has to be provided even for datasets of satisfactory quality, taking into consideration important details like soil type, number of samples per site, distribution of depositions and measurement techniques. Second, it is important to consider the vital role of the geotechnical engineer in appreciating and recognizing the complexities of soil behavior and the inherent limitation of "simplistic" empirical geotechnical models used in the prediction of such behavior.

Current Study Calibrations. For the present calibration of resistance factors for shallow foundations, a target reliability range of 3.0 ($p_f = 0.135\%$) to 3.5 ($p_f = 0.023\%$) will be examined. This range encompasses the nonredundant target reliability used for deep foundations ($\beta = 3.0$) to the target reliability assigned in the current LRFD Bridge Design Specifications for shallow foundations. There are two major reasons

at this stage for leaving the target reliability as a range: (1) using the different resistance factors obtained from the target reliability range allows evaluation of the associated range of equivalent factors of safety and hence identification of suitability to WSD and (2) shallow foundation design includes two distinct groups of foundations for which the controlling limit state is different. By and large, shallow foundations on soil are controlled by the SLS, and, therefore, the target reliability of the ULS and the associated resistance factor are of secondary practical importance and must be evaluated against the serviceability limits. In contrast, for foundations built on rock, the ULS is by and large the controlling criterion as either structural or geotechnical failure will take place before the limit settlement will be mobilized. As such, the chosen target reliability actually controls the safety of the structure. An additional aspect affecting the aforementioned discussion is the fact that the uncertainty in the determination of capacity for foundations on rock is of higher complexity (as it is subjected to discontinuities that control the rock strength), and, hence, a possible logical outcome of the proposed range is the use of two different target reliabilities: one for shallow foundations on soil and the other for shallow foundations on rock.

Examined Target Reliability Range. Resistance factors for three target reliabilities—3.0 ($p_f = 0.135\%$), 3.25 ($p_f = 0.058\%$), and 3.5 ($p_f = 0.023\%$)—are examined as a first stage in the present study for the uncertainty established by the databases and selected methods of analysis. Figure 92 illustrates the range of resistance factors calculated based on a typical range of bias and a wide range in the uncertainty of the resistance using load characteristics from *NCHRP Report 507*'s calibration for the three examined target reliabilities. Considering "typical" values of resistance with a lognormal distribution, with a bias of 1.5, and a COV of 0.3, the resistance factors for the target reliabilities of 3.00, 3.25, and 3.50 are 0.64, 0.58, and 0.53, respectively. The three resistance factors roughly translate into a cost difference of 20% between the higher and the lower resistance factor (assuming, for simplicity, direct relations among load, size, and cost).

4.3.3 Load Conditions, Distributions, Ratios, and Factors

The loading conditions are taken as those presented in Table 49 and Section 4.2.3.3. The actual load transferred from the superstructure to the foundations is, by and large, unknown because very little long-term research has been focused on the subject. The load uncertainties are taken, therefore, as those used for superstructure analysis. The *LRFD Bridge Design Specifications* (AASHTO, 2007) provide four load combinations for the standard strength limit state (dead, live, vehicular, and wind loads) and two for the extreme limit states (earthquake
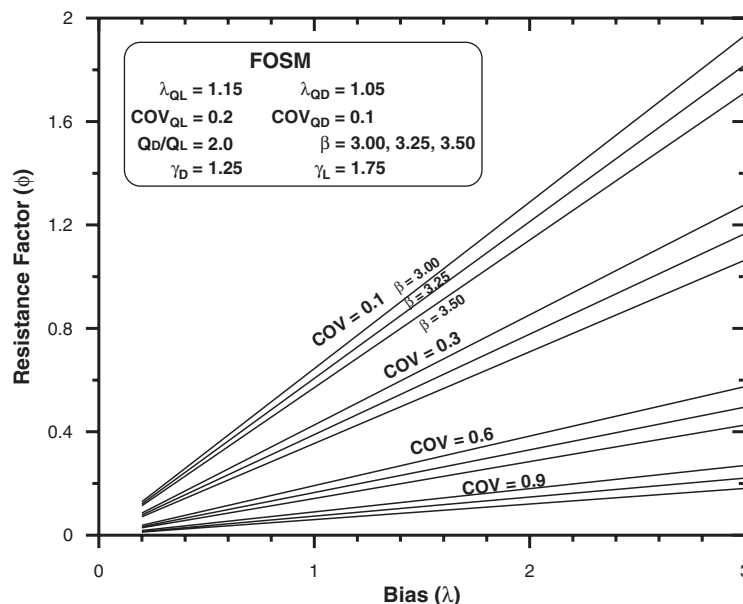
Figure 92. Calculated resistance factors as a function of the bias and COV of the resistance for the chosen vertical loading distributions and ratios under the range of the examined target reliabilities.

and collision loads). The load combination for Strength I (Z) was therefore applied in its primary form, as shown in the following limit state:

$$Z = R - D - LL \qquad (118)$$

where R = the strength or resistance of the footing, D = dead load, and LL = vehicular live loads. The probabilistic characteristics of the random variables D and LL are provided in Table 49 for vertical loads and in Section 4.2.3.3 for lateral loads. For the strength or resistance (R), the probabilistic characteristics are developed in Chapters 3 and 4, based on the databases for the various methods and conditions of analysis.

Paikowsky et al. (2004) examined the influence of the ratio of dead load to live load, demonstrating very little sensitivity of the resistance factors to that ratio, with overall decrease of the resistance factors with the increase in the ratio of dead load to live load. Large ratios of dead load to live load represent conditions of bridge construction typically associated with very long bridge spans. The relatively small influence of the ratio of dead load to live load on the resistance factor led Paikowsky et al. (2004) to use a typical ratio of 2.0, knowing that the obtained factors are by and large applicable for long span bridges, being on the conservative side. This ratio was adopted, therefore, for the present study calibrations as well. Discussion of the ratio of dead load to live load for lateral loads is presented later in this chapter.

4.4 Examination of the Factor $N\gamma$ as a Source of Uncertainty in Bearing Capacity Analysis

4.4.1 Overview

Section 3.5 examined the uncertainty in the bearing capacity of footings in/on granular soils subjected to vertical-centric loading. This load type pertains to 173 case histories of database UML-GTR ShalFound07. A summary of the bias is presented as a flow chart in Figure 60 and histograms and relations between measured and calculated capacities in Figures 61 to 65. The analysis of the data indicated the following:

1. Overall, the mean bias (measured over predicted capacity) was greater than 1 ($m_\lambda = 1.59$ for $n = 173$) pointing out a systematic capacity underprediction.
2. The mean bias (m_λ) of the footings on natural soil conditions was 1.0, and the mean bias (m_λ) of the footings on controlled soil conditions was 1.64.
3. Previous findings suggested resistance factors based on the separation between natural and controlled soils, using the above findings (Paikowsky et al., 2008; Amatya et al., 2009; Paikowsky et al., 2009b).

A clear variation exists between the cases of the foundations on natural soils and the cases of the foundations on controlled soils by a factor of 1.6. The source of this large variation in the

bias was further investigated, especially other parameters that could affect this variation and could be the source for the large bias in the prediction. Section 1.5.2 discusses the fact that no closed-form analytical solution exists for the bearing capacity problem formulation once the soil weight effect beneath the foundation is considered. The factor N_γ has been, therefore, evaluated by many researchers with varying results, as demonstrated in Figure 11. The investigation of the factor N_γ using the robust database assembled for this study is presented in the following section in view of the aforementioned bias findings.

4.4.2 The Uncertainty in the Bearing Capacity Factor N_γ

For foundations tested on the surface of granular soils, the bearing capacity (Equation 19) becomes a function of the term $\gamma\, N_\gamma$ only, as the cohesion and embedment terms are zeroed. The bearing capacity factor N_γ can then be back-calculated and the obtained factor (termed $N_{\gamma Exp}$) can be evaluated against that proposed by Vesić (1973) (termed $N_{\gamma Vesić}$) and used in this study (see Equation 29 and Table 26). The bias of the term N_γ can be defined as the following:

$$\lambda_{N\gamma} = \frac{N_{\gamma Exp}}{N_{\gamma Vesic}} = \frac{q_u/(0.5\gamma Bs_\gamma)}{2(N_q+1)\tan\phi_f} \qquad (119)$$

One hundred and twenty five relevant cases were investigated in which the foundation was tested on the ground surface, and the groundwater was below the zone of the foundation influence. Figure 93 presents the scatter and exponential fit of the
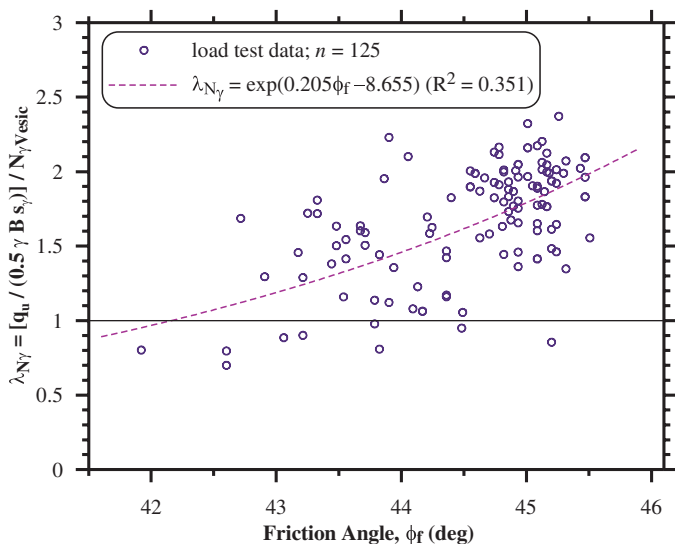
bias in N_γ obtained for soils with friction angles between 42° and 46°. The data points representing the bias in N_γ presented in Figure 93 suggest a clear trend in which the bias N_γ increased as the soil's internal friction increased beyond about $\phi_f \geq 43°$.

The best fit line of the bias $\lambda_{N\gamma}$ versus internal friction ϕ_f, as expressed in Figure 93, can be used to develop an expression for a modified bearing capacity factor N_γ that would better match the experimental data:

$$N_{\gamma Exp} = \exp(0.205\phi_f - 8.655)N_{\gamma Vesic}$$

$$\text{for } 42.5° \leq \phi_f \leq 46° \qquad (120)$$

The large scatter of the data results in a coefficient of determination (R^2) of 0.351 for Equation 120.

4.4.3 Re-examination of the Uncertainty in Bearing Capacity of Footings in/on Granular Soils Accounting for the Bias in the Factor N_γ

The effect of the bias in N_γ established in Section 4.4.2 is examined in this section by comparing the bias of the calculated bearing capacity under different loading conditions to the bias established for N_γ. Figures 94 to 98 describe the bias of the calculated bearing capacity for soil friction angles between 42.5° and 46.0° (for which Equation 120 is valid) for different loading conditions. For the case of vertical-centric loading (Figure 94), the bias of the bearing capacity calculation overlaps that of N_γ, suggesting that the bias observed for the investigated cases can be mostly attributed to the bias in N_γ. This

Figure 93. The ratio ($\lambda_{N\gamma}$) of the back-calculated bearing capacity factor N_γ (based on experimental data) and the bearing capacity factor proposed by Vesić (1973) versus soil friction angle.
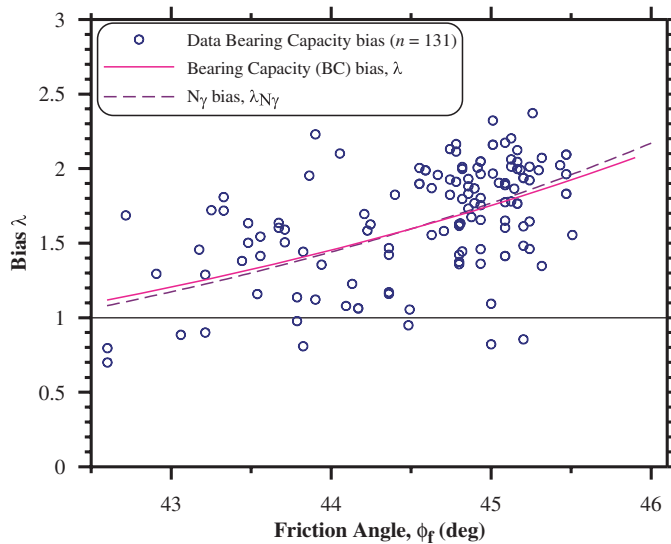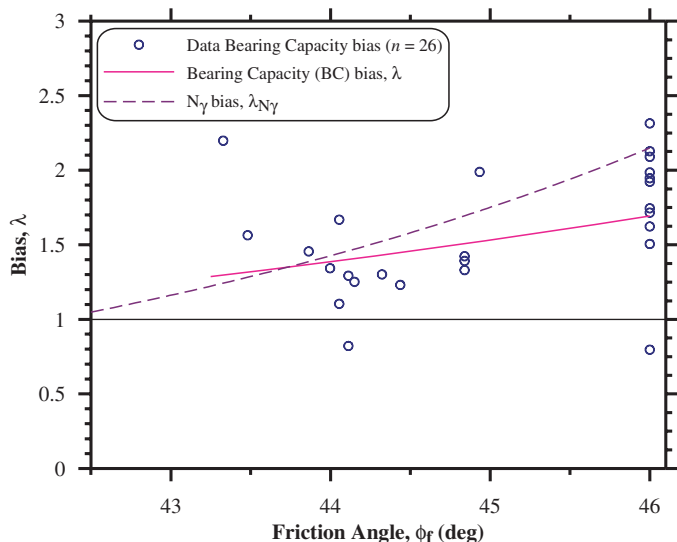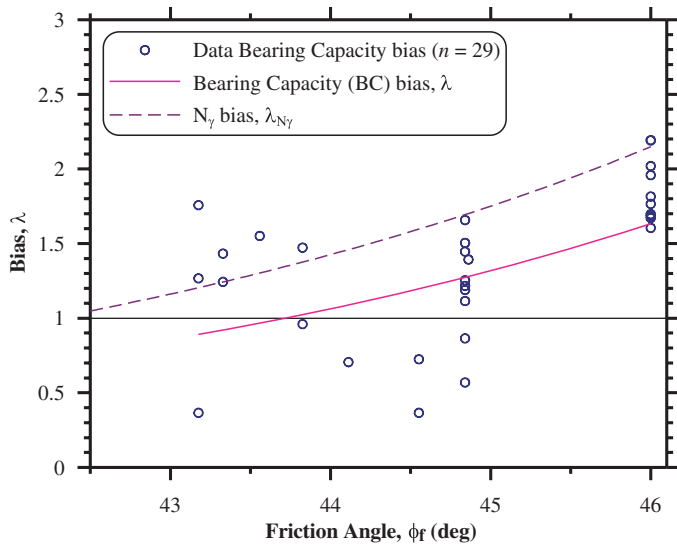

Figure 94. The ratio between measured and calculated bearing capacity (bias λ) compared to the bias in the bearing capacity factor N_γ ($\lambda_{N\gamma}$) versus the soil friction angle for footings under vertical-centric loadings.
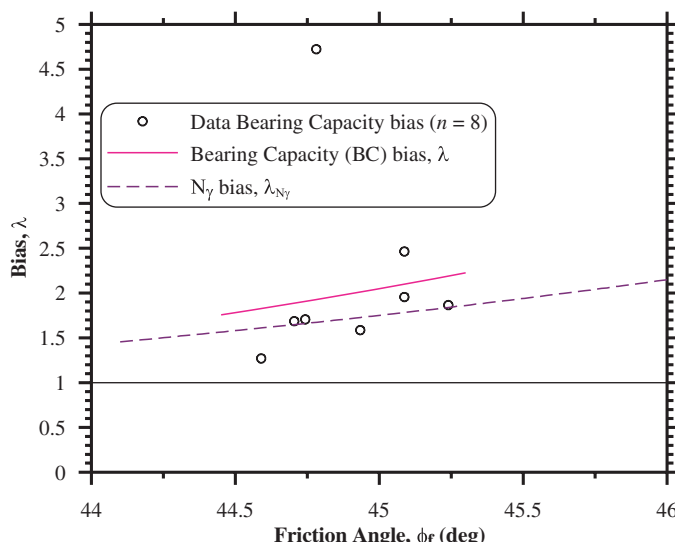
Figure 95. The ratio between measured and calculated bearing capacity (bias λ) compared to the bias in the bearing capacity factor N_γ (λ_{N_γ}) versus the soil friction angle for footings under vertical-eccentric loadings.

Figure 97. The ratio between measured and calculated bearing capacity (bias λ) compared to the bias in the bearing capacity factor N_γ (λ_{N_γ}) versus the soil friction angle for footings under inclined-eccentric, positive moment loadings.

conclusion is subjected, however, to the fact that most of the cases are related to surface loading, hence, used for establishing the bias in N_γ. For the cases related to vertical-eccentric and inclined-centric loading (Figures 95 and 96), the data suggests that the trends are similar, and, hence, the bias in N_γ may be a significant contributor to the bias in the bearing capacity calculations. The biases do not overlap because the cases involved in eccentric and inclined loading are highly sensitive to many other factors that affect the bearing capacity. The cases

involved in inclined-eccentric loading (Figures 97 and 98) have a small number of data cases and the bearing capacity is highly sensitive to the loading conditions. Overall, the data presented in Figures 94 to 98 suggest that the bias in the bearing capacity factor N_γ is a major contributor to the uncertainties in the bearing capacity estimation regardless of the load combinations acting on the footing.

Figure 96. The ratio between measured and calculated bearing capacity (bias λ) compared to the bias in the bearing capacity factor N_γ (λ_{N_γ}) versus the soil friction angle for footings under inclined-centric loadings.
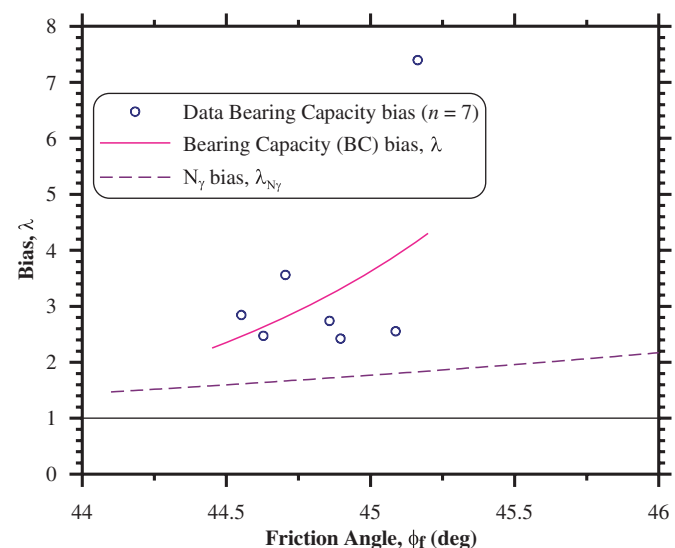

Figure 98. The ratio between measured and calculated bearing capacity (bias λ) compared to the bias in the bearing capacity factor N_γ (λ_{N_γ}) versus the soil friction angle for footings under inclined-eccentric, negative moment loadings.

4.5 Examination of Footing Size Effect on the Uncertainty in Bearing Capacity Analysis

Figure 99 presents the ratio of measured to calculated bearing capacity (the bias λ) versus footing width for vertical-centric loaded footings on/in natural and controlled soils. Overall, no easily identifiable trend appears in Figure 99 other than a general trend of some increase in the bias with the increase in footing size for natural soils, subjected to the presented scatter.

Figure 100 shows the mean bias of the bearing resistance versus the footing size for all the cases in controlled and natural soil conditions combined. The 95% confidence interval of the mean bias versus the footing size is also presented for friction angles less than and greater than 43° (the reason for making $\phi_f = 43°$ the separator is related to the uncertainty in the factor N_γ presented in Section 4.4). The following observations related to the database on which Figure 100 was based can be made: smaller footings were tested on soils with larger friction angles, $\phi_f \geq 43°$, and larger footings were tested on soils with smaller friction angles, $\phi_f < 43°$.

Overall, it can be concluded that what can be perceived as a reduction in the bias with an increase in the foundation size seems to be more associated with the bias in N_γ associated with the internal friction angle. Other conclusions are difficult to derive due to the small number of cases associated with large footings (i.e., 1 to 3 cases for footings greater than 1 m) as compared to 135 cases in the small footing category.

4.6 In-Depth Re-Examination of the Uncertainty in Bearing Capacity of Footings in/on Granular Soils Under Vertical-Centric Loading

4.6.1 Identification of Outliers and Fit of Distributions for Calibrations

4.6.1.1 Overview

The bearing capacity of footings in granular soils is highly controlled by the bearing capacity factor N_γ, in particular for foundations on or near the surface. The factor N_γ is very sensitive to the magnitude of the soil's internal friction angle ϕ_f as expressed by Equation 29, presented in Table 26, and illustrated in Figure 11. Section 4.3 investigated the source of the bias underlying the bearing capacity analysis, demonstrating that the bias increases with the increase in the internal friction angle (when exceeding 42.5°) and is closely associated to the bias in the expression of N_γ as illustrated in Figures 94 to 96.

The varying bias with the soil's internal friction angle suggests that the development of the resistance factors should follow this trend, unless a correction to the methodology is developed and the expression of N_γ is modified. The latter, although it may have some advantages, is problematic for several reasons, including the need to change an established methodology and modifications of an expression based on a database that, while extensive, may be modified in the future. As the resistance factors should be developed considering the
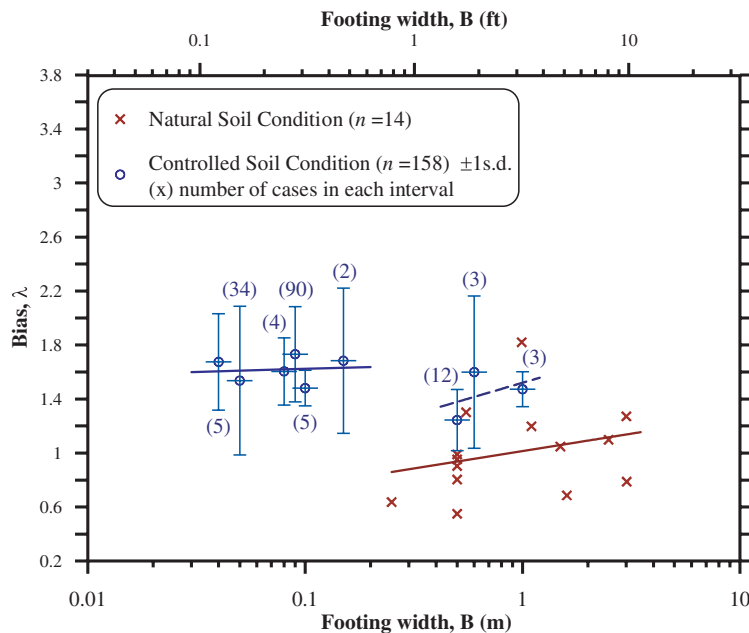
Figure 99. Variation of the bias in bearing resistance versus footing size for cases under vertical-centric loadings: controlled and natural soil conditions.
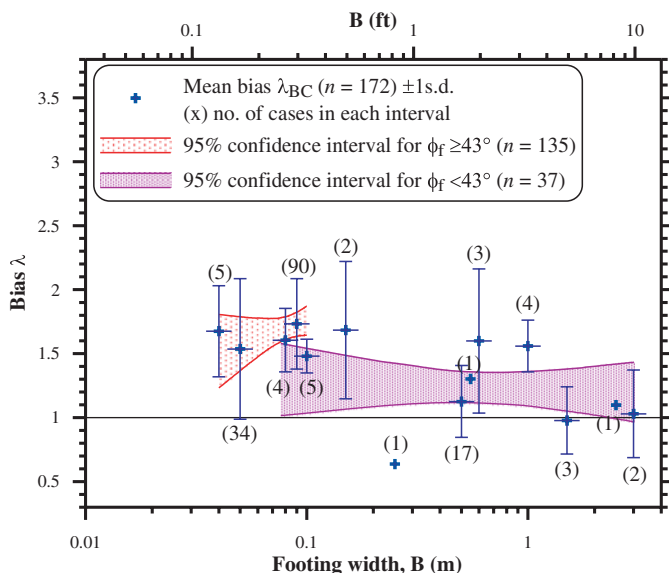
Figure 100. Variation of the bias in bearing resistance versus footing size for cases under vertical-centric loadings: $\phi_f \geq 43°$ and $\phi_f < 43°$.

Figure 101. Standard normal quantile of bias data (measured over predicted bearing capacity) for $\phi_f = 45 \pm 0.5°$ and predicted quantiles of normal and lognormal distributions.

bias change with the soil's internal friction angle, ϕ_f, it is also reasonable to pursue the identification of data outliers for subsets based on the magnitude of ϕ_f.

4.6.1.2 Outliers and Examination of Fit of Distributions for $\phi_f = 45° \pm 0.5$

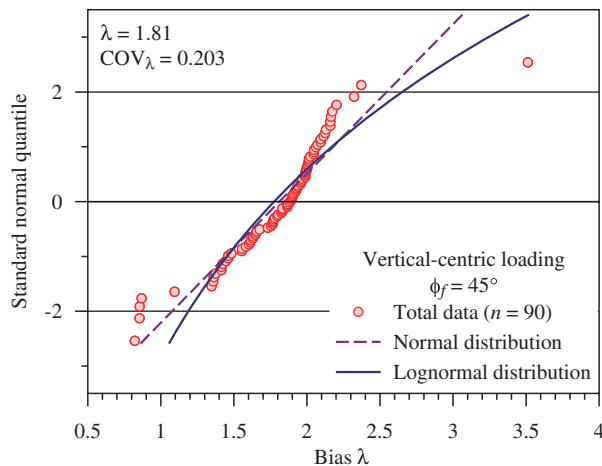The largest dataset in the UML-GTR ShalFound07 database is for footings tested under vertical-centric loadings. Subsets of data are formed for each identifiable internal friction angle, $\phi_f (\pm 0.5°)$. The largest subset is for $\phi_f = 45 \pm 0.5°$ (90 cases), the mean and COV of the bias for which are found to be 1.81 and 0.203, respectively. Figure 101 presents a comparison of a standard normal quantile of the bias data to predicted quantiles of the theoretical normal and lognormal distributions. At least one possible outlier, a footing with a bias of 3.51, can be observed for both the normal and the lognormal distributions. Removal of this data point can result in a better fit of the dataset to the normal distribution, which is further quantified by the goodness-of-fit test. In this sense, the outliers identified here imply that their removal improves the dataset so it better fits a theoretical distribution.

The χ-squared goodness-of-fit (GOF) tests have been carried out to test the fit of the theoretical normal and lognormal distributions to follow the bearing resistance bias for $n = 90$ cases, along with the datasets after the removal of some identifiable outliers. Table 54 lists in detail a number of trials and the corresponding χ-squared values obtained from the GOF tests. If the χ-squared values obtained for an assumed distribution are greater than the acceptable χ-squared values of a certain

significance level (usually of 1% or 5%), the distribution is rejected. For $n = 90$, the χ-squared value for the lognormal distribution is 63.0 and the χ-squared value for the normal distribution is 228.9, both of which are greater than the χ-squared values of 21.66 at the 1% significance level and 16.92 at the 5% significance level, respectively. Hence, both distributions do not fit the data well and are rejected by the χ-squared GOF test. The smaller χ-squared value for the lognormal distribution (in comparison to the χ-squared value of the normal distribution) for this dataset suggests, however, that the lognormal distribution provides a better fit.

It can be seen from the trials outlined in Table 54 that the removal of outliers from either or both the higher and the lower tails of the bias distribution does not result in an acceptable χ-squared value for either the normal or the lognormal distribution. Hence, the removal of outliers from the distribution tails does not render normal or lognormal distribution acceptable, while a comparatively better fit fluctuates between normal and lognormal distribution, based on the χ-squared GOF test. Hence, all the available data for the cases in/on soil with $\phi_f = 45°$ have been used for the resistance factor calibration without the identification and removal of outliers and assumed to follow lognormal distribution.

In Figure 101, there are four footings with a bias smaller than 1.0, the smallest being $\lambda = 0.82$, for which the assumed lognormal distribution overpredicts the bias in the lower tail region, which is more critical than the higher tail region (because bias less than 1.0 means the calculated resistance was more than the actual resistance). This circumstance is examined in Section 4.6.2.4 following the resistance factor calibration in order to ensure that the resistance factor developed for $\phi_f = 45°$ results in acceptable risk in design.

Table 54. χ-squared values for the fitted lognormal and normal distributions for vertical-centric loading cases on/in soil with an internal friction angle (ϕ_f) of 45°.

n	χ-squared values		Comments
	Lognormal distribution	Normal distribution	
90	63.0	228.9	Mean = 1.81, COV = 0.203; all data for ϕ_f = 45°
89	515.0	60.3	Mean = 1.79, COV = 0.179; highest bias (3.51) removed (data beyond 2s.d.)
89	60.3	428.0	Mean = 1.822, COV = 0.195; case with 3rd lowest bias (0.87) removed; this case is on the lower bias tail and the farthest from theoretical lognormal quantile
88	57.9	724.0	Mean = 1.83, COV = 0.186; 2 cases with 2nd and 4th lowest biases (0.85 and 0.87) removed; in lower bias tail and farthest two from theoretical lognormal quantile
87	805.0	43.6	Mean = 1.83, COV = 0.185; 2nd and 4th lowest bias cases (0.85 and 0.87) and the case with the highest bias (3.51) removed
87	62.5	927.0	Mean = 0.81, COV = 0.161; 2nd and 4th lowest bias cases (0.85 and 0.87) and the case with the 2nd highest bias (2.37) removed
87	57.5	1,418.0	Mean = 1.84, COV = 0.177; 2nd, 3rd and 4th lowest bias cases (0.85, 0.85 and 0.87) removed

Note: Acceptable χ-squared value for significance level of 1% is 21.666 and for significance level of 5% is 16.919.

4.6.1.3 Outliers and DFs for Internal Friction Angles Other than 45°

Procedures similar to those described in Section 4.6.1.2 have been performed for the data subsets of ϕ_f other than 45°. For ϕ_f = 44° (n = 30, m_λ = 1.40 and COV = 0.250), both the normal and lognormal distributions are accepted by the χ-squared GOF test for the 1% significance level. The lognormal distribution provides a better fit, with a χ-squared value of 13.74 versus 17.82 for the normal distribution.

For ϕ_f = 43°, 42°, 38°, 36°, and 32°, although the normal distributions provide better fits than the lognormal distributions, lognormal distributions have been considered. This is done because lognormal distribution is naturally expected to better represent the dataset of a ratio (i.e., bias) restricted by values greater than zero or due to similar behavior, small dataset, and so forth as further detailed. For ϕ_f = 43° (n = 14, m_λ = 1.34, and COV = 0.283), the χ-squared value is 18.53 for normal versus 22.69 for lognormal. For ϕ_f = 42° (n = 4, m_λ = 1.60, and COV = 0.416), the χ-squared value is 12.20 for normal versus 12.74 for lognormal. For ϕ_f = 38° (n = 12, m_λ = 1.26, and COV = 0.215), the χ-squared value is 16.75 for normal versus 74.62 for lognormal. The minimum bias of 0.55, which is overpredicted by the lognormal distribution for this dataset, will be examined following the resistance factor calibration. For ϕ_f = 36° (n = 4, m_λ = 1.20, and COV = 0.233), the χ-squared value is 19.78 for normal versus 21.61 for lognormal, and, for ϕ_f = 32° (n = 4, m_λ = 1.25, and COV = 0.347), the χ-squared value is 10.77 for a normal distribution versus 11.15 for lognormal.

For ϕ_f = 35° (n = 4), the mean bias is found to be 2.00 and the bias COV is 0.528, which is exceptionally high compared to the COVs for the datasets of the closer-in-magnitude friction angles, which is around 0.2. Though the GOF test shows that both normal and lognormal distributions are acceptable, with lognormal being a better fit, the case with the highest bias, λ = 3.57, has been considered an outlier. The comparison of the standard normal quantiles of the dataset and the theoretical distributions is shown in Figure 102(a). The resulting dataset after the removal of this case has a mean of 1.47 and COV of 0.088 (examination of the database shows that the remaining three cases are from the same site, hence explaining the very small COV). Comparison of the standard normal quantiles of the filtered dataset and the theoretical distributions is shown in Figure 102(b). Lognormal distribution is considered for this dataset also. Hence, only one outlier was removed from the total dataset, resulting in 172 cases used for the resistance factor calibration for vertical-centric loading.

4.6.2 The Statistics of the Bias as a Function of the Soil's Internal Friction Angle and Resulting Resistance Factors

4.6.2.1 In-Depth Examination of Subsets Based on Internal Friction Angle

Tables 55 through 57 present the biases evaluated for the bearing capacity estimation according to the soil's friction angles. The corresponding resistance factors have been obtained for a target reliability index β_T of 3.0 (exceedance probability of 0.135%). Table 55 presents the cases in controlled soil conditions while Table 56 shows the cases in natural soil conditions. Table 57 presents all the cases in the
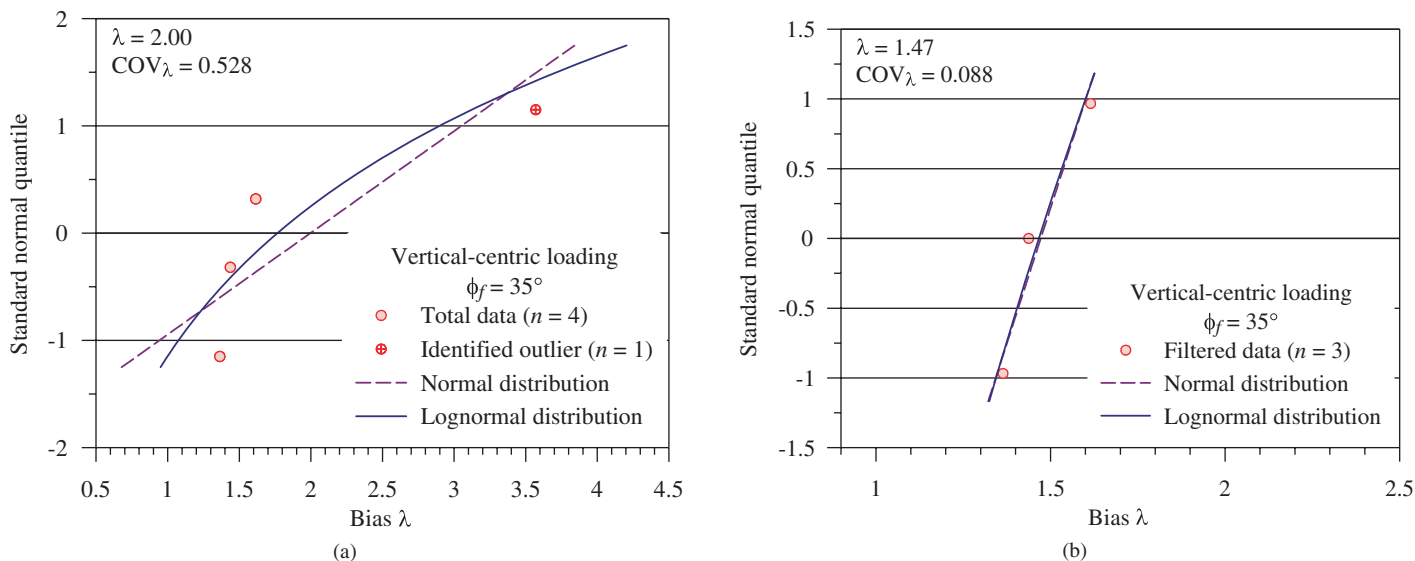
Figure 102. Standard normal quantile of bias data for $\phi_f = 35 \pm 0.5°$ and predicted quantiles of normal and lognormal distributions (a) for all data and (b) with the outlier removed.

database, both controlled and natural soil conditions, under vertical-centric loadings. All the cases in the controlled soil conditions are in soils with relative densities above 35%.

Graphical presentation of the bias in bearing resistance estimation versus soil friction angle is shown in Figure 103. The error bars represent one standard deviation of the mean bias for each friction angle, taken as a range of $\phi_f \pm 0.5°$, and the

number in parentheses represents the number of cases in each of the friction angles' subsets.

4.6.2.2 Factor Development Based on Data Trend

The bias in bearing resistance estimation for the cases under vertical-centric loading, both in/on controlled and natural soil

Table 55. Statistics of bearing resistance bias and the resistance factors corresponding to soil friction angles in controlled soil conditions for vertical-centric loading.

Friction angle ϕ_f (±0.5 deg)	n	Bias		Resistance factor ϕ ($\beta_T = 3$)	
		Mean λ	COV$_\lambda$	MCS	Preliminary
46	2	1.81	0.071	1.655	1.00
45	90	1.81	0.203	1.194	1.00
44	30	1.40	0.250	0.807	0.80
43	14	1.34	0.283	0.700	0.70
42	4	1.60	0.416	0.700	0.70
39	1	1.02	--	--	--
38	11	1.32	0.122	1.081	1.00
36	3	1.34	0.079	1.206	1.00
35	3	1.47	0.088	1.300	1.00
43 to 46	136	1.67	0.247	0.971	0.95
38 ± 3	22	1.38	0.225	0.855	0.85
all angles	158	1.63	0.252	0.934	0.90

Table 56. Statistics of bearing resistance bias and the resistance factors corresponding to soil friction angles in natural soil conditions for vertical-centric loading.

Friction angle ϕ_f	n	Bias		Resistance factor ϕ ($\beta_T = 3$)	
		Mean λ	COV$_\lambda$	MCS	Preliminary
33 ± 2.5 (all angles)	14	1.00	0.329	0.457	0.45

Table 57. Statistics of bearing resistance bias and the resistance factors corresponding to soil friction angles in controlled and natural soil conditions combined, for vertical-centric loading.

Friction angle ϕ_f (±0.5 deg)	n	Bias		Resistance factor ϕ ($\beta_T = 3$)	
		Mean λ	COV$_\lambda$	MCS	Preliminary
46	2	1.81	0.071	1.655	1.00
45	90	1.81	0.203	1.194	1.00
44	30	1.40	0.250	0.807	0.80
43	14	1.34	0.283	0.700	0.70
42	4	1.60	0.416	0.700	0.70
39	2	0.83	0.330	0.378	0.35
38	12	1.26	0.215	0.804	0.80
36	4	1.20	0.233	0.727	0.70
35	3	1.47	0.088	1.300	1.00
34	2	1.09	0.135	0.865	0.85
33	3	1.03	0.126	0.836	0.80
32	4	1.25	0.347	0.542	0.50
30.5	2	0.98	0.423	0.339	0.30
43 to 46	136	1.67	0.247	0.971	0.95
36 ± 3	36	1.23	0.296	0.619	0.60
all angles	172	1.58	0.278	0.838	0.80

conditions, can be expressed by the best fit line in Figure 103 and in Equation 121, for which the coefficient of determination is 0.200. This line shows that the bearing resistance bias (λ_{BC}) increases with an increase in the soil friction angle:

$$\lambda_{BC} = 0.308\exp(0.0372\phi_f) \qquad (121)$$

The details provided in Tables 55 and 56 indicate that the data available for controlled soil conditions relate to soils with higher friction angles compared to that for natural soil conditions. The bias expressed by Equation 121 has been used to develop resistance factors for the whole range of soil friction angles for both controlled and natural soil conditions.

Based on Tables 55 and 56, the COVs of the bias for all the controlled and natural soil condition cases are 0.252 and 0.329, respectively. Hence, COV$_\lambda$ of 0.25 and 0.35 may be taken to represent the COVs of the biases for the controlled soil and nat-
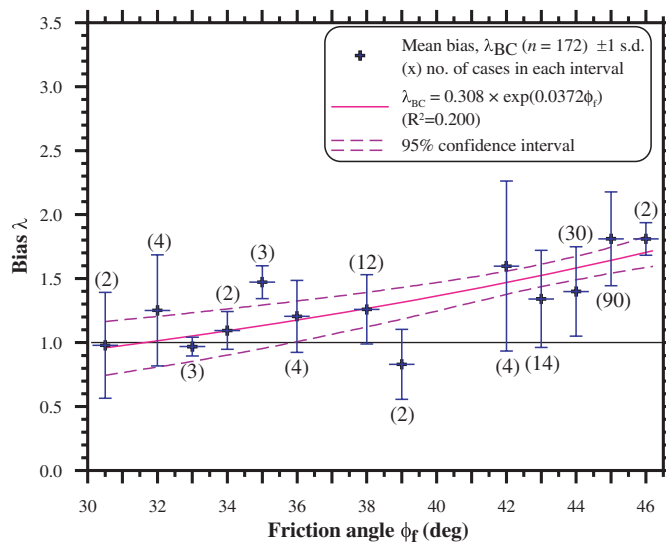
Figure 103. Bearing resistance bias versus average soil friction angle (taken ϕ_f ± 0.5°) including 95% confidence interval for all cases under vertical-centric loading.

Table 58. Resistance factors for vertical-centric loading cases based on the bias versus ϕ_f best fit line of Equation 121 and the COV of natural versus controlled soil conditions.

Soil friction angle ϕ_f (deg)	Mean bias λ (Equation 121)	Resistance factor ϕ ($\beta_T = 3$)			
		Soil Conditions			
		Natural (COV$_\lambda$ = 0.35)		Controlled (COV$_\lambda$ = 0.25)	
		MCS	Rec.*	MCS	Rec.
30	0.94	0.403	0.40	0.542	0.50
35	1.13	0.485	0.45	0.652	0.60
37	1.22	0.524	0.50	0.703	0.70
38	1.27	0.545	0.50	0.732	0.70
40	1.36	0.584	0.55	0.784	0.75
≥45	1.64	0.704	0.65	0.946	0.80

*Rec. = Recommended

ural soil conditions, respectively. Table 58 presents the resistance factors calculated using these statistics for friction angles ranging from 30° to ≥45°, on foundations in/on natural and controlled soil conditions.

Figure 104 presents the recommended resistance factors for controlled and natural soil conditions detailed in Table 58. Figure 104 also presents a comparison of the recommended resistance factors to those obtained in Table 57 (based on the database) and the 95% confidence interval of the bearing resistance bias. It can be observed that the recommended resistance factors follow the trend in the bearing resistance

bias with the soil friction angle. The cases for which a small resistance factor was developed based on a very small subset (two cases each) could be justifiably overruled in the context of the established trend and the large datasets supporting it.

4.6.2.3 Recommended Resistance Factors

The recommended resistance factors for vertical-centric loading cases are presented for different friction angles in Table 59 based on the values calculated and recommended in Table 58. The values in Table 59 are applicable for soils with relative densities greater than 35%. Further consideration is necessary for soils with friction angles less than 30° combined with relative densities less than 35%. For these soils, which are in a very loose state, it is recommended either to consider ground improvement to a depth of at least twice the footing width (subjected to a settlement criterion), ground replacement, or an alternative foundation type.

4.6.2.4 Examination of the Recommended Resistance Factors

A rough estimate of the equivalent factor of safety (FS) for a resistance factor of ϕ, developed using a ratio of dead load to live load of 2.0; dead-load, load factor of 1.25; and live-load,
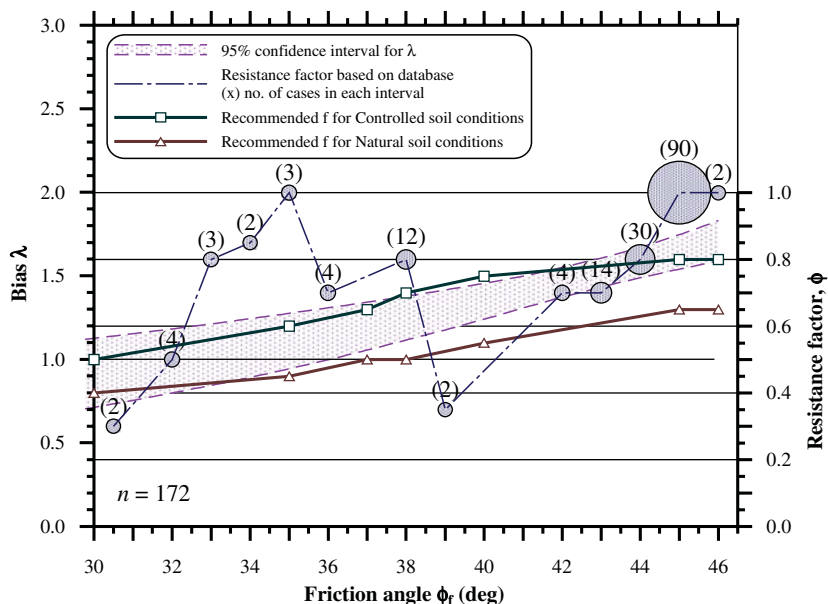
Figure 104. Recommended resistance factors for soil friction angles (taken ϕ_f ±0.5°) between 30° and 46°, with comparisons to 95% confidence interval and resistance factors obtained for the cases in the database; the bubble size represents the number of data cases in each subset.

Table 59. Recommended resistance factors for vertical-centric loading cases.

Soil friction angle ϕ_f (deg)	Recommended resistance factor ϕ ($\beta_T = 3$)	
	Soil conditions	
	Natural	**Controlled**
30–34	0.40	0.50
35–36	0.45	0.60
37–39	0.50	0.70
40–44	0.55	0.75
≥ 45	0.65	0.80

load factor of 1.75 was presented by Paikowsky et al. (2004) and expressed by the following equation:

$$FS \approx 1.4167/\phi \tag{122}$$

The highest recommended resistance factor in Table 59 is $\phi = 0.80$ for $\phi_f \geq 45°$, developed assuming the data follow a lognormal distribution. A rough estimate of the equivalent factor of safety for this resistance factor is given by Equation 122 as 1.77. A safe design requires that the condition in Equation 123 is met:

$$\frac{q_{calc}}{FS} \leq q_{meas} \tag{123}$$

where q_{calc} is calculated bearing capacity and q_{meas} is measured bearing capacity. The minimum allowable bias for the given FS is, therefore, the reciprocal of the FS, i.e., the minimum bias for which the design will be safe is $1/FS = 0.565$. This bias is much smaller than the smallest bias of the dataset, $\lambda = 0.82$, for which the standard normal quantile is seen to be over-predicted by the assumed lognormal distribution (see Figure 101). A bias of 0.82, therefore, results in a safe design, and all the footing cases in the database are safe upon the application of the developed resistance factor. It can, therefore, be concluded that the methodology of utilizing the trend and the assumption of the lognormal distribution for the bias is acceptable for resistance factor calibration and is justified by the outcome.

4.7 In-Depth Re-Examination of the Uncertainty in Bearing Capacity of Footings in/on Granular Soils Under Vertical-Eccentric Loading

4.7.1 Examination of the Bias for Controlling Parameters

The investigation presented in Section 4.4.3 and Figure 95 suggested that the bias in the bearing capacity factor N_γ can be associated with the general trend of the bias for the bearing

capacity analysis of footings under vertical-eccentric loading. The relations shown in Figure 95 are not similar to those in Figure 94 (investigating footings under vertical-centric loading); hence, additional evaluation is required for cases not under vertical-centric loading.

The variation of the bearing capacity bias with the soil's friction angle is presented in Figure 105 for cases under vertical-eccentric loading (each error bar represents one standard deviation). It can be observed that for $\phi_f = 35 \pm 0.5°$ the mean bias of the seven cases is higher than for the other soil friction angles with a relatively lower COV. These seven cases are related to a single site and compiled from the DEGEBO literature. Hence, for the determination of the best fit line of the bias versus the friction angle, these seven cases were excluded. The trend in Figure 105 suggests a possible decrease in the bias with the increase in the friction angle, which is contrary to the trend established for the case of vertical-centric loading (see Figure 94) or the trend seen in Figure 95 for the soil's friction angles in the range of 43.5° to 46.0°. The data in Figure 105 suggest that no clear, unique correlation exists between the bias and the soil's internal friction angle, and, even upon the exclusion of the aforementioned seven cases, the coefficient of determination (R^2) is 0.01, essentially indicating that a correlation does not exist. The data in Figure 105 may indicate, therefore, that either for the eccentric loading and/or the available data for such cases, factors other than the soil's friction angle contribute significantly to the bias.

Figure 106 presents the relationship between the bias of vertical-eccentric loading of foundations and the magnitude of the eccentricity normalized by the foundation's width, i.e., e/B. Forty-three cases have been tested with load eccentricity
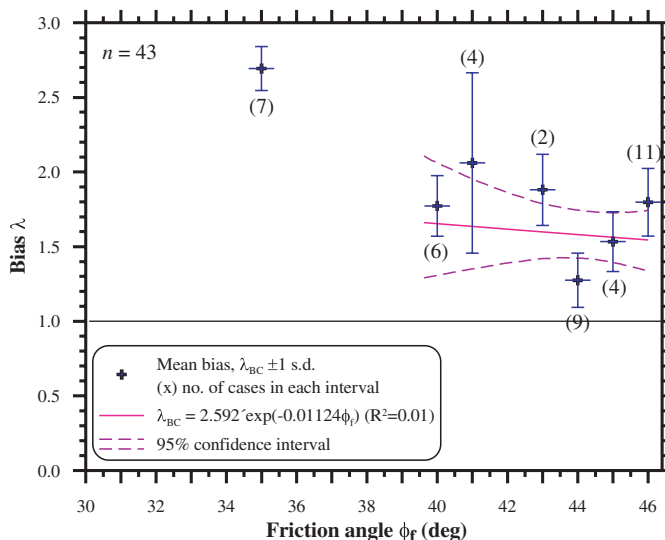
Figure 105. Bearing resistance bias versus soil friction angle for cases under vertical-eccentric loadings (seven cases for ϕ_f = 35° [all from a single site] have been ignored for obtaining the best fit line).
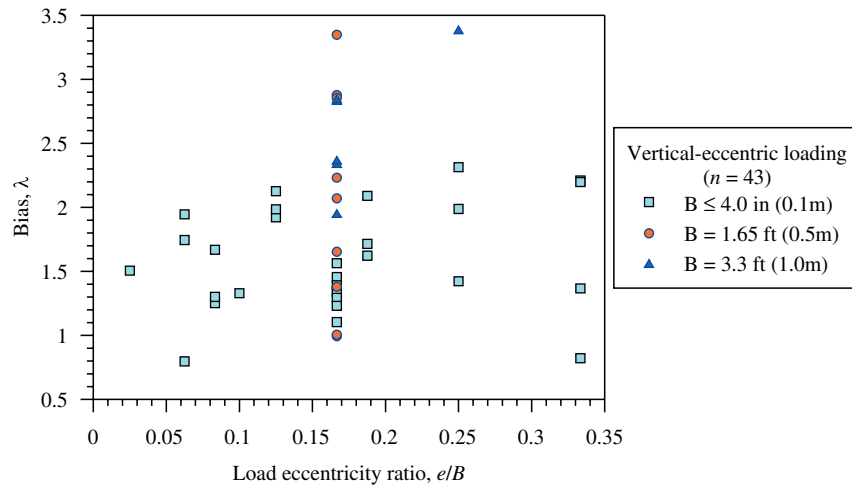
Figure 106. Bearing resistance bias versus load eccentricity ratio e/B for vertical-eccentric loading.

ratios ranging from 0.025 to 0.333 (1/40 to 1/3), with a majority of them having an eccentricity ratio of 1/6. It can be seen that while the larger foundations mostly have higher biases, there appears to be no correlation between the bearing resistance bias and the load eccentricity ratio. The large scatter that appears for the small foundations may be related to the physical difficulties of conducting such tests where eccentric loads need to be applied to a small footing.

A closer examination of the relationship between the bias and the magnitude of the eccentricity is presented in Figure 107 for a given eccentricity ratio of $e/B = 1/6$ versus friction angle ϕ_f. Cases with various footing widths are available for this eccentricity ratio only (see Figure 106), while tests with other load eccentricity ratios mostly utilize footings of widths less than or equal to 4 in ($\approx$0.1 m). While a best fit line for these data would show a decrease in the bias with an increase in ϕ_f,

the data related to small footings only are relevant to higher friction angles. Figure 107 thus emphasizes that the effect of the footing size on the bearing resistance bias when testing eccentrically loaded foundations is more significant compared to the effect of the soil's friction angle. Hence, calibrating resistance factors using this dataset, based on ϕ_f, cannot be justified, as has been done for the vertical-centric loading cases.

4.7.2 Identification of Outliers

The data presented in Figures 105 and 107 lead to the conclusion that in the absence of a clear underlying factor to explain the bias, resistance factors may be developed for both natural and controlled soil conditions and a range of ϕ_f and then compared to the resistance factors developed for vertical-centric loading.
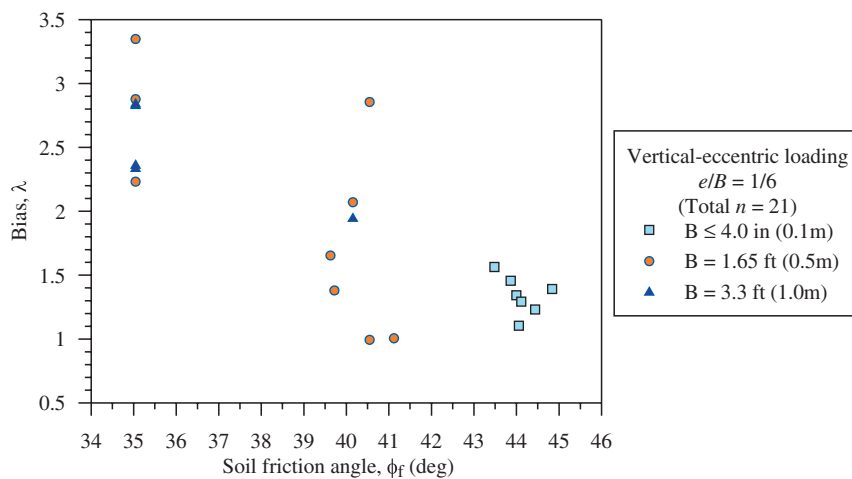
Figure 107. Change in bearing resistance bias with soil friction angle for tests with a load eccentricity ratio of e/B = 1/6.
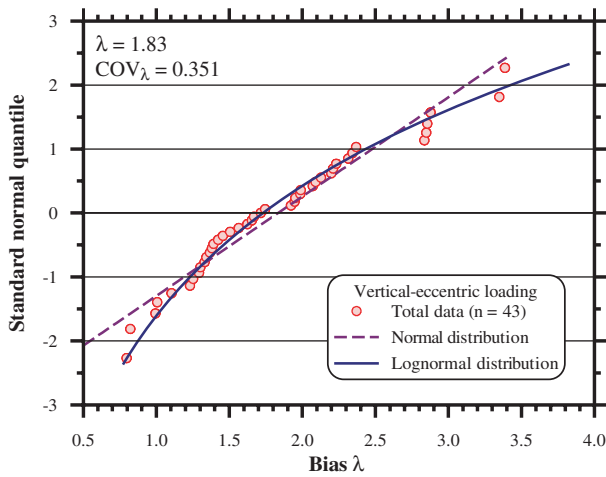
Figure 108. Standard normal quantile of the bias for all vertical-eccentric loading cases and the predicted quantiles of theoretical distributions.

Figure 108 presents the standard normal quantile of the dataset with the theoretical predictions of normal and lognormal distributions. The presented relations visually suggest a good match between the lognormal distribution and the data. The χ-squared GOF tests verify that the data follow the lognormal distribution better than the normal distribution (accepted both at the 1% and 5% significance levels), with χ-squared values of 8.34 for lognormal distribution versus 11.74 for normal distribution. As the data follow the lognormal distribution, no outliers are identified.

4.7.3 The Statistics of the Bias as a Function of the Soil's Internal Friction Angle and Resulting Resistance Factors

The bias in the bearing resistance estimation for footings under vertical-eccentric loadings evaluated for subsets of each $\phi_f\,(\pm0.5)°$ are presented in Table 60. The associated resistance

factors remain essentially at 1.0, with the exception of four cases related to $\phi_f = 41°$, for which a large scatter had been observed (see Figure 105). In addition, the amount of data available for some of the ϕ_f subsets is comparatively small. It has also been concluded in Section 4.5 that using the available data, the effect of footing size on the bias cannot be isolated from the effect of the soil friction angle. All these conditions lead to the issue of whether it is practical and appropriate to use the dataset for vertical-eccentric loading conditions alone for the resistance factor calibration of this loading situation.

Since vertical-centric loading is the simplest loading mode, the uncertainties involved in estimating the resistance of footings under vertical-eccentric loading are assumed to be not less than those involved in the case of footings under vertical-centric loading. This assumption is based on the following: (1) when the source of the lateral load is not permanent, the foundation supports vertical-centric loading only, and (2) very often the magnitudes of the lateral loads (and hence eccentricity) are not known at the bridge foundation design stage (see Section 3.1, in particular, Section 3.1.7). This means that the resistance factors for vertical-eccentric loading conditions have to be either equal to or less than the ones recommended for the vertical-centric loading in Table 59.

4.7.4 Examination of the Recommended Resistance Factors for Vertical-Eccentric Loading

The bias mean for vertical-eccentric loading is slightly higher than the bias mean for vertical-centric loading (1.83 versus 1.58); hence, the same resistance factors used for vertical-centric loadings are recommended for vertical-eccentric loadings.

Based on Equations 122 and 123, the minimum allowable bias for the highest resistance factor of 0.80 is 0.565. The bearing resistance biases of all the cases under vertical-eccentric loading in the database (the minimum being $\lambda = 0.80$) are thus

Table 60. Statistics of bearing resistance bias and the resistance factors corresponding to soil friction angles in controlled soil conditions for vertical-eccentric loading.

Friction angle ϕ_f (±0.5 deg)	n	Bias		Resistance factor ϕ ($\beta_T = 3$)	
		Mean λ	COV$_\lambda$	MCS	Preliminary
46	11	1.80	0.227	1.109	1.00
45	4	1.53	0.199	1.021	1.00
44	9	1.27	0.182	0.889	0.85
43	2	1.88	0.238	1.122	1.00
41	4	2.06	0.604	0.426	0.40
40	6	1.77	0.203	1.168	1.00
35	7	2.69	0.148	2.063	1.00
43 to 46	26	1.58	0.257	0.892	0.85
40 to 46	36	1.67	0.325	0.772	0.75
all angles	43	1.83	0.351	0.783	0.75

safe upon the application of the recommended factors. A different approach may be taken, assuming the eccentric loads are permanent, hence, allowing for resistance factors higher than those applied for vertical-centric loading. This condition is examined via the effective width (B') versus the actual width of footings under vertical-centric loading, i.e., both foundation sizes are examined (B based on ϕ for vertical-centric and B' based on ϕ for vertical-eccentric) and the larger foundation size prevails. Such examination allows review of the recommended resistance factors for vertical-centric versus vertical-eccentric conditions. A limited examination of this issue follows.

In Figure 105, the mean bias of vertical-eccentric loading for friction angles between 40° and 46° is 1.60. Assuming the mean bias to remain a constant at 1.60 for all friction angles and the COV of the bias of the bearing resistance to be related to natural and controlled soil conditions, i.e., 0.35 and 0.30, respectively, the obtained resistance factors are as follows:

Natural soil conditions, for all ϕ_f : $\phi = 0.65$ (ϕ obtained from MCS = 0.687)
Controlled soil conditions, for all ϕ_f : $\phi = 0.75$ (ϕ obtained from MCS = 0.796)
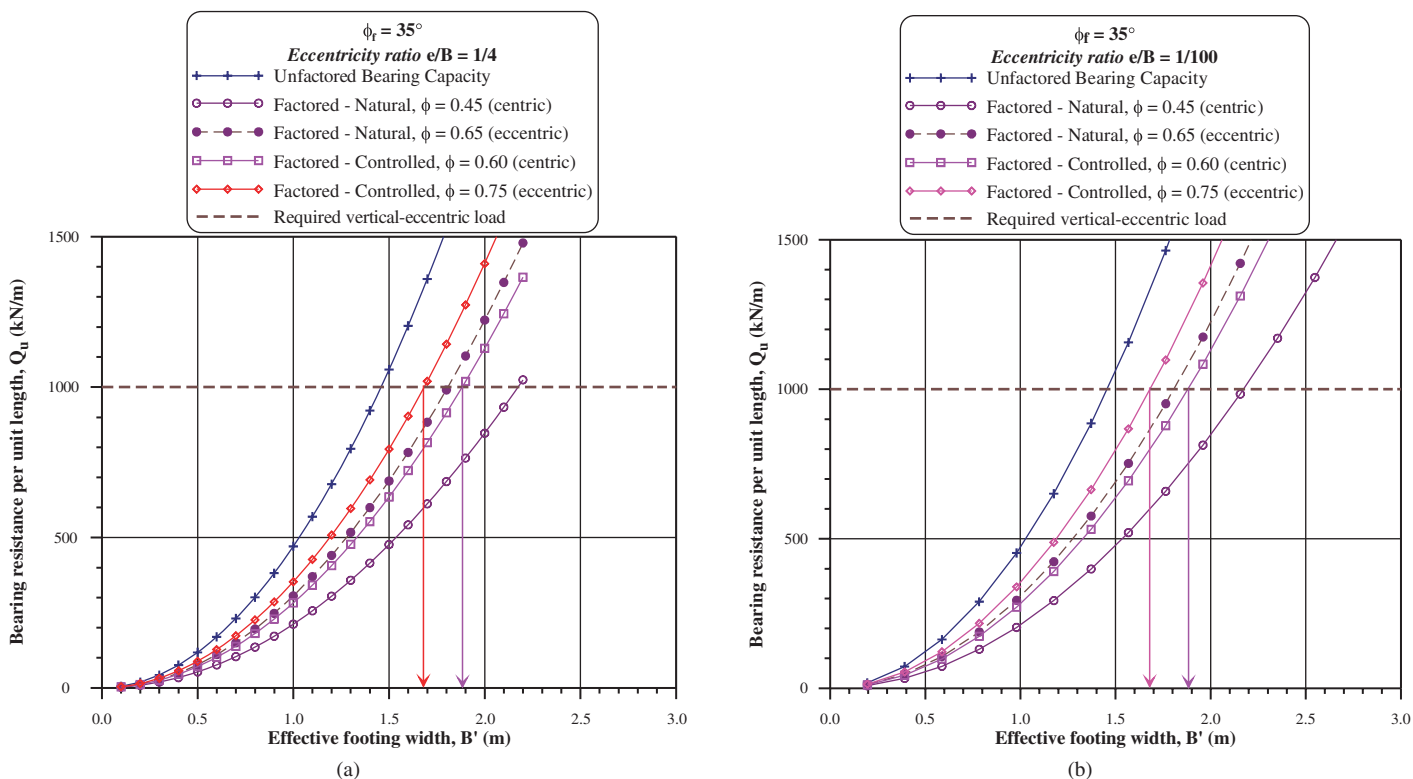
Taking these two separate databases, one for vertical-centric and the other for vertical-eccentric, two sets of resistance factors, one for controlled soil conditions and one for natural soil conditions can be obtained, as presented in Table 61. Table 61 demonstrates that the recommended resistance factors based on the extensive data available from vertical-centric load tests, although they may be conservative, will be also safe when applied for footings designated to be subjected to load-eccentricity. This is validated when compared to the resistance factors developed based on vertical-eccentric load tests (under the aforementioned assumptions) shown in Table 61 as well.

An additional examination of the effect of the eccentricity ratio (ratio of load eccentricity to footing width) on the designed footing was carried out. A strip foundation on the surface of soil with a unit weight of 124.7pcf (19.6 kN/m³) was analyzed, hence eliminating the effects of the foundation's shape and depth. Bearing resistances of the strip footing under an eccentric load with a given eccentricity ratio, altered from 1/4 to 1/100, were estimated using the bearing capacity equation and expressed as bearing resistance versus the effective footing width B' ($B - 2e$), (Meyerhof, 1953). Because the effective footing width is used, the effect of eccentricity is "eliminated" and the vertical-eccentric load case is essentially transferred to the vertical-centric case, i.e., the resulting effective footing width is the same regardless of the load eccentricity ratio. For example, for a required factored load of 369 ton/ft (1,000 kN/m), the required effective footing width (B') using the recommended ϕ of 0.60 for a ϕ_f of 35° has been found to be about 6.25 ft (1.90 m) for eccentricity ratios of 1/4 as well as 1/100. In Figures 109(a) and 109(b), the bearing resistance versus the effective footing width plots have been presented for $e/B = 1/4$ and 1/100, respectively, for a frictional soil with an internal friction angle (ϕ_f) of 35°.

It should be noted that the design (physical) footing width in both cases is different as $B = B' + 2e$ and hence depends on the magnitude of the eccentricity. Based on the examination above, it can be said that the recommended resistance factors using the vertical-centric test data results in an acceptable design for vertical-eccentric loading conditions and that separate sets of resistance factors are not required. The test results in the UML-GTR ShalFound07 database for vertical-eccentric loadings did not enable evaluation of the performance of Meyerhof's effective width model (1953), i.e., the uncertainty in defining $B' = B - 2e$ or the ability of the eccentricity ratio to exceed the limiting compression contact value of 1/6. Some discussion of the subject using other sources follows.

Table 61. Comparison of the recommended resistance factors based on vertical-centric loading to those obtained based on Figure 105 for vertical-eccentric loading.

| Soil friction angle ϕ_f | Resistance factor ϕ ($\beta_T = 3$) | | | |
| | Controlled soil conditions | | Natural soil conditions | |
	Recommended Vertical-centric and vertical-eccentric	Vertical-eccentric based on Figure 105	Recommended Vertical-centric and vertical-eccentric	Vertical-eccentric based on Figure 105
30°–34°	0.50		0.40	
35°–36°	0.60		0.45	
37°–39°	0.70	0.75	0.50	0.65
40°–44°	0.75		0.55	
≥ 45°	0.80		0.65	

Figure 109. *Comparison of the required effective footing widths for different eccentricity ratios: (a)* **e/B = 1/4** *and (b)* **e/B = 1/100** *for a strip footing resting on a soil with internal friction angle (*ϕ_f*) = 35°.*

The limiting eccentricity value of $e/B = 1/6$ is developed from a theory assuming a linear stress distribution under a rigid footing subjected to eccentric loading (the combination of centric load and a moment similar to the stress distribution in a beam). As such, when the eccentricity ratio is 1/6, the foundation is subjected to compression with one edge under no (zero) stress. When the eccentricity ratio exceeds 1/6, the foundation is expected to be subjected to "tension," hence the contact area between the foundation and the soil decreases. It is well understood that the load distribution under the foundation depends on the relative stiffness of the foundation/soil system and, hence, is not necessarily linear. Expected load distributions under vertical-centric loading proposed by Terzaghi and Peck (1948) were verified experimentally by Paikowsky et al. (2000) using tactile sensor technology and demonstrating concave stress load distribution across a rigid footing in granular soil. The effect of eccentricity (not presented in Paikowsky et al., 2000) was measured as one side stress concentration supporting the one-sided extensive slip surfaces developing under an eccentrically loaded foundation as illustrated in Figure F-3 (Appendix F) by Jumikis (1956).

A theoretical study was presented by Michalowski and You (1998) examining Meyerhof's aforementioned effective width rule (1953) in calculations of the bearing capacity of shallow foundations. Michalowski and You developed a limit analysis solution for eccentrically loaded strip footings and assessed

the effective width rule. The isometric slip lines developed by Michalowski and You invoking the kinematic approach of limit analysis resemble qualitatively the above described experimental observations. Michalowski and You concluded that for smooth footings, realistic footing models, and cohesive soils, Meyerhof's effective width rule is a reasonable account of eccentricity in bearing capacity calculations. It is only for significant bonding at the soil interface (i.e., no separation or perfect adhesion) and for large eccentricities (e.g., e/B greater than 0.25) that the effective width rule significantly underestimates bearing capacity (for clays). For cohesive-frictional soil, this underestimation decreases with an increase in the internal friction angle, becoming more and more "accurate" with limited eccentricity.

The examination and discussion presented in Sections 4.6 and 4.7 lead to the following recommendations:

1. The use of resistance factors developed and recommended for vertical-centric loading (see Table 59) could and should be extended to be used with vertical-eccentric loading.
2. The rule of effective foundation size ($B' = B - 2e$) proposed by Meyerhof (1953) is not overly conservative and results in realistic bearing capacity predictions for the foundation-soil conditions expected to be encountered in bridge construction (rough surface foundations on granular soils).

3. The independence of the calculated effective foundation size (B') from the magnitude of the eccentricity and the aforementioned recommendations/observations provide a solution for the design problems presented by various DOTs (see Section 3.1.7), in which the eccentricity is unknown at the early design stage. The solution justifies the calculated foundation size during early design to be referred to as the effective foundation that can then be modified by twice the eccentricity at the final design stage.

4. In light of the presented material, there is no clear evidence allowing an increase in the foundation eccentricity ratio for permanent loading beyond $e/B = 1/6$.

5. For combined loading (permanent and variable), an argument can be made that the eccentricity ratio can be increased to $e/B = 1/3$ for which half of the foundation is under "tension" conditions. Some performance-based design codes (e.g., DIN 1054) allow that limit. As no clear data exists to support such an increase, it is recommended that until further research is carried out in the area, the eccentricity of the combined loading will be limited to $e/B \leq 1/4$, as allowed in the AASHTO standard specifications (4.4.8) or recommended in Section 8.4.3.1 of FHWA-NHI-06-089 *Soils and Foundation Manual.* (FHWA, 2006).

4.8 In-Depth Re-Examination of the Uncertainty in Bearing Capacity of Footings in/on Granular Soils Under Inclined-Centric Loading

### 4.8.1 Examination of the Bias for Controlling Parameters

In the case of footings under inclined-centric loadings, an additional factor involved is the load inclination to the verti-

cal, when compared to the case of footings under vertical-centric loadings. Figure 110 examines the variations in the bias versus the angle of load inclination (to the vertical), according to footing sizes. The scatter shows that there is no clear trend of the bias associated with either the load inclination angle or the footing size. All the larger footings ($B \geq 1.65$ ft) were tested under inclined loads with $\theta = 0°$ (inclination along the footing length, see Figure 17), while the smaller footings were subjected to inclined loads with $\theta = 90°$ (inclination along the footing width). Although it appears that the bias increases with an increase in the load inclination for $\theta = 0°$ while for $\theta = 90°$ the bias decreases with an increase in the inclination angle, it is difficult to isolate the effect of the footing size, except in the vicinity of load inclination of 10°. For the tests with inclination angles around 10° carried out on different footing sizes, it can be observed that the orientation switched between $\theta = 0°$ and 90° has no effect on the bias, which suggests that no correlation exists with the orientation of the load. This observation should be qualified, however, by the fact that the dataset for loading orientations between 0° and 90° is not sufficiently large to make a general statement. The resistance factors can thus be further examined in relation to the soil's friction angle.

The total number of data points available for inclined-centric loading is 39 (bias mean = 1.43 and COV = 0.295), while the soil friction angles ranged from 46 ($\pm0.5°$) to 38 ($\pm0.5°$). As a result, the identification of outliers based on the data subset for each ϕ_f ($\pm0.5°$) may not be practical because of the small data subsets. The standard normal quantiles of the data and those predicted by the developed normal and lognormal distributions are presented in Figure 111. A visual observation clearly shows that the data fits the normal distribution, while for the data to follow the lognormal distribution, some outliers in the lower tail region (especially
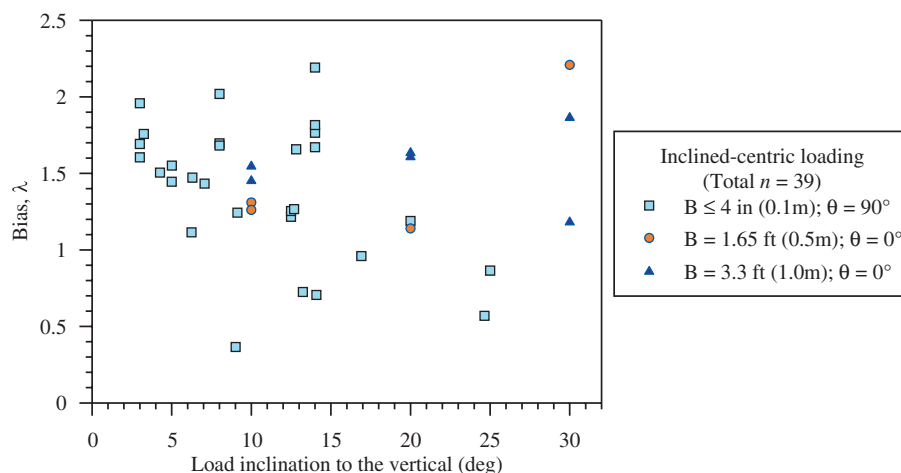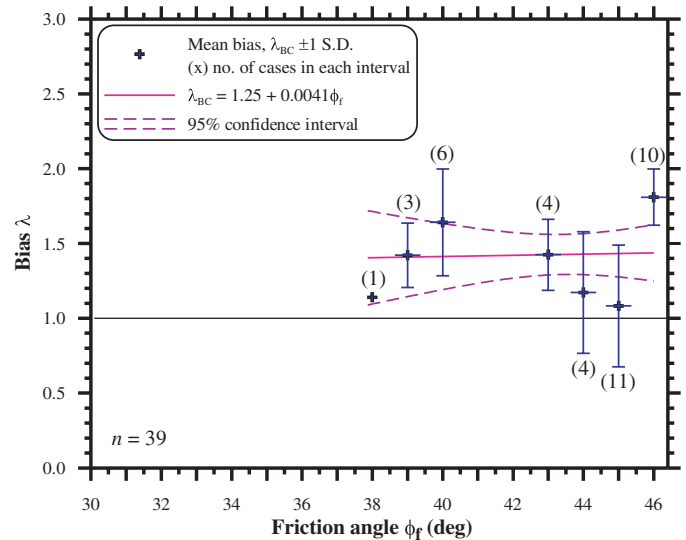

Figure 110. Bias versus load inclination for footings under inclined-centric loading.
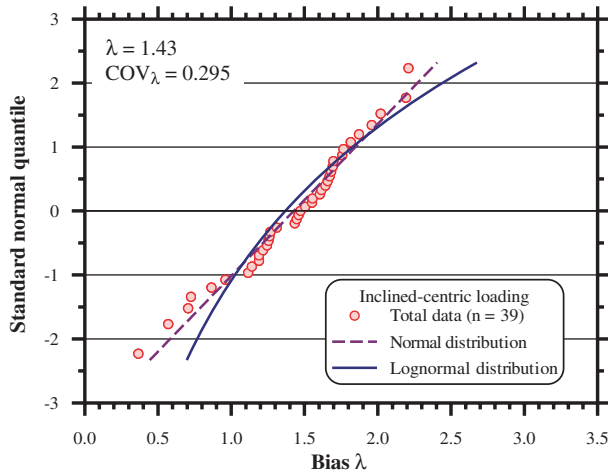
Figure 111. Standard normal quantile of bias data for all data for inclined-centric loading and predicted quantiles of theoretical distributions.

Figure 112. Variation of the bias in bearing resistance versus soil friction angle for cases under inclined-centric loadings.

with biases of less than 1.0) need to be removed. However, lognormal distribution has been assumed to be followed by the resistance bias without removing the outliers because the lower tail region (where the resistance bias is less than 1.0) is a critical region for determination of the resistance factors as it is associated with the area of concern in which the loading may exceed the resistance. It should be noted that in such a case, the use of a lognormal distribution would result in a more conservative resistance factor evaluation than otherwise. Other practices, such as "fitting" the distribution to the tail (ignoring the bulk of the data), should be discouraged and are not perceived as mathematically or otherwise justifiable.

Further examination of the variation of bias with the magnitude of the soil's friction angle is presented in Figure 112 for cases under inclined-centric loading (each error bar represents 1 standard deviation). The best fit line suggests that the

bias gradually increases with an increase in the soil friction angle. The resistance factor is calibrated using the mean obtained by the best fit line.

4.8.2 The Statistics of the Bias as a Function of the Soil's Internal Friction Angle and Resulting Resistance Factors

The statistics of the bearing resistance bias for the cases under inclined-centric loadings are presented in Table 62 for subsets of each $\phi_f(\pm 0.5°)$, while the best fit line obtained from the regression analysis of the biases available for $38° < \phi \le 46°$ in Figure 112, is provided by Equation 124.

$$\lambda = 1.25 + 0.0041\phi_f \qquad (124)$$

Table 62. Statistics of bearing resistance bias and the resistance factors corresponding to soil friction angles in controlled soil conditions for inclined-centric loading.

Friction angle ϕ_f (±0.5 deg)	n	Bias		Resistance factor ϕ ($\beta_T = 3$)	
		Mean λ	COV$_\lambda$	MCS	Preliminary
46	10	1.81	0.104	1.555	1.00
45	11	1.08	0.376	0.442	0.45
44	4	1.17	0.347	0.520	0.50
43	4	1.43	0.166	1.055	1.00
40	6	1.64	0.217	1.050	1.00
39	3	1.42	0.151	1.088	1.00
38	1	1.14	--	--	--
43 to 46	29	1.39	0.322	0.665	0.65
all angles	39	1.43	0.295	0.737	0.70

Table 63. Recommended resistance factors for inclined-centric loading cases.

Soil friction angle ϕ_f (deg)	Mean bias λ (from Eq. 5)	Resistance factor ϕ ($\beta_T = 3$)			
		Soil conditions			
		Natural		Controlled	
		($COV_\lambda = 0.40$)		($COV_\lambda = 0.35$)	
		MCS	Rec*	MCS	Rec
38	1.41	0.522	0.45	0.605	0.45
42	1.42	0.526	0.45	0.610	0.50
45	1.43	0.530	0.50	0.614	0.50
46	1.44	0.533	0.50	0.618	0.55

*Rec = recommended.

The COV of the bias (COV_λ) obtained for the data is used as a reference value; thus, a COV_λ of 0.35 is adopted for controlled soil conditions (even though a maximum COV_λ of 0.376 was obtained for $\phi_f = 45°$), and a COV_λ of 0.40 is adopted for natural soil conditions. Table 63 presents the resistance factors for inclined-centric loading cases for ϕ_f ranging from 38° to 46° using Equation 124 to obtain the bias for each soil friction angle and COV_λ values of 0.35 and 0.40, assumed based on the uncertainty evaluation.

The minimum bias for the highest resistance factor obtained using the equivalent factor of safety relationship in Equation 122 is 0.423 (0.60/1.4167). The minimum biases of the data are 0.37 and 0.57 (both with $\phi_f = 45 \pm 0.5°$), which means that the resistance factor needs to be reduced further. The required resistance factor for $\lambda = 0.37$ is approximately 0.52 ($= 0.37 \times 1.4167$), which can be taken as 0.50. Hence, the resistance factors for both controlled soil conditions and natural soil conditions are rounded off to a much lower number than resistance factors obtained from the MCS.

4.9 In-Depth Re-Examination of the Uncertainty in Bearing Capacity of Footings in/on Granular Soils Under Inclined-Eccentric Loading

4.9.1 Extent of Database

The number of reliable data points for the inclined-eccentric loading cases for which the positive and negative loading eccentricities could be clearly distinguished are 15 in total. Eight were tested under a positive loading eccentricity, and seven were tested under a negative loading eccentricity. The resistance factors obtained using the bias statistics for these cases have been used here for guidance only.

4.9.2 Inclined-Eccentric, Positive Loading Eccentricity Condition

Table 64 summarizes the bias statistics for the eight footing cases under inclined-eccentric, positive (or reversible) loading eccentricity. The resistance factor obtained based on the bias statistics was 0.65, but as could be observed in all other cases of loading, the recommended resistance factor may be taken as low as 0.50.

4.9.3 Inclined-Eccentric, Negative Loading Eccentricity Condition

Table 65 summarizes the bias statistics for the seven footing cases under inclined-eccentric, negative loading eccentricity. The preliminary resistance factor obtained based on the bias statistics was 1.00 for the available cases of soil friction angle, but

Table 64. Statistics of bearing resistance bias and the resistance factors corresponding to soil friction angles in controlled soil conditions for inclined-eccentric, positive (or reversible) loading eccentricity.

Friction angle ϕ_f (± 0.25 deg)	n	Bias		Resistance factor ϕ ($\beta_T = 3$)	
		Mean λ	COV_λ	MCS	Preliminary
45.0	5	2.52	0.505	0.687	0.65
44.5	3	1.55	0.158	1.158	1.00
all angles	8	2.16	0.506	0.587	0.55

Table 65. Statistics of bearing resistance bias and the resistance factors corresponding to soil friction angles in controlled soil conditions for inclined-eccentric, negative loading eccentricity.

Friction angle ϕ_f (± 0.25 deg)	n	Bias		Resistance factor ϕ ($\beta_T = 3$)	
		Mean λ	COV_λ	MCS	Preliminary
45.0	4	3.78	0.640	2.043	1.00
44.5	3	2.96	0.187	0.703	0.70
all angles	7	3.43	0.523	0.887	0.85

as could be observed in all other cases of loading, the recommended resistance factor may be conservatively reduced to 0.80.

4.10 Summary of Recommended Resistance Factors for Footings in/on Granular Soils

Tables 66 and 67 present the resistance factors recommended for use in the design of shallow foundations in/on granular soils (controlled soil conditions and natural soil conditions, respectively) with soil friction angles (ϕ_f) in the range of 30° to 45° and relative density (D_R) ≥ 35%. The resistance factors for controlled soil conditions are to be used when the foundations are placed in/on compacted engineering fills extending to a depth of no less than two (2.0) times the foundation width below the foundation base. The internal friction angle in such cases is to be determined by laboratory testing. Use of the resistance factors for natural soil conditions is recommended when the foundations are placed on/in the in situ soil, and the soil's internal friction angle is assumed to be evaluated from correlations with Standard Penetration Testing.

4.11 Goodman's (1989) Semi-Empirical Bearing Capacity Method for Footings in/on Rock

4.11.1 Identification of Outliers

The χ-squared GOF tests have been carried out on the datasets containing all the cases and subsets: (1) cases with measured friction angle, (2) cases with measured rock discontinuity spacing s′, and (3) cases with both friction angle and s′

Table 67. Recommended resistance factors for shallow foundations on natural deposited granular soil conditions.

| Soil friction angle ϕ_f | Loading conditions | | | |
| | Vertical-centric or -eccentric | Inclined-centric | Inclined-eccentric | |
			Positive	Negative
30°–34°	0.40	0.40	0.35	0.65
35°–36°	0.45			0.70
37°–39°	0.50		0.40	
40°–44°	0.55	0.45		0.75
≥ 45°	0.65	0.50	0.45	

Notes:
(1) ϕ_f determined from Standard Penetration Test results.
(2) Granular material is assumed to extend below the base of the footing at least two (2.0) times the width of the foundation.
(3) The resistance factors were evaluated for a target reliability (β_T) = 3.0.

measured. Figure 113 presents the standard normal quantile of the unfiltered bias data for all cases with the theoretical normal and lognormal distributions based on the calculated mean and standard deviation. The χ-squared values of the normal and lognormal distributions are found to be 121.28 and 18.79, respectively. The match observed in Figure 113 and the GOF test results indicate that the lognormal distribution is the matching underlying distribution for the data with an acceptance level of the GOF test at 1% (for which the acceptable highest χ-squared value is 21.67). These results also mean that no outliers need to be identified for the dataset of all cases.

Figures 114 and 115 present the standard normal quantiles of the unfiltered bias data for the cases with measured rock friction angle and measured rock discontinuity spacing, respectively, along with the relations predicted from the theoretical

Table 66. Recommended resistance factors for shallow foundations on granular soils placed under controlled conditions.

| Soil friction angle ϕ_f | Loading conditions | | | |
| | Vertical-centric or -eccentric | Inclined-centric | Inclined-eccentric | |
			Positive	Negative
30°–34°	0.50	0.40	0.40	0.70
35°–36°	0.60			
37°–39°	0.70	0.45	0.45	0.75
40°–44°	0.75	0.50	0.50	0.80
≥ 45°	0.80	0.55		

Notes:
(1) ϕ_f determined by laboratory testing.
(2) Compacted controlled fill or improved ground are assumed to extend below the base of the footing to a distance to at least two (2.0) times the width of the foundation (B). If the fill is less than 2B thick, but overlays a material equal or better in strength than the fill itself, then the recommendation stands. If not, then the strength of the weaker material within a distance of 2B below the footing prevails.
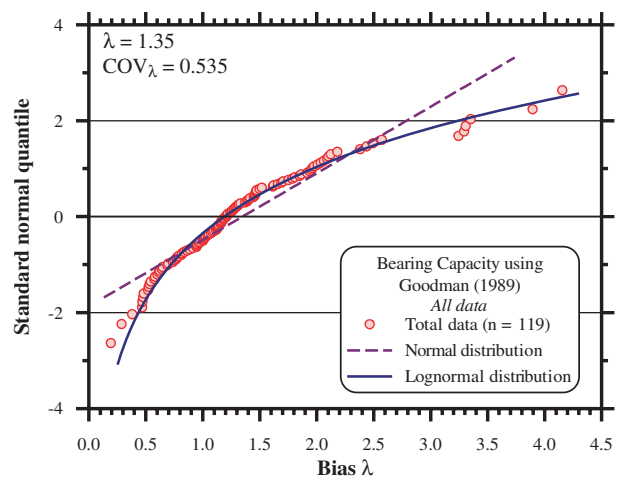(3) The resistance factors were evaluated for a target reliability (β_T) = 3.0.

Figure 113. Comparison of the unfiltered bias for bearing capacity calculated using the Goodman (1989) method for all data and the theoretical normal and lognormal distributions.
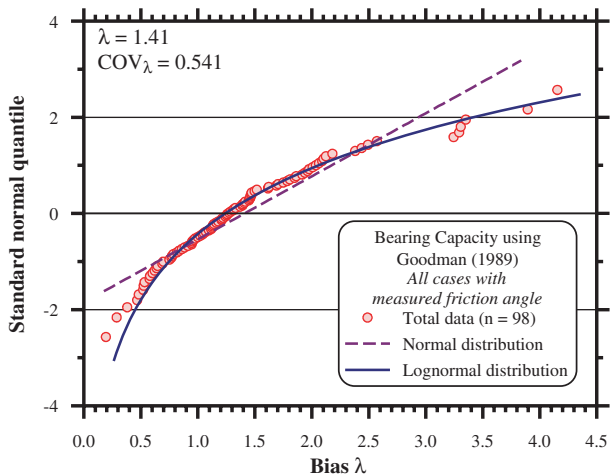
Figure 114. Comparison of the unfiltered bias for bearing capacity calculated using the Goodman (1989) method for all data on rocks with measured friction angles and the theoretical normal and lognormal distributions.
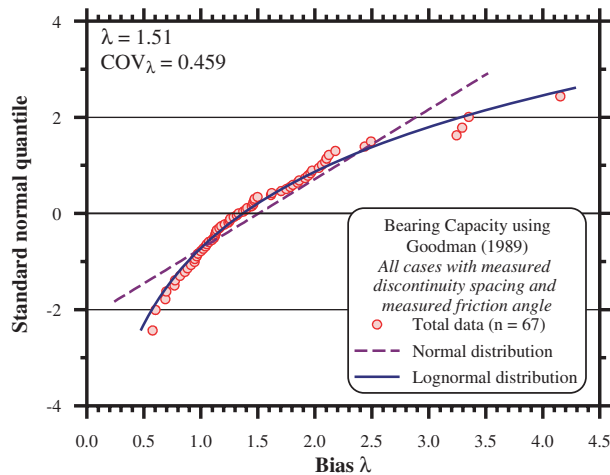
Figure 116. Comparison of the unfiltered bias for bearing capacity calculated using the Goodman (1989) method for all data on rocks with measured discontinuity spacing and friction angle and the theoretical normal and lognormal distributions.

normal and lognormal distributions. For the dataset of cases with measured friction angle presented in Figure 114, the χ-squared value for the normal distribution is found to be 64.35 while that for the lognormal distribution is 15.60, which is accepted with a significance level of 5%. For the dataset of cases with measured rock discontinuity spacing presented in Figure 115, the χ-squared value for the normal distribution is found to be 113.92 while that for the lognormal distribution is 11.99, which is also accepted with a significance level of 5%.

Figure 115. Comparison of the unfiltered bias for bearing capacity calculated using the Goodman (1989) method for all data on rocks with measured discontinuity spacing s' and the theoretical normal and lognormal distributions.
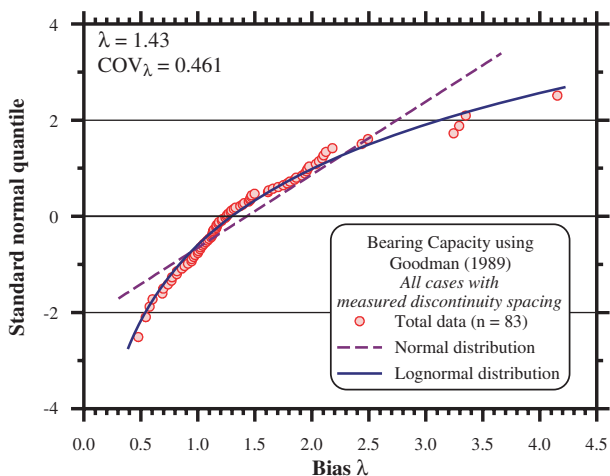
Figure 116 examines the standard normal quantile for the resistance bias dataset of cases with both friction angle and discontinuity spacing measured along with the predicted relations for the theoretical normal and lognormal distributions. The χ-squared value from the GOF tests obtained for the normal distribution is 66.27 while that for the lognormal distribution is 11.77.

Based on the data and analyses of Figures 113 to 116, it can be concluded that the bias associated with Goodman's (1989) analysis of shallow foundations on rock as an entire set and its subsets match the lognormal distribution, and no outliers exist for the examined datasets.

4.11.2 Calibration of Resistance Factors

Table 68 shows the resistance factors (ϕ) obtained from the MCS using one million samples for each dataset considered. As can be expected, the uncertainties in the estimated bearing resistance decrease with the increase in the available reliable information, thereby increasing the confidence of the estimated resistances, and thus resulting in higher resistance factors. When all data are used, without differentiating between data for which the rock properties information is available from the field and testing and data for which rock properties information is estimated by the outlined procedure, the recommended resistance factor is 0.30. The resistance factor can be increased to 0.45 when the relevant rock properties, i.e., rock friction angle and rock discontinuity spacing, are measured values.

Figures 113 and 114 indicate that the assumed lognormal distribution overpredicts the bias in the lower tail regions of the

Table 68. Calibrated resistance factors for different datasets of resistance bias obtained using Goodman's (1989) method.

Dataset	No. of cases	Bias		Resistance factor ϕ ($\beta_T = 3$)	
		Mean λ	COV$_\lambda$	MCS	Recommended
All data	119	1.35	0.535	0.336	0.30
Measured friction angle, ϕ_f	98	1.41	0.541	0.346	0.35
Measured spacing, s′	83	1.43	0.461	0.437	0.40
Measured friction angle, ϕ_f, and s′	67	1.51	0.459	0.464	0.45

data for all cases as well as for the cases with measured ϕ_f, respectively. The minimum bias observed for both of these datasets is 0.19, and the second lowest is 0.29 (for both, the rock discontinuity spacing s′ is based on AASHTO [2007]). A rough estimate of the equivalent factor of safety for a given calibrated resistance factor is given by Equation 122, while the equivalent minimum allowable bias for which the design will be safe for the given resistance factor is given by the reciprocal of the equivalent factor of safety (Equation 123). Thus, the minimum allowable biases for the recommended resistance factors are the following: (1) 0.21 for $\phi = 0.30$, (2) 0.25 for $\phi = 0.35$, (3) 0.28 for $\phi = 0.40$, and (4) 0.32 for $\phi = 0.45$, respectively. Except for the single case of the minimum bias of 0.19 (which can be taken as a marginal case), the results imply safe design when $\phi = 0.30$ is taken, i.e., all the data result in safe design on the application of the recommended resistance factors.

4.12 Carter and Kulhawy's (1988) Semi-Empirical Bearing Capacity Method for Footings in/on Rock

4.12.1 Identification of Outliers

The information and analyses presented in Section 3.8.2 suggest that the bearing resistance bias obtained using the Carter and Kulhawy (1988) method depends on the type of foundation, i.e., a rock socket drilled into rock or a shallow foundation in/on the rock. It is also observed that a systematic variation exists in the bearing resistance bias with the rock quality. When examining both factors, the data suggested (Section 3.8.2.2) that the bias variation attributed to the foundation type is actually controlled by the bias relation to the rock quality within the independent databases for each of the foundation types. As such, GOF tests have been carried out on the datasets categorized according to the rock RMR and the resistance factors developed for each of these subgroups.

Comparisons of the standard normal quantiles of the datasets for (1) the total cases in/on rocks, (2) the cases in/on rocks with RMR $\geq$ 85, and (3) the cases in/on rocks with 65 $\leq$ RMR < 85 are presented in Figures 117, 118 and 119, respectively. Except in the case of Figure 119, it can be observed that the lognormal distribution fits the data better than the normal distribution.

The χ-squared GOF tests have been carried out for all the data subsets, classified according to rock RMR values, to check the suitability of the assumption that the datasets can be modeled by lognormal distributions. The χ-squared values obtained for the normal distribution (N) and the lognormal distribution (LN), respectively are the following: (1) 481.64 for N and 16.22 for LN for the total cases for rocks ($n = 119$); (2) 15.87 for N and 15.61 for LN for RMR $\geq$ 85 ($n = 23$); (3) 18.97 for N and 31.82 for LN for 65 $\leq$ RMR < 85 ($n = 57$); (4) 11.58 for N and 9.12 for LN for 44 $\leq$ RMR < 65 ($n = 17$); and (5) 13.34 for N and 10.43 for LN for 3 $\leq$ RMR < 44 ($n = 22$). The χ-squared values at the 1% and 5% significance levels are 21.66 and 16.92, respectively; hence, the GOF tests show that a majority of the data subsets follow lognormal distributions and that no outliers need to be identified.

4.12.2 Calibration of Resistance Factors

Based on the datasets, for a majority of which the GOF tests show that lognormal distributions can be assumed to model the bias distribution, the resistance factors have been calibrated using MCS using one million samples. These factors are presented in Table 69. If no RMR information is available, the rec-
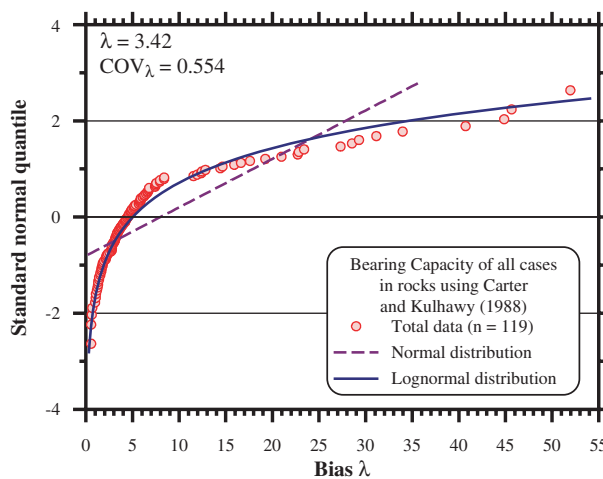
Figure 117. Comparison of the unfiltered bias for bearing capacity calculated using the Carter and Kulhawy (1988) method for total cases in/on rocks in the database and the theoretical normal and lognormal distributions.
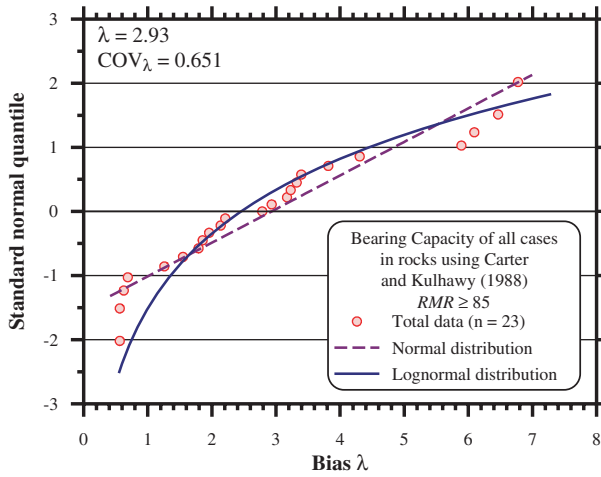
Figure 118. Comparison of the unfiltered bias for bearing capacity calculated using the Carter and Kulhawy (1988) method for all cases in rocks with RMR ≥ 85 and the theoretical normal and lognormal distributions.
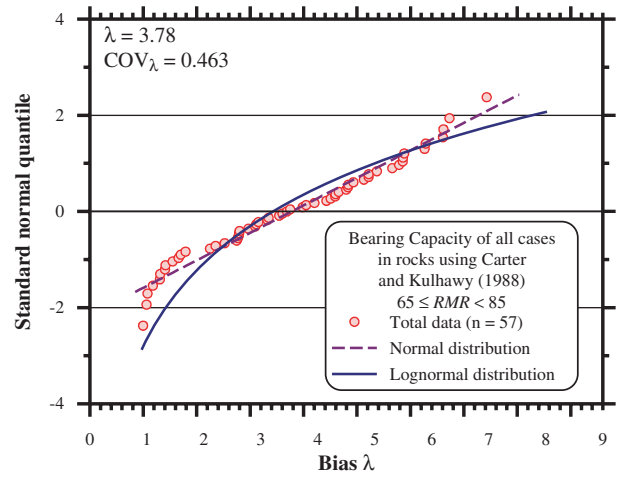
Figure 119. Comparison of the unfiltered bias for bearing capacity calculated using the Carter and Kulhawy (1988) method for all cases in rocks with 65 ≤ RMR < 85 and the theoretical normal and lognormal distributions.

ommended ϕ is 0.35. When the rock has RMR ≥ 85 the recommended ϕ is 0.50. For rocks with RMR lower than 85, $\phi = 1.00$.

4.13 Summary of Recommended Resistance Factors for Shallow Foundations in/on Rock

Table 70 summarizes (based on the information presented in Tables 68 and 69) the recommended resistance factors to be used in evaluation of the bearing capacity of shallow foundations on rock. The resistance factors for both examined methods are presented along with the efficiency factors providing a measure for the relative efficiency of the methods.

Goodman's (1989) method performed exceptionally well consistently, regardless of rock quality. Improvement in the method's performance with an increase in knowledge translates into an increase in the resistance factor and the associated method efficiency.

The performance of the Carter and Kulhawy (1988) method has a "built-in" safety that increases as the rock quality decreases. As such, the method's bias changes with the rock

quality (expressed via RMR), and a calibration was required following the rock quality designation. The relatively higher resistance factors are a byproduct of the large bias of the method and, hence, do not represent efficient design as expressed by the low efficiency factor of the method's application compared to Goodman's (1989) method.

4.14 Sliding Friction Resistance

4.14.1 Parametric Study Evaluating the Resistance Factor as a Function of the Ratio of Dead to Live Load

The probabilistic characteristics of the parameter contributing directly to the sliding friction resistance, the friction coefficient ratio (f_c), have been presented in Section 3.9 and summarized in Table 48. The uncertainties in the friction coefficient ratio (f_c) follow one-to-one transformation to the sliding resistance, i.e., the mean of sliding resistance = vertical load × (mean of $f_c \times \tan \phi_f$) and the standard deviation (s.d.) of sliding resistance = vertical load × (s.d. of $f_c \times \tan \phi_f$). Hence,

Table 69. Calibrated resistance factors for different datasets of resistance bias obtained using Carter and Kulhawy's (1988) method.

Dataset	No. of cases	Bias		Resistance factor ϕ ($\beta_T = 3$)	
		Mean λ	COV$_\lambda$	MCS	Recommended
All cases	119	8.00	1.240	0.372	0.35
RMR ≥ 85	23	2.93	0.651	0.535	0.50
65 ≤ RMR < 85	57	3.78	0.463	1.149	1.00
44 ≤ RMR < 65	17	8.83	0.651	1.612	1.00
3 ≤ RMR < 44	22	23.62	0.574	5.295	1.00

Table 70. Recommended resistance factors for foundations in/on rock based on $\beta_T = 3.0$ ($p_f = 0.135\%$).

Method of analysis	Equation	Application	ϕ	Efficiency factor ϕ/λ (%)
Carter and Kulhawy (1988)	$q_{ult} = q_u\left(m + \sqrt{s}\right)$	All	0.35	4.4
		RMR ≥ 85	0.50	17.1
		$65 \leq RMR < 85$		26.5
		$44 \leq RMR < 65$	1.00	11.3
		$3 \leq RMR < 44$		4.2
Goodman (1989)	For fractured rocks: $q_{ult} = q_u\left(N_\phi + 1\right)$ For non-fractured rocks: $q_{ult} = q_u\left(\dfrac{1}{N_\phi - 1}\left\{N_\phi\left(\dfrac{s'}{B}\right)^{(N_\phi-1)/N_\phi} - 1\right\}\right)$	All	0.30	22.2
		Measured ϕ_f	0.35	24.8
		Measured s'	0.40	28.0
		Measured s' and ϕ_f	0.45	29.8

Table 71. Resistance factors obtained from MCS simulations for footings, either cast in place or prefabricated, in soils with various friction angles, along with the effect of ratios of lateral dead load to lateral live load.

(a) Cast-in-place footings

ϕ_f obtained from	Resistance factor from MCS ($\phi_{\tau MCS}$)							
	At-rest earth pressure				Active earth pressure			
	LFD/LFL = 2	LFD/LFL = 4	LFD/LFL = 5	LFD/LFL = 7	LFD/LFL = 2	LFD/LFL = 4	LFD/LFL = 5	LFD/LFL = 7
SPT	0.469	0.455	0.452	0.447	0.507	0.498	0.496	0.492
CPT	0.516	0.499	0.494	0.488	0.558	0.545	0.542	0.537
Lab test	0.558	0.535	0.530	0.523	0.603	0.585	0.581	0.576

(b) Prefabricated footings

ϕ_f obtained from	Resistance factor from MCS ($\phi_{\tau MCS}$)							
	At-rest earth pressure				Active earth pressure			
	LFD/LFL = 2	LFD/LFL = 4	LFD/LFL = 5	LFD/LFL = 7	LFD/LFL = 2	LFD/LFL = 4	LFD/LFL = 5	LFD/LFL = 7
SPT	0.195	0.193	0.193	0.191	0.211	0.212	0.211	0.211
CPT	0.217	0.213	0.212	0.210	0.234	0.233	0.232	0.232
Lab test	0.239	0.234	0.232	0.230	0.258	0.256	0.255	0.253

Table 72. Recommended resistance factors for sliding resistance (ϕ_τ) for soil friction angles based on different tests and lateral pressure due to at-rest or active earth pressure for cast-in-place and prefabricated footings.

ϕ_f obtained from	Resistance factor for sliding friction (ϕ_τ) ($\beta_T = 3$)			
	At-rest earth pressure		Active earth pressure	
	Cast in-place [1]	Prefabricated [2]	Cast in-place [1]	Prefabricated [2]
SPT	0.40		0.45	
CPT	0.45	0.20	0.50	0.20
Lab test [3]	0.50		0.55	

[1] $\tan\delta_s = 0.91 \tan\phi_f$;   [2] $\tan\delta_s = 0.53 \tan\phi_f$,   [3] Any laboratory shear strength measurement of ϕ_f

the form of the limit state function for sliding resistance is essentially the same as that for the bearing resistance (see Equation 118), which can be expressed as

$$Z_\tau = R_\tau - \text{LFD} - \text{LFL} \tag{125}$$

where Z_τ is the load combination for sliding, R_τ is sliding resistance of a footing, LFD is lateral load due to dead load, and LFL is lateral load due to live load. A summary of the uncertainties in the lateral loads and the load factors as recommended in AASHTO (2007) are presented in Section 4.2.3.3.

Analogous to the calibration of resistance factors for the bearing resistance, the influence of the ratio of lateral dead load to the lateral live load has been studied and presented here.

Based on the loadings for the design example bridges considered in the current research study, it is found that the ratios of LFD to LFL range from 4 to 7. As a result, the resistance factors for sliding resistance have been calibrated for LFD to LFL ratios varying from 2 to 7 and the corresponding results are presented in Table 71 for cast-in-place and prefabricated footings.

4.14.2 Resistance Factors

The calculated resistance factors presented in Table 71 suggest that the ratio of LFD to LFL does not have a pronounced effect on the magnitude of the resistance factors. As a result, selected resistance factors are recommended for use for sliding resistance of footings on granular materials as presented in Table 72.

CHAPTER 5

Design Examples

5.1 Introduction

Seven detailed design examples are presented in Appendix H. The presented examples include (1) Examples 1 through 4 of FHWA's *Geotechnical Engineering Circular No. 6* (GEC6), Appendix C (Kimmerling, 2002); (b) the foundations of the central pier and the east abutment of the Billerica, Massachusetts, B-12-025 Bridge; and (c) the foundation of the south abutment of the Marlborough, Massachusetts, N-08-013 Bridge.

The ULS of bridge foundations (bearing capacity) is analyzed in the following examples according to the presented methodology and the AASHTO design specifications with LRFD resistance factors, as given in the current AASHTO (2007) specifications, as well as with the new resistance factors for bearing resistance developed in this research project. The analysis is based on the conditions that are given in the examples' references, i.e., footing geometry as designed, soil conditions, and loading. For design completion, the SLS is analyzed as well, using several settlement analysis methods and a range of factors. Summary graphs and tables are provided for the calculations in all examples, and detailed calculations are shown for two design examples: (1) Example 1 from FHWA, in which the footing rests on natural soil and the applicable resistance factor depends on the way the soil parameters are derived and (2) the Central Pier of the B-12-025 Billerica Bridge, in which the footing rests on controlled soil.

5.2 Loading Conventions and Notations

The loading conventions and the corresponding notation used in this report are as presented in Figure 120, unless otherwise stated in the design examples. The vertical-centric loading is F_1; F_2 and F_3 are horizontal loadings along the transverse (x_2-direction or z-direction) and longitudinal (x_3-direction or y-direction) directions of the bridge, respectively. M_3 is the moment about the longitudinal direction (x_3- or y-axis) due to transverse loading and M_2 is the moment about the z-axis (transverse direction) due to longitudinal loading. The load eccentricity across the footing width is $e_B = M_2/F_1$ and across the footing length is $e_L = M_3/F_1$. The resultant load inclination is given by $\sqrt{F_2^2 + F_3^2}/F_1$.

5.3 Examples Summary

In Appendix H, the figures present for the different examples the performance versus footing size, referring to the effective footing size. The discussion in Appendix H of the example refers to geometrical size, which includes, for example, eccentricity. The limiting eccentricity in all examples was assumed to be $e = B/6$. Table 73 provides a summary of major findings from the design examples referring to the full geometrical width. Overall, the use of the new, recommended resistance factors for the strength limit states resulted in foundations with varied relations to the actual design, i.e., in five cases the designed foundations under the new factors are smaller, and in two cases the foundations are larger. In most cases, the foundations are controlled by limiting eccentricity, especially if the contribution of negative eccentricity is not adopted.

As in other instances in which designs are compared to each other, the introduction of calibrated factors in RBD methodology provides mixed results in terms of economics. Overall, no significant change in economics can be pointed out; the design improvement and the systematic approach are, however, a major improvement to the existing guidelines.
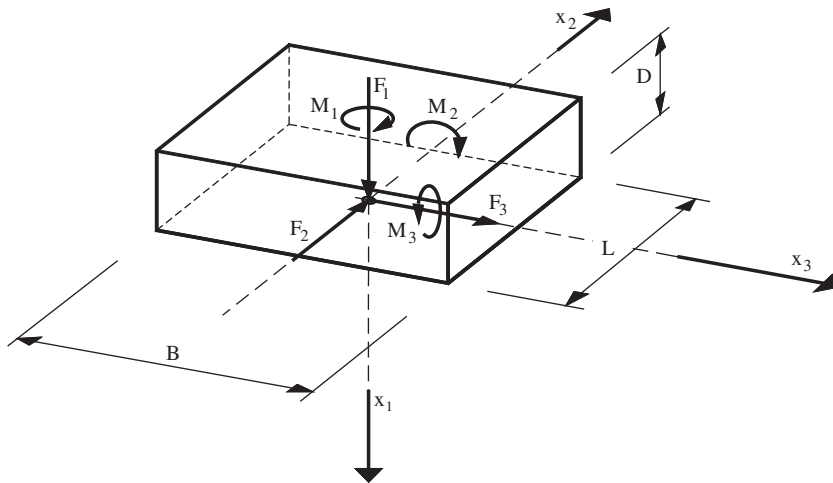
Figure 120. Loading conventions and notation used.

Table 73. Design example details summary.

Example	Reference	Foundation and soil condition	Dominant limit state	Maximum load eccentricity (ft)	Eccentricity to footing side ratio	Design foundation size, B × L (ft × ft)			Design in reference	Settlement method used in reference
						Strength LS		Service LS		
						Recommended ϕ	$\phi = 0.45$	$\phi = 1.0$		
1	GEC6 - Example 1	Bridge pier on natural soil deposits	Service	0.36	$e_2/B = 0.23/B$ $e_3/L = 0.36/L$	9.75×9.75 (ϕ = 0.35 to 0.40)	9.5×9.5	50.0×50.0 (Schm78: 19.5×19.5) (Hough: 16.25×16.25)	16.0×16.0	Hough (1959)
2	Billerica Bridge Central Pier	Pier footing on gravel fill	Strength	0.50	$e_2/B = 0.50/B$ $e_3/L = 0.095/52.4 = 0.0018$	6.0×52.4 (C2 load, ϕ = 0.70) 8.9×52.4 (C7 load, ϕ = 0.45)	8.9×52.4	4.5×52.4 (Schm78: 4.3×52.4) (Hough: 2.0×52.4)	13.1×52.4	Peck et al. (1974)
3	Billerica Bridge East Abutment	Abutment footing on gravel fill	Strength	2.31	$e_2/B = 2.31/B$ $e_3/L = $ n.a.	15.5×61.65 (ϕ = 0.45)	15.5×61.65	13.9×61.65 (including Schm78 and Hough)	12.5×61.7	Peck et al. (1974)
4	GEC6 - Example 2	Integral bridge abutment on structural fill	Limiting eccentricity	1.00	$e_2/B = 1.00/B$ $e_3/L = $ n.a.	6.0×82.0 (ϕ = 0.45)	6.0×82.0	6.0×82.0 (Schm78 and Hough: 6.0×82.0*)	9.8×82.0	Hough (1959)
5	GEC6 - Example 3	Stub seat-type bridge abutment on structural fill	Limiting eccentricity	1.39	$e_2/B = 1.39/B$ $e_3/L = $ n.a.	8.35×82.0 (ϕ = 0.45)	8.35×82.0	(8.35<B<14.75)×82.0 (Schm78 and Hough: 8.35×82.0)	10.5×82.0	Hough (1959)
6	GEC6 - Example 4	Full height bridge abutment on natural soil	Limiting eccentricity	3.15	$e_2/B = 3.15/B$ $e_3/L = $ n.a.	18.9×82.0 (ϕ = 0.40)	18.9×82.0	18.9×82.0 (Schm78 and Hough: 18.9×82.0*)	17.1×82.0	Hough (1959)
7	Marlborough Bridge South Abutment	Single span abutment footing on rock	Limiting eccentricity if not considered pos/neg contribution	7.38	$e_2/B = 7.38/B$ $e_3/L = 0$	4.0×38.4	4.0×38.4	4.0×38.4 AASHTO (2008)	10.5×38.4	AASHTO (2008) Eq. 10.6.2.4.4-3

References

AASHTO (1994). *AASHTO LRFD Bridge Design Specifications,* SI units, 1st ed., AASHTO, Washington, DC.

AASHTO (1997). 1997 Interim Revisions to the *Standard Specifications for Highway Bridges,* 16th ed., 1996. AASHTO, DC.

AASHTO (2001). 2001 Interim *AASHTO LRFD Bridge Design Specifications,* 2nd ed., 1998. AASHTO, Washington, DC.

AASHTO (2006). Interim Revisions to *AASHTO LRFD Bridge Design Specifications,* 3rd ed., 2004. AASHTO, Washington, DC.

AASHTO (2007). *AASHTO LRFD Bridge Design Specifications,* 4th ed., AASHTO, Washington, DC.

AASHTO (2008). Interim Revisions to *AASHTO LRFD Bridge Design Specifications,* 4th ed., 2007. AASHTO, Washington, DC.

AIJ (2002). *Recommendations for Limit State Design of Buildings.* Architectural Institute of Japan (in Japanese).

Allen, T. M. (2005). *Development of Geotechnical Resistance Factors and Downdrag Load Factors for LRFD Foundation Strength Limit State Design,* Publication No. FHWA-NHI-05-052, Federal Highway Administration, Washington, DC, 41 pp.

Amatya, S., Paikowsky, S. G., Lesny, K., and Kisse, A. (2009). "Uncertainties in the Bearing Capacity of Shallow Foundations and the Factor N_γ Using an Extensive Database." *Proc. GI Conference International Foundation Congress & Equipment Expo 2009 (IFCEE),* ASCE GSP No. 186, Orlando, FL, March 15–19, 2009, 403–410.

ARMY EM 1110-1-2908 (1994). *Engineering and Design—Rock Foundations,* Dept. of the Army, U.S. Army Corps of Engineers, Washington, DC.

Ayyub, B., and Assakkaf, I. (1999). *LRFD Rules for Naval Surface Ship Structures: Reliability-Based Load and Resistance Factor Design Rules.* Naval Surface Warfare Center, Carderock Division, U.S. Navy, West Bethesda, MD.

Ayyub, B., Assakkaf, I., and Atua, K. (2000). "Reliability-Based Load and Resistance Factor Design (LRFD) of Hull Girders for Surface Ships." *Naval Engineers Journal,* Vol. 112, No. 4, July, 279–296.

Barker, R. M., Duncan, J. M., Rojiani, K. B., Ooi, P. S. K., Tan, C. K., and Kim, S. G. (1991). *NCHRP Report 343: Manuals for the Design of Bridge Foundations.* Transportation Research Board, National Research Council, Washington, DC.

Barton, N. R., Lien, R., and Lunde, J. (1974). "Engineering Classification of Rockmasses for the Design of Tunnel Support." *Rock Mechanics,* May, 189–236.

Becker, D. E. (1996). "Eighteenth Canadian Geotechnical Colloquium: Limit State Design for Foundations. Part II. Development for the National Building Code of Canada." *Canadian Geotechnical Journal,* Vol. 33, No. 6, 984–1007.

Becker, D. E. (2003). "Limit States Foundation Design Code Development in Canada." *Proc. International Workshop on Limit State Design in Geotechnical Engineering Practice (LSD2003),* 37–38. (Full paper on CD-ROM, World Scientific.)

Bell, A. L. (1915). "Lateral Pressure and Resistance of Clay, and the Supporting Power of Clay Foundations." *Minutes of Proc. of the Institution of Civil Engineers,* 199, January 12, 233–336.

Bienen, B., Byrne, B. W., Houlsby, G. T., and Cassidy, M. J. (2006). "Investigating Six-Degree-of-Freedom Loading of Shallow Foundations on Sand." *Géotechnique,* Vol. 56, No. 6, 367–379.

Bieniawski, Z. T. (1973). "Engineering Classification of Jointed Rock Masses." *Transactions of the South African Institute of Civil Engineers,* Vol. 15, No. 12, 335–344.

Bieniawski, Z. T. (1974). "Geomechanics Classification of Rock Masses and Its Application in Tunnelling." *Proc. 3rd International Congress of the International Society for Rock Mechanics,* Vol. 2, Part A, Denver, CO, 27–32.

Bieniawski, Z. T. (1976). "Rock Mass Classifications in Rock Engineering." *Proc. Symposium on Exploration for Rock Engineering,* Balkema, Cape Town, 76–106.

Bieniawski, Z. T. (1978). "Determining Rock Mass Deformability: Experience from Case Histories." *Int. Journal Rock Mechanics Min. Sci. and Geomech.,* Abstract, Vol. 15, No. 5, 237–248.

Bieniawski, Z. T. (1979). "The Geomechanics Classification in Rock Engineering Classifications." *Proc. 4th Int. Congr. On Rock Mech.,* Vol. 2, International Society for Rock Mechanics (ISRM), Montreux, September 2–8, 1979, 41–48.

Bieniawski, Z. T. (1974). "Geomechanics Classification of Rock Masses and its Application in Tunnelling." *Proc. 3rd International Congress of the International Society for Rock Mechanics,* Vol. 2, part A, Denver, CO, pp. 27–32.

Bieniawski, Z. T. (1989). *Engineering Rock Mass Classification.* Wiley, New York.

Bishoni, B. L. (1968). "Bearing Capacity of a Closely Jointed Rock." Ph.D. Dissertation, Georgia Institute of Technology, 120 p.

Bolton, M. D., and Lau, C. K. (1993). "Vertical Bearing Capacity for Circular and Strip Footings on Mohr-Coloumb Soil." *Canadian Geotechnical Journal,* Vol. 30, No. 6, 1024–1033.

Bowles, J. E. (1996). *Foundation Analysis and Design,* 5th ed, McGraw-Hill Inc., New York.

Brady, B. H. G., and Brown, E. T. (1985). *Rock Mechanics for Underground Mining.* Chapman & Hall, London.

Briaud, J. L., and Gibbens, R. (1997). *Large-Scale Load Tests and Database of Spread Footings on Sand,* FHWA-RD-97-068. FHWA, U.S. DOT, Washington, DC, 228 pp.

Brinch Hansen, J. (1961). "A General Formula for Bearing Capacity." *Akademiet for de Tekniske Videnskaber,* Geoteknisk Institut, Bullentin No. 11, Copenhagen, 38–46.

Brinch Hansen, J. (1970). "A Revised and Extended Formula for Bearing Capacity." *Akademiet for de Tekniske Videnskaber,* Geoteknisk Institut, Bullentin No. 28, Copenhagen, 5–11.

Brook, N., and Dharmaratne, P. G. R. (1985). "Simplified Rock Mass Rating System for Mine Tunnel Support." *T. I. Min. Metall. A* 94, 148–154.

Buisman, A. S. K. (1940). "Grondmechanica." In *Toegepaste Mechanica, Deel IV* (ed. Klopper, J.), Delft, The Netherlands (in Dutch).

Butterfield, R. (1993). "A New Approach to Safety Factors for Shallow Foundations: Load Combination Factors as a Basis for Risk Assessment." In B. O. Skipp, ed., *Risk and Reliability in Ground Engineering,* Thomas Telford, London, 112–125.

Butterfield, R., Houlsby, G. T., and Gottardi, G. (1996). "Standardized Sign Conventions and Notation for Generally Loaded Foundations." *Géotechnique,* Vol. 47, No. 5, 1051–1054.

Butterfield, R., and Ticof, J. (1979). "Discussion: Design Parameters for Granular Soils." *Proc., 7th European Conference on Soil Mechanics and Foundation Engineering,* Vol. 4, Brighton, UK, 259–262.

Byrne, B. W., and Houlsby, G. T. (2005). "Investigating 6 Degree-of-Freedom Loading on Shallow Foundations." In S. Gouvernc and M. Cassidy, eds., *Proceedings of the First International Symposium on Frontiers in Offshore Geotechnics,* Taylor & Francis Group, London, 477–482.

Canadian Geotechnical Society (2006). *Canadian Foundation Engineering Manual,* 4th ed., 488 pp.

Caquot, A., and Kérisel, J. (1953). "Sur le Terme de Surface dans le Calcul des Foundations en Milieu Pulvérulent." *Proc., 3rd Int. Conf. on Soil Mechanics and Foundation Engineering,* Vol. I, Zürich, 336–337.

Carder, D. R., Pocock, R. G. and Murray, R. T. (1977). "Experimental Retaining Wall Facility—Lateral Stress Measurements with Sand Backfill." *Transport and Road Research Laboratory Report No. LR 766,* Crowthorne, Berkshire, UK.

Carter, J. P., and F. H. Kulhawy (1988). *Analysis and Design of Foundations Socketed into Rock.* Report No. EL-5918. Empire State Electric Engineering Research Corporation and Electric Power Research Institute, New York, 158.

Casagrande, A. (1948). "Classification and Identification of Soils." *Transactions of the American Society of Civil Engineers,* Vol. 113, 901–930.

CEN (2004). *prEN 1997-1 Geotechnical Design—General Rules.* European Committee for Standardization.

Chen, W. F. (1975). "Limit Analysis and Soil Plasticity." *Developments in Geotechnical Engineering* 7, Elsevier, Amsterdam.

Cheney, R. S., and Chassie, R. G. (1982). *Soils and Foundations Workshop Manual,* FHWA-NHI-88-009. FHWA, U.S. DOT, Washington, DC, 338 pp.

Clough, G. W., and Duncan, J. M. (1991). "Earth Pressures." In *Foundation Engineering Handbook,* 2nd ed., H-Y Fang, ed., Van Nostrand Reinhold, New York.

Coates, D. F., and Patching, T. H. (1968) "A Recommended Rock Classification for Rock Mechanics Purposes." *CIM Bull.* (October), 1195–1197.

Cornell, C. (1969). "A Probability-Based Structural Code." *Journal of American Conc. Institute,* Vol. 66, No. 12, 974–985.

Cummings, R. A., Kendorski, F. S., and Bieniawski, Z. T. (1982). *Caving Rock Mass Classification and Support Estimation.* U.S. Bureau of Mines Contract Report #J0100103. Engineers International Inc., Chicago.

D'Appolonia and the University of Michigan (2004). Final Report for NCHRP Project 12-55, Load and Resistance Factors for Earth Pressures on Bridge Substructures and Retaining Walls. (Unpublished document.)

Das, B. M. (1981). "Bearing Capacity of Eccentrically Loaded Surface Footings on Sand." *Soils and Foundations,* Vol. 21, No. 1, 115–119.

De Beer, E. E. (1967). "Proefondervindelijke bijdrage tot de studie van het gransdragvermogen van zand onder funderingen op staal; Bepaling von der vormfactor sb." *Annales des Travaux Publics de Belgique,* 68, No. 6, 481–506; 69, No. 1, 41–88; No. 4, 321–360; No. 5, 395–442; No. 6, pp. 495–522.

De Beer, E. E. (1970). "Experimental Determination of the Shape Factors and the Bearing Capacity Factors of Sand." *Géotechnique,* 20, No. 4, 387–411.

De Beer, E. E., and Ladanyi, B. (1961). "Etude Expérimentale de la Capacité Protante du Sable sous des Fondations Circulaires Établies en Surface." *Proc., 5th Int. Conf. on Soil Mechanics and Foundation Engineering,* Paris, Vol. 1, 577–581.

Deere, D. U. (1968). "Geological Considerations." In *Rock Mechanics in Engineering Practice,* R. G. Stagg and D. C. Zienkiewicz, eds., Wiley, New York, 1–20.

Deere, D. U., and Miller, R. P. (1966). *Engineering Classification and Index Properties for Intact Rock,* Technical Report No. AFWL-TR-65-116. Air Force Weapons Lab, Kirtland Air Force Base, New Mexico.

Deere, D. U., and Deere, D. W. (1988). *The Rock Quality Designation (RQD) Index in Practice, Rock Classification Systems for Engineering Purposes, ASTM STP* 984, American Society for Testing and Materials, Philadelphia, 91–101.

DEGEBO Deutsche Forschungsgesellschaft für Boden-mechanik

DIN EN 1997-1 (2008). *Geotechnical Design, Part I: General Rules.* Beuta-Verlag, Berlin.

DIN 4017 (2006). *Berechnung des Grundbruchwiderstands von Flachgründungen.* Normenausschuss Bauwesen (NABau), Deutsches Institut für Normung e. V., Berlin.

Döerken, W. (1969). Der Einfluss der Aussermittigkeit auf die Grundbruchlast lotrecht beanspruchter Oberflaechengruendungen auf nichtbindigen Boeden, Mitteilungen aus dem Institut fuer Verkehrswasserbau, Grundbau und Bodenmechanik der Technischen Hochschule Aachen, Heft 44.

Douglas, K. J. and Mostyn, G. (1999). "Strength of Large Rock Masses—Field Verification." In *Proc. 37th U.S. Rock Mechanics Symposium,* Vail, CO, June 6–9, 1, 271–276.

Duncan, J. M. and Seed, R. B. (1986). "Compaction-Induced Earth Pressures under K_0–Conditions." *Journal of Geotechnical Engineering,* Vol. 112, No. 1, 1–22.

Eastwood, W. (1955). "The Bearing Capacity of Eccentrically Loaded Foundations on Sandy Soils." *The Structural Engineer,* Vol. 33, No. 1, 181–187.

Edelbro, C. (2004). "Evaluation of Rock Mass Strength Criteria." Licentiate thesis, Lulea University of Technology, Department of Civil and Mining Engineering, Division of Rock Mechanics, Sweden.

Ellingwood, B., Galambos, T., MacGregor, J., and Cornell C. (1980). *Development of a Probability-Based Load Criterion for American National A58.* National Bureau of Standards Publication 577, Washington, DC.

Ellingwood, B., MacGregor, J. G., Galanbos, T. V., and Cornell, C. A. (1982). "Probability Based Load Criteria: Load Factors and Load Combinations." *Journal of the Structural Division,* Vol. 108, No. 5, 978–997.

Eurocode 7 (EC7) (2005) (DIN EN 1997-1). *Geotechnical Design, Part I: General Rules.* Deutsches Institut für Normung e.V., Berlin.

FHWA (2006). Soils *and Foundations Workshop—Reference Manual Volume 2,* FHWA-NHI-06-089. Washington, DC.

Foik, G. (1984). Die Tragfähigkeit überwiegend horizontal beanspruchter Fundamente auf dicht gelagertem Sand. Mitteilungen aus dem Fachgebiet Grundbau und Bodenmechanik, Universität—Gesamthochschule—Essen, Heft 8.

Franklin J. A. and Dusseault, M. (1989). *Rock Engineering.* McGraw Hill, Inc., New York.

Franklin, J. A. and Gruspier, J. E. (1983). *Evaluation of Shales for Construction Projects,* Ministry of Transportation and Communications, Ontario, Research and Development Branch, 98 pp.

Galambos, T., and Ravindra, M. (1978). "Properties of Steel for Use in LRFD." *Journal of Structural Engineering,* Vol. 104, No. 9, 1459–1468.

Gifford, D., Kraemer, S., Wheeler, J., and McKown, A. (1987). *Spread Footings for Highway Bridges,* FHWA/RD-86/185. FHWA, U.S. DOT, McLean, VA, October, 229 pp.

Giraudet, P. (1965). "Recherches Experimentales sur les Fondations Soumises a des Efforts Inclines ou Excentres." *Annales des Ponts et Chaussees,* Vol. 3, 168–193.

Goel, R. K., Jethwa, J. L. and Paithankar, A. G. (1995). "Correlation Between Barton's Q and Bieniawski's RMR—A New Approach." Technical Note, *Int. j. Rock Mech. Min.,* Vol. 33, No. 2, 179–181.

Goodman, R. E. (1980). *Introduction to Rock Mechanics.* Wiley, New York, 478 pp.

Goodman, R. E. (1989). *Introduction to Rock Mechanics,* 2nd ed. Wiley, New York.

Gottardi, G. (1992). *Modellazione del Comportamento di Fondazoni Superficiali su Sabbia Soggette a Diverse Condizioni di Carico,* Dottorato di ricerca in ingegneria geotecnica, Instituto di Costruzioni Marittime e di Geotecnica, Universita di Padova.

Gottardi, G., and Butterfield, R. (1993). "On the Bearing Capacity of Surface Footings on Sand under General Planar Loads." *Soils and Foundations,* Vol. 33, No. 3, 68–79.

Gottardi, G., and Butterfield, R. (1995). "The Displacement of a Model Rigid Surface Footing on Dense Sand under General Planar Loading." *Soils and Foundations,* Vol. 35, No. 3, 71–82.

Gudehus, G. (1981). *Bodenmechanik.* Ferdinand Enke Verlag, Stuttgart

Hasofer, A., and Lind, N. (1974). "Exact and Invariant Second-Moment Code Format." *Journal of the Engineering Mechanics Division,* Vol. 100, No. 1, 111–121.

Hatanaka, M., and Uchida, A. (1996). "Empirical Correlation between Penetration Resistance and Internal Friction Angle of Sandy Soil." *Soils and Foundations,* Vol. 36, No. 4, 1–10.

Haubrichs, K. (1993). Widerstand eines dicht gelagerten Sandes gegen Beanspruchungen infolge ausmittig-schraeg oder exzentrisch belasteter starrer Einzelfundamente. Mitteilungen aus dem Fachgebiet Grundbau und Bodenmechanik der Universitaet Essen, Heft 18, Ed. Prof. Dr.-Ing. H. Nendza, Verlag Glueckauf GmbH, Essen.

Hirany, A. and Kulhawy, F. H. (1988). *Conduct and Interpretation of Load Tests on Drilled Shaft Foundations: Detailed Guidelines,* Report EL-5915. Electric Power Research Institute, Palo Alto, CA, July, 374 pp.

Hoek, E. (1983). "Strength of Jointed Rock Masses," 23rd Rankine Lecture. *Geotechnique,* Vol. 33, No. 3, 187–223.

Hoek, E. and Brown, E. T. (1980). *Underground Excavations in Rock.* The Institution of Mining and Metallurgy, London, 527 pp.

Hoek, E. and Brown, E. T. (1988). "The Hoek-Brown Failure Criterion—a 1988 Update." *Proc. 15th Canadian Rock Mech. Symp,* ed. J. H. Curran, Toronto, Civil Engineering Department, University of Toronto, 31–38.

Hoek, E. and Brown, E. T. (1997). "Practical Estimates of Rock Mass Strength." *International Journal of Rock Mechanics and Mining Sciences and Geomechanics Abstracts,* Vol. 34, No. 8, December, 1165–1186.

Hoek, E., Carranza-Torres, C., and Corkum, B. (2002). "Hoek-Brown Failure Criterion—2002 Edition." *Proceedings of the 5th North American Rock Mechanics Symposium and 17th Tunneling Association of Canada Conference: NARMS-TAC 2002,* July 7–10, University of Toronto, 267–271.

Hoek, E., Kaiser, P. K., and Bawden, W. F. (1995). *Support of Underground Excavations in Hard Rock,* Balkema, Rotterdam, 215 pp.

Hoek, E. and Marinos, P. (2000). "Predicting Squeeze." *Tunnels and Tunneling International,* November, 45–51.

Honjo, Y., and Amatya, S. (2005). "Partial Factors Calibration Based on Reliability Analyses for Square Footings on Granular Soils." *Géotechnique,* Vol. 55, No. 6, 479–491.

Honjo, Y., and Kusakabe, O. (2002). "Proposal of a Comprehensive Foundation Design Code: Geocode 21 ver.2." In *Foundation Design Codes and Soil Investigation in View of International Harmonization and Performance-based Design,* Y. Honjo, O. Kusakabe, K. Matsui, M. Kouda, and G. Pokharel, eds., Balkema, 95–106.

Honjo, Y., Kusakabe, O., Matsui, K., Kikuchi, Y., Kobayashi, K., Kouda, M., Kuwabara, F., Okumura, F., and Shirato, M. (2000). "National Report on Limit State Design in Geotechnical Engineering: Japan." *Proc. International Workshop on Limit State Design in Geotechnical Engineering (LSD2000),* Melbourne, 217–240.

Honjo, Y., Suzuki, M., Shirato, M., and Fukui, J. (2002). "Determination of Partial Factors for a Vertically Loaded Pile Based on Reliability Analysis." *Soils and Foundations,* Vol. 42, No. 5, 91–109.

Horn, A. (1970). *Sohlreibung und räumlicher Erdwiderstand bei massiven Gründungen in nichtbindigem Boden.* Straßenbau und Straßenverkehrstechnik, Bundesminister für Verkehr, Abt. Straßenbau.

Hough, B. K. (1959). "Compressibility as the Basis for Soil Bearing Value." *Journal of the Soil Mechanics and Foundations Division,* Vol. 85, Part 2.

Hunt, R. E. (1986). *Geotechnical Engineering Analysis and Evaluation.* McGraw-Hill Inc., New York.

Hvorslev, M. J. (1937). *Iber die Festigkeitseigenschaften Gestörter Bindiger Böden.* København.

Ingra, T. S., and Baecher, G. B. (1983). "Uncertainty in Bearing Capacity of Sands." *Journal of Geotechnical and Geoenvironmental Engineering,* Vol. 109, No. 7, 899–914.

International Code Council. (2008). *2008 New York City Building Code,* ICC, New York, NY.

ISRM—International Society for Rock Mechanics (1981). *Suggested Methods for Rock Characterization, Testing and Monitoring,* ISRM Commission on Testing Methods, E. T. Brown (ed.), Pergamon, Oxford, UK.

Jaky, J. (1944). "The Coefficient of Earth Pressure at Rest." *Journal for Society of Hungarian Architects and Engineers,* 355–358.

Jaky, J. (1948). "Pressure in Silos." *Proc. 2nd Intl. Conference on Soil Mechanics and Foundation Engineering,* Rotterdam, Vol. 1, 103–107.

JRA (1996). *Specifications for Highway Bridges IV: Substructures (SHB).* Japan Road Association, Tokyo.

Jumikis, A. R. (1956). "Rupture Surfaces in Sand under Oblique Loads." *Journal of Soil Mechanics and Foundation Design,* Vol. 82, No. 1, 1–26.

Kanda, J., and Shah, H. (1997). "Engineering Role in Failure Cost Evaluation for Buildings." *Structural Safety,* Vol. 19, No. 1, 79–89.

Kim, S. G., Barker, R. M., Duncan, J. M., and Rojiani, K. B. (1991). "Part 3—Engineering Manual for Retaining Walls and Abutments." In *NCHRP Report 343: Manuals for the Design of Bridge Foundations,* Barker et al., Transportation Research Board, National Research Council, Washington, DC, 115–159.

Kimmerling, R. E. (2002). *Geotechnical Engineering Circular No. 6—Shallow Foundations,* FHWA-IF-02-054. FHWA, U.S. DOT, Washington, DC, 310 pp.

Kisse, A. (2008). Entwicklung eines Systemgesetzes zur Beschreibung der Boden-Bauwerk-Interaktion flachgegruendeter Fundamente auf Sand. Heft 34 der Mitteilungsreihe des Instituts fuer Grundbau und Bodenmechanik, Hrsg. Prof. Dr.-Ing. W. Richwien, VGE Verlag GmbH, Essen.

Kisse, A., and Lesny, K. (2007). Reliability-based Design of the Foundation of an Offshore Wind Energy Converter Using the Single Surface Hardening Model. In *Applications of Statistics and Probability in Civil Engineering, Proc. 10th International Conference,* eds. Kanda, J., Takada, T., and Furuta, H., June 31–July 3, 2007, Tokyo.

Kobayashi, K., Kuwabara, F., and Ogura, H. (2003). "Limit State Design Development for Building Foundations." *Proc. of 5th Japan Conference on Structural Safety and Reliability,* 901–908.

Kulhawy, F. H. (1978). "Geomechanical Model for Rock Foundation Settlement." *Journal of the Geotechnical Engineering Division,* Vol. 104, No. 2, February, 211–227.

Kulhawy, F. H. and Goodman, R. E. (1980). "Design of Foundations on Discontinuous Rock." *Proceedings of the International Conference on Structural Foundations on Rock,* International Society for Rock Mechanics, Vol. I, A. A. Balkema, Rotterdam, 209–220.

Kulhawy, F. H. and Goodman, R. E. (1987). "Foundations in Rock." In *Ground Engineer's Reference Book,* F. G. Bell, ed., Butterworths, London.

Kulhawy, F. and Mayne, P. (1990). *Manual on Estimation of Soil Properties for Foundation Design,* Report EPRI-EL-6800. Electric Power Research Institute, Palo Alto, CA.

Kulhawy, F. H. and Phoon, K. K. (2002). "Observations on Geotechnical Reliability-Based Design Development in North America." In *Foundation Design Codes and Soil Investigation in View of International Harmonization and Performance Based Design,* Y. Honjo, O. Kusakabe, K. Matsui, M. Kouda, and G. Pokharel, eds., A. A. Balkema, 31–50.

Kulicki, J. M., Prucz, A., Clancy, C. M., Mertz, D. R., and Nowak, A. S. (2007). Final report for NCHRP Project 20-07/186, Updating the Calibration Report for the AASHTO LRFD Code. (Unpublished document.)

Ladanyi, B., Dufour, R., Larocque, G. S., Samson, L., and Scott, J. S. (1974). "Report of the Subcommittee on Foundations and Near-Surface Structures to the Canadian Advisory Committee on Rock Mechanics." 55 pp.

Lambe, W. T., and Whitman, R. V. (1969). *Soil Mechanics.* Wiley, New York.

Laubscher, D. H. (1977) "Geomechanics Classification of Jointed Rock Masses—Mining Applications." *T. I. Min. Metall. A* 86 (1977), A1–A8.

Lauffer, H. 1958. "Gebirgsklassifizierung fur den Stollenbau." *Geologie and Bauwesen,* Vol. 24, No. 1, 46–51.

Lesny, K. (2001). Entwicklung eines konsistenten Versagensmodells zum Nachweis der Standsicherheit flachgegruendeter Fundamente. *Mitteilungen aus dem Fachgebiet Grundbau und Bodenmechanik der Universität Essen, Heft 27, Hrsg.: Prof. Dr.-Ing. W. Richwien, Verlag Glueckauf, Essen.*

Lesny, K. (2006). "The Role of Favourable and Unfavourable Actions in the Design of Shallow Foundations According to Eurocode 7." In *Foundation Analysis and Design—Innovative Methods* (*Geotechnical Special Publication No. 153*), (Proceedings of Sessions of Geoshanghai, June 6–8, Shanghai), 119–126.

Lesny, K., and Kisse, A. (2004). "Safety of Shallow Foundations in Limit State Design." *Proc. Int. Workshop on Risk Assessment in Site Characterization and Geotechnical Design,* Bangalore, India, 97–10.

Lesny, K., Kisse, A., and Richwien, W. (2002). "Proof of Foundation Stability Using a Consistent Failure Model." *Proceedings of the International Conference on Probabilistics in Geotechnics—Technical and Economic Risk Estimation,* Graz, Austria, 95–103.

Lesny, K., Perau, E., Richwien W., and Wang, Z. (2000). Some Aspects on Subsoil Failure of Vertical Breakwaters. Forschungsbericht aus dem Fachbereich Bauwesen, Heft 83, Universitaet Essen.

Lesny, K., and Richwien, W. (2002). A Consistent Failure Model for Single Footings Embedded in Sand. In *Foundation Design Codes and Soil Investigation in View of International Harmonization and Performance,* Honjo, Y., Kusakabe, O., Matsui, K., Kouda, M., and Pokharel, G., eds., Swets & Zeitlinger, Lisse, The Netherlands, 159–165.

Liao, S. S. C., and Whitman, R. V. (1986). "Overburden Correction Factors for SPT in Sand." *Journal of Geotechnical Engineering,* Vol. 112, No. 3, 373–377.

Lo, K. Y., and Hefny, A. M. (2001). "Foundation on Rock." *Geotechnical and Geoenvironmental Handbook,* R. K. Rowe, ed., Kluwer Academic Publishers, 305–335.

Lutenegger, A. J., and DeGroot, D. J. (1995). "Settlement of Shallow Foundations on Granular Soils" (report of research conducted for Massachusetts Highway Department, transportation research project contract #6332, task order #4).

Marinos, P., and Hoek, E. (2001). "Estimating the Geotechnical Properties of Heterogeneous Rock Masses Such as Flysch." *Bull. Eng. Geol. Env.,* Vol. 60, No. 2, 85–92.

Martin, C. M., and Houlsby, G. T. (2000). Combined Loading of Spudcan Foundations on Clay: Laboratory Test. *Géotechnique,* Vol. 50, No. 4, 325–338.

Martin, C. M., and Houlsby, G. T. (2001). Combined Loading of Spudcan Foundations on Clay: Numerical Modelling. *Géotechnique,* Vol. 51, No. 8, 687–699.

Matula, M., and Holzer, R. (1978). "Engineering Typology of Rock Masses." In *Proc. Felsmekanik Kolloquium, Grundlagen und Andwendung der Felsmekanik,* Karlsruhe, Germany, 107–121.

Mayne, P. W., Christopher, B. R., and DeJong, J. (2001). *Manual on Subsurface Investigations,* FHWA NHI-01-031. National Highway Institute and FHWA, U.S. DOT, Washington, DC.

Mayne, P. W. and Kulhawy, F. H. (1982). "K_o—OCR Relationships in Soil." *Journal of the Geotechnical Engineering Division,* Vol. 108, No. 6, 851–872.

Mayne, P. W. and Poulos, H. G. (2001). "Discussion: Approximate Displacement Influence Factors for Elastic Shallow Foundations." *Journal of Geotechnical and Geoenvironmental Engineering,* Vol. 127, No. 1, 100–102.

Meyerhof, G. G. (1953). "The Bearing Capacity of Foundations under Eccentric and Inclined Loads." *Proc., 3rd Int. Conf. on Soil Mechanics and Foundation Engineering,* Vol. 1, Zürich, 440–445.

Meyerhof, G. G. (1963). "Some Recent Research on the Bearing Capacity of Foundations." *Canadian Geotechnical Journal,* Vol. 1, No. 1, 16–26.

Meyerhof, G. (1994). "Evolution of Safety Factors and Geotechnical Limit State Design," Second Spencer J. Buchanan Lecture. Texas A&M University, College Station, TX, Nov. 4.

Meyerhof, G. G., and Koumoto, T. (1987). "Inclination Factors for Bearing Capacity of Shallow Footings." *Journal of Geotechnical and Geoenvironmental Engineering,* Vol. 131, No. 9, 1013–1018.

Michalowski, R. (1997). "An Estimate of the Influence of Soil Weight on Bearing Capacity Using Limit Analysis." *Soils and Foundation,* Vol. 37, No. 4, 57–64.

Michalowski, R. L., and You, L. (1998). "Effective Width Rule in Calculations of Bearing Capacity of Shallow Footings." *Journal of Computers and Geotechnics,* Vol. 23, No. 4, 237–253.

Montrasio, L. (1994). *Un Metodo per il calcolo die cedimenti di fondazioni su sabbia soggette a carichi eccentrici e inclinati,* Dottorato di ricerca in Ingegneria Geotecnica, Universita di Milano (in Italian).

Montrasio, L., and Nova, R. (1997). "Settlements of Shallow Foundations on Sand: Geometrical Effects." *Géotechnique,* Vol. 47, No. 1, 49–60.

Muhs, H. (1971). Die experimentelle Untersuchung der Grenztragfaehigkeit nichtbindiger Boeden bei lotrechter Belastung. Degebo-Mitteilungen, Heft 27.

Muhs, H., and Weiss, K. (1969). "The Influence of the Load Inclination on the Bearing Capacity of Shallow Footings." *Proc., 7th Int. Conf. on Soil Mechanics and Foundation Engineering,* Vol. 2, Mexico City, 187–194.

Munfakh, G. A., Arman, A., Collin, J. G., Hung, J. C-J., and Brouillette, R. P. (2001). *Shallow Foundations Reference Manual,* FHWA NHI-01-023. Federal Highway Administration, U.S. DOT, Washington, D.C.

NAVAC (*Naval Facilities Engineering Command Design Manual 7.01*) (1986). Naval Facilities Engineering Command, Alexandria, VA.

Nendza, H. and Nacke, C. (1986). Der Einfluss der Lagerungsdichte auf die Tragfaehigkeit ueberwiegend horizontal beanspruchter und auf Sand gegruendeter Fundamente. Mitteilungen aus dem Fachgebiet Grundbau und Bodenmechanik der Universitaet Essen, Heft 12, Ed. Prof. Dr.-Ing. H. Nendza, VerlagGlueckauf GmbH, Essen.

Nova, R., and Montrasio, L. (1991). "Settlements of Shallow Foundations on Sand." *Géotechnique,* Vol. 41, No. 2, 243–256.

Nowak, A. (1999). *NCHRP Report 368: Calibration of LRFD Bridge Design Code.* Transportation Research Board, National Research Council, Washington, DC.

NRC (1995). *National Building Code.* National Research Council of Canada, Ottawa.

OHBDC (1979, 1983, 1993). *Ontario Highway Bridge Design Code.* Ministry of Transportation, Downsview, Ontario, Canada.

Okahara, M., Fukui, J., Shirato, M., Matsui, K., and Honjo, Y. (2003). "National Report on Geotechnical Codes in Japan." *Proc. 12th Asian Regional Conference on Soil Mechanics and Geotechnical Engineering.*

O'Neill, M. W. and Reese, L. C. (1999). *Drilled Shafts: Construction Procedures and Design Methods,* ADSC-TL-4, FHWA-IF-99-025. FHWA, U.S. DOT, Washington, DC.

Orr, T. L. L. (2002). "Eurocode 7—A Code for Harmonized Geotechnical Design." *Foundation Design Codes and Soil Investigation in View of International Harmonization and Performance Based Design,* Y. Honjo, O. Kusakabe, K. Matsui, M. Kouda, and G. Pokharel, eds., Balkema, 3–12.

Oumeraci, H., Kortenhaus, A., Allsop, W., de Groot, M., Crouch, R., Vrijling, H., and Voortman, H. (2001). *Probabilistic Design Tools of Vertical Breakwaters,* Balkema, Lisse, the Netherlands.

Ovesen, N. K. (1989). "General Report/Discussion Session 30: Codes and Standards." *Proc. 12th International Conference on Soil Mechanics and Foundation Engineering,* Vol. 4, Rio de Janeiro, 2751–2764.

Paikowsky, S. G. (1989). "A Static Evaluation of Soil Plug Behavior with Application to the Pile Plugging Problem." D.Sc. Dissertation, M. I. T., Cambridge, MA.

Paikowsky, S. (2005). "Serviceability in the Design of Bridge Foundations." *Proceedings of the International Workshop on the Evaluation of Eurocode 7.* March 31–April 1, Trinity College, Dublin, 251–261.

Paikowsky, S. G., Amatya, S., Lesny, K. and Kisse, A. (2009b). "Developing LRFD Design Specifications for Bridge Shallow Foundations." *Proc. IS-GIFU2009 2nd Intl. Symposium on Geotechnical Safety and Risk,* June 11–12, Gifu, Japan.

Paikowsky, S. (with contributions by Birgisson, G., McVay, M., Nguyen, T., Kuo, C., Baecher, G., Ayyub, B., Stenerson, K., O'Mally, K., Chernauskas, L., and O'Neill, M.) (2004). *NCHRP Report 507: Load and Resistance Factor Design (LRFD) for Deep Foundations.* Transportation Research Board of the National Academies, Washington, DC.

Paikowsky, S. G., Palmer, C. J., and DiMillio, A. F. (2000). "Visual Observation and Measurement of Aerial Stress Distribution under a Rigid Strip Footing." In *Performance Confirmation of Constructed Geotechnical Facilities (Geotechnical Special Publication No. 94),* (Proceedings of the 17th International Conference on Soil Mechanics and Geotechnical Engineering, October 5–9, Alexandria, Egypt), 148–169.

Paikowsky, S. G., Fu, Y., Amatya, S., and Canniff, M. (2009a). "Uncertainty in Shallow Foundations Settlement Analysis and Its Utilization in SLS Design Specifications." *Proc. 17th International Conference on Soil Mechanics and Geotechnical Engineering,* IOS Press, Fairfax, VA.

Paikowsky, S. G., Fu, Y., and Lu, Y. (2005). Final Report for NCHRP Project 20-07/Task 183, LRFD Foundation Design Implementation and Specification Development. (Unpublished document.)

Paikowsky, S. G., and Hajduk, E. L. (1997). "Calibration and Use of Grid-Based Tactile Pressure Sensors in Granular Material." *Geotechnical Testing Journal,* GTJODJ, Vol. 20, No. 2, June, 218–241.

Paikowsky, S. G., Lesny, K., Amatya, S., Canniff, M., Kisse, A., and Muganga, R. (2008). Quarterly Report for NCHRP Project 24-31, LRFD Design Specifications for Shallow Foundations. Geosciences Testing & Research, Inc., North Chelmsford, MA.

Paikowsky, S. G., and Lu, Y. (2006). "Establishing Serviceability Limit State in the Design of Bridge Foundations." In *Foundation Analysis and Design—Innovative Methods* (*Geotechnical Special Publication No. 153*), (Proceedings of Sessions of Geoshanghai, June 6–8, Shanghai), 49–58.

Paikowsky, S. G., Player, C. M., and Connors, P. J. (1995). "A Dual Interface Apparatus for Testing Unrestricted Friction of Soil along Solid Surfaces." *Geotechnical Testing Journal,* GTJODJ, Vol. 18, No. 2, 168–193.

Paikowsky, S. G., Xi, F., and Hajduk, E. L. (1996). "Closure to a Discussion on 'A Dual Interface Apparatus for Testing Friction of Soil Along Solid Surfaces' by Paikowsky, Player, and Connors." *Geotechnical Testing Journal,* Vol. 19, No. 4, December, 447–451.

Palmström A. (1982). "The Volumetric Joint Count—A Useful and Simple Measure of the Degree of Rock Mass Jointing." IAEG Congress, New Delhi.

Palmström, A. (1995). "Rmi—A Rock Mass Characterization System for Rock Engineering Purposes." Ph.D. thesis, University of Oslo, Norway, 400 pp.

Paolucci, R. and Pecker, A. (1997). "Seismic Bearing Capacity of Shallow Strip Foundations on Dry Soils." *Soils and Foundations,* Vol. 37, No. 3, 95–105.

Peck, R. P., Hanson, W. E., and Thornburn, T. H. (1974). *Foundation Engineering,* 2nd ed., Wiley, New York.

Perau, E. (1995). *Ein systematischer Ansatz zur Berechnung des Grundbruchwiderstands von Fundamenten.* Mitteilungen aus dem Fachgebiet Grundbau und Bodenmechanik der Universität Essen, Heft 19, Hrsg.: Prof. Dr.-Ing. W. Richwien, Essen: Glückauf-Verlag.

Perau, E. (1997). "Bearing Capacity of Shallow Foundations." *Soils and Foundations,* Vol. 37, No. 4, 77–83.

Phoon, K. K. and Kulhawy, F. H. (1999). "Characterization of Geotechnical Variability." *Canadian Journal of Geotechnical Engineering,* Vol. 36, No. 4, 612–624 (including Discussion and Reply, Vol. 38, 2001, pp. 213–215).

Claudio Cherubini and Concetta I. Giasi (2001). Characterization of geotechnical variability *and* Evaluation of geotechnical property variability: Discussion. *Canadian Journal of Geotechnical Engineering,* Vol. 38, No. 1, 213.

Phoon, K. K. and Kulhawy, F. H. (2001). Characterization of geotechnical variability *and* Evaluation of geotechnical property variabil-

ity: Reply. *Canadian Journal of Geotechnical Engineering,* Vol. 38, No. 1, 214–215.

Phoon, K. K., and Kulhawy, F. H. (2002). "EPRI Study on LRFD and MRFD for Transmission Line Structure Foundations." In *Foundation Design Codes and Soil Investigation in View of International Harmonization and Performance,* Honjo, Y., Kusakabe, O., Matsui, K., Kouda, M., and Pokharel, G., eds., Swets & Zeitlinger, Lisse, The Netherlands, 253–261.

Phoon, K., Kulhawy, F., and Grigoriu, M. (1995). *Reliability-Based Design of Foundations for Transmission Line Structures,* Report TR-105000. Electrical Power Research Institute, Palo Alto, CA.

Phoon, K. K., Kulhawy, F. H., and Grigoriu, M. D. (2000). "Reliability-Based Design for Transmission Line Structure Foundations." *Computers and Geotechnics,* Vol. 26, No. 3–4, 169–185.

Prakoso, W. A. (2002). *Reliability-Based Design of Foundations on Rock Masses for Transmission Line and Similar Structures.* Ph.D. dissertation, Cornell University.

Prandtl, L. (1920). *Ueber die Haerte plastischer Koerper.* Nachrichten der Gesellschaft der Wissenschaften, Berichte der mathem.-physikal. Klasse, 74–85.

Prandtl, L. (1921). Ueber die Eindringfestigkeit (Haerte) plastischer Baustoffe und die Festigkeit von Schneiden. Zeitschrift für angewandte Mathematik und Mechanik 1, Band 1, 15–20.

Priest, S. D. and Hudson, J. A. (1976). "Discontinuity Spacings in Rock." *International Journal of Rock Mechanics and Mining Sciences and Geomechanics Abstracts,* Vol. 13, No. 5, May, 135–148.

Rabcewicz, L. v. (1964). "The New Austrian Tunneling Method. Part 1." *Water Power* (November), 511–515.

Rabcewicz, L. v. (1965). "The New Austrian Tunneling Method. Part 2." *Water Power* (January), 19–24.

Rabcewicz, L. v. (1975). "Tunnel Under Alps Uses New, Cost-Saving Lining Method." *Civil Engineering* (October), 66–68.

Ramamurthy, T., and Arora, V. K. (1993). *A Classification for Intact and Jointed Rocks, Geotechnical Engineering of Hard Soils-Soft Rocks,* Balkema, Rotterdam, 235–242.

Ramelot and Vanderperre (1950). "Les fondations de pylônes électriques: leur résistance au renversement, leur stabilité, leur calcul." IRSIA, *Comptes rendus de recherches, No. 2.*

Reissner, H. (1924). "Zum Erddruckproblem." *Proc., 1st Int. Congress of Applied Mechanics,* Delft, 295–311.

Romana, M. (1985). "New Adjustment Ratings for Application of Bieniawski Classification to Slopes." In *Proc. International Symposium on the Role of Rock Mechanics,* Zacatecas, 49–53.

Rosenblueth, E., and Esteva, L. (1972). *Reliability Basis for Some Mexican Codes,* ACI Publication SP-31. American Concrete Institute, Detroit, MI.

Rubinstein, R. Y. (1981). *Simulation and the Monte Carlo Method.* Wiley, New York, 278 pp.

Sabatini, P. J., Bachus, R. C., Mayne, P. M., Schneider, J. A., and Zettler, T. E. (2002). *Geotechnical Engineering Circular No. 5: Evaluation of Soil and Rock Properties,* FHWA-IF-02-034. Federal Highway Administration, U.S. DOT, Washington, DC.

Schmertmann, J. H. (1970). "Static Cone to Compute Static Settlement over Sand." *Journal of Soil Mechanics and Foundation Division,* Vol. 96, No. 3, 1011–1043.

Schmertmann, J. H., Brown, P. R., and Hartman, J. P. (1978). "Improved Strain Influence Factor Diagrams." *Journal of the Geotechnical Engineering Division,* Vol. 104, No. 8, 1113–1135.

Schneider, J. (2000). "Safety—A Matter of Risk, Cost and Consensus." *Structural Engineering International,* Vol. 10, No. 4, 266–269.

Schofield and Wroth (1968). *Critical State Soil Mechanics,* McGraw Hill, Maidenhead.

Schultze, J. (1952). "Der widerstand des Baugrundes gegen schraege Sohlpressungen." *Die Bautechnik,* Vol. 29, No. 1, 19–34.

Simpson, B., and Driscoll, R. (1998). *Eurocode—A Commentary,* Report 344. Building Research Establishment (BRE), UK.

Sjöberg, J. (1997). "Estimating Rock Mass Using the Hoek-Brown Failure Criterion and Rock Classification." Lulea University of Technology, Department of Civil and Mining Engineering, Division of Rock Mechanics, Sweden.

Sowers, G. F. (1979). *Introductory Soil Mechanics and Foundations: Geotechnical Engineering,* 4th ed., MacMillan, New York, 621 pp.

Sowers, G. B. and Sowers, G. F. (1970). *Introductory Soil Mechanics and Foundations,* 3rd ed., MacMillan, New York, 556 pp.

Steenfelt, J. S. (1977). "Scale Effect on Bearing Capacity Factor N_γ." *Proc., 9th Int. Conf. on Soil Mechanics and Foundation Engineering,* Vol. 1, Tokyo, 749–752.

Stille, H., Groth, T., and Fredriksson, A. (1982). "FEM-analysis of Rock Mechanical Problems with JOBFEM." Stiftelsen Bergteknisk Fonkning—BeFo, Stockholm, 307, 1/82.

Szerszen, M. M. and Nowak, A. S. (2003). "Calibration of Design Code for Buildings (ACI 318): Part 2—Reliability Analysis and Resistance Factors." *ACI Structural Journal,* Vol. 100, No. 3, 383–391.

Taly, M. (1997). *Design of Modern Highway Bridges.* McGraw-Hill, Inc., 1,368 pp.

Terzaghi, K. (1946). "Rock Defects and Loads on Tunnel Supports." In *Rock Tunneling with Steel Supports* (eds., R. V. Proctor and T. L. White), 17–99, Youngstown, OH, Commercial Shearing and Stamping Company.

Terzaghi, K. (1943). *Theoretical Soil Mechanics.* Wiley, New York.

Terzaghi K., and Peck R. B. (1948). *Soil Mechanics in Engineering Practice.* Wiley, New York.

Thoft-Christensen, P., and Baker, M. (1982). *Structural Reliability Theory and Its Application.* Springer-Verlag, New York.

Ticof, J. (1977). *Surface Footings on Sand under General Planar Loads.* Ph.D. thesis, University of Southampton, UK.

Tonias, D. (1995). *Bridge Engineering: Design, Rehabilitation, and Maintenance of Modern Highway Bridges,* McGraw-Hill, Inc., New York, 470 pp.

Uesugi, M. and Kishida, H. (1986). "Frictional Resistance at Yield between Dry Sand and Mild Steel." *Soils and Foundations,* Vol. 26, No. 4, 139–149.

Vesic, A. (1963). "Bearing Capacity of Deep Foundations in Sand." *Highway Research Record 39: Stresses in Soils and Layered Systems,* National Academy of Sciences, National Research Council, Washington, DC, 112–153.

Vesić, A. (1973). "Analysis of Ultimate Loads of Shallow Foundations." *Journal of the Soil Mechanics and Foundations Division,* Vol. 99, No. 1, 54–73.

Vesić, A. (1975). "Bearing Capacity of Shallow Foundations." In *Foundation Engineering Handbook,* H. F. Winterkorn and H. Y. Fang, eds., Van Nostrand Reinhold, New York, 121–147.

Vollpracht, H.-J., and Weiss, K. (1975). Anhang 1: Großmaßstäbliche Belastungsversuche zur Untersuchung des Gleitvorgangs. *Berichte aus der Bauforschung, Die Grenztragfähigkeit von flach gegründeten Streifenfundamenten unter geneigter Belastung nach Theorie und Versuch.*

Wickham, G. E., Tiedemann, H. R., and Skinner, E. H. (1972). "Support Determination Based on Geologic Predictions." *Proc. North American Rapid Excavation and Tunneling Conf.,* Chicago, 43–64.

Williams, G. W., Duncan, J. M. and Sehn, A. L. (1987). "Simplified Chart Solution of Compaction-Induced Earth Pressures on Rigid

Structures." *Geotechnical Engineering Report,* Virginia Polytechnic Institute and State University, Blacksburg, VA.

Williamson, D. A. (1980). "Uniform Rock Classification for Geotechnical Engineering Purposes." *Transportation Research Record 783,* TRB, National Research Council, Washington DC, 9–14.

Williamson, D. A. (1984). "Unified Rock Classification System." *Bull Assoc. Eng. Geol.* XXI (3), 345–354.

Withiam, J. L. (2003). "Implementation of the AASHTO LRFD Bridge Design Specifications for Substructure Design." *Proc. International Workshop on Limit State Design in Geotechnical Engineering Practice (LSD2003),* 37–38. (Full paper in CD-ROM, World Scientific.)

Withiam, J., Voytko, E., Barker, R., Duncan, M., Kelly, B., Musser, S., and Elias, V. (1998). *Load and Resistance Factor Design (LRFD) of Highway Bridge Substructures,* FHWA HI-98-032. FHWA, U.S. DOT, Washinton, DC.

Wolff, T. F. (1989). "Pile Capacity Prediction Using Parameter Functions." In *Predicted and Observed Axial Behaviors of Piles: Results of a Pile Prediction Symposium* (Geotechnical Special Publication No. 23), ASCE, 96–106.

Wyllie, D. C. (1992). *Foundations on Rock,* E & FN Spon, London.

Yoon, G. L., and O'Neill, M. W. (1997). "Resistance Factors for Single Driven Piles from Experiments." In *Transportation Research Record 1569,* Transportation Research Board, National Research Council, Washington, DC, 47–54.

Zienkiewicz, O. (2005). *The Finite Element Method,* 6th ed., Elsevier, Amsterdam.

Zhang, L. (2003). "Limit State Design Experiences in Hong Kong and Mainland China." *Proc. 12th Asian Regional Conference on Soil Mechanics and Geotechnical Engineering.*

Zhang, L., and Einstein, H. (1998). "End Bearing Capacity of Drilled Shafts in Rock." *Journal of Geotechnical and Geoenvironmental Engineering,* Vol. 124, No. 7, 574–584.

Zhang, L., Tang, W., and Ng, C. (2001). "Reliability of Axially Loaded Driven Pile Groups." *Journal of Geotechnical and Geoenvironmental Engineering,* Vol. 127, No. 12, 1051–1060.

Zhu, F., Clark, J. I., and Phillips, R. (2001). "Scale Effect of Strip and Circular Footings Resting on Dense Sand." *Journal of Geotechnical Geoenvironmental Engineering,* Vol. 127, No. 7, 613–621.

Zhu, M., and Michalowski, L. (2005). "Shape Factors for Limit Loads on Square and Rectangular Footings." *Journal of Geotechnical Geoenvironmental Engineering,* Vol. 131, No. 2, 223–231.

Unpublished Material

Appendixes to the contractor's final report for NCHRP Project 24-31 are not published herein but are available on the TRB website (www.trb.org) by searching for "NCHRP Report 651". The appendix titles are the following:

- Appendix A: Alternative Model Background
- Appendix B: Findings—State of Practice, Serviceability and Databases
- Appendix C: Questionnaire Summary
- Appendix D: UML-GTR ShalFound07 Database
- Appendix E: UML-GTR RockFound07 Database
- Appendix F: Shallow Foundations Modes of Failure and Failure Criteria
- Appendix G: Bias Calculation Examples
- Appendix H: Design Examples

Abbreviations and acronyms used without definitions in TRB publications:

AAAE	American Association of Airport Executives
AASHO	American Association of State Highway Officials
AASHTO	American Association of State Highway and Transportation Officials
ACI–NA	Airports Council International–North America
ACRP	Airport Cooperative Research Program
ADA	Americans with Disabilities Act
APTA	American Public Transportation Association
ASCE	American Society of Civil Engineers
ASME	American Society of Mechanical Engineers
ASTM	American Society for Testing and Materials
ATA	Air Transport Association
ATA	American Trucking Associations
CTAA	Community Transportation Association of America
CTBSSP	Commercial Truck and Bus Safety Synthesis Program
DHS	Department of Homeland Security
DOE	Department of Energy
EPA	Environmental Protection Agency
FAA	Federal Aviation Administration
FHWA	Federal Highway Administration
FMCSA	Federal Motor Carrier Safety Administration
FRA	Federal Railroad Administration
FTA	Federal Transit Administration
HMCRP	Hazardous Materials Cooperative Research Program
IEEE	Institute of Electrical and Electronics Engineers
ISTEA	Intermodal Surface Transportation Efficiency Act of 1991
ITE	Institute of Transportation Engineers
NASA	National Aeronautics and Space Administration
NASAO	National Association of State Aviation Officials
NCFRP	National Cooperative Freight Research Program
NCHRP	National Cooperative Highway Research Program
NHTSA	National Highway Traffic Safety Administration
NTSB	National Transportation Safety Board
PHMSA	Pipeline and Hazardous Materials Safety Administration
RITA	Research and Innovative Technology Administration
SAE	Society of Automotive Engineers
SAFETEA-LU	Safe, Accountable, Flexible, Efficient Transportation Equity Act: A Legacy for Users (2005)
TCRP	Transit Cooperative Research Program
TEA-21	Transportation Equity Act for the 21st Century (1998)
TRB	Transportation Research Board
TSA	Transportation Security Administration
U.S.DOT	United States Department of Transportation